THE BIOEFFICACY OF FLAVOKAWAIN C AGAINST COLON CANCER AND THE UNDERLYING MECHANISTIC INSIGHTS

PHANG CHUNG WENG

THESIS SUBMITTED IN FULFILMENT OF THE REQUIREMENTS FOR THE DEGREE OF DOCTOR OF PHILOSOPHY

FACULTY OF SCIENCE
UNIVERSITY OF MALAYA
KUALA LUMPUR

2017

UNIVERSITY OF MALAYA

ORIGINAL LITERARY WORK DECLARATION

Name of Candidate: PHANG CHUNG WENG

Matric No: SHC120009

Name of Degree: DOCTOR OF PHILOSOPHY

Title of Project Paper/Research Report/Dissertation/Thesis ("this Work"):

THE BIOEFFICACY OF FLAVOKAWAIN C AGAINST COLON CANCER AND THE UNDERLYING MECHANISTIC INSIGHTS

Field of Study: BIOCHEMISTRY AND MOLECULAR BIOLOGY

I do solemnly and sincerely declare that:

(1) I am the sole author/writer of this Work;
(2) This Work is original;
(3) Any use of any work in which copyright exists was done by way of fair dealing and for permitted purposes and any excerpt or extract from, or reference to or reproduction of any copyright work has been disclosed expressly and sufficiently and the title of the Work and its authorship have been acknowledged in this Work;
(4) I do not have any actual knowledge nor do I ought reasonably to know that the making of this work constitutes an infringement of any copyright work;
(5) I hereby assign all and every rights in the copyright to this Work to the University of Malaya ("UM"), who henceforth shall be owner of the copyright in this Work and that any reproduction or use in any form or by any means whatsoever is prohibited without the written consent of UM having been first had and obtained;
(6) I am fully aware that if in the course of making this Work I have infringed any copyright whether intentionally or otherwise, I may be subject to legal action or any other action as may be determined by UM.

Candidate's Signature Date:

Subscribed and solemnly declared before,

Witness's Signature Date:

Name:

Designation:

ABSTRACT

In the present study, flavokawain C, a natural-occuring chalcones, showed higher cytotoxic activity against HCT 116 cells in comparison to other cell lines tested and minimal toxicity on normal colon cell line (CCD-18Co). Cytotoxic activity of FKC was found to be caused by the activation of intrinsic, extrinsic and endoplasmic reticulum stress-mediated apoptotic pathways.This was associated with an increase in reactive oxygen species and a decrease in SOD activity. A sustained ERK1/2 activation and inactivation of PI3K/Akt were also observed. Cell cycle was found to be arrested at S phase and G_2/M in HCT 116 and HT-29 cells, respectively after FKC treatment. Down-regulation of Cdk2 and Cdk4, up-regulation of p53, $p21^{Cip1}$ and $p27^{Kip1}$, and hypophosphorylation of pRb were observed. Proteomic analysis identified 35 proteins that changed in abundance (17 increased and 18 decreased). These proteins were found to be involved in cell death and survival, cellular growth and proliferation, cell cycle, protein synthesis, post-translational modification and amino acid metabolism. In *in vivo* study, FKC treatment inhibited HCT 116 tumor growth with no obvious toxicity. Induction of apoptosis and reduction in cell proliferation were shown in FKC-treated tumors. Five differentially abundant proteins from serum were also identified via proteomic analysis which can be used as potential biomarkers. Thus FKC holds great promise for use in molecular target-based chemopreventive and chemotherapeutic strategies.

ABSTRAK

Dalam kajian ini, flavokawain C (FKC), sebatian semula jadi jenis kalkon, kesan sitotoksik, FKC menunjukkan aktiviti sitotoksik lebih tinggi terhadap HCT 116 berbanding dengan sel-sel lain tetapi ketosikan yang minima terhadap sel kolon normal (CCD-18Co). Aktiviti sitotoksik FKC didapati disebabkan oleh pengaktifan laluan intrinsik, ekstrinsik dan tekanan endoplasma retikulum apoptosis. Ini diiringi dengan peningkatan bagi spesies oksigen reaktif (ROS) dan penurunan dalam aktiviti SOD. FKC juga didapati menyebabkan tekanan terhadap endoplasma retikulum, seperti yang ditunjukkan oleh peningkatan GADD-153 dalam kedua-dua sel tersebut. Kekekalan ERK1/2 aktivasi and inaktivasi PI3K/Akt juga diperhatikan. Kitaran sel didapati diberhentikan di fasa S dan G_2/M dalam sel-sel HCT 116 and HT-29, masing-masing selepas FKC rawatan. Penurunan Cdk2 dan Cdk4, peningkatan p53, $p21^{Cip}$ dan $p27^{Kip1}$ dan pRb hipofosforilan diperhatikan. Analisis proteomik mengenal pasti 35 protein yang berubah kelimpahan (17 meningkat dan 18 menurun). Protein-protein tersebut ini terlibat dalam kematian dan kehidupan sel, pertumbuhan dan pembiakan sel, kitran sel, sintesis protein, pengubahsuaian pasca-translasi dan metabolisma asid amino. Untuk kajian *in vivo*, rawatan FKC merencat pertumbuhan HCT 116 tumor tanpa ketoksikan jelas. Induksi apoptosis dan pengurangan percambahan sel ditunjukkan dalam tumor dirawat FKC. Lima protein yang mengalami perubahan 'abundance' dari serum telah digenalpasti melalui analisis proteomik yang mempunyai potensi sebagai penanda biology. Oleh itu, FKC mempunyai potensi yang besar untuk digunakan dalam strategi kemopreventif dan kemoterapeutik berasaskan sasaran molekul.

ACKNOWLEDGEMENTS

First and foremost, I owe my deepest gratitude to my supervisor, Prof. Datin Dr. Sri Nurestri Abd Malek, who has supported and guided me throughout the thesis and the years of research. I especially thank her for being so patient and helping me not only in research but also inspiring me with her passion for research.

Secondly, I would like to express my sincere appreciation and gratitude to my co-supervisor, Assoc. Prof. Dr. Saiful Anuar Karsani. His invaluable guidance and support as well as insightful idea and advice have contributed greatly to the thesis.

I am indebted to my labmates and friends for their help and encouragement throughout the study. Special thanks to Dr Gautam Sethi from National University of Singapore (NUS) for his help and guidance in the western blot work. I would also like to express my gratefulness to Prof. Dr. Mahmood Ameen Abdulla Hassan and Pouya Hassandarvish from the Department of Biomedical Science, Faculty of Medicine, and the staffs from Department of Pathology, Faculty of Dentistry and Animal Experimental Unit, Faculty of Medicine for their assistance in my *in vivo* study.

I would like to take this opportunity to acknowledge the financial support (MyPhD) of the Ministry of Higher Education. Also, I gratefully acknowledge the University of Malaya who funded my PhD project (High Impact Research MoE Grant UM.C/625/1/HIR/MoE/SC/02 and PPP grant PG121-2015B).

Last, and most importantly, this thesis would not have been possible without the never-ending help and support of my parents. I am deeply grateful to them.

To them, I dedidate this thesis

TABLE OF CONTENTS

LIST OF FIGURES

LIST OF TABLES

LIST OF SYMBOLS AND ABBREVIATIONS

AIF	:	Apoptosis inducing factor
APS	:	Ammonium persulfate
ATCC	:	American Tissue Culture Collection
BCL-2	:	B-cell lymphoma 2
BrdU	:	Bromodeoxyuridine
BSA	:	Bovine serum albumin
CHAPS	:	3-[(3-cholamidopropyl) dimethyl-ammonio]-1-propanesulfonate
DCFH-DA	:	2',7'-Dichlorodihydrofluorescein Diacetate
DMSO	:	Dimethyl sulfoxide
DR	:	Death receptor
DTT	:	Dithiothreitol
EDTA	:	Ethylenediaminetetraacetic acid
ER	:	Endoplasmic reticulum
FKA	:	Flavokawain A
FKB	:	Flavokawain B
FKC	:	Flavokawain C
FITC	:	Fluorescein isothiocyanate
GMM	:	gymnogrammene
HRP	:	Horseradish peroxidase
HSP	:	Heat shock protein
IC_{50}	:	Half maximal inhibitory concentration
IAA	:	Iodoacetamide
IEF	:	Isoelectric focusing
IHC	:	Immunohistochemistry

IPG	:	Immobilised pH gradient
JC-1	:	5,5',6,6'-tetrachloro-1,1',3,3'-tetraethylbenzimidazolylcarbocyanine iodide
JNK	:	c-Jun N-terminal kinase
kDa	:	kiloDalton
MALDI	:	Matrix assisted laser desorption/ionisation
MAPK	:	Mitogen-activated protein kinase
MS	:	Mass spectrometry
m/z	:	Mass to charge ratio
MMP	:	Mitochondrial membrane potential
NF-κB	:	Nuclear factor-kappa β
NCBI	:	National Centre for Biotechnology Information
PAGE	:	Polyacrylamide gel electrophoresis
PARP	:	Poly adenosine diphosphate (ADP)-ribose polymerase
pI	:	Isoelectric point
PI	:	Propidium iodide
PBS	:	Phosphate buffered saline
PBST	:	Phosphate buffered saline with Tween-20
PMF	:	Peptide mass fragment
PS	:	Phosphatidylserine
qPCR	:	Quantitative polymerase chain reaction
ROS	:	Reactive oxygen species
SD	:	Standard Deviation
SDS	:	Sodium dodecylsulfate
SAR	:	Strucuture-activity relationship
SOD	:	Superoxide dismutase

SRB	:	Sulforhodamine B
TEMED	:	Tetramethylethylenediamine
TdT	:	Terminal deoxynucleotidyl transferase
TUNEL	:	Terminal deoxylnucleotidyl transferase dUTP nick end labelling
TOF	:	Time-of-flight
XIAP	:	X-chromosome linked inhibitor of apoptosis protein
2-DE	:	Two dimensional gel electrophoresis

LIST OF APPENDICES

CHAPTER 1: INTRODUCTION

Plants have been, and remain to be, an important source of bioactive molecules with novel structures and mechanisms of actions. Recently, there has been increasing interest in the use of natural compounds as a basis for drug development. In cancer treatment, the approach to the development of anti-cancer drugs has undergone major changes, from a strategy of selecting compounds that kill particular tumor cells towards a more mechanistic strategy in which the selection is based on their capability to modulate the molecular targets that underlie cell transformation. These treatments often have fewer side effects as they are more selective of the tumor cells over the host cells, since only the tumor cells are so dependent on the target molecule.

By knowing the ability of the treatment on how it interferes with cellular functions in cancer may provide a novel understanding of molecular basis underlying cancer development and progression (Millimouno *et al.*, 2014). Therefore, numerous efforts have been directed at the identification of biologically active targets of naturally-occurring compounds from plants. Many potential novel anticancer molecular targets have been identified and validated such as protein lipid kinase like phosphoinositide 3-OH kinase, proteasomes, chaperone proteins, as well as chromatin associated and hypoxia associated proteins (Blume-Jensen & Hunter, 2001; Workman & Kaye, 2002). The search for novel drugs is still a priority for cancer therapy as chemotherapeutic drug resistance and cancer recurrence becoming more and more frequent.

The use of natural dietary agents as alternative treatment for cancer has became widely accepted due to their therapeutic benefits, wide safety margin and cost-effectiveness (Amin *et al.*, 2009). Chalcones are naturally occurring flavonoids and can be found in a variety of vegetables, fruits and medicinal plants. They have been shown to exhibit remarkable cytotoxic and apoptotic activities against a number of cancer cell

lines and in animal models. The substitution of different functional groups in chalcone structure give rise to many chalcone derivatives that target various signaling molecules or pathways such as growth factors, transcription factors, protein kinases, inflammatory cytokines, and angiogenesis, all of which are often deregulated in cancers (Jandial *et al.*, 2014). The flavokawains are among the most active naturally-occurring chalcone in Kava root extract. Several recent studies have shown that treatment with flavokawains caused apoptosis and cell cycle arrest in many cancer cell lines (Abu *et al.*, 2013). It was therefore of interest to investigate the anti-cancer potential of yet another chalcone, flavokawain C (FKC) and a structurally related chalcone, gymnogrammene (GMM). GMM only differs from FKC at C-2' and C-4 in which the C-4 hydroxyl in FKC is replaced by a methoxy group whilst the C-2' methoxyl group in FKC is replaced by a hydroxyl moiety (Figure 3.1).

Colorectal cancer (CRC) is one of the three most dreadful malignancies reported worldwide besides lung and breast cancer. It is the third most commonly diagnosed cancer, ranking after lung and breast (Ferlay *et al.*, 2015). CRC is normally characterized by its invasiveness and highly metastatic potential which have attributed to increasing cancer-related deaths (Bresalier *et al.*, 1984; Schluter *et al.*, 2006). CRC incidences differ considerably between western and non-western countries. In recent years, a gradual increase in CRC incidence has been reported in Asian and less developed countries (Torre *et al.*, 2015). Studies have suggested that lifestyle and environmental factors rather than genetic susceptibility are primarily responsible for the increasing occurence of CRC (Haggar & Boushey, 2009b). The incidence of CRC could be reduced through the early diagnosis of cancer and removal of benign polyp precursors. Unfortunately, a great majority of patients are diagnosed at the late-stage where the cancer has spread outside of the colon and thus surgery is not the best option (de Wit *et al.*, 2013; Worthley & Leggett, 2010). Patients with advanced cancers are

usually resistant to a variety of cytotoxic agents. Therefore, new preventive and therapeutic agents are urgently needed.

Despite advances in clinical diagnostics and therapeutic modalities, cancer incidences have been increasing over the years and there is limited success in extending the survival of patients. The unsuccessful outcomes in many forms of chemotherapy in most cancer patients is often caused by its failure to induce cell death and growth arrest in cancer particularly the apoptosis signaling pathways (Housman *et al.*, 2014). A number of conventional drugs have restricted clinical application due to the dose-limiting toxicity and resistance by tumor cells. Thus there has been a growing effort in the search for a better chemotherapeutic drug that targeting apoptotic cell death pathway and inhibiting proliferation of cancer cells.

Apoptosis is a form of programmed cell death that functions in the maintenance of tissue homeostasis by counterbalancing cell proliferation and eliminating damaged or transformed cells. Apoptosis is the fastest and cleanest way to remove unwanted cells without provoking an inflammatory reaction as in the case of necrosis. This makes it the ideal way for eliminating cells in cellular differentiation and immunosurveillance mechanisms (Pohle *et al.*, 2004). Apoptosis occurs as a result of caspase activation which causes the collapse of cellular infrastructure via internal proteolytic cleavage, leading to cytoskeletal disintegration, DNA fragmentation and metabolic derangement (Melet *et al.*, 2008). Apart from that, inhibition of the signaling pathways that regulate the cell cycle progression may also lead to cytostatic and even apoptotic effects in cancer cells (Lin *et al.*, 2008). The underlying mechanisms of cell death via apoptosis remains poorly understood even though many key apoptotic proteins have been found. This is due to the crosstalk and the mechanisms that link among these proteins in the

apoptotic pathways have not been fully characterized. Thus manipulation of apoptosis pathways in cancer treatment still remains a daunting task.

Targeting signal transduction pathways is the first approach to the current paradigms of molecularly-targeted cancer therapeutics (Ortega *et al.*, 2010). Proteins are the main components of the metabolic pathways that control and execute biological functions of cells in living organisms (Mesri, 2014). Dysregulation of protein expression and cellular signaling pathways is the cause of several chronic diseases such as neurodegenerative diseases, cancer and metabolic disorders. Proteomics is a large-scale analysis of the structures and functions of proteins in defined biological systems. In cancer research, it has been extensively used to discover new diagnostic or prognostic markers, improve the understanding of cancer pathogenesis as well as develop a new therapy options (Alaiya *et al.*, 2000). A two-dimensional gel electrophoresis (2DE) approach is a popular and versatile method for the separation of complex protein mixtures, and quantification as well as identification of individual proteins in cells, tissue or fluids. The post-translational modifications and/or spliced forms of the same protein can be detected which allows us to gain more information on cellular phenotype (Alvarez-Chaver *et al.*, 2014). Furthermore, advancement in mass spectrometry technology, coupled with the availability of protein sequence databases and software tools for data acquisition, allows for a more rapid, effective and sensitive way for the characterization of proteins (Mesri, 2014).

The efficiency and selectivity of killing against particular tumor types by newly found compounds in clinical settings still remains one of the major challenges. Animal models are widely used to address a variety of research questions regarding to drug treatment response in cancer research, as the results obtained would more reflective of the effects of the drug in cancer patients. In addition, the tumor microenvironment and

host cells (such as fibroblast, endothelial cells, nerve cells and immune cells, etc) may also contribute to tumor development and progression (de Wit *et al.*, 2013). Human tumor xenografts have been used as predictive preclinical models for cancer therapeutics. It allows us to assess the efficacy, safety and toxicity of new anticancer drugs in order to gain scientific merit before proceeding to human clinical trials or further clinical development (DeSantis *et al.*, 2014; Kerbel, 2003; Workman *et al.*, 2010).

1.1 Objectives of study

General objective:

To evaluate the anti-cancer activity of flavokawain C by postulating its potential molecular mechanisms in regulating cell death in cancer.

The aims of the current study are as follows:

1. To evaluate the dose- and time-dependent effect of flavokawain C and gymnogrammene (flavokawain C analogue) on cell proliferation against a panel of cancer cell lines (A549, CaSki, MCF-7, HCT 116, HT-29) and a non-cancerous cell line (CCD-18Co).
2. To investigate the apoptotic-inducing activity of flavokawain C on selected cancer cell lines and its potential signaling pathways.
3. To further identify the signaling factors and pathways that may be involved in mediating the anti-proliferative and apoptotic acitivities of flavokawain C on selected cancer cell line at the proteomic and genomic levels.
4. To develop and use a human xenograft tumor model to investigate the anti-tumor effect of flavokawain C.

CHAPTER 2: LITERATURE REVIEWS

2.1 Natural products as a source of anti-cancer drug discovery

Natural products have historically served mankind as the source of all kind of medicine. Higher plants contributed for most of these remedial agents. From 1981 to 2013, over one third (38%) of all FDA-approved drugs were of natural origin, consisting of original natural products, synthetic products based on natural product models and semi-synthetic compounds derived from natural products. Plant products represent 47% of the total FDA-approved natural products (Patridge *et al.*, 2016).

The history of plant as a source of anti-cancer agents dated back to the late 1950s with the discovery of the vinca alkaloids (vincristine and vinblastine) by Robert Noble and Charles Beer from the Madagascar periwinkle plant which was used by various cultures for the treatment of diabetes, and followed by in the late 1960s with the isolation of podophyllotoxins and its derivatives (Bhanot *et al.*, 2011; Moudi *et al.*, 2013). Between 1960 and 1982, over 114,000 plant-derived extracts had been tested by the National Cancer Institute (NCI) on human cancer cell lines and this had led to discovery of many compounds with a range of cytotoxic activities (Paul *et al.*, 2010). Since then, numerous active ingredients in plants or herbs have been discovered was found to be potentially useful for the development of therapeutic agents. The bioactive compounds also serve as lead structures for the transformation into new, more potent and effective compounds (Srivastava *et al.*, 2005). They can be used as molecular probes in the study of signaling pathways affecting cell cycle progression (David *et al.*, 2002).

The two most common methods for the discovery of these bioactive compounds is through ethnobotany/ethnopharmacology, and targeting plant families which are known

to be rich in biologically active compounds (Rates, 2001). Examples of plant-based anti-cancer drugs which are in clinical use or under clinical trial are taxol (paclitaxel®) from the bark of the Pacific yew tree, vincristine (Oncovin®) from *Catharanthus roseous,* camptothecin from *Camptotheca acuminate*, etc and chemically modified plant-derived compounds such as topotecan, irinotecan, taxotere, etoposide, teniposide, etc (Du, 2003; Lu *et al.*, 2003; Slichenmyer & Von Hoff, 1991).

2.1.1 Chalcones

Chalcone or 1,3-diaryl-2-propen-1-one belong to family of flavonoids which is synthesized via the shikimate pathway. Chalcones act as the precursor for open-chain flavonoids and isoflavonoids, which present abundantly in a variety of plant species (Orlikova *et al.*, 2011). In nature, chalcones are common natural pigments of flowers, intermediates in flavonoid biosynthesis, and can act as defensive compounds against microorganisms, insects and ultraviolet radiation (Albuquerque *et al.*, 2014; Batovska & Todorova, 2010). The structural skeleton of chalcones consists of two aromatic rings joined by an open chain three-carbon unit α, β-unsaturated carbonyl system (Orlikova *et al.*, 2011). Chalcones have a broad structural diversity in plants as a result of their differential gene expression. For example, hydroxyl, methoxy, methylenedioxy, methyl, isoprenyl, and glycosyl derivatives as well as dimers, oligomers, and the β-hydroxyl (or oxy) chalcones (Cazarolli *et al.*, 2013).

The chalcones and its derivatives can also be synthesized via Claisen-Schmidt condensation. This reaction involves cross-Aldol condensation of an aromatic aldehyde and appropriate ketones by acid catalyzed or base catalyzed reactions, and followed by dehydration (Rayees Ahmad *et al.*, 2016). The green approach has been applied to the synthesis of chalcones using solvent-free conditions, heterogenous catalysts, cesium salts of 12-tungstophosphric acid as nanocatalysts, microwave and ultrasound

irradiation, and grinding techniques (Calvino *et al.*, 2006; Rafiee & Rahimi, 2013; Rayees Ahmad *et al.*, 2016). The chalcone structure, atom numbering of chalcones, the designation of the aryl rings as A and B are shown in Figure 2.1.

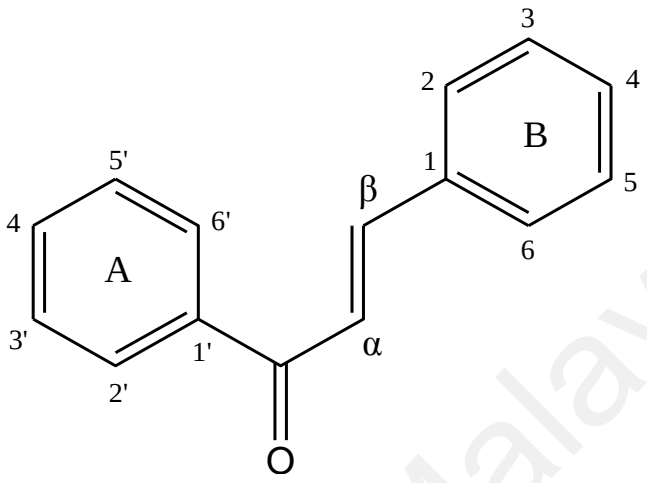

Figure 2.1: Structure of chalcone

Numerous studies have reported that natural and synthetic chalcones show a broad range of biological activities, including anticancer (Srinivasan *et al.*, 2009), antioxidant (Miranda, Stevens *et al.*, 2000), cytotoxic (Vogel *et al.*, 2008), anti-mitotic (Boumendjel *et al.*, 2008), anti-proliferative (Loa *et al.*, 2009), anti-inflammatory (Kim *et al.*, 2007), anti-HIV (Wu *et al.*, 2003), antimalarial (Dominguez *et al.*, 2001), anti-tubercular (Chiaradia *et al.*, 2008), anti-viral (Onyilagha *et al.*, 1997), antibacterial (Avila *et al.*, 2008) and antifungal activities (Batovska *et al.*, 2007). Some example of chalcone compounds such as metochalcone, sofalcone and hesperidin methylchalcone have been marketed for treatment of various health conditions (Zhou & Xing, 2015). Thus chalcone derivatives have received increasing attention amongst researchers because of its diverse pharmacological applications. However, much of the mechanistic bases of the biological activities of chalcones are still not fully understood.

2.1.2 Structure-activity relationship of chalcones for anti-cancer activity

Chalcones have been shown to exert cytotoxic activity against many cancer cells by affecting multiple signaling targets and pathways which include apoptosis, cell cycle, proteosome, angiogenesis, tubulin polymerization and NF-κB (Albuquerque *et al.*, 2014). Structure-activity relationship (SAR) studies showed that the activities of some chalcones varied widely and are closely related to their structural features. Modification in the substitution pattern and type of functional groups in chalcones resulted in different inhibitory effect against various molecular targets involved in carcinogenesis (Mahapatra *et al.*, 2015).

The presence of a double bond in conjugation with carbonyl functionality at the core of chalcone scaffold is believed to be the main pharmacophore as its partial or full removal causes a loss of bioactivity (Batovska & Todorova, 2010). The double bond can exist both in the cis- and trans-forms, and can easily be cyclized to form flavonones via Michael addition (Singh *et al.*, 2014). α, β-unsaturated carbonyl system of chalcones has a high tendency towards thiols as compared to hydroxyl and amino groups. It has been found to be responsible for the inhibition of ubiquitin-proteasome system (UPS) by interacting with the proteasome and deubiquitinating enzymes (DUB) (Bazzaro *et al.*, 2011; Issaenko & Amerik, 2012). Inhibition of DUB activity has been shown to stabilise and up-regulate tumor supressors p53, $p27^{Kip1}$ and $p16^{Ink4A}$ (Issaenko & Amerik, 2012).

Structure-activity relationship studies also found that replacement of aryl with heteroaryl ring and/or substitution of aryl ring A and B with electron donating/withdrawing groups resulted in the inhibition of VEGF2, MMP, 5α-reductase, proteasome and ABCG2 (Mahapatra *et al.*, 2015). Multiple methoxy substitutions on both phenyl ring A and B and their substitution pattern has been shown to cause

inhibition of JAK/STAT signaling and kinase activity such as aurora kinases and ErbB family of receptor tyrosine kinases (RTKs) whereas multiple hydroxyl substitution on phenyl ring B showed inhibition of CDC25B phosphatase which resulted in inhibition of cell cycle in G_2 or S-phase and mitotic arrest occurs (Mahapatra *et al.*, 2015). For this reason there has been a continuous search for naturally occurring or synthesized chalcones with potent anticancer properties.

2.1.3 Flavokawains: Phytochemistry and biological properties

Recently, one class of chalcones (flavokawain) have emerged as potential candidates for anti-cancer agents candidates (Abu *et al.*, 2013). Several studies have shown that flavokawains are cytotoxic, induce apoptosis as well as block the different stages of the cell cycle in a number of different human cancer cell lines *in vitro* and *in vivo* models, with minimal cytotoxic effect on noncancerous cells (Abu *et al.*, 2013). The structures of flavokawain A, B and C are shown in Figure 2.2.

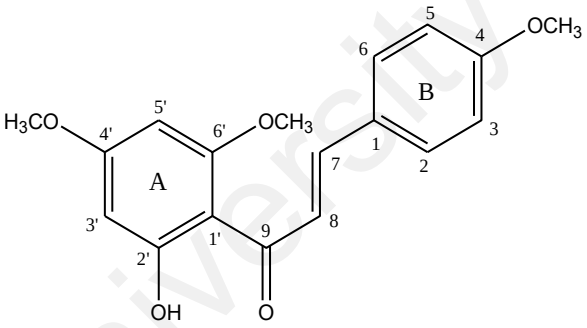

flavokawain A

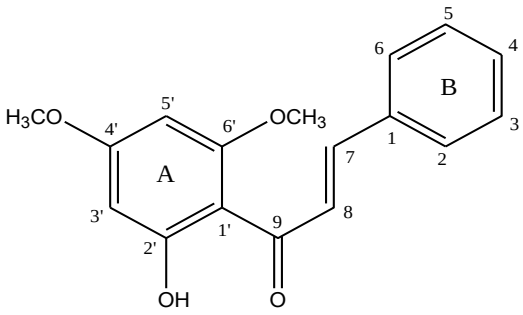

flavokawain B

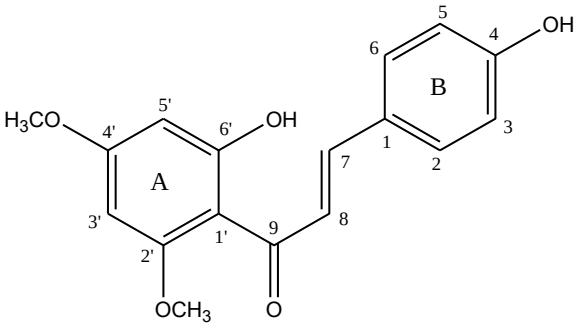

flavokawain C

Figure 2.2: Structure of flavokawain A, B and C.

Flavokawain C can be found in Kava (*Piper methysticum* Forst) root which grows naturally in Fiji and other South Pacific Islands and constitute up to 0.012% of kava extracts (Dharmaratne *et al.*, 2002). In the Pacific Islands, kava kava extracts have been traditionally prepared from macerated roots with water and coconut milk and used for centuries as a beverage for ceremonial purposes and social events without any side effects (Cote *et al.*, 2004; Whitton *et al.*, 2003). The plant has been used in traditional medicine to treat both acute and chronic gonorrhoea, vaginitis, leucorrhea, menstrual problems, venereal diseases, nocturnal incontinence and other ailments of the genitourinary tracts as it has an antiseptic effect on urine (Bilia *et al.*, 2004). Kava-kava extracts have also been commercialised as dietary supplement for stress, anxiety, insomnia, restlessness and muscle fatigue (Weiss *et al.*, 2005). However, kava-kava extracts were withdrawn from the market in several countries in 2002 as it had been reported to cause liver toxicity. The cause of liver toxicity may be due to: (i) the commercial extraction process used for the crude root powder which may result in chemical changes and (ii) consumption in high doses (Whitton *et al.*, 2003). Some studies have found an unusually low incidence of several cancers in kava drinking countries, including in the Pacific Islands, Fiji, Vanuatu and Western Samoa, despite the presence of a large number of smokers in these populations, especially among men (Steiner, 2000).

A previous study has shown that flavokwain C exhibited cytotoxic activity against three bladder cancer cell lines (T24, RT4 and EJ cells) with an IC_{50} of less than 17 µM (Zi & Simoneau, 2005). Li *et al* (2008) reported that FKC exhibited a mild cytotoxic effect against human hepatoma cells (HepG2) and normal liver cells (L-02) with IC_{50}, 57.04 and 59.08 µM respectively (Li *et al.*, 2008). The structure-activity relationship of chalcones involving B-rings showed that the hydroxyl group at the *o*-position on B-ring of flavokawain C play an important role in the inhibition of melanogenesis (IC_{50} value

of 6.9 µM) in B16 melanoma cells and it was more active compared to flavokawain B (IC_{50} value of 7.7 µM) (Jeong *et al.*, 2015). However, to the best of our knowledge, there is no report on the cytotoxic activity of flavokawain C on colon cancer cells and no investigation on its apoptotic activity towards the cancer cells.

Besides flavokawiain C, recent studies demonstrated that flavokawain B induced apoptosis and cell cycle arrest in colon, bladder, oral, lung cancer cells and also tumor cells such as osteosarcoma, synovial sarcoma and uterine leiomyosarcoma (An *et al.*, 2012; Eskander *et al.*, 2012; Ji *et al.*, 2013; Kuo *et al.*, 2010; Lin *et al.*, 2012; Sakai *et al.*, 2012). In addition, flavokawain A was shown to induce apoptosis and cell cycle arrest in bladder cancer cells (p53 wild type and mutant) and breast cancers (MCF-7 and MDA-MB231) (Abu *et al.*, 2014; Tang *et al.*, 2008; Zi & Simoneau, 2005).

2.2 Cancer

According to the statistics by GLOBOCAN 2012, an estimated 14.1 million new cancer cases and 8.2 million cancer-related deaths are reported in 2012. Cancer is a complex genetic disease characterized by uncontrolled growth of abnormal cells to produce a population of cells that have acquired the ability to multiply and invade surrounding and distant tissues (Grady, 2004b). Cancer develops through multi-stages and progress over a protracted period due to the accumulation of mutations in genomic DNA. The mutations result in the malfunction of tumor suppressor genes, oncogenes, and key cellular genes that involved in cell death, cell proliferation, survival, differentiation, and genome integrity which contribute to tumor formation. Some cancers are caused by inherited essential DNA repair genes (Macaluso *et al.*, 2003). Conceptually, carcinogenesis can be thought of as occurring in three steps: initiation, which is the irreversible alteration of cancer-related genes; promotion, the clonal expansion of the initiated cells, which is reversible if detected; and progresssion, the

final stage, which is characterized by the transformation of a benign mass of cells into a malignant tumor, driven by the acquisition of additional mutations (Bevers *et al.*, 2014).

Oncogenes code for proteins that promote cell transformation or cancer formation and usually result from mutations of normal genes (proto-oncogenes) through point mutation, gene amplication or chromosomal rearrangements, and are highly expressed in cancer. Tumor suppressor genes code for proteins that function as negative regulators of cell growth or regulators of cell death, and some function in DNA repair and cell adhesion (Grady, 2004a). The lost of function of tumor suppressor genes can lead to the predisposition of cancer. The accumulation of multiple mutations allows the cells to circumvent the multiple regulatory mechanisms that maintain homeostasis in the organs. These mutations can be resulted from inheritance of mutated allele, epigenetic mechanisms, exposure to carcinogens, DNA replication errors and chemical instability of DNA (Baba, 2007).

Genetic alterations alone cannot explain all tumor development. It is accepted that the interaction of cancer cells with the microenvironment, the surrounding non-neoplastic cells, the immune system, and other epigenetic events are relevant determinants in tumor promotion and metastasis (Ungefroren *et al.*, 2011). In addition, the growth of malignant cells is dictated by the manifestation of six essential alterations in cell physiology as suggested by Hanahan and Weinberg (2011): self-sufficiency in growth signals, insensitivity to growth-inhibitory (antigrowth) signals, evasion of programmed death (apoptosis), limitless replicative potential, sustained angiogenesis, and tissue invasion and metastasis. This can be further intensified by the lack of a broad knowledge of the signaling pathways within a cancer cell where the particular affected pathway(s) and acquired mutations vary across the different cancer sites (Hanahan & Weinberg, 2011). Until now, there is yet a comprehensive and detailed explanation on

how this required set of mutations are able to transform normal cells into highly malignant cancer cells and take place over the course of the patients' lifetime.

2.3 Colorectal cancer

2.3.1 Structure and function of colon

The colon, like the rest of the gastrointestinal tract, is composed of various tissues organized into four layers: the mucosa, the submucosa, the muscularis propria and the serosa as shown in Figure 2.3. The mucosa itself contains three layers: the epithelium, the lamina propria and the muscularis mucosae. The columnar epithelial cells are folded into finger-like invaginations or crypts which represent the functional unit of the colon, and supported by lamina propria. The main functions of the colon are the absorption of water and electrolytes, and fecal lubrication (Kasdagly *et al.*, 2014). The colon host a broad range of microorganisms that play essential roles in the fermentation of undigested nutrients, the synthesis of essential vitamins, and the establishment of a proper immune system throughout postnatal life (Kasdagly *et al.*, 2014).

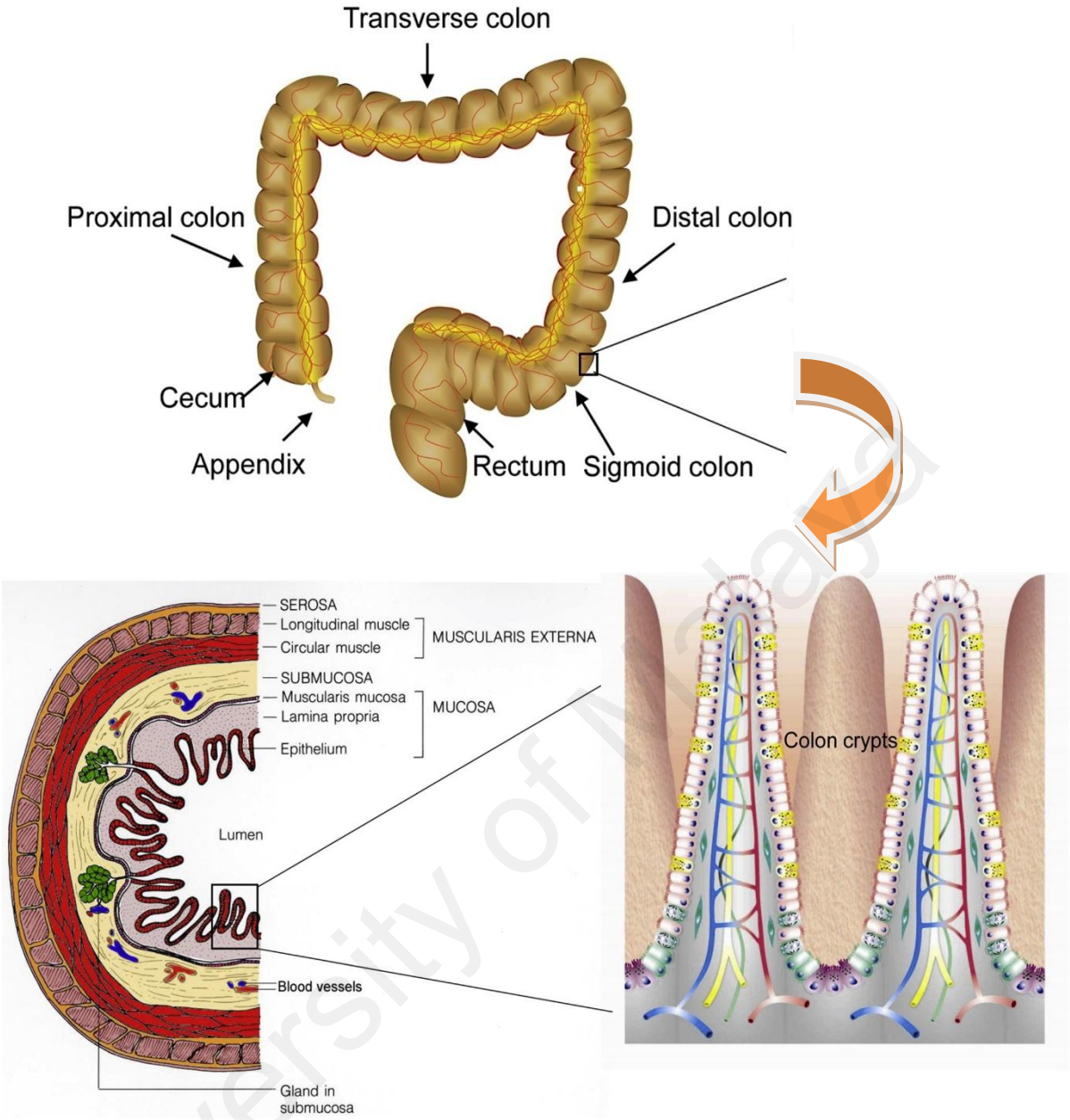

Figure 2.3: Morphology of the colon

(Retrieved from Kasdagly, Radhakrishnan, Reddivari, Veeramachaneni, & Vanamala, 2014)

2.3.2 Epidemiology

Colorectal cancer (CRC) is the third most common malignancy and fourth most common cause of death worldwide, with an estimated 1.4 million new cases of CRC diagnosed and a mortality of 693,900 in 2012 (Torre *et al.*, 2015). It is the third most common cancer in men (746,000 cases) and the second in women (614,000 cases) worldwide (Ferlay *et al.*, 2015). In Malaysia, it is the second most common cancer as reported by National Cancer Registry in 2007, with the highest incidence rate occurs among the chinese followed by the Malays and Indians (Abu Hassan *et al.*, 2016). There are large geographic differences in the incidence of CRC globally. The highest incidence rates are found in developed countries (mainly western countries) such as Australia, New Zealand, United States, and Europe as compared with developing countries (Ng & Wong, 2013). The incidence rate in United States has been found to be declining and this has been attributed to increasing screening rates. However, the incidence of CRC has been rapidly increasing in several historically low-risk countries, and some countries in Asia such as Japan, Korea, Bangkok, Singapore and China (Sano *et al.*, 2016; Torre *et al.*, 2015).

2.3.3 Staging and treatments

The selection of treatment for CRC depends mainly on the stages of tumor progression (stage I through IV) which is classified according to TNM staging system. In the TNM classification, 'T' refers to the depth of tumor invasion, 'N' refers to the presence of metastasis to regional lymph node, and 'M' refers to presence of distant metastasis (Greene & Sobin, 2008).

Surgical resection has been the primary treatment for CRC. The extend of resection is based on the depth of invasion, histologic grade and nodal status (Van Schaeybroeck *et al.*, 2014). Adjuvant therapy includes chemo-, radiotherapy or in combination of both

approaches has been used to reduce the risk of recurrence particurly for patients with high-risk stage II and stage III cancer after surgery (Van Schaeybroeck *et al.*, 2014). The conventional chemotherapy regimens consist of 5-fluorouracil, capecitabine, irinitecan and oxaliplatin or a combination of these drugs. These drugs have also been used to treat patients with metastatic CRC. Another treatment option is the targeted therapy involves the use of antibody inhibitors of the VEGF (bevacizumab, regorafenib and ramucirumab) and the EGFR (cetuximab and panitumumab) (Van Schaeybroeck *et al.*, 2014).

There is a higher chance of cure for CRC if it is detected at early stages. However, most CRC cases are detected at the advanced stages at the time of initial diagnosis where most patients are diagnosed with liver metastasis and it becomes more difficult to treat. Once CRC has metastasized, the five-year overall survival rate drops to 10% (Haggar & Boushey, 2009a).

2.3.4 Risk factors

Studies have shown that rising of CRC incidences in developing countries can be attributed to the adoption a western lifestyle and dietary habits such as diets rich in red and processed meats, sugar and fats, but poor in fruits, vegetables, and fiber, as well as increasing age, family history and having diabetes mellitus (Acevedo *et al.*, 2012; Su *et al.*, 2013; Virk *et al.*, 2010). Studies have also shown that the disparity in CRC incidence and mortality has been related to race, gender and ethnicity. This occurrence of CRC incidence has been found to be correlated with environmental factors and genetic characteristics (Boyle & Leon, 2002; Sung *et al.*, 2005). Overweight or obesity is now established as a risk factor for colon cancer where studies have found that the elevation of insulin and insulin-like growth factor (IGF-1) was associated with colon carcinogenesis (Kasdagly *et al.*, 2014).

2.4.5 Molecular pathogenesis of CRC

It is generally accepted that most CRC arise from an adenomatous polyp (adenoma). Some might develop from serrated adenomas, hyperplastic polyps, dysplasia and flat adenomas that can be found in the inflamed colon in association with inflammatory bowel disease (Tanaka, 2009). The malignancy potential of an adenomous polyp depends on its size, growth pattern, and grade of dysplasia.

Studies have suggested that the aberrant activation of self-renewal pathways of stem cells such as Wnt or β-catenin signaling pathways due to genetic mutations causes uncontrolled crypt cell division. This leads to the adenoma formation and eventually turns into into malignancy (Humphries & Wright, 2008; Tanaka, 2009). Figure 2.4 shows the stages of CRC from the formation of an early adenoma to carcinoma which penetrates through the submucosal and muscularis externa layers to reach the serosal side of the coloretal wall. Further accumulation of genetic mutations can result in metastasis which commonly spread to the liver via lymph nodes (Bretthauer, 2011). The common affected pathways are shown in Figure 2.5 which include Wnt signaling, and the signaling pathways involving receptor tyrosine kinase [epidermal growth factor receptor (EGFR), vascular endothelial growth factor (VEGF), insulin-like growth factor 1 (IGF1R), and MET], transforming growth factor (TGF)-β1 receptor, phosphoinositide 3-kinase (PI3K), Akt and p53 (Palma *et al.*, 2015).

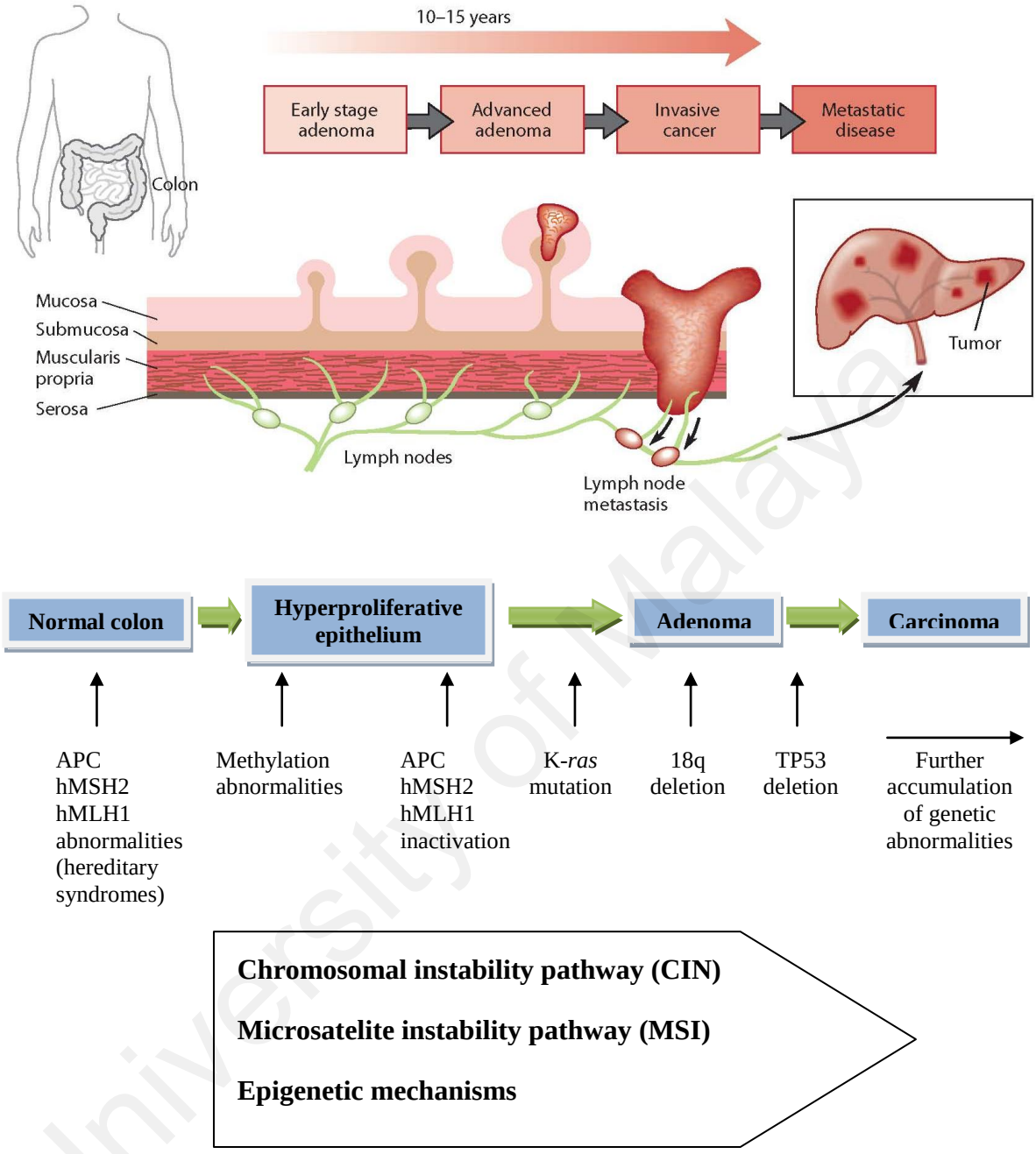

Figure 2.4: **A schematic representation of adenoma-carcinoma sequence and the proposed sequence of molecular genetic events in the evolution of colon cancer.** CRC develop from benign precursor polyps on the mucosal surface of large intestine and progress to invasive adenocarcinomas, through series genetic changes over a long-time period. Eventually spread to the intestinal lymph nodes and metastasize to liver. Each stage of CRC progression are accompanied by involvement of unique molecular features which depend on whether they display CIN, MSI or epigenetic mechanisms

(Retrieved from Bretthauer, 2011)

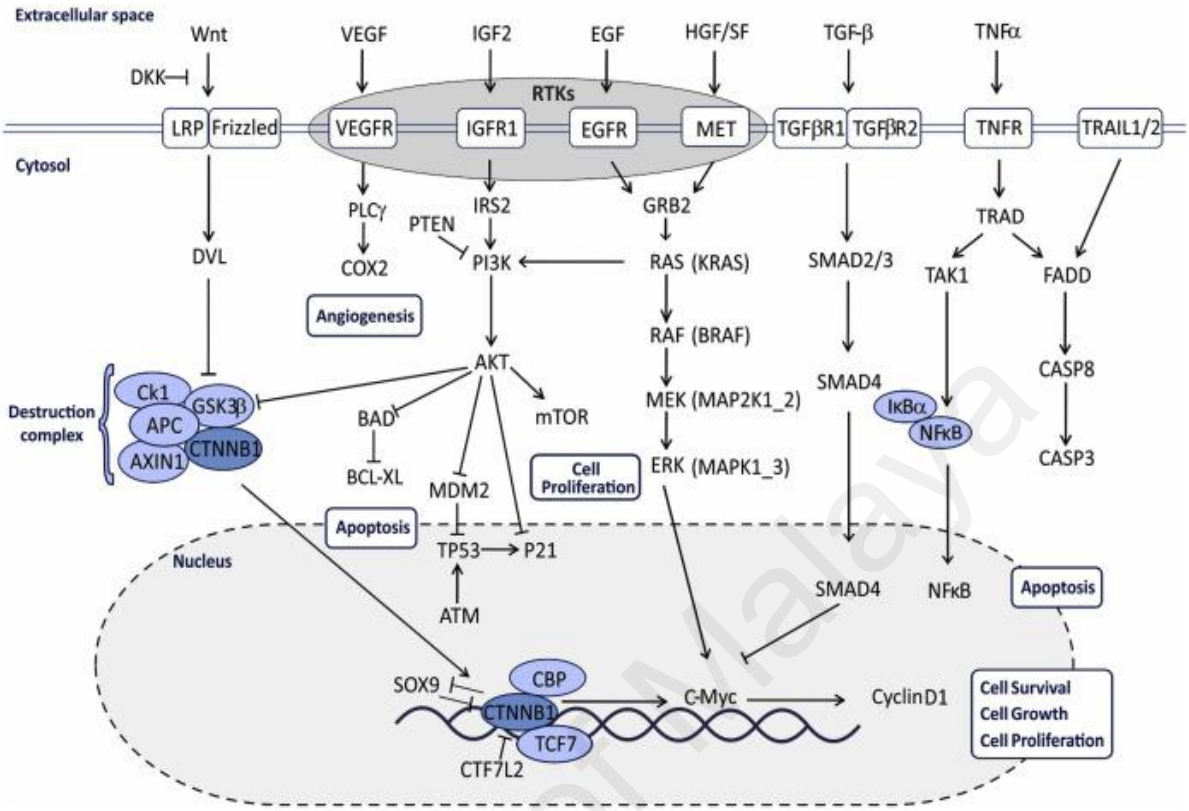

Figure 2.5: A Schematic representation of the main pathways affected in CRC.

(Retrieved from Palma et al, 2015)

The majority of CRC cases are sporadic (approximately 85%) and occurs in average risk patients aged 50 and older without obvious predisposing risk factors. It is developed through randomly acquired somatic mutations in several of the genes affected in hereditary cancers or their deregulation by epigenetic alterations. The remaining cases (less than 10%) have hereditary forms of CRC which occurs at younger ages due to germline mutations in specific genes (Rao & Yamada, 2013). Carcinogenesis of CRC is a multistep process, which arises through a sequential accumulation of genetic and epigenetic alterations in the adenoma to carcinoma transition and this model was first proposed by Fearon and Vogelstein (Fearon & Vogelstein, 1990). Since then, numerous genetic and non-genetic alterations have been found to be involved in the transformation. There are two major forms of genetic instability in CRC: microsatellite instability (MSI) and chromosomal instability (CIN).

2.4.5.1 Chromosomal instability (CIN)

CIN is characterized by consecutive accumulation of chromosomal abnormalities and loss of heterozygosity (LOH). It is found to be more common than MSI in CRC cases (about 80%). This pathway is associated with mutations or allelic loss of the adenomatous polyposis coli (APC) gene, KRAS gene, the deleted in colorectal cancer (DCC) gene and TP53 gene. Inactivation of APC causes the activation of β-catenin/Wnt signaling pathway which is responsible for tumor progression and malignant transformation (Pino & Chung, 2010). Germline mutation of APC causes familial adenomatous polyposis (FAP) which is characterized by the development of large numbers of polyps in the colorectal mucosa and accounts for 1-2% of all hereditary CRC (Van Schaeybroeck *et al.*, 2014).

2.4.5.2 Microsatellite instability (MSI)

MSI is characterized by a defective DNA mismatch-repair function caused by mutations in DNA mismatch repair (MMR) genes such as hPMS1, hPMS2 and hMSH6, hMLH1 and hMSH2 genes. It is often associated with mutations in specific target genes such as transforming growth factor β receptor II (TGFβRII), β-catenin, BAX, PTEN and $p16^{INK4A}$. In sporadic CRC, the loss of MMR gene is caused by epigenetic silencing. MSI is also a characteristic molecular defect in hereditary nonpolyposis colorectal cancer (HNPCC) (Soreide *et al.*, 2006).

2.4.5.3 Epigenetic modification

Epigenetic modification of genes has recently been implicated in CRC pathogenesis. It involves heritable changes in gene expression without alteration in the primary DNA sequence. Epigenetic alterations in CRC include histone modifications, aberrant DNA methylation, chromatin remodelling and noncoding RNAs especially microRNA expression (Jia & Guo, 2013). In CRC, CpG islands in cell cycle regulatory genes, DNA repair genes and tumor suppressor genes are frequently methylated which result in repression of transcription such as APC, RUNX3, MLH1, MGMT, CDKN2A and RASSF1A. These CpG-rich regions are mostly present close to the promoter region of almost 50% of all human genes (Vaiopoulos *et al.*, 2014).

2.3.6 Chemotherapy

Chemotherapy is one of the main strategies for reducing the rate of cancer progression and metastasis or, in some cases, curing the tumor. DNA-alkylating agents are the most widely used anti-cancer drugs in chemotherapy such as cisplatin, doxorubicin and methotrexate (Cheung-Ong *et al.*, 2013). Most chemotherapeutic drugs are not only selectively targeting the tumor cells but they are also known to damage the normal cells with high proliferation rate such as the bone marrow cells and hair matrix keratinocytes which results in a compromised immune system and hair loss (Sak, 2012). The standard chemotherapy regimens for CRC involve the use of cytotoxic drugs (5-fluorouracil and leucovorin, oxalipatin (FOLFOX) and irinotecan (FOLFIRI)) and monoclonal antibodies (cetuximab, bevacizumab or panitunumab) either alone or in combination (Cartwright, 2012). The administration of these drugs or drug combination is likely to associate with some side effects.

The treatment strategy for cancer depends on the clinical staging. Patients diagnosed with early stage I and II cancer are curable with radiotherapy or surgery with adjuvant chemotherapy. However, late stages of cancer (Stage III to IV) must be treated with aggressive chemotherapy as they are usually resistant to a variety of cytotoxic agents due to the presence of multiple genetic alterations. The survival rate following resection remains poor, except in patients with an early-stage of the disease. A majority of cancer patients eventually relapse after resection (Siegel *et al.*, 2012). Chemotherapy is thus important for treatment of advanced stage cancer and prevents cancer reoccurrence.

2.3.7 Molecular targeted approaches for cancer prevention and therapy

The remarkable understanding of the molecular mechanisms underlying malignant transformation, together with the great advances in molecular technologies in cancer research has led to the development of targeted therapies which offer more personalized approaches to cancer treatment. Targeted therapy refers to agents that selectively target specific molecular pathways involved in tumor growth, progression and survival while sparing the normal cells. It is different from conventional cytotoxic drugs which affect all rapidly dividing cells (Ortega *et al.*, 2010). It continues to be the most promising and actively pursued area of research in anticancer drug discovery. Two approaches have been approved by the US FDA for use in clinical practice: (i) monoclonal antibodies such as bevacizumab targets the VEGR-A and cetuximab targets EGFR, and (ii) small-molecule inhibitor such as gefitinib, erlotinib and imatinib target the tyrosine kinase part of EGFR (Burrell & Swanton, 2014).

A number of reports have attempted to reveal the mechanism of action and molecular targets responsible for the various bioactivities of chalcones. Chalcones have been shown to target multiple molecules and affect multiple steps of carcinogenesis from tumor initiation, progression, invasion and metastasis (Zhang *et al.*, 2013). Chalcones are promising compounds to be used in molecular targeted therapy. As the structure of chalcones are easy to be chemically modified, they can be used as the basic building blocks for the synthesis of novel agents (Jandial *et al.*, 2014). In addition, chlacones have been reported to be less toxic towards normal cells, thus the commonly reported chemotherapy side effect can be avoided (Orlikova *et al.*, 2011).

2.3.8 Limitation and obstacles of current therapies

Despite remarkable clinical successes in targeted therapy has been achieved, there is still lack of desired results in the treatment of many cancers. Tumor heterogeneity and occurrence of drug resistance have been found to be the reasons for the failure in the therapy (Huang *et al.*, 2014b). Human tumors are traditionally thought to be monoclonal in origin, there is now increasing evidence of intra-tumor heterogeneity as well as inter-tumor heterogeneity as the results of both genetic and non-genetic influences. The variation in phenotypic and functional features include cellular morphology, gene expression (including the expression of growth factor receptors and non-receptor signaling molecules which drive cancer survival and progression), metabolism, motility, angiogenesis, proliferation and metastasis (Marusyk & Polyak, 2010). The intra-tumor heterogeneity could be driven by genetic complexity and differentiation of cancer stem cells (Michor & Polyak, 2010). This phenomenon is believed to arise from Darwinian-like clonal evolution (Marusyk *et al.*, 2012). Tumor heterogeneity is further influenced by ongoing alterations of the microenvironment components around or within tumor regions such as lymphatic vasculature, densities of blood, numbers and types of infiltrating normal cells, and compositions extracellular matrix (Marusyk & Polyak, 2010).

Resistance to targeted therapies can occur either from the outset (intrinsic resistance) due to the presence of concurrent aberrations or through adaptive responses (acquired resistance) during treatment such as loss of the target, outgrowth of resistant clones or the activation of alternative signaling pathways. This resistance can also arise through acquisition of new mutations that activate signaling pathways necessary for tumour growth (Arnedos *et al.*, 2014). The mechanisms of resistance are directly connected to specific gene alterations such as KRAS-mutated tumors that show resistance to anti-EGFR therapy (Diaz *et al.*, 2012). All these factors have resulted in variation of patient

responses to targeted therapy and the main reason for the resistance to cancer therapy. Thus, the use of several targeted drugs in combination could be more effective than single targeted drug.

2.3.9 Biomarkers

Biomarkers are referred to as biological entities whose level of expression or activity could be used in clinical applications to either determine the onset of cancer (diagnostic), predict the response of patients to treatment (predictive) or predict development of cancer and prospect of recovery (prognostic) (Nibbe & Chance, 2009). Biomarkers have been integrated into early clinical trials and development of targeted therapies in order to screen for the patients who are potentially responsive to such targeted agents (Luo & Xu, 2014). It can also be used to determine the recurrence of the cancer and whether the target molecules are inhibited by the treatment (Henry & Hayes, 2012). The use of ideal biomarkers able to improve early detection of cancer, shorten the period of clinical trial, and reduce the healthcare cost (de Wit *et al.*, 2013) .

Currently, the screening methods for CRC includes colonoscopy, sigmoidoscopy, immunochemical faecal occult blood test (FIT) and fecal occult blood test (FOBT) (Van Schaeybroeck *et al.*, 2014). Colonoscopy and sigmoidoscopy are invasive methods, costly, time-consuming, and uncomfortable, and may bring adverse outcome as bowel preparation is needed. They are difficult to be implemented on a population-wide basis (Garborg *et al.*, 2013). Although FOBT and FIT is non-invasive and inexpensive, it lacks the required specificity and may give false positive results (Elfant, 2015). Taking into consideration the heterogeneous nature of cancer and tumor microenvironment, it is implausible to use a single marker to characterize a tumor and determine the appropriate treatment for patients (Kelloff & Sigman, 2012). Carcinoembryonic antigen (CEA) is

the only blood biomarker in clinical use for CRC detection and has been used to monitor CRC recurrence (Su *et al.*, 2012).

Serum/plasma is an attractive target for the discovery of potential biomarkers. Serum biomarkers are convenient to be measured via non-invasive method. However, most biomarkers in clinical practice are still lack the needed specificity and sensitivity. This is due to the high sample-variation among cancer patients and the present of a wide dynamic range of serum proteins (Dunn *et al.*, 2011; Wu *et al.*, 2008). Therefore, the search for a promising serum tumor marker for predicting responses to drug therapies is necessary. Mouse xenograft models have recently been used to search for the serum biomarkers. The use of this approach can minimize the biological heterogeneity where blood samples can be obtained at defined stages of tumor development and under controlled breeding conditions (Kuick *et al.*, 2007).

2.4 Deregulation of cell death pathways in cancer

In addition to mutations in genes that regulate cell survival, cancers also carry mutations in genes that regulate cell death. Defects in cell death mechanisms cause cancer formation and growth. It can also cause resistance to treatment as the maintenance of homeostasis in tissues depends on both the regulation of cell proliferation and cell death (Fulda, 2010).

Cell death is of major importance in regulating an organism's development, tissue homeostasis and stress response, and interconnects with cell survival and proliferation (Jain *et al.*, 2013). Generally, cell death can be classified into apoptosis, necrosis and autophagy (lysosomal cell death). Both apoptosis and autophagy are active cellular self-destruction and are the preferred form of cell death in cancer therapy, although some forms of necrosis are also under consideration and studied.

2.4.1 Apoptosis

Apoptosis is a form of programmed cell death, which is energy-dependent, genetically controlled and a highly regulated form of cell death in which individual cells undergo regulated self-destruction in response to physiological and pathological stimuli (Duprez *et al.*, 2009; Steller, 1995). It plays important roles in maintenance of tissue homeostasis and normal embryonic development in the adult organism by regulating the cell numbers precisely and removing unneeded cells (Steller, 1995). It also play important role in our body to defend against potentially harmful cells, such as cancer cells, cells infected with viruses, self-reactive lymphocytes (Steller, 1995). The dysregulation of apoptosis has been implicated in the pathogenesis of many human diseases, including cancer, diabetes, neurodegenerative disorders, sepsis, stroke, myocardial infarction, ischemia and autoimmune diseases (Duprez *et al.*, 2009)

Apoptosis is characterized by typical cellular morphological and biochemical features. These characteristics include loss of cell-cell contact, detachment, cell shrinkage (loss of K^+ and water), nuclear condensation, internucleosomal DNA leakage (CAD activation), membrane blebbing, nuclear fragmentation and cell-self-fragmentation into apoptotic bodies. These apoptotic bodies are quickly removed by phagocytes and neighbour cells which are attracted by membrane-exposure of phosphatidylserine that serves as an 'eat me' signal. In cell culture, the cells eventually undergo secondary necrosis where they lose membrane integrity and lyse (Jain *et al.*, 2013).

In mammals, there are three main apoptotic signaling pathways which are categorized based on their source of the stimuli: (i) the intrinsic or mitochondria-mediated, (ii) the extrinsic or death receptor-mediated, and (iii) endoplasmic reticulum stress-mediated pathway. All three pathways lead to the activation of caspases which are responsible for the execution of the apoptotic process (Majors *et al.*, 2007). Apart from caspases, apoptosis-inducing factor (AIF) and endonuclease G (EndoG) are specifically involved in the regulation of apoptosis. An overview of the intrinsic and extrisnic apoptotic cell death pathways is shown in Figure 2.6.

In contrast, necrosis is characterised by inflammation and wide-spread injury in response to tissue damage caused by toxin, hyperthermia, hypoxia and ishcemia. Cells typically swell, lose membrane integrity and subsequently release their intracellular contents which trigger the host inflammation response (Fink & Cookson, 2005). Although initially it was considered as an accidental mode of cell death, there is now increasing evidence suggesting that necrotic cell death is regulated by specific signaling pathways (Fulda *et al.*, 2010).

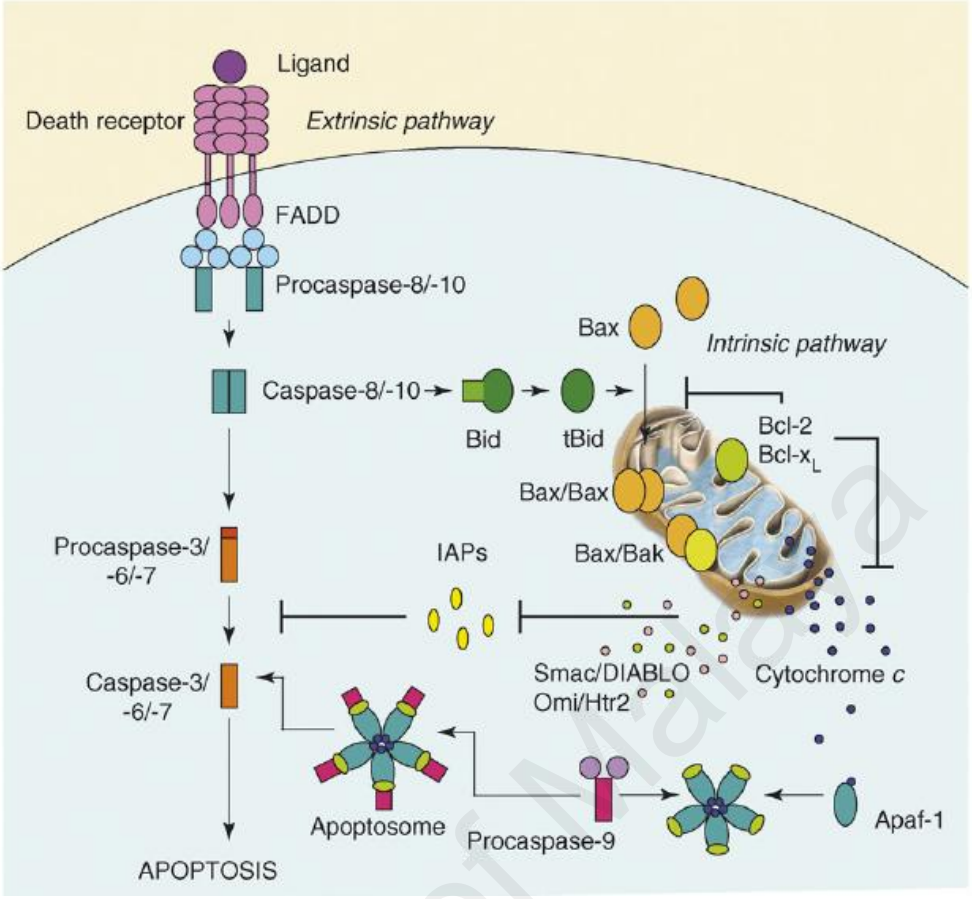

Figure 2.6: Overview of intrinsic and extrinsic apoptotic pathways

(Retrieved from Ramalho *et al.*, 2008)

2.4.1.1 Caspases

Caspases belong to a family of cysteine-activated aspartate-specific proteases, which are synthesized as catalytically-dormant tripartite proenzymes (zymogens) consisting of a prodomain of variable length, followed by a large (p20), and a small (p10) catalytic subunit (Salvesen & Dixit, 1999). Caspases can be classified into two groups: upstream initiator and downstream effector caspases. Initiator caspases (caspase 8 and 9) are capable of autocatalytic activation by distinct pro-apoptotic stimuli, which in turn, cleave the inactive form of effector caspases (caspase 3 and 7), thereby activating them (Neutzner *et al.*, 2012; Watson, 2004). Effector caspases are responsible for the cleavage of intracellular proteins, next to an aspartate residue. The substrates for

caspasese are: (i) apoptotic regulators (ii) structural elements of the cytoskeleton and the nucleus, (iii) cellular DNA repair proteins, and (iv) cell cycle regulatory proteins. The action of caspases on these substrates causes the induction and amplification of cellular pathways which lead to morphological features of apoptotic cell death (Ulivieri, 2010). The function of caspases is highly regulated by a group of inhibitor of apoptosis proteins (IAPs).

2.4.1.2 Intrinsic or mitochondrial pathway

In the intrinsic apoptotic pathway, the signal leading to cell death typically originates from within the cell itself (Brouckaert *et al.*, 2005). It can be initiated by cellular or genotoxic stresses induced by irradiation or chemotherapeutics, trophic factor withdrawal, nutrient deprivation, heat shock, oxidative stress, hypoxia, ER stress, loss of interactions with the extracellular matrix or chemical toxins (Prehn *et al.*, 2013; Brouchaert *et al.*, 2005). The mitochondria play a major role in the initiation and execution of the intrinsic pathway of apoptosis apart from being a site of electron transport and generating cellular ATP (Harris & Thompson, 2000; Zeestraten *et al.*, 2013).

Apoptotic signaling in this pathway causes two major changes in the mitochondria: an increased in permeabilization of the outer mitochondrial membrane and a reduction of the inner membrane potential. This results in the release of pro-apoptotic proteins from mitochondria into cytoplasm. These proteins are cytochrome-c, Smac/DIABLO, Omi/HtrA2, AIF and Endo G (Huang *et al.*, 2007).

The release of cytochrome c from mitochondria is a key stage in the intrinsic pathway. This is tightly regulated by the Bcl-2 family proteins. Cytochrome c binds to the apoptosis-activating factor 1 (Apaf1) after released into cytosol. Apaf-1 then changes from a closed to an open conformation and is stabilized by the binding of ATP

to the nucleotide binding domain. This causes heptamerization of Apaf-1 which binds to pro-caspase-9 through the N-terminal caspase recruitment domain (CARD), forming a wheel-like structure called apoptosome. Pro-caspase-9 is activated through conformation changes upon binding into the apoptosome. The activated caspase-9 in turn proteolytically activates caspase-3/7. The activated caspase-3/7 then cleaves a myriad of substrates (Reubold *et al.,* 2011). However, caspase-9 and caspase-3/7 activation is antagonized by endogenous inhibitor of caspases (IAPs). The IAPs themselves are antagonized by the Smac/DIABLO and Omi/HtrA2 released from the mitochondria. Smac/DIABLO binds to IAPs via IAP-binding motif, and promote their auto-ubiquitination for degradation (Berthelet & Dubrez, 2013).

2.4.1.3 BCL2 family of apoptosis regulator

The release of cytochrome c from the mitochondria is modulated by the ratio of pro- and anti-apoptotic proteins of the Bcl-2 family (Hengartner, 2000). Inappropriate expression of Bcl-2 family members has been implicated in oncogenesis (Korsmeyer, 1995). Generally, all members consist of at least one of four conserved motifs known as Bcl-2 homolog domains (BH1, BH2, BH3 and BH4). It consists of three distinct subgroups: (i) pro-apoptotic members (Bak and Bax) lack the N-terminal BH4 domain, (ii) antiapoptotic members (Bcl-xL and Bcl-2) contain all four BH domains and (iii) pro-apoptotic members that share homology only at the BH3 domain (BH3-only proteins) such as Bad, Bik and Bim (Deng *et al.*, 2007).

(a) Pro-apoptotic BCL2 family members

Bax is found as a monomeric protein in the cytosols or loosely bound to the mitochondrial surface or endoplasmic reticulum in normal cells. Low expresssion of Bax is often found in colorectal cancer due to the frameshift mutation in (G)8 tract of Bax gene (Katkoori *et al.*, 2010). After exposure of cells to apoptotic stimuli, Bax

undergoes conformational change to exposure its C-terminal hydrophobic domain, which enable Bax to integrate into the mitochondrial outer membrane. Bax then oligomerizes to form a channel, resulting in the permeablization of the outer mitochondrial membrane. At the same time, Bak proteins which normally resides in the outer mitochondrial membrane also undergoes a conformation change that results in its deeper insertion in the outer mitochondrial membrane, forming larger pores (Hengartner, 2000; Tzifi *et al.*, 2012). Alternatively, studies have suggested that Bax/Bak can induce the opening of permeability transition pore (PTP) by interacting with mitochondrial voltage dependent anion channel (VDAC) (Javadov & Karmazyn, 2007). The opening of PTP results in the loss of mitochondria membrane potential, swelling of the mitochondria matrix and rupture of the outer mitochondria membrane. This eventually leads to the release of cytochrome c and other apoptogenic factors (Kroemer, 2003; Sugiyama *et al.*, 2002). In addition, Bcl-2 family proteins can directly regulate the activation of caspases by binding to adaptor molecules such BAR, the endoplasmic reticulum-localized protein (Bap31) and Aven (Hengartner, 2000).

(b) Anti-apoptotic BCL2 family members

In cancer cells, the amount of anti-apoptotic proteins have been found to be greater compared to pro-apoptotic proteins (Tamm *et al.*, 2001). Anti-apoptotic Bcl-2 proteins such as Bcl-2 and Bcl-xL can bind with pro-apoptotic proteins of the Bcl-2 family and thus antagonising them (Tamm *et al.*, 2001). Therefore, they prevent permeabilization of the mitochondrial outer membrane and maintain the mitochondria membrane potential by inhibiting pore formation, resulting in the prevention of the release of different apoptosis-activating molecules such as cytochrome c and Smac/DIABLO (Harris & Thompson, 2000; Jain *et al.*, 2013)

2.5.1.4 Extrinsic or death receptor pathway

The death receptor pathway is mainly initiated by the ligation of cell-surface death receptors with their cognate ligands as shown in Figure 2.7 (Fulda & Debatin, 2006). Death receptors are cell surface receptors which belong to members of the tumor necrosis factor (TNF) family that consist of more than 20 proteins and are involved in a broade range of functions, including regulation of cell survival and death, differentiation, and immune response (Fulda & Debatin, 2006).

The death receptor consists of an extracellular region containing varying numbers of cystein-rich domains (CRDs) that allow them to recognize and bind with their ligands with great specificity. It contains a cytoplasmic death domain (DD) consisting of about 80 amino acids that are responsible for transmitting the death signal from the cell's surface to intracellular signaling pathways (Fulda & Debatin, 2006; Zeestraten *et al.*, 2013). The most extensive studied death receptors are TNF-receptor 1 (TNF-R1/p55/CD 120a), TNF-related apoptosis-inducing ligand receptor 1 (TRAIL-R1/DR 4), receptor 2 (TRAIL-R2/DR5/APO-2/KILLER) and Fas (CD95/APO-1) (Guicciardi & Gores, 2009).

The binding of receptors with their specific ligands causes receptor trimerization. It occurs via recruiting the adaptor proteins through their complementary death domains (DDs). Examples of adaptor proteins are TNF receptor-associated death domain protein (TRADD) and FAS-associated death domain protein (FADD). Pro-caspase-8 or -10 then binds to adaptor proteins through its complementary death effector domains (DEDs), to form intracellular death-inducing signaling complex (DISC). DISC provokes autoproteolytic activation pro-caspase-8/-10 which then cleaves and activates executioner caspases (caspase-3, -6 and -7) (Barnhart *et al.*, 2003).

Activation of caspase-8/10 at the DISC can be inhibited by cellular FLICE-like inhibitory protein (c-FLIP) (Guicciardi & Gores, 2009). There are two splice variants of FLIP: a long form (c-$FLIP_L$) and a short form (c-$FLIP_S$). c-$FLIP_L$ shows a strong structurally similarity to caspase-8 which contains two DEDs and a catalytically inactive caspase-like domain. However, it lacks the amino acid residues for its catalytic activity, especially the cysteine of the catalytic center. c-$FLIP_L$ compete with pro-caspase-8 to bind to the FADD in the DISC formation process (Krueger *et al.*, 2001) Thus they block the activation of caspase-8 which in turn inhibits the activation of apoptosis triggered by death receptors. cFLP_L is upregulated by activation of nuclear factor-kappaB (NF-κB) (Safa, 2012). High level of c-FLIP has been found in various tumor cells and has been correlated with resistance to chemotherapy-induced apoptosis (Fulda & Debatin, 2006).

A link between the extrinsic and intrinsic pathways is created via caspase 8-mediated cleavage of Bid. Truncated Bid (tBid) translocates to the mitochondria, where it activates Bax and Bak, causing permeabilization of the outer mitochondria membrane. This causes the release of cytochrome c and Smac/DIABLO from mitochondria, and subsequent activation of the caspase-3. This mechanism creates an amplication loop to accelerate apoptosis in death receptor apoptosis pathway (Watson, 2004; Yin, 2000)

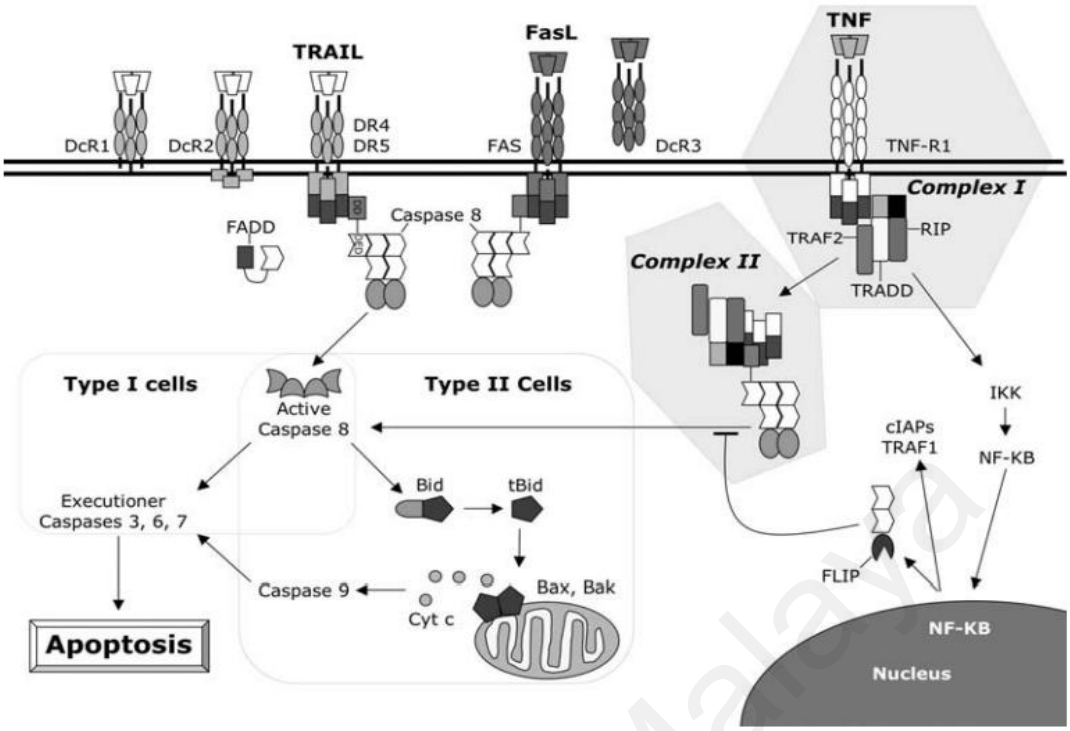

Figure 2.7: The extrinsic pathway of apoptosis

(Retrieved from Ricci & Deiry, 2007)

2.5.1.5 Endoplasmic reticulum stress pathway

Targeting endoplasmic reticulum (ER) stress signaling pathways in cancer has received a great deal of attention. Manipulation of this pathway can lead to apoptotic cell death and increase the sensitivity of tumor towards chemotherapeutic agents (Selimovic *et al.*, 2011). ER plays an essential role in the proper folding and post-translational modification of secreted and membrane proteins, maintenance of calcium homeostasis and lipid biosynthesis (Jin *et al.*, 2014). Accumulation of unfolded proteins and a severe calcium depletion within the ER can lead to ER stress (Mekahli *et al.*, 2011). Cancer cells grow under ER stress due their dysregulation of protein synthesis and nutrient deprivation. They overcome the ER stress by triggering an adaptive response called unfolded protein response (UPR) in order to reduce the load of unfolded protein and restore the ER function (Clarke *et al.*, 2014).

As shown in Figure 2.8, this response is mediated through three ER trans-membrane receptors: protein kinase RNA (PKR)-like ER kinase (PERK), inositol requiring enzyme 1 (IRE1) and activating transcription factor 6 (ATF6). Under normal conditions, all these ER stress receptors remain inactive through binding with the ER chaperone, GRP78/Bip. Under ER stress, GRP78 dissociates from these receptors, leading to their activation and initiation of UPR (Tabas & Ron, 2011).

If ER stress persists or is aggravated, it can cause the switching from pro-survival to pro-apoptosis response via the intrinsic or extrinsic-mediated pathways to eliminate damaged cells (Jin *et al.*, 2014; McGuckin *et al.*, 2010). This apoptotic pathway is mainly mediated by the transcription factor CHOP/GADD153 (Tabas & Ron, 2011). CHOP has been found to up-regulate pro-apoptotic proteins such as Bim, Puma, Bax, and DR5, and down-regulate Bcl-2 (Nishitoh, 2012). ER stress can also cause oxidative stress by enhancing ROS generation in the mitochondria through the induction of cytoplasmic calcium released from the ER (Tabas & Ron, 2011). Interestingly, CHOP can induce the expression of ERO1α which activates the calcium release channel IP3R1 to release the stored calcium in ER (Nishitoh, 2012), and suppress the expression of antioxidant genes (Tabas & Ron, 2011).

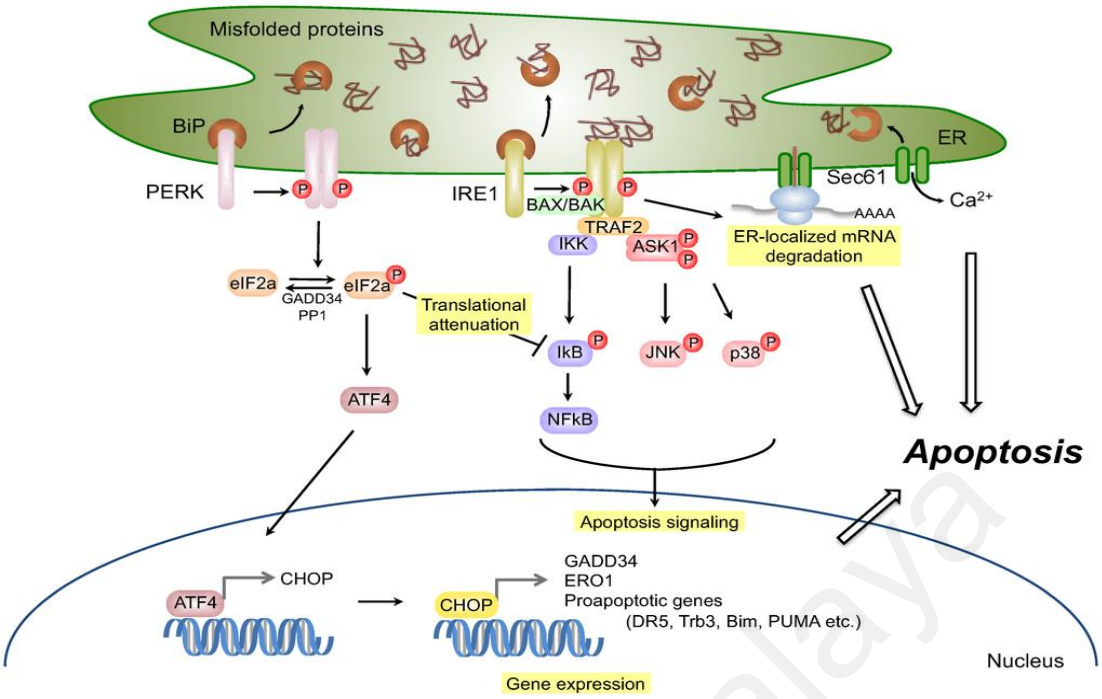

Figure 2.8: A schematic diagram of the role of the ER stress-CHOP pathway

(Retrieved from Kadowaki & Nishitoh, 2013)

2.4.2 Oxidative stress and cancer

Persistent oxidative stress is known to initiate apoptotic cascades in cancer cells. Oxidative stress arises due to disturbance between pro-oxidant generation and antioxidant protection which can lead to damage of organelles and macromolecules (Reuter *et al.*, 2010). ROS are mainly formed as byproducts of the respiratory chain through the mitochondria and are catalyzed by NADPH oxidases or xanthine oxidase (Liu & Wang, 2015). It is well-known that a moderate increase in ROS can stimulate cell growth and proliferation. However, excessive ROS accumulation causes cellular injury resulting in damage to DNA, protein and lipid membrane (Hu *et al.*, 2005). ROS generation is counterbalanced by the action of antioxidant enzymes. The imbalance between the level of ROS and the endogenous antioxidants can result in oxidative stress which can cause apoptosis in cells (Wang & Yi, 2008).

Superoxide dismutase (SOD) is a key antioxidant enzyme which protects cells against oxidative stress. The mitochondrial manganese-containing SOD (Mn-SOD) and cytosolic copper/zinc-containing SOD (Cu/Zn-SOD) are two main enzymes responsible for catalyzing the conversion of superoxide anions ($O_2^{\bullet -}$) into hydrogen peroxide, which is then eliminated by glutathione peroxidase and catalase (Kuninaka *et al.*, 2000). Previous studies have shown that higher Mn-SOD activity was found in colorectal cancer and was associated with a relatively poor survival of the patients (Janssen *et al.*, 1998). Thus therapies that can affect the SOD activity and increase ROS generation in colon cancer could aid in the elimination of cancer cells or improved therapeutic intervention.

2.4.3 Cell cycle and cancer

Deregulation of the cell cycle contributes to the uncontrolled proliferation in human cancers. Inhibiting the signaling pathways that regulate cell cycle progression may lead to cytostatic and even apoptotic effects in cancer cells (Lin *et al.*, 2008). The cell cycle can be divided into four in which the periods of DNA synthesis (S phase) and mitosis (M phase) are separated by gaps called G_1 and G_2 (Han *et al.*, 2012). G_0 phase refers to as quiescent phase where the cells remain non-proliferating for a few days or up to years, or enter the cell cycle when stimulated by specific growth factors (Figure 2.9).

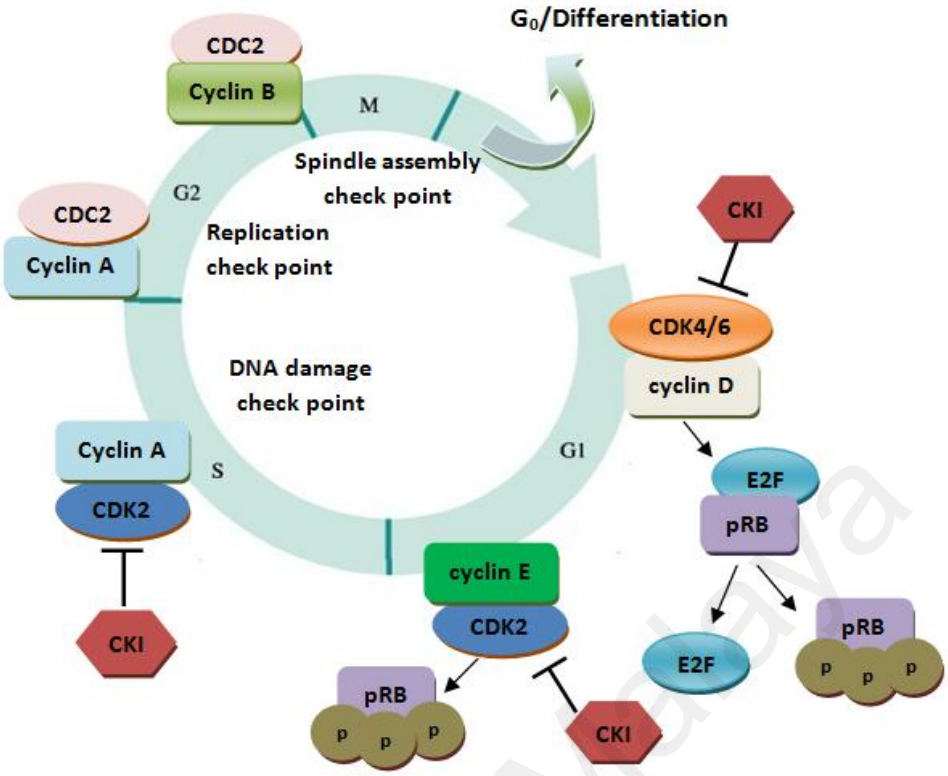

Figure 2.9: A schematic diagram of cell cycle in mammalian cells

The entry of cells from one phase to another is regulated by a family of cyclin-dependent kinases (CDKs) through binding with their respective regulatory subunits (cyclins), which then trigger different downstream processes of the cycle by phosphorylating appropriate target proteins (Vermeulen *et al.*, 2003). The activity of CDK-cyclin complex is, in turn, inhibited by binding to CDK inhibitors (CKIs) or degradation of cyclins (Vermeulen *et al.*, 2003). The endogenous CDK inhibitors consist two families: INK4 family ($p15^{INK4b}$, $p16^{INK4a}$, $p18^{INK4a}$ and $p19^{ARF}$) which bind to the CDKs of CDK4/6-cyclin D complex whereas Kip/Cip family ($p21^{CIP}$,$p27^{KIP}$ and $p57^{KIP2}$) binds to the cyclins of CDK2/cyclin A or E complex (Donjerkovic & Scott, 2000).

The G_1/S transition is a key point in the cell cycle at which cells no longer require growth factor stimuli for subsequent progression once the cycle has passed this phase. The key step in the G_1/S-phase of the cell cycle involves the phosphorylation of the

retinoblastoma protein (pRb) by CDK4/cyclin D or CDK6/cyclin D. This causes the release of bound transcriptional factor E2F from pRb and the free E2F is allowed to enter the nucleus to initiate the transcription of genes such as cyclins that are essential for progression to the S-phase. During the late G_1 phase, CDK2/cyclin E complex phosphorylate several substrates including pRb. $p27^{KIP1}$ is normally bound to CDK2/cyclin E complex and delays its activity. Throughout the S phase, CDK2/cyclin complex is activated which leads to DNA replication. In order to progress to mitosis, CDC2 must be activated by binding with cyclin A or cyclin B (Pietenpol & Stewart, 2002). Figure 2.8 shows the schematic diagram of the cell cycle in mammalian cells.

Defects in a number of cell cycle regulators have resulted in unrestrained proliferation in human cancers, even without being stimulated by mitogenic signals. Approximately 90% of human cancers have abnormalities in some component of the retinoblastoma pathway and this may include inappropriate activation of CDKs/cyclins, down-regulation of endogenous CKIs or mutation/deletion in the Rb gene itself. Ths may lead to the deregulation of S-phase progression and loss of G_1 checkpoint function (Giacinti & Giordano, 2006).

The loss of cell cycle checkpoint frequently occurs in human cancers. The p53 is a tumor suppressor protein and a key player in the G1/S checkpoint, and is the most frequently mutated protein in human cancers. Upon DNA damage or other stresses, p53 arrests the cell cycle in G_1 by inducing $p21^{CIP1}$ until the damage is repaired. If repair is not possible, apoptosis is initiated by inducing various pro-apoptotic factors (PUMA, Bax, NOXA) or entering an irreversible G_0 phase (senescence) (Pietenpol & Stewart, 2002).

In addition, the cell cycle checkpoints are also tightly controlled by the SCF (SKP1/CUL1/F-box protein complex) or APC/C ubiquitin ligases that promote the ubiquitination of key checkpoint effectors, leading them to proteasomal degradation. Deregulation of the proteolytic system has been found in cancers and contribute to its uncontrolled proliferation. For example, up-regulation of SKP2 (another component of SCF) was observed in many cancers and this resulted in the increased degradation of $p27^{KIP1}$ (Zheng *et al.*, 2016).

2.4.4 Extracellular regulated protein kinases 1/2 (ERK1/2)

Mitogen-activated protein kinase (MAPK) superfamily contains three major kinases: extracellular regulated protein kinases 1/2 (ERK1/2), c-Jun N-terminal kinase (JNK) and p38 signals. These kinases are known to relay, amplify and integrate signals from a diverse range of stimuli in controlling cellular proliferation, differentiation, development, inflammatory responses and apoptosis (Zhang & Liu, 2002).

ERK1/2 signaling pathway plays an important role in colorectal oncogenesis (Fang & Richardson, 2005). ERK1/2 is the downstream component of many growth factor receptors, particularly EGFR. Upon activation of the receptors, membrane-bound GTP-loaded Ras recruits and activates one of the Raf kinases. Raf phosphorylates two serine residues on MEK1/2 which in turn activate ERK1/2. Activated ERK1/2 translocates to the nucleus where it regulates the activities of transcription factors by phosphorylation. The Ras/Raf/MEK/ERK signaling pathway is affected by Ras and BRAF mutation, and up-regulation of EGF receptor and ligands (Roberts & Der, 2007).

Studies have found that the most critical factors of cell fate are determined by the duration of ERK activation and its subcellular localization. A short duration of ERK activation favours cell proliferation while prolonged activation causes cell death via activation of apoptosis, autophagy and senescence. ERK activity is associated with

DNA damage and increased ROS generation (Cagnol & Chambard, 2010). Dangi et al (2006) reported that over-activation of ERK causes the cell cycle arrest through induction of $p21^{CIP1}$ (Dangi *et al.*, 2006). Chemotherapeutic drugs such as doxorubicin, cisplatin and carboplatin have been found to induce an prolonged activation of ERK which is required for triggering apoptosis in cancer cells (Park *et al.*, 2012; Singh *et al.*, 2007; Wang *et al.*, 2000). However, it is still not clear how does the activation regulate the cell death of cancer.

2.5.5 AKT/PI3K signaling pathway

Akt (also known as protein kinase B) belongs to a family of serine/threonine kinases which acts a critical downstream mediator of phosphoinositide 3-kinase (PI3K) signaling pathway (Itoh *et al.*, 2002). Activated Akt has been shown to promote tumor progression and growth in human carcinoma including colorectal, breast, pancreas and lung through promotion of cell cycle progression and inhibition of apoptosis (Itoh *et al.*, 2002). ERK pathway is often co-activated with Akt signaling pathway (Lee *et al.*, 2006). It has been recognized as potential prognostic marker and molecular target for cancer therapy (Baba *et al.*, 2011).

Akt is activated by the phosphorylation on two residues at Thr308 by pyruvate dehydrogenase kinase (PDK1) and Ser473 by PDK2. Hyperactivation of Akt in cancers often resulted in the loss of tumor suppressor protein PTEN, mutation of PIK3CA and KRAS, and overexpression of tyrosine kinase receptors (RTKs) (Danielsen *et al.*, 2015). The downstream signaling effects of PI3K/Akt are involved in the inhibition of apoptosis and activation of survival pathways. Akt inhibits apoptosis through phosphorylation of bad, bax and caspase-9. It also inhibits p53-mediated apoptosis by phosphorylating MDM2 and FoxOs (Cardone *et al.*, 1998; Duronio, 2008). Akt promotes cell growth and survival by indirectly activating the NF-κB through the

phosphorylation of I-κB kinase, and activation of mTOR pathway (Hahn-Windgassen *et al.*, 2005; Ozes *et al.*, 1999). Akt regulates the cell cycle machinery by directly inhibiting the activity of $p21^{CIP1}$ and $p27^{KIP1}$ via phosphorylation. It also stabilizes the cyclin D1 by phosphorylating GSK-3β (Zhang *et al.*, 2011).

2.6 Proteomics

The human genome project (HGP) was started two decades ago and has successfully completed the large-scale sequencing of human genome. The project has provided us an overview of genes involving in human diseases. However, there is still an incomplete understanding of the function of some of the genes due to the lack of experimental evidence at the protein level (Legrain *et al.*, 2011).

It has been estimated that there is approximately 100,000 RNA transcripts (alternative splicing) or the equivalent of about 40,000 genes may give rise to approximately 10^6 proteins (including post-translational modifications) (Tunon *et al.*, 2010). Proteins reflect the true status of cells as they are implicated in almost all biological functions of the cells from the catalysis of biochemical reactions within the intermediary metabolism to the processing and integration of internal and external signals. Proteins are dynamic and are constantly undergo turnover. Certain proteins may function within a multiprotein complex (Schmidt *et al.*, 2014).

The term 'Proteome' was first introduced in 1995 and was defined as the total protein complement of a genome (Wasinger *et al.*, 1995). Proteomic is the study and characterization of a complete set of proteins present in a cell, organ, or organism at a given time (Graves & Haystead, 2002). In general, proteomic approaches have been used for (a) proteome profiling, (b) comparison and analysis of differential protein abundance between two or more samples such as healthy and disease states (c) the localization and identification of posttranslational modifications of proteins, and (d) the

study of protein-protein interactions (Chandramouli & Qian, 2009; Dominguez *et al.*, 2007). Proteomics is considered to bridge the gap between genomic information and biologic function and disease phenotypes (Jimenez & Verheul, 2014). Understanding the interactions among the proteins within the cells, and their post-translational modifications and localization may hold the key to know on how the biological systems in response to abnormal physiological conditions or drug treatments (Rao *et al.*, 2014)

2.6.1 Methodology overview: 2D gel electrophoresis

Proteomics is a multi-step methodology which generally requires the four basic steps as shown in Figure 2.10: (i) extraction of proteins from cells, tissues or biofluids, with sequential purification or fractionation steps in some cases, (ii) the separations of proteins, (iii) the imaging of the protein spots and lastly, (iv) the identification of unknown proteins which is generally conducted through mass spectrometry (MS) analysis and the use of various algorithms to identify list of candidates in libraries by in silico approach (Rabilloud & Lelong, 2011). Currently, the proteomic approaches available consist of gel-based and gel-free applications.

Since its introduction over 30 years ago (O'Farrell, 1975), two-dimensional polyacrylamide gel electrophoresis (2-D PAGE) has evolved dramatically and emerged as one of the main methods for the analysis of complex protein mixtures extracted from biological samples. The detailed descriptions are given in the section on Materials and Methods. In this technique, proteins are separated by two different physiochemical properties.

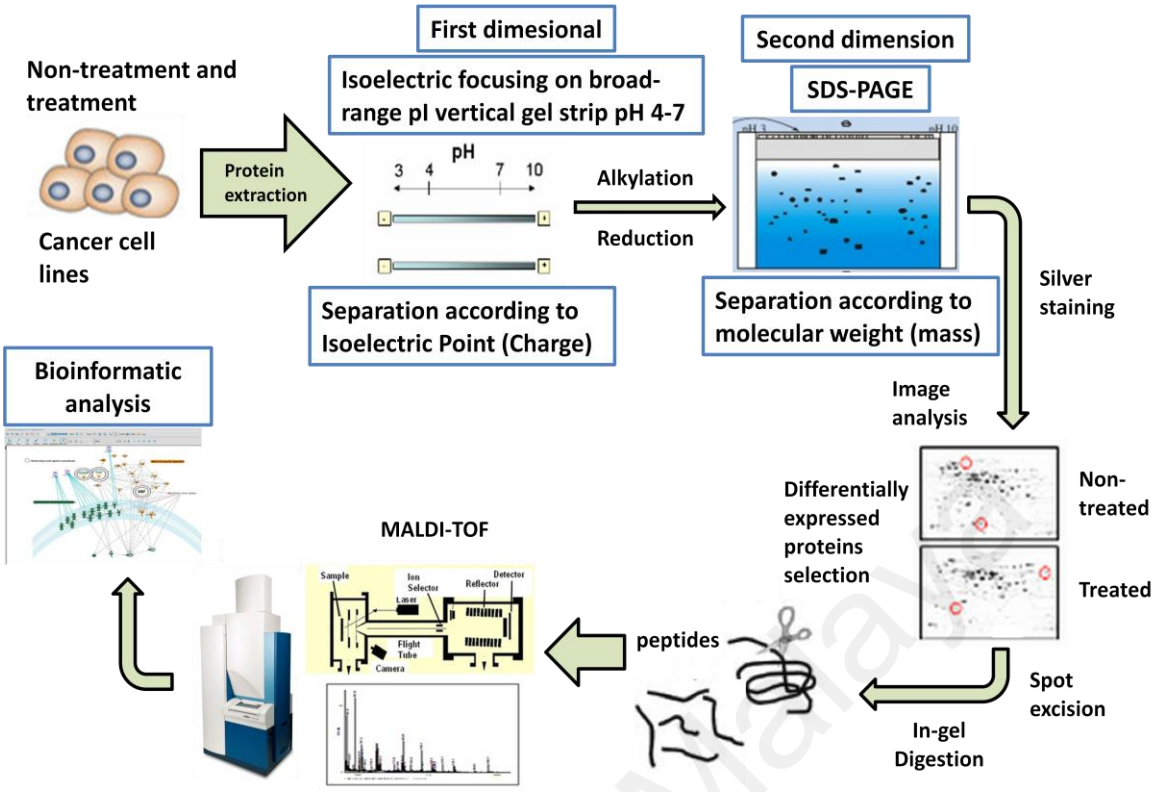

Figure 2.10: Flow chart of the characterization of candidate proteins in cell lysates via 2D electrophoresis and MALDI-TOF-MS

In the first dimension, separation is carried out on immobilized pH gradient (IPG) strips which separates the proteins based on their isoelectric point (pI) and refers to isoelectric focusing (IEF). The use of IPG strip eliminates the problem of gradient instability and enhances the reproducibility and sample loading capacity. The pI of a denatured protein is the pH at which the net charge on the protein is zero, which is determined by its amino acid composition (type and number of N- and C-terminal amino acids) and by any post-translational modifications. (Rabilloud & Lelong, 2011).

In the second dimension, proteins are separated in denaturing conditions based on their molecular weight. This is carried out by sodium dodecyl sulfate-polyacrylamide gel electrophoresis (SDS-PAGE) in a discontinuous buffer system. Before the separation, the isoelectrically focused strips must undergo two-step equilibration steps.

The equilibrium buffer containing tris-HCl (pH 8.8), glycerol, urea, DTT, IAA and SDS (Pomastowski & Buszewski, 2014).

Once the proteins have been separated on the gels, they can be visualized by various dye stainings. Silver staining of proteins on 2D gels is the most sensitive commonly used stain which offer high level of sensitivity of between 2 to 10 ng/ protein spot and spot volume linearity over a 8 to 10-fold concentration range from 0.04 ng/mm^2 to 2.0 ng/mm^2 (Cristea *et al.*, 2004). This is followed by downstream analysis involves capturing the images from stained 2D-gels and converted into digital data using scanner. The images are analyzed with image analysis software. For protein identification, the particular spots of the 2-DE gels are isolated for further processing and subjected to mass spectrometry (Aebersold & Mann, 2003).

2.6.2 MALDI-TOF/TOF and mass spectrometry (MS)

The great advances in proteomic research is mainly driven by the increase in sensitivity of MS and the availability of gene and protein sequence databases, allowing a more rapid and accurate way in identification and characterization of protein (Mesri, 2014). MS consists of three main components: (i) ion source such as matrix assisted laser desorption ionisation (MALDI) and electrospray ionization (ESI), (ii) one or several mass analyzers such as quadrupole, ion-trap, time-of-flight (TOF) and Fourier transform ion cyclotron resonance (FT-MS) analyzers, and (iii) an ion detector (Chandramouli & Qian, 2009). Basically, protein analysis by MS occurs in three major steps: Firstly, proteins are converted into gas-phase ions in vacuum by the ion sources. Secondly, the ions are accelerated in an electric field towards the high vacuum chamber of mass analyzer, which separates them according to their mass-to-charge ratio (m/z). Lastly, the m/z value and relative abundance of each ions are recorded by ion detectors (Chandramouli & Qian, 2009).

MALDI is typically coupled to TOF mass analyzer to measure the mass of intact peptides. MALDI has recently been coupled to tandem TOF-TOF or hydrid quadrupole-TOF analyzers separated by collision cell, allowing to generate fragment ion spectra (CID spectra) of MALDI-generated precursor ions as shown in Figure 2.11 (Aebersold & Mann, 2003). MALDI is based on the use of organic matrices that has a strong absorption at the laser wavelength (often a pulsed nitrogen laser at 337 nm) that able to desorb and ionize simple peptide mixtures in a relatively soft manner (Chaurand *et al.*, 1999). The ions formed are mainly protonated and carry a single charge (Croxatto *et al.*, 2012). The flight time of the ions is recorded by comparing the laser pulse time to the time of the ion reaching the detector (Kollipara *et al.*, 2011).

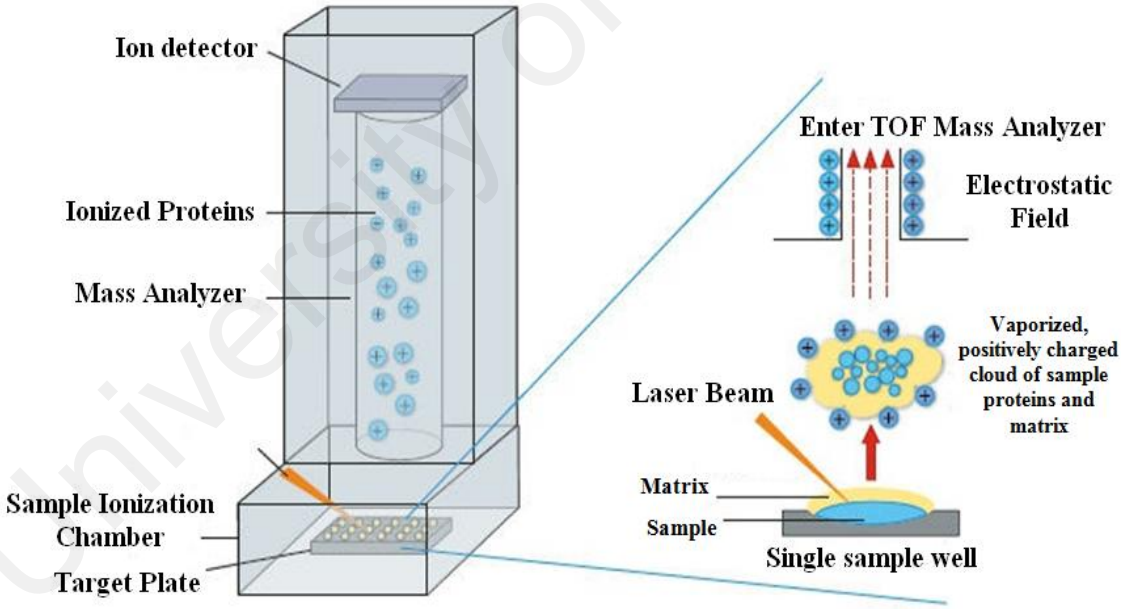

Figure 2.11: Schematic diagram of MALDI-TOF instrument.

(Retrieved from Schreiber, 2015)

2.6.3 Protein identification and bioinformatic tools

The principle behind the protein identification by MALDI-TOF/TOF-MS/MS is the use of in-gel protease digestion and tandem mass spectrometry. Based on this method, the proteins are first digested with an proteolytic enzyme with a known cleavage specificity and trypsin is the most commonly used protease that cleaves at the C-terminal side of arginine and lysine residues which generate a mixture of peptides that are unique to that protein. The masses of the resulting peptide fragments are then analyzed by MS to produce a profile of ion peaks (peptide mass fingerprint) (Barrett *et al.*, 2005). Tandem mass spectrometry (MS/MS) which employs two steps of mass analysis and separated by a fragmentation step, giving a series of peptide fragment ion for each individual peptides whose masses are measured in the second analyzer. Collision induced dissociation (CID) is the most common method of ion fragmentation where the selected parent ion undergoes fragmentation by collision with high pressurized inert gas, resulting in cleavage of the amide bond to form 'b' or 'y'-type fragment ions. The acquired MS/MS spectrum is the record of *m/z* values and intensities of the resulting fragment ions of the parent ion and is most widely used for protein identification. This fragmentation pattern provide more information about the protein structure (Han *et al.*, 2008).

The acquired MS/MS spectra are searched against a protein sequence database using database search algorithm to identify the peptides. A number of database search algorithms are available for interpretation of MS data including the widely used commercial programs, SEQUEST and Mascot (Baldwin, 2004; Barrett *et al.*, 2005). Raw mass spectrometry spectra need to be converted into generic lists of monoisotopic masses and intensity before inputted to protein identification algorithms. The identification of proteins are performed by matching a list of experimental peptide masses with theoretical peptide masses generated from the same proteolytic digested

protein sequences in databases. From this comparison, a confidence score along with the matched hits are generated. The scoring algorithm is probability-based in which protein with highest score indicates highest degree of similarity between the experimental and theoretical spectra (Aebersold & Mann, 2003).

In addition to the sequence databases, the increasing size and complexity of the experimental database lead to the development of many bioinformatic tools and databases containing biological information that describe the biological process, molecular function and cellular localization of the proteins. Several web-based algorithms such as Uniprot knowledge base (Uniprot), Ensembl and HPRD can functionoally interpret the proteins and may help to identify falsely annotated protein hits (Schmidt *et al.*, 2014). Bioinformatic tools such as STRING, Panther pathways and IPA (Ingenuity pathway analysis) has been used to predict the proteins interaction and map out the protein network based on literature mining (Laukens *et al.*, 2015).

2.6.4 Pitfalls of 2D electrophoresis and MS-based proteomics

Despite the advancements made in 2-DE, the application of 2-DE is hampered by some technical limitations. Generally, the methodology is often considered tedious, time-consuming and lacking in automation, however, it still remains an efficient way for direct separation and visualization of complex mixtures of diverse proteins and is highly reproducible (Magdeldin *et al.*, 2014). Large quantity of protein is required for the analysis and this is considered as major limitation for the detection of low abundant proteins (Patterson & Aebersold, 2003). However, higher loading capacity can be achieved by using low narrow pH-range IPG gels, pooling of multiple protein spots, sub-cellular fractionation and protein enrichment methods (Chevalier, 2010).

The other weakness of 2-DE lies in its inability to cope with highly hydrophobic proteins (especially membrane and cytoskeletal proteins) which tend to precipitate

during IEF, and those with isoelectric points at either extremes of the pH scale (Chandramouli & Qian, 2009). Different treatments and protein extraction methods such as using strong detergents and chaotropes are needed to ensure the solubilization of hydrophobic proteins to avoid their aggregation and precipitation (Fountoulakis & Takacs, 2001).

There are also problems with quantitation due to the low dynamic range of stains and incidence of comigrating proteins (Pietrogrande *et al.*, 2003). Identification of proteins by MS can be compromised by the comigration which can result in false-positive identifications and low confidence score (Gygi *et al.*, 2000). Nonetheless, commercial software such as progenesis samespot are available which allows relative quantitation of protein abundances from 2-DE gels by comparing of protein spot intensities across several gels (Berth *et al.*, 2007). Therefore, an improvement or a combination of different proteomic technologies would be necessary to identify more disease-related proteins.

2.6.5 Applications of proteomics in cancer research and drug discovery

2-DE and mass spectrometry-based proteomics have been widely used in large scale analysis of differentially abundant proteins in a broad range of diseases. The proteome is not static but undergoes dynamic changes based on the cell type and the responses to various environmental stimuli and progression of disease (Mesri, 2014). Proteomics has become important in drug design and development as proteins are the most common drug targets such as receptors, enzymes and transporters, or the signal transduction pathways in which proteins are involved (Mara & Marina, 2013).

In cancer research, the current proteomics approaches are mainly aimed at assessing the protein profiling of various types of cancers, identifying the abnormal expressed proteins in tumor tissues compared to normal tissues as well as biomarkers for

diagnostic and treatment purposes (Honda *et al.*, 2013). The balance of cell survival and death is governed by the content and functional state of the proteins through multiple mechanisms. Alterations of protein function and expression will lead to deregulation of the signaling pathways that give the survival advantage to cancer cells (Calvo *et al.*, 2005). Comparative proteomic analysis along with the availability of the bioinformatic approaches have been used to unravel the intracellular signaling pathways that underline the development of cancer as well as cancer drug resistance. This may serve as a guide for the development of novel therapeutic targets (Guo *et al.*, 2013).

In addition, many potential tumor-associated protein biomarkers have been discovered using proteomic approach especially from serum and urine (Hudler *et al.*, 2014). The biomarkers have been associated with the molecularly targeted therapy to provide basis for stratification of the patients in clinical trials and assessing the status of the cancer progression relative to diagnosis and drug treatment (Cho, 2007). Besides diseases, proteomics has been used to identify early markers in blood and other body fluids or tissues of drug induced damage and toxicity to the body organs (Merrick, 2008; Witzmann & Grant, 2003). Through an understanding of both biological mechanisms and pharmacological effects of drug, proteomics has been a useful tool to speed up the process of drug development and to make more a efficient clinical trial designs (Savino *et al.*, 2012).

2.6 *In vivo* studies for drug discovery

The current challenges of drug development from initial discovery of a promising drug candidate to final medication are the time-consuming and relatively expensive which can take 12 to 15 years and the costs exceed $1 billion, and often resulted in low success rate as some drugs turn to be ineffective or have intolerable side effects during clinical trials (Hughes *et al.*, 2011). The primary goal of drug development is to identify a molecule with desired effect in the human body without causing any side effects or secondary diseases, while to establish its quality, safety and efficacy for treating patients (Kraljevic *et al.*, 2004). Animal models have been used in pre-clinical studies and their research outcome has aided in bridging the translational gap between laboratory findings and clinical intervention (Denayer *et al.*, 2014).

Prior to progression into clinical trials in human volunteers and patients, *in vivo* study is required for validation of the activity and safety of the new compounds (Hughes *et al.*, 2011). The advancement in molecular techniques has increased the demand for *in vivo* study in drug discovery which can be either using mammalian or non-mammalian models. Mammals such as rats, mice, dogs and rabbits are classically used to evaluate the effects of new therapies before they are tested in human patients (Doke & Dhawale, 2015). Mammals are preferable for *in vivo* study as they share many common genes with humans as well as similarities in aspects of anatomy, metabolism and physiology (Bradley, 2002).

With the recognition of many biological mechanisms and protein functions that are implicated in cancer development from earlier findings and the advent of genomic technologies, alternative non-mammalians models such as using nematode worm *Caenorhabditis elegans*, zebrafish, and fruit fly *Drosophila melanogaster* have been developed and increasingly used in cancer drug discovery (Pandey & Nichols, 2011). In

addition, *in vivo* studies is essential to study the mechanisms underlying the onset of malignancies such as the use of transgenic animals which allow the evaluation of phenotypic endpoints due to the consequence of gene manipulation, however they are expensive and difficult to establish (Levitzki & Klein, 2010). Therefore, selection of a suitable and predictive animal model is important to address clinical questions.

The athymic nude mouse has been widely used by cancer researchers and drug developers. It is an immunodeficient mouse which resulted from the mutation in the FoXN1 (fork-head box N1) gene. This mutation causes congenital dysgenessis of the thymus (deficiency of T lymphocytes) and hairless skin (Zhang *et al.*, 2012). Thus this makes it a perfect host for the maintenance of human tumor xenografts without causing rejection response. Due to this reason, the nude mice xenograft model is being increasingly utilized as experimental models in cancer research for studying the efficacy of the drugs on human tumor growth *in vivo* as well as investigating the molecular mechanisms of the drugs (Kelland, 2004). It has also been used in many studies to understand the characteristics and mechanisms of tumor development and metastasis, and develop a new diagnostic method for cancer (Kelland, 2004; Sharkey & Fogh, 1984).

CHAPTER 3: MATERIALS AND METHODS

3.1 Materials

3.1.1 Drugs and reagents

Flavokawain C (FKC) and gymnogrammene (GMM) were obtained from the Extrasynthase (Genay, France) while cisplatin were obtained from Sigma and all compounds were dissolved in dimethyl sulfoxide (DMSO) (Sigma).

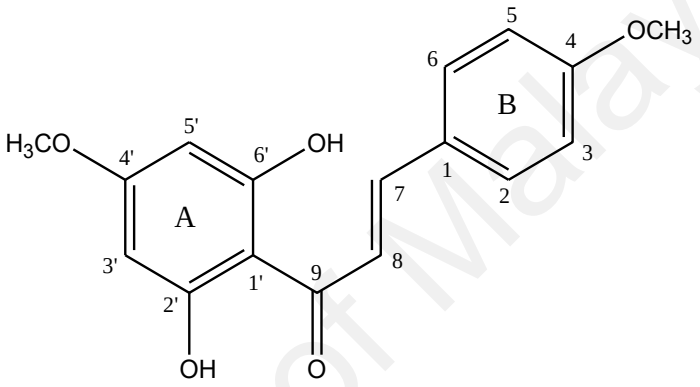

Gymnogrammene

Figure 3.1: Molecular structure GMM

3.1.2 Cell lines

The human cell lines used were the colon carcinoma cell line (HCT 116), colon adenocarcinoma cell line (HT-29), hormone-dependent breast carcinoma cell line (MCF7), lung adenocarcinoma epithelial cell line (A549), cervical carcinoma cell line (CaSki) and the non-cancer colon cell line (CCD-18Co). The cell lines were purchased from the American Tissue Culture Collection (ATCC, USA).

3.1.3 Chemicals, reagents and kits

i) Cell culture

Material	Source
RPMI, McCoy's 5A and EMEM	Sigma
Foetal Calf Serum (FBS)	Sigma
Amphotericin B (250µg/ml)	PAA Laboratories
Penicillin-Streptomycin (100µg/ml)	PAA Laboratories
Sodium pyruvate (11mg/ml)	Sigma
Non-essential amino acid (100X)	Sigma
10X Phosphate Buffered Saline (PBS)	Nacalai Tesque

ii) SRB assays

Materials	Source
Trichloroacetic acid	Sigma
Sulforhodamine B	Sigma
Acetic acid	Merck
Tris Base	Sigma

iii) Morphological analysis

Materials	Sources
Hoechst 33342	Sigma
Propidium iodide (PI)	BD Pharmingen

iv) Flow cytometry analysis

Materials	Source
Annexin V-FITC Apoptosis Detection kit	BD Pharmingen
BD MitoScreen Kit	BD Pharmingen
Apo-BrdU TUNEL assay Kit	Invitrogen
Caspase-3, -8 and -9 staining kit (CaspILLUME)	Genetex

v) Proteomics

Materials	Source
Acrylamide	Nacalai Tesque
Methylbis acrylamide	Merck
Urea	Merck
Thiourea	Merck
Dithiotheriol (DTT)	Gold Biotechnology
Iodoacetamide (IAA)	Merck
IPG buffer (pH 4 -7)	GE healthcare
CHAPS	Gold Biotechnology
85% Glycerol	Merck
Agarose	Gold Biotechnology
Sodium carbonate	Merck
Sodium thiosulphate	Merck
Sodium acetate trihydrate	Merck
Formaldehyde	Merck
Silver nitrate	Nacalai Tesque
Ammonium carbonate	Sigma
Potassium ferricyanide	Sigma
EDTA disodium salt dihydrate (Titriplex III)	Merck
Absolute ethanol	Merck
Ziptip	Merck

vi) Real-time PCR

Materials	Source
RNAqueous-4Total RNA isolation kit	Applied Biosystems
High capacity RNA to cDNA kits	Applied Biosystems
Taqman Fast Advanced Master Mix	Applied Biosystems

3.1.4 Antibodies and reagents

i) Western blot

Materials	Source
30% Acrylamide/Bis solution	Bio-rad
Mitochondrial/cytosol fractionation kit	BioVision
Bradford reagent	Bio-rad
Blocking one	Nacalai Tesque
Western Bright ECL	Advansta
Nitrocellulose membrane	Bio-rad
Tween 20	Sigma
Tris Base	Nacalai Tesque
Glycine	Merck
Sodium persulphate (SDS)	Merck
Bromophenol blue	Nacalai Tesque
Temed	Merck

i) Western blot - continued

Antibody	Supplier	Catalogue No.	Host/Clonality	Dilution
PARP-1 (cleaved p25)	GeneTex	GTX61017	Rabbit monoclonal	1:1000
DR-5	GeneTex	GTX102436	Rabbit polyclonal	1:1000
Diablo [Y12]	GeneTex	GTX161004	Rabbit monoclonal	1:1000
p53	GeneTex	GTX70214	Mouse monoclonal	1:1000
AIF	Pierce	MA5-15880	Mouse monclonal	1:1000
c-IAP1	Pierce	PA5-29085	Rabbit polyclonal	1:1000
c-IAP2	Pierce	PA5-29643	Rabbit polyclonal	1:1000
XIAP	Pierce	PA5-20067	Rabbit polyclonal	1:1000
Caspase-3	Santa Cruz	sc-277	Rabbit polyclonal	1:1000
p21	Santa Cruz	sc-817	Mouse monoclonal	1:1000
p27	Santa Cruz	sc-528	Rabbit polyclonal	1:1000
DR4	Santa Cruz	sc-65312	Mouse monoclonal	1:1000
Cdk2	Santa Cruz	sc-6248	Mouse monoclonal	1:1000
Cdk4	Santa Cruz	sc-260	Rabbit polyclonal	1:1000
Cyclin D1	Santa Cruz	sc-753	Rabbit polyclonal	1:1000
Cyclin E	Santa Cruz	sc-481	Rabbit polyclonal	1:1000
c-$FLIP_L$	Santa Cruz	sc-8346	Rabbit polyclonal	1:1000
survivin	Santa Cruz	sc-47750	Mouse monoclonal	1:1000
Bak	Santa Cruz	sc-832	Rabbit polyclonal	1:1000
Bax	Santa Cruz	sc-493	Rabbit polyclonal	1:1000
Bcl-2	Santa Cruz	sc-509	Mouse monoclonal	1:1000
Bcl-xL	Santa Cruz	sc-8392	Mouse monoclonal	1:1000
Bid	Santa Cruz	sc-11423	Rabbit polyclonal	1:1000
GAD153	Santa Cruz	sc-575	Rabbit polyclonal	1:1000
p-ERK (Thr202/Tyr204)	Santa Cruz	sc-7383	Mouse monoclonal	1:1000
ERK2	Santa Cruz	sc-153	Rabbit polyclonal	1:1000
Akt1/2/3	Santa Cruz	sc-56878	Mouse monoclonal	1:1000
p-p38 (Thr180/Tyr182)	Cell Signaling	#9216S	Mouse monoclonal	1:1000
p38	Cell Signaling	#9212S	Rabbit polyclonal	1:1000
p-JNK (Thr183/Tyr185)	Cell Signaling	#9251S	Rabbit polyclonal	1:1000
JNK	Cell Signaling	#9252	Rabbit polyclonal	1:1000
p-AKT (Ser473)	Cell Signaling	#4060S	Rabbit polyclonal	1:1000
Cytochrome c	Cell Signaling	#4280	Rabbit monoclonal	1:1000
p-pRb	Cell Signaling	#9307S	Rabbit polyclonal	1:1000
pRb	Cell Signaling	#9309	Mouse monoclonal	1:1000
Caspase-8	Cell Signaling	#9746S	Mouse monoclonal	1:1000
p-PI3K	Cell Signaling	#4228	Rabbit polyclonal	1:1000
β-actin	Cell Signaling	#3700S	Mouse monoclonal	1:2000
COX IV	Cell Signaling	#4850	Rabbit monoclonal	1:1000

* 'p-' indicates phosphorylated

i) Western blot - continued

Secondary antibody	Supplier	Catalogue No.	Dilution
Goat anti-mouse IgG-HRP	Santa Cruz	sc-2030	1:10,000
Goat anti-rabbit IgG-HRP	Santa Cruz	sc-2031	1:10,000

ii) Immunohistochemistry

Antibody	Supplier	Catalogue number	Host/Clonality
Cleaved caspase-3	Cell Signaling	#9661S	Rabbit monoclonal
Ki67	Santa Cruz	Sc-15402	Rabbit polyclonal

Materials	Source
Sodium citrate	Sigma
Citrate acid	Sigma
Peroxidase Blocking Reagent	Dako
Antibody diluent	Dako
Envision Detection System, Peroxidase/DAB+, Rabbit/Mouse kit	Dako

3.1.5 Laboratory instruments

Instruments	Sources
Class II Biosafety Carbinet	ESCO, USA
CO_2 incubator	ESCO, USA
TC10 Cell counter	Bio-Rad Laboratories, Hercules, CA, USA
Accuri C6 Flow cytometer	BD Biosciences, San Diego, CA, USA
ChemiDoc XRS Imaging System	Bio-rad, Hercules, CA, USA
Synergy H1Microplate reader	BioTek, Winooski, VT, USA

3.2 Methods

3.2.1 Cell culture

Cells were propagated using the following growth media: RPMI for MCF7, CaSki and HT-29 cell lines; McCoy's 5A for HCT 116 cell line; and EMEM for CCD-18Co cell line; and all media supplemented with 10% heat-inactivated fetal bovine serum, 1% penicillin/streptomycin, 1% amphotericin B. CCD-18Co was cultured in Eagle minimum essential medium (MEM; Sigma) and supplemented with 10% heat-inactivated FBS, 1% penicillin/Streptomycin, 1% amphotericin B, 1% non-essential amino acid, and 1% sodium pyruvate. This mixture is referred to as complete media.

Cells were routinely maintained in 25 cm^2 or 75 cm^2 tissue culture flask in a 5% CO_2 incubator (ESCO, USA) at 37˚C, and given new media every 2 to 3 days until 90% confluency. Cells were passaged when they reached 70–90% confluency and media was aspirated from the flask and cells washed twice with 5 ml PBS. Following the removal of PBS, accutase was added and the cells incubated for 5 minutes at 37˚C. Fresh complete media was added to the detached cells and the mixture centrifuged at 1000 rpm for 5 minutes. The pellet was resuspended in 1 ml fresh complete media. The viability of the cells was determined before and after treatment using the tryphan blue dye exclusion assay. To preprare cells for freezing, cells were detached as described above and the pellet resuspended in a solution containing 40% media, 50% FBS and 10% DMSO. The cells were frozen at –70˚C overnight before transferring to liquid nitrogen tank. Frozen cell stocks were stored in liquid nitrogen (–196˚C). To recover cells from freezing, aliquots were thawed rapidly, and then centrifuged at 1000 rpm for 5 minutes. The pellet was resuspended in fresh complete media and transferred into tissue culture flask.

3.2.2 *In vitro* cytotoxicity screening: Sulforhodamine B assay

The cytotoxicity assay is based on the protocol described by Houghton *et al*. (2007). This method is based on the measurement of the total protein mass of viable cells. Cells were seeded (4500 cells/well) in sterile 96-well plates in growth medium. They were incubated and cultured overnight to allow cell attachment. Following overnight incubation, the cells were treated with various concentrations of FKC or GMM (5, 10, 21, 42, 84, 166 and 333 µM) and further incubated for 24, 48 and 72 hours in 5% CO_2 incubator at 37°C. Untreated cells in 0.5% DMSO served as control. After the treatment period, the cells were fixed in 50 µl of ice-cold trichloroacetic acid (10% w/v) and incubated at 4˚C for 1 hour. The cells were then washed and stained with 50 µl of 0.4% SRB and left for 30 minutes at room temperature. They were then washed with 1% acetic acid (Merck) to remove any unbound dye and 100 µl of 10 mM Tris buffer (pH 10.5) was then added to dissolve protein-bound dye. The absorbance of dye eluted from viable cells was then measured (at 492 nm) using a microplate reader (BioTek). All experiments were performed in triplicates. Data were presented as means±SD. Trypan blue exclusion assay was used to determine the numbers of live and dead cells in each treatment. The live and dead cells were counted in a 1:1 mixture of cell suspension and 0.4% (w/v) trypan blue solution in a hemocytometer chamber using a cell counter (Bio-Rad). IC_{50} was defined as the concentration (µM) of compound which caused 50% inhibition or cell death. A final concentration of 0.5% (v/v) DMSO was used (considered to be non-toxic). The IC_{50} value for each test sample was extrapolated from the graph of the percentage inhibition versus concentration of test sample. Dose- and time-dependent studies were performed to determine suitable doses and time for induction of apoptosis in cells. The percentage of inhibition and cell viability of each of the test samples was calculated according to the following formula:

$$\% \text{ of inhibition} = \frac{OD_{control} - OD_{sample}}{OD_{control}} \times 100\%$$

$$\% \text{ cell viability} = \frac{OD_{sample}}{OD_{control}} \times 100\%$$

Where $OD_{control}$: Absorbance of negative control and OD_{sample}: Absorbance of sample

3.2.3 Morphological assessment by phase contrast and fluorescence microscopy

Cells (2.7×10^5 cells/well) cultured in 6-well plates were treated with 0.5% DMSO or FKC at concentrations equivalent to; and also two and three times higher than the IC_{50} value for 48 hours. To evaluate the changes in cellular morphology, the cells were examined using a phase contrast inverted microscope (Zeiss AxioVert A1) after 48 hours at ×40 magnification. The morphological features of apoptotic cells observed included chromatin condensation, cell-volume shrinkage, and membrane-bound apoptotic bodies (Karmakar *et al.*, 2007).

To evaluate changes in nuclear morphology induced by apoptosis, Hoechst 33342/propidium iodide (PI) double staining was used. After 48 hours incubation, cells were harvested and washed with ice-cold PBS. The cells were then suspended in Hoechst 33342 (10 µg/ml) and incubated at 37˚C in a CO_2 incubator for seven minutes. After incubation, the cells were counter-stained with propidium iodide (2.5 µg/ml) and incubated in the dark for 15 minutes. The stained cells were then mounted onto glass microscope slides and observed immediately under fluorescence microscope (Leica DM160008). The images were captured with a digital camera (Leica DFC 310 FX).The cells were then classified as follows: live cells (normal nuclei, blue chromatin with organized structure); early apoptotic cells (bright blue chromatin, which is highly condensed or fragmented); late apoptotic cells (bright pink chromatin, highly condensed or fragmented; necrotic (red, enlarged nuclei with normal structure) (Klamt & Shacter, 2005).

3.2.4 Analysis of plasma membrane alteration

Apoptotic cells were quantified by Annexin V-FITC Apoptosis Detection Kit (BD Pharmingen) using flow cytometry. FITC-conjugated Annexin V was used to measure the loss of asymmetry of phosphatidylserine on apoptotic cell membranes while propidium iodide (PI) was used to differentiate early apoptotic from late apoptotic and necrotic cells (Chen *et al.*, 2006). Briefly, cells were seeded at a density of 2.7×10^5 cells in 6-well plates for overnight and then treated with FKC in 0.5% DMSO at concentrations equivalent to; and also two and three times higher than the IC_{50} values, for 24 and 48 hours. After treatment, adherent and floating cells were harvested and washed with PBS. The cells were then incubated in 100µl of annexin V-PI labeling solution containing both annexin V-FITC (3 µl) and PI (3 µl) for 15 minutes at room temperature in the dark. After incubation, the cells were resuspended in 400µl of binding buffer before being analyzed using flow cytometer (Accuri C6) with cell counts of 10,000. The cell population were quantified in a percentage based on the four quadrants from a dot plot of FL1 (Annexin V) versus FL2 (PI): lower left (viable cells, Annexin V(-)/PI(-)), lower right (early apoptotic cells, Annexin V(+)/PI(-)), upper right (late apoptotic cells, Annexin V(+)/PI(+)) and upper left (dead cells/debris, PI(+), Annexin V(-)). The control was the well containing cells in 0.5% DMSO without FKC.

3.2.5 Analysis of changes in mitochondrial membrane potential ($\Delta\Psi_m$)

The loss of mitochondrial membrane potential was assessed using lipophilic cationic fluorochrome JC-1 (5,5',6,6'-tetrachloro-1,1',3,3'-tetraethyl benzimidazolyl carbocyanine iodide). The assay was carried out using BD MitoScreen kit as per manufacturer's protocol. Approximately 1×10^6 cells were treated with FKC in 0.5% DMSO at concentrations equivalent to; and also two and three times higher than the IC_{50} values for 24 and 48 hours. Following treatment, the cells were harvested and washed twice with PBS. The cells were then suspended in 500 µl of JC-1 working

solution and incubated at 37˚C for 30 minutes after which they were analyzed with flow cytometry (Accuri C6) where 10,000 events were recorded per analysis. In healthy cells, JC-1 accumulates as aggregates in the mitochondria and emits red fluorescence, whereas in apoptotic cells, the JC-1 remains in monomeric form in the cytoplasm and fluoresces green. The red and green fluorescence were detected at FL-2 and FL-1 channels, respectively in flow cytometer. The change in membrane potential was determined by calculating the ratio of mean fluorescence intensity between the FL1 and FL2 channels. The results were analyzed by calculating the ratio of JC-1 dimers to JC-1 monomers. A higher ratio indicated a higher membrane depolarization of mitochondria in cells. Untreated cells in 0.5% DMSO served as the control.

3.2.6 Detection of DNA fragmentation by TUNEL assay

DNA fragmentation was assessed using the TUNEL (terminal deoxynucleotidyl transferase-mediated dUTP nick end-labelling) assay kit (APO-BrdU; invitrogen), according to the instructions provided by the manufacturer. Cells were grown in 60 mm petri dishes and exposed to FKC in 0.5% DMSO at concentrations equivalent to; and also two and three times higher than their IC_{50} valuesfor 48 hours. Both detached and attached cells were harvested and fixed with 4% formaldehyde and permeabilized using 70% ethanol overnight. For detection of fragmented DNA, the cells were washed and incubated with DNA labeling solution containing TdT enzyme and Brd UTP for one hour at 37˚C. After incubation, the cells were labeled with FITC-labeled anti-BrdU antibody followed by staining with propidium iodide/RNase for 30 minutes. The cells were then analyzed using Accuri C6 flow cytometer. Untreated cells in 0.5% DMSO served as the control.

3.2.7 Assay for activation of caspase-3/8/9

Caspases are key mediators of cell death. Caspase activity assay was performed using Caspases-3,-8 and -9 Staining Kit (CaspILLUME, Genetex). Briefly, cells at a density of 1×10^6 were cultured in 60 mm petri dish. The cells were then treated with FKC in 0.5% DMSO at concentrations equivalent to; and also two and three times higher than their IC_{50} values for 48 hours. After incubation, the cells were harvested and incubated with 1 µl of *in situ* marker (FITC-DEVD-FMK for caspase-3, FITC-IETD-FMK for caspase-8 and FITC-LEHD-FMK for caspase-9) for 20 minutes in 5% CO_2 at 37˚C before being analyzed by flow cytometry (Accuri C6) and BD CFlow software. The results were analyzed by determining the percentage of activated caspase-3, -8 and -9 in comparison to the control. Untreated cells in 0.5% DMSO served as the control.

3.2.8 Cell cycle analysis

Cell cycle arrest analysis was performed using PI staining and flow cytometry. This assay is based on the measurement of the DNA content of nuclei labeled with PI. Cells (2.7×10^5 cells/well) were grown in a 6-well plate and exposed to FKC (20, 40, 60 µM for HCT 116 cells while 40, 60, 80µM for HT-29 cells). Both detached and attached cells were harvested and then pelleted by centrifugation. The cell pellets were fixed and permeabilized by suspension in 5 ml ice-cold 70% ethanol at –20˚C overnight. Following incubation, the cells were washed twice with PBS and resuspended in 500 µl of staining buffer containing 50 µg/ml propidium iodide, 100 µg/ml RNase, 0.1% sodium citrate and 0.1% Trition-X-100) and incubated in the dark at room temperature for 30 minutes. Cell cycle phase distribution was determined using Accuri C6 flow cytometer (Accuri C6) and BD CFlow software. The DNA content of at least 15,000 cells was counted per sample and the percentage of cells in various phases (G_0, G_1, S and G_2/M phases) of cell cycle was evaluated using Modfit software. Untreated cells in 0.5% DMSO served as the control.

3.2.9 Mitochondrial/cytosolic isolation and proteins extraction

Isolation of cytosolic and mitochondrial proteins was performed according to the manufacturer's instructions (BioVision). Briefly, HCT 116 cells were seeded at 2×10^6 cells per 25 mm^2 culture flask treated with or without FKC (60 µM) at 12, 24 and 48 hours. Cells were washed twice with ice-cold PBS and collected by centrifugation at 600×g for 5 minutes at 4°C. The cells were resuspended in cytosolic extraction buffer and incubated on ice for 10 minutes. After incubation, the cells were homogenized in an ice-cold dounce tissue grinder. Homogenates were centrifuged at 700×g for 10 minutes to remove unbroken cells. The supernatant was collected and centrifuged again at 10,000×g for 30 minutes at 4°C. The resulting supernatant was collected as cytosolic fraction. The pellet was then resuspended with mitochondrial extraction buffer and centrifuged at 10,000×g for 10 minutes and the supernatant was collected as the mitochondrial fraction. The protein concentrations of the fractions were measured using Bradford method (Bio-Rad Laboratories) and the fractionated protein were analyzed by western blotting.

3.2.10 Western blot analysis

Western blot analysis was used to evaluate the levels of apoptosis related proteins in HCT 116 and HT-29 cells following the indicated FKC treatment (60 µM for HCT 116 cells and 80 µM for HT-29 cells). Cells seeded at 1×10^6 cells per petri dish (60mm) treated with FKC for 6, 12, 18, 24 and 48 hours after overnight incubation. Cells were washed with cold phosphate buffer saline (PBS) and harvested. Cells were lysed in lysis buffer containing 250 mmol/L NaCl, 20 mmol/L HEPES, 2 mmol/L EDTA (pH 8.0), 0.5 mmol/L EGTA, 0.1% Triton X-100, 1.5 ug/mL aprotinin, 1.5 ug/mL leupeptin, 1 mmol/L phenylmethylsulfonylfluoride (PMSF) and 1.5 mmol/L $NaVO_4$. Lysates were then centrifuged at 13,300 rpm, 4°C for 10 minutes and the supernatants were collected. Protein concentrations were measured with Bradford method (Bio-Rad Laboratories).

Proteins were denatured by boiling for five minutes at 100˚C. Equal amounts of protein (50µg) were loaded onto a 10% or 12% SDS-PAGE gel for electrophoresis and electroblotted onto a nitrocellulose membrane (Bio-Rad) and blocked with Blocking One (Nacalai Tesque, Inc). The membranes were probed with specific primary antibodies in a blocking buffer overnight at 4°C. After blocking, the blots were washed with Tris-buffered saline containing 0.1% Tween-20 (TBST) three times to remove unbound antibody, followed by incubation with HRP-conjugated secondary antibodies (1: 10,000 dilution) for 1 hour at room temperature. Protein bands were visualized using enhanced chemiluminescence (Western Bright ECL, Advansta) and images were captured on a ChemiDoc XRS Imaging System (Bio-rad Hercules, CA, USA). The membranes were stripped and reprobed with different antibodies as necessary. β-actin was used as the internal standard for the total cell lysate and cytoplasmic fractions, whereas COX IV was used as the control for the mitochondrial fractions. Densitometric quantification of the bands was performed using ImageJ software and the results were expressed as fold change relative to the control after normalization to β-actin.

3.2.11 Reactive oxygen species (ROS) assay

Intracellular levels of ROS in cancer cells were determined using DCFH-DA. HCT 116 and HT-29 cells were seeded at a density of 7,500 cells per well in 150 µl of media in 96 well plates. After 24 hours, HCT 116 and HT-29 cells were treated with 60 µM and 80 µM of FKC, respectively and incubated for 4 hours. After the treatment with FKC, the cells were washed twice with PBS and added with HBSS (Hank's Balanced Salt Solution) containing DCFH-DA (20µM). Then cells were incubated at 37°C for 30 minutes in the dark. DCF fluorescence intensity was measured by fluorescence microplate reader (BioTek) with excitation source at 480 nm and emission at 530 nm.

3.2.12 SOD (superoxide dismutase) inhibition activity

The SOD activity was measured using SOD assay Kit-WST (Sigma) which is a colorimetric assay used for the measurement of total antioxidant capacity. HCT 116 and HT-29 cells were seeded at a density of 7,500 cells per well in 96 well plates and allowed to adhere overnight. HCT 116 and HT-29 cells were then treated with 60 and 80 µM of FKC for 4 hours. After the treatment, cells were harvested and collected by centrifugation. The cell pellets were then lysed and centrifuged at high speed (13,300 rpm for 15 minutes at 4°C). The supernatants were collected and protein concentration was determined by Bradford assay. Cell lysates (35 µg) was added to sample well and blank2 well, and 20 µl of ddH_2O (doubled distilled water) was added to blank1 and blank3 wells. WST working solution (20 µl) was added to each well and 20 µl of enzyme working solution was added to sample and blank 1 wells then mixed thoroughly. Then, the plate was incubated at 37˚C for 20 minutes. The absorbance was read at 450 nm using an Elisa microplate reader. The SOD activity was calculated according to the following equation:

$$\text{SOD activity} = [(A_{blank1} - A_{blank3}) - (A_{sample} - A_{blank2})] / (A_{blank1} - A_{blank3}) \times 100$$

where A_{blank1}, A_{blank2}, A_{blank3} and A_{sample} were the absorbances of blank1, blank2, blank3, and sample wells.

3.2.13 Two-dimensional gel electrophoresis (2-DE)

3.2.13.1 Protein extraction and quantification

For treatment, HCT 116 cells were exposed to 60 µM of FKC (Extrasynthase, France) dissolved in media containing DMSO and incubated for 48 hours before harvesting. Control cells were exposed to an equal amount of media containing only 0.5% DMSO. Cells were detached using accutase solution (Invitrogen), washed with PBS twice and harvested by centrifugation. Cell pellets were resuspended in lysis buffer (7M urea, 2M thiourea, 4% [w/v] CHAPS, 2% [v/v] pharmalytes [pH 4–7] and 40mM DTT) supplemented with protease inhibitor cocktail (Nacalai tesque) and incubated for 30 minutes in 4˚C with gentle shaking every 15 minutes. Cell lysates were centrifuged for 30 mins at 13,000×g at 4˚C and the supernatants (containing soluble proteins) were harvested. Protein concentration was determined by Bradford assay with bovine serum albumin (BSA) as standard (Bio-Rad).

3.2.13.2 First dimension: Isoelectric focusing (IEF)

A total of 150 µg of protein was solubilized in a final volume of 450 µl of urea rehydration buffer (7M urea, 2M thiourea, 2% CHAPS, 0.5% [v/v] pharmalyte [pH 4–7] and 0.002% [w/v] bromophenol blue) and loaded on 24 cm IPG strips (pH 4–7, nonlinear, GE Healthcare). Following overnight rehydration, strips were focused for 65100Vhr at 20˚C using an Ettan IPGphor 3 IEF system (GE Healthcare, Wauwatosa, WI, USA) with a maximum current of 0.05 mA per strip using the following protocol: 500V for 1 hour (linear); 500V–1000V for 7 hours (gradient); 1kV to 8kV for 4 hours (gradient); and 8kV for 5.10 hours (linear). Upon completion of IEF, the strips were stored at –80˚C until use.

3.2.13.3 Second dimension: SDS-PAGE

Focused strips were reduced for 15 minutes in sample buffer [6M urea, 75 mM tris-HCl (pH 8.8), 2% (w/v) SDS, 29.3 % (v/v) glycerol and 0.002% of 1% (w/v) bromphenol blue] containing 20 mM DTT, and alkylated for 15 minutes in sample buffer containing 12.5 mM iodoacetamide. Second-dimension separation then performed using Ettan Dalt Twelve Electrophoresis System (GE healthcare) on 12% acrylamide gels. The gels were run in running buffer [(25 mM tris-HCl, 0.1% SDS (w/v) and 192 mM glycine] at 10mA/gel for 30 minutes, followed by a 30mA/gel run until the bromophenol blue dye front was about 1.0 cm from the bottom of the gels.

3.2.13.4 Silver staining

Protein spots on 2DE gels were visualized by silver staining according to protocols from the PlusOne Silver Staining Kit (GE Healthcare). For analytical gels, the complete protocol was used. For MS protein identification, a modified protocol where glutaraldehyde was omitted from the sensitization step and formaldehyde omitted from the silver reaction step was used (Yan *et al.*, 2000). Gel images were acquired using ImageScanner III (GE Healthcare).

3.2.13.5 Image analysis

Gel image analysis was performed using Progenesis SameSpot software version 4.1 (Nonlinear Dynamics). Briefly, gel images were aligned to a reference gel selected by the program. Spot detection and background subtraction was then performed. This was followed by spot filtering to remove artefacts and missed spots. Protein spot volumes were calculated as the percentage of the total spot volumes in the gel, corresponding to pixel intensity localized within the area of each spot and divided by the sum of all spots in the gel. Spot volumes on all gels were normalized against the reference gel. One-way analysis of variance (ANOVA) followed by correction for false discovery rate (FDR)

(p<0.05) was performed to identify protein spots that have significantly changed in abundance between the samples. A protein spot is deemed to have changed in abundance when p<0.05 with a fold change of at least 2×.

3.2.13.6 In-gel tryptic digestion

Protein spots of interest were manually excised from silver-stained preparative 2DE gels. In-gel digestion was then performed using MS-grade trypsin gold (Promega). Briefly, excised spots were destained in 15 mM potassium ferricyanide in 50 mM ammonium bicarbonate solution. They were then placed in 100% acetonitrile (ACN) for 15 minutes. The destained and rehydrated gel spots were digested in trypsin solution (7 ng/ul) in 50 mM ammonium bicarbonate at 37°C for 16–18 hours. Prior to mass spectrometric analysis, the peptides were extracted, concentrated and desalted using C_{18} ZipTip (Millipore).

3.2.13.7 Protein identification by tandem mass spectrometry

Tryptic peptides (4µl) were spotted onto a clean Matrix-Assisted Laser Desorption/Ionisation (MALDI) plate and co-cyrstallized with 4 µl of α-cyano-4-hydroxycinnamic acid MALDI matrix (Sigma). Mass spectra were then acquired using a MALDI-TOF/TOF mass spectrometer (ABISCIEX TOF/TOF 5800, Applied Biosystems). After filtering trypsin, keratin-, and matrix-contaminant peaks, up to 20 precursor ions were selected for subsequent MS/MS fragmentation according to mass range, signal intensity, signal to noise ratio, and absence of neighbouring masses in the MS spectrum. Database searching was then carried out using Mascot version 2.2.07 (http://www.matrixscience.com) via Protein Pilot Software version 4.5 (ABSCIEX) combining MS and MS/MS data against Homo Sapiens (human) database from SwissProt 51.6 and NCBInr Mar12 (www.expasy.org). The parameters used were protein taxon, Homo sapiens; carbamidomethylation and methionine oxidation as

variable modifications; ion mode, [M+H]; mass values, monoisotopic. Up to 1 missed tryptic cleavage was allowed with a mass tolerance of 100 ppm and 0.2 Da. Positive identification was based on a Mascot score of above the significance level (p<0.05).

3.2.13.8 *In silico* analysis

Canonical sequences of identified proteins were used in all bioinformatics analysis. Gene symbols and abundance levels of the identified proteins were imported into the Ingenuity Pathway Analysis (IPA; Ingenuity Systems Inc., Redwood City, CA) software. The biological relationships between proteins as networks and functional pathways were then predicted using the Ingenuity Pathway Knowledge Base (IPKB). Overlapping canonical pathways from IPA that shared common proteins in the dataset were also analyzed and reported. Statistical scores were then calculated using Fischer's right tailed exact tests to calculate a *p*-value indicating the probability that each biological function assigned and the canonical pathways to that data set is not due to chance alone. We also cross referenced all identified proteins with the Human Protein Reference Database (HPRD) and Uniprot Knowledgebase (UniProtKB) to further predict possibile protein functions.

3.2.13.9 Analysis of mRNA expressions of identified proteins by reverse transcription quantitative PCR (RT-qPCR)

Total RNA was extracted from 1×10^7 HCT 116 cells using the RNAqueous-4PCR Kit (Ambion). The purity and concentration of mRNA were assessed using a NanoDrop2000 spectrophotometer (Thermo Fisher Scientific Inc., Wilmngton, DE, USA) and the integrity was examined using an Agilent 2100 Bioanalyzer (Agilent Technologies Inc., Mississauga, ON, Canada), and stored at –80°C. Total RNA (2µg) was reverse transcribed to cDNA using a high-capacity cDNA Reverse Transcription kit (Applied Biosystems). All mRNA expression analysis were performed using

StepOnePlus Real-Time PCR instrument (Applied Biosystems, Carlsba, CA, USA), according to the manufacturer's protocol using specific Taqman gene expression assays (Applied Biosystems). The PCR reactions were initiated with a 20 minutes incubation at 95°C followed by 40 cycles of 95°C for 1 seconds and 60°C for 20 seconds. Gene expression levels were analyzed using the StepOne software v2.2.2 and the ΔΔCt method was used to calculate the relative expression levels of each gene. ΔCt values were normalized against β-actin. All experiments were performed in triplicates. Table 3.1 shows the list of the gene and corresponding accession number investigating in this study. Endogenous control used in this study is β-actin.

Table 3.1: List of primers used for the quantitative real-time PCR

No.	Genes	Amplicon length
1.	HSPA1A	124
2.	HMOX1	82
3.	EEF2	121
4.	P4HB	66
5.	RAD23B	115
6.	SKP1	140
7.	ATP5H	85
8.	TCEB1	120
9.	EIF5A	142
10.	SFPQ	74
11.	EIF3I	94
12.	RANBP1	145
13.	ACTB	63

3.2.14 *In vivo* studies

3.2.14.1 Animals

Female BALB/c nude mice were purchased from BioLASCO Taiwan Co. Ltd. The mice were aged about 6 weeks at the time of the beginning of the treatment with FKC. All mice were maintained in a specific pathogen free facility supplied with high efficiency particulate air (HEPA) filters and provided with rodent chow and water *ad libitum*. All animal care and treatment were conducted in accordance with the accepted guidelines for the use and care of laboratory animals established by the Animal Experimental Unit (AEU) in the Faculty of Medicine, University of Malaya. All procedures were performed in accordance with the protocol approved by the Faculty of Medicine Institutional Animal Care and Use Committee (FOM IACUC) (Reference number: 2013-06-07/ISB/R/PCW).

3.2.14.2 Tumor implantation and drug administration

HCT 116 cells were harvested from sub-confluent cultures by overlaying the monolayer with a solution of accutase in CO_2 incubator. Cells were then washed twice and resuspended in PBS. The number of detached cells was adjusted to achieve a final concentration of 6×10^6 cells in 0.1 ml PBS. Cell viability was determined by trypan blue dye exclusion and only suspensions consisting of single cells with cell viability greater than 95% were used for tumor implantation in nude mice. Before tumor inoculation, all mice were anaesthetized with ketamine (80 mg/kg) and xylazine (10 mg/kg). HCT 116 cells (6×10^6 in 0.1 ml PBS) were inoculated subcutaneously into the lower right flank of each mouse. Treatment started once the tumors reached a volume of 75–150 mm^3, the mice were randomly divided into control and treatment groups (n =5). The mice were divided into three groups as shown below. The control group was given intraperitoneal injection (i.p.) of vehicle solution (0.9% saline containing 4% DMSO and 5% Tween 80) while treatment group mice were given i.p. of 1 mg/kg and 3 mg/kg of FKC thrice

weekly. Cisplatin was used as standard with the same concentration used for FKC but once a week for the same duration of treatment.

(G1) with colon cancer and no treatment with FKC (vehicle control)

(G2) with colon cancer and given i.p. of 1 mg/kg of FKC

(G3) with colon cancer and given i.p. of 3 mg/kg of FKC

(G4) with colon cancer and given i.p. of 3 mg/kg of cisplatin (positive control)

Doses have been based on previous studies by Lin *et al* (2012) showing activity at these concentrations of a structurally similar compound (flavokawain B). The solutions were filtered through 0.22 µm before administering to the mice. Body weight and tumor sizes of each mouse were recorded and measured (average of three measurements per week throughout the experiment). After 19 days of treatment, the mice were sacrificed and tumor and organs were excised and weighed. The mouse organs include the heart, spleen, liver, lungs and kidneys were collected and examined for toxicity of the drugs. The blood sample were collected for biochemical and proteomic analysis.

3.2.14.3 Tumor volume and body weight measurement

Tumor volume was measured using vernier calipers and calculated according to the formula: $(D \times d^2)/2$, where D represents the large diameter or length of the tumor and d represent the small diameter or width (DePinto *et al.*, 2006). The anti-tumor effect of the compound was measured as the mean tumor volume inhibition (%T/C) by comparing the mean tumor volumes from the treatment group with that of the control group at a particular time point using the following formula: [1–(mean tumour volume in the treatment group/mean tumor volume in the control group) x 100] (Huang *et al.*,

2014a). The toxicity of the compound was evaluated based on body weight loss of the mice following the treatment. Other abnormal clinical observations, such as diarrhea, lethargy, ataxia, abnormal breathing, loss of appetite, decreased movement or any other apparent signs of illness were also recorded (Lin *et al.*, 2008; Nakamura *et al.*, 2000).

3.2.14.4 Toxicology studies

Briefly, the tumor, liver, kidneys, heart, lungs and spleen collected from all mice were fixed in 10% formalin in PBS for overnight. Sections of 5 µm thickness were sliced from paraffin-embedded tissues and placed on microscope slides. The slides were then stained with Hematoxylin and Eosin (H&E), and analyzed for pathological damage by light microscopy (Olympus, Tokyo, Japan) connected to a Nikon camera. Cross sections of the tumors were then prepared as described above, stained with Hematoxylin and Eosin (H&E), and were studied for presence of apoptotic and necrotic cells (Aisha *et al.*, 2012). All pathological analysis was performed by Prof. Dr. Mahmood Ameen Abdulla Hassan from Department of Biomedical Science, Faculty of Medicine, University of Malaya (Malaysia). Blood samples were taken from the mice before euthanasia. Levels of creatinine, urea nitrogen, alanine aminotransferase (ALT), alkaline phosphatase (ALP) and aspartate aminotransferase (AST) were measured using the standard automated analyzer at the Central Diagnostic Laboratory, University of Malaya Medical Center.

3.2.14.5 TUNEL assay/Detection of apoptosis

DNA fragmentation in apoptotic cells was determined by the terminal deoxynucleotidyl transferase-mediated nick end labeling (TUNEL) assay with the ApopTag in situ apoptosis detection kit (Merck). The paraffin-embedded sections were cut at 5 μm thickness and dried overnight. Sections were then deparaffinized, rehydrated, and boiled in 10 mM citrate buffer (pH 6.6) for 20 minutes in a microwave. After the slides were incubated with Peroxidase blocking reagent (Dako) for 10 minutes, they were treated with equilibration buffer (75 μl/5 cm^2) for 10 min. Incubation with terminal deoxynucleotidyl transferase (TdT) (55 μl/5 cm^2) in the presence of modified nucleotides was carried out for 1 hour at 37°C, which resulted in the labeling of DNA fragments with the digoxigenin nucleotide. The reaction was stopped by incubating with stop-wash buffer for 10 minutes. The digoxigenin nucleotide was incubated with anti-digoxigenin peroxidase for 30 minutes in humidified chamber and then developed with DAB chromogenic substrate for 5 minutes. Sections were manually counterstained with hematoxylin, dehydrated through xylene, and mounted under a glass coverslip. The sections were examined and imaged using an Olympus light microscope connected to Nikon camera. TUNEL-positive cells were identified by a brown stain over the nucleus.

3.2.14.6 Immunohistochemistry (IHC)

IHC was used to detect the expression of active apoptosis executor protein (cleaved caspase-3) and proliferation marker (Ki67). The paraffin-embedded sections cut at 5 μm thickness were mounted on positively charged silanized slides (Fisher Scientific) and dried overnight. The sections were deparaffinized in 100% xylene, dehydrated in a gradient ethanol series (100%, 95%, and 70% ethanol/water [vol/vol]), and rehydrated in PBS (pH 7.5). For antigen retrieval, the sections were boiled in a 10mM sodium citrate solution (pH 6.6) for 20 minutes, followed by a cooling period at room

temperature for 20 minutes. Endogenous peroxidase activity was blocked by peroxidase-blocking reagent (Dako) for 10 minutes and then the sections were then rinsed with phosphate-buffered saline (PBS). Primary antibodies were then applied to the sections for 45 minutes and then washed with PBS three times, followed by secondary antibodies (Envision System-HRP, Dako) for 30 minutes at room temperature. Dilutions of primary antibodies were as follows: cleaved caspase-3 (1:300) and Ki67 (1:50). Detection was carried out using Dako Real Envision Detection System, Peroxidase/DAB+, Rabbit/Mouse kit (Dako, Japan), and staining was developed by 3,3'-diaminobenzidine (DAB) substrate for 5 minutes. The sections were washed with distilled water to stop the reaction and counter-stained with hematoxylin. Slides were dehydrated, cleared with xylene and mounted with cover slips, and then examined under a light microscope (Li *et al.*, 2014). Ki67-positive cells were identified by a brown stain over the nucleus while caspase-3-positive cells were identified by a brown stain over the cytoplasm.

3.2.14.7 Serum sample collection and protein estimation

Blood samples were obtained from the mice in tubes without additive and allowed to clot at room temperature for 1 hour. Serum was separated by centrifugation at 3000 rpm for 10 minutes at 4˚C and stored at –80˚C until use. Total protein determinations were performed by the Bradford assay (BioRad laboratories).

3.2.14.8 2-DE and MALDI-TOF/TOF MS

Approximately 125 µg of protein samples was calculated and subjected for 2D-electrophoresis and MALDI TOF/TOF-MS/MS according to the protocol as described in 3.2.13 and Table 3.2.

Table 3.2: IPGphor running conditions for serum from nude mice (for sample in-gel rehydration)

Gel length	24 cm
Temperature	20˚C
Current maximum	0.05 mA per IPG strip
Voltage maximum	8,000 V
IPGs	pH 4 – 7
Sample application	In-gel loading
IPG DryStrip rehydration	16 – 18 hours
Initial IEF	500 V, 1 hour
IEF to the steady state	Gradient from 500 to 1,000 V within 7 hours Gradient from 1,000 to 8,000 V within 3 hours 8,000 V to the steady state for 7.10 hours
Total volt hours	**76588 Vhrs**

3.2.15 Statistical analysis

Data were expressed as mean ± SD of triplicates. Statistical analysis of data was performed using SPSS Statistics 17.0 and differences with a $p<0.05$ were considered significant. The following notion was used: * indicated $p<0.05$, compared with the non-treated group.

CHAPTER 4: RESULTS

4.1 Growth inhibitory effects of FKC and GMM on selected cancer cell lines and normal cell line

The cytotoxic activities of FKC on the various human cancer cell lines (HCT 116, HT-29, A549, CaSki and MCF7) and normal coloncell line (CCD-18Co). The cells were exposed to various concentrations of FKC and GMM and subjected to SRB assay. This assay estimates cytotoxicity based on the total protein content, which is proportional to the number of cells (Vichai & Kirtikara, 2006). The extent of cytotoxicity of test compounds was based on their IC_{50} values and their effectiveness compared with chemotherapeutic drugs (cisplatin). IC_{50} value was defined as the concentration of drug that inhibited cell growth by 50%.

As shown in Table 4.1 and Figure 4.1, cell viability was reduced in the cancer cell lines tested in comparison with the control in a dose-dependent manner and HCT 116 cells was found to be most sensitive towards FKC (compared to other cancer cell lines) with an IC_{50}value of 12.75±0.17 µM. A comparison of the growth inhibitory effects of FKC against a chemotherapeutic drug, cisplatin is shown in Table 4.1. The IC_{50} of FKC was found to be comparable to cisplatin (IC_{50} 13.12±1.24 µM) in HCT 116 cells. In the case of normal colon cells, FKC exhibited moderate cytotoxic effect against CCD-18Co cells which was less toxic compared to cisplatin, indicating a possible cytotoxic selectively towards colon cancer cells. In addition, a structurally related compound, gymnogrammene (GMM) was also evaluated for its cytotoxic activity against human cancer cell lines. GMM exhibited no cytotoxic activity against all other tested cell lines. Figure 4.2 shows that FKC decreased the growth of HCT 116 and HT-29 cells in a time-dependent manner at 20, 40 and 60 µM for HCT 116 cells and 40, 60 and 80 µM for HT-29 cells. Growth was found to be arrested after treatment with 60µM of FKC in

HCT 116 while in HT-29 cells was 60 and 80 µM. The results show that FKC can suppress HCT 116 and HT-29 cells growth in a dose- and time-dependent manner. In the study, HCT 116 cells were selected and subjected for further investigation on the potential underlying mechanism(s) of cell death induced by FKC.

Table 4.1: Cytotoxic activities of FKC and GMM on various cancer cell lines and human normal cell line (CCD-18Co) for 72 hours treatment in comparison to cisplatin.

Cell lines	IC_{50} in µM		
	FKC	GMM	Cisplatin
HCT 116	12.75 ± 0.17	> 300	13.12 ± 1.24
HT-29	39.00 ± 0.37	> 300	34.35 ± 1.57
MCF-7	47.63 ± 5.93	> 300	> 300
A549	40.28 ± 2.11	> 300	19.47 ± 4.37
CaSki	39.88 ± 0.45	> 300	124.05 ± 3.08
CCD-18Co	160.86 ± 2.45	> 300	108.90 ± 2.91

The IC_{50} value indicates a concentration of compounds which caused 50% reduction in cell viability based on SRB assay. Cisplatin was used as standard. Each value is expressed as mean±SD of three replicates of three independent experiments.

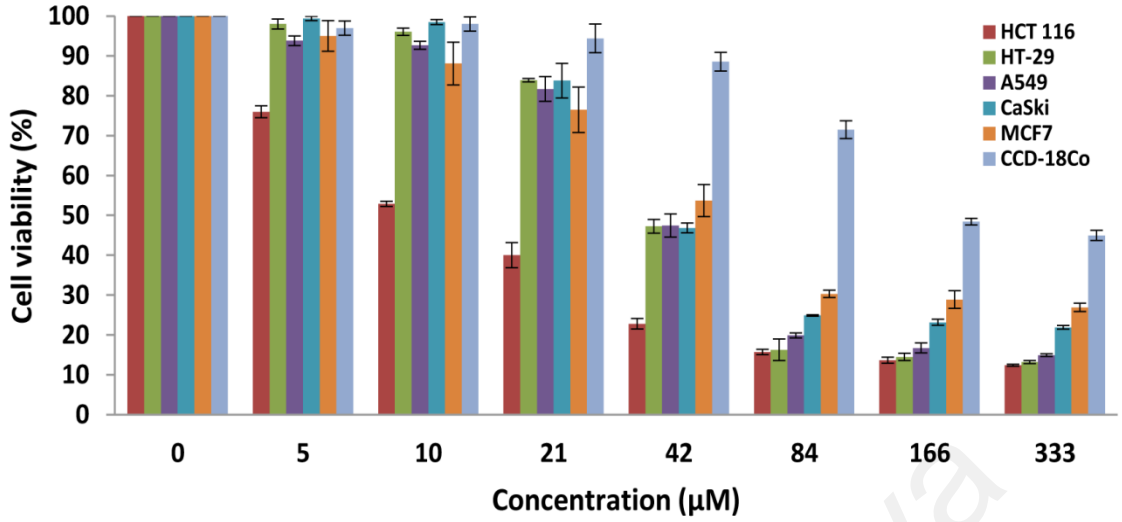

Figure 4.1: Effect of FKC on cell viability on the selected human cancer cell lines and normal colon cells. Each cell lines were seeded at 4.5×10^3 cells per well in 96-well plates. After 24 hours, the cells were treated with various concentration of FKC (5–333µM) for 72 hours, and the results were expressed as inhibition of proliferation which was determined by SRB assay as described in Materials and Methods. In comparison to control, the inhibition of cell proliferation was increased in dose-dependent manner. All data shown are the mean±standard deviation (SD) of triplicates obtained from three independent experiments. Cell viability in FKC-treated cells was expressed as a percentage of viable cells compared to control cells.

A.

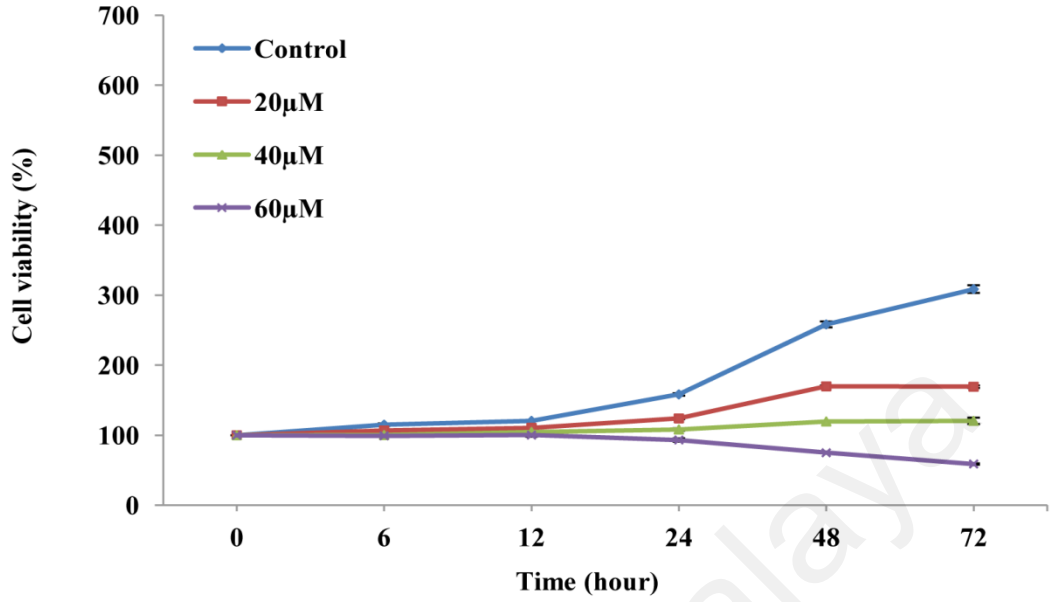

B.

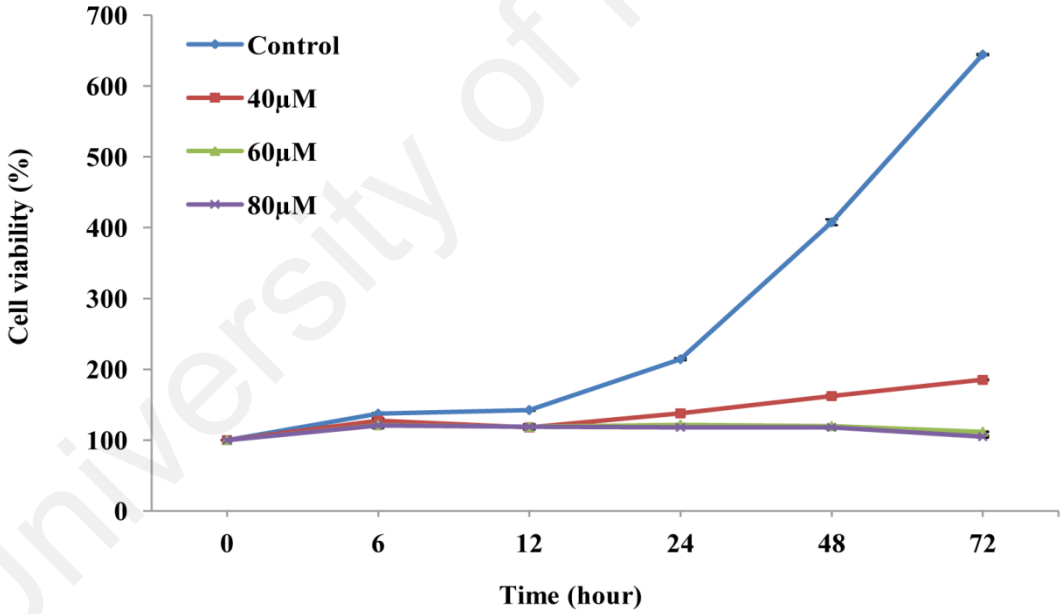

Figure 4.2: Inhibition of cell proliferation and viability by FKC in human cancer cell lines. (A) and (B) HCT 116 cells (4.5×10^3 cells/well) and HT-29 (6×10^3 cells/well) were seeded in a 96-well for overnight and then treated with FKC (20, 40 and 60 µM for HCT 116 cells while 40, 60 and 80 µM for HT-29 cells) at increasing time points (6, 12, 24, 48 and 72 hours). All data shown are the mean±standard deviation (SD) of triplicates obtained from three independent experiments. Cell viability in FKC-treated cells was expressed as a percentage of viable cells compared to control cells.

4.2 Cellular and nuclear morphological studies of HCT 116 and HT-29 cells upon FKC treatment

To determine whether the cytotoxic effect of FKC was associated with the induction of apoptosis, morphological changes of cells were evaluated using phase-contrast microscopy. As shown in Figures 4.3 and 4.4, control cells observed under phase-contrast microscopy were in tightly packed groups and retained the typical epithelial morphology. After treatment of HCT 116 and HT-29 cells with FKC at various concentrations for 48 hours, it was observed that cell numbers were reduced and the cells were shrunken. The cells also displayed fewer cell to cell interactions, vacuolation in the cytoplasm, membrane blebbing, nuclear disintegration and formation of apoptotic bodies.

In order to distinguish between live, early or late apoptotic and necrotic cells, cells treated with FKC were evaluated by double staining with Hoechst 33342 and propidium iodide (PI) to examine the changes in nuclear morphology in HCT 116 and HT-29 cells. Untreated cells showed dull blue colour indicating healthy and viable cells. After treatment for 48 hours, a population of cells showed bright blue and pink fluorescence with condensed or fragmented nuclei was observed indicating the presence of early and late apoptotic cells, respectively in both cell lines. In addition, it was observed that some cells were undergoing necrosis-like cell death after being treated with 60 µM of FKC for 48 hours (red coloured) in HCT 116 cells. The results obtained thus far indicated that the cytotoxic effect of FKC on HCT 116 and HT-29 cells was associated with induction of apoptosis. Further experiments were necessary to validate the initial observation.

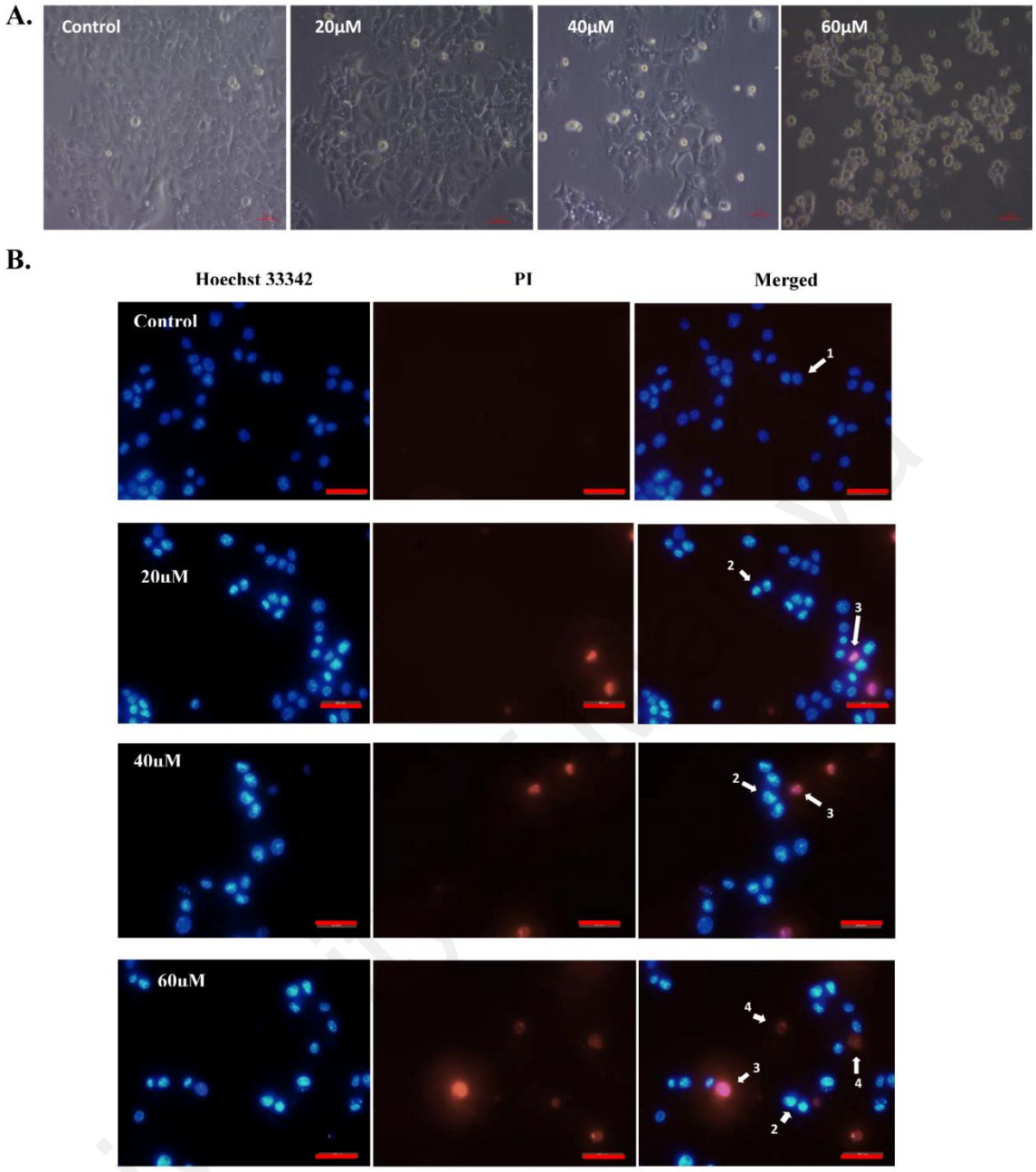

Figure 4.3: Cellular and nuclear morphological changes in HCT 116 cells upon FKC treatment. HCT 116 cells were treated with FKC at the indicated concentrations for 48 hours, and subsequently observed under an inverted phase contrast microscope at magnification of ×40. (A) Control cells showing normal morphology (well spread and normal nuclei structure) while treated cells showing the typical morphological features of apoptosis include cell shrinkage, condensed or fragmented nuclei, membrane blebbing, increased vacuolation formation and formation of apoptotic bodies. (B) Representative fluorescence microscopy images of HCT 116 and HT-29 cells stained with Hoechst 34222 and PI after treated without or with the indicated concentrations of FKC for 48 hours and visualized using fluorescence microscope at magnification of ×40 (Red scale bar=50μm). Arrows labelled with the following number and letter indicates: (1) viable cells with normal nuclei; (2) early apoptotic cells with highly condensed chromatin or fragmented chromatin (b); (3) late apoptotic cells with highly condensed chromatin or fragmented chromatin; (4) dead cells/necrosis. Untreated cells in 0.5% DMSO served as the control.

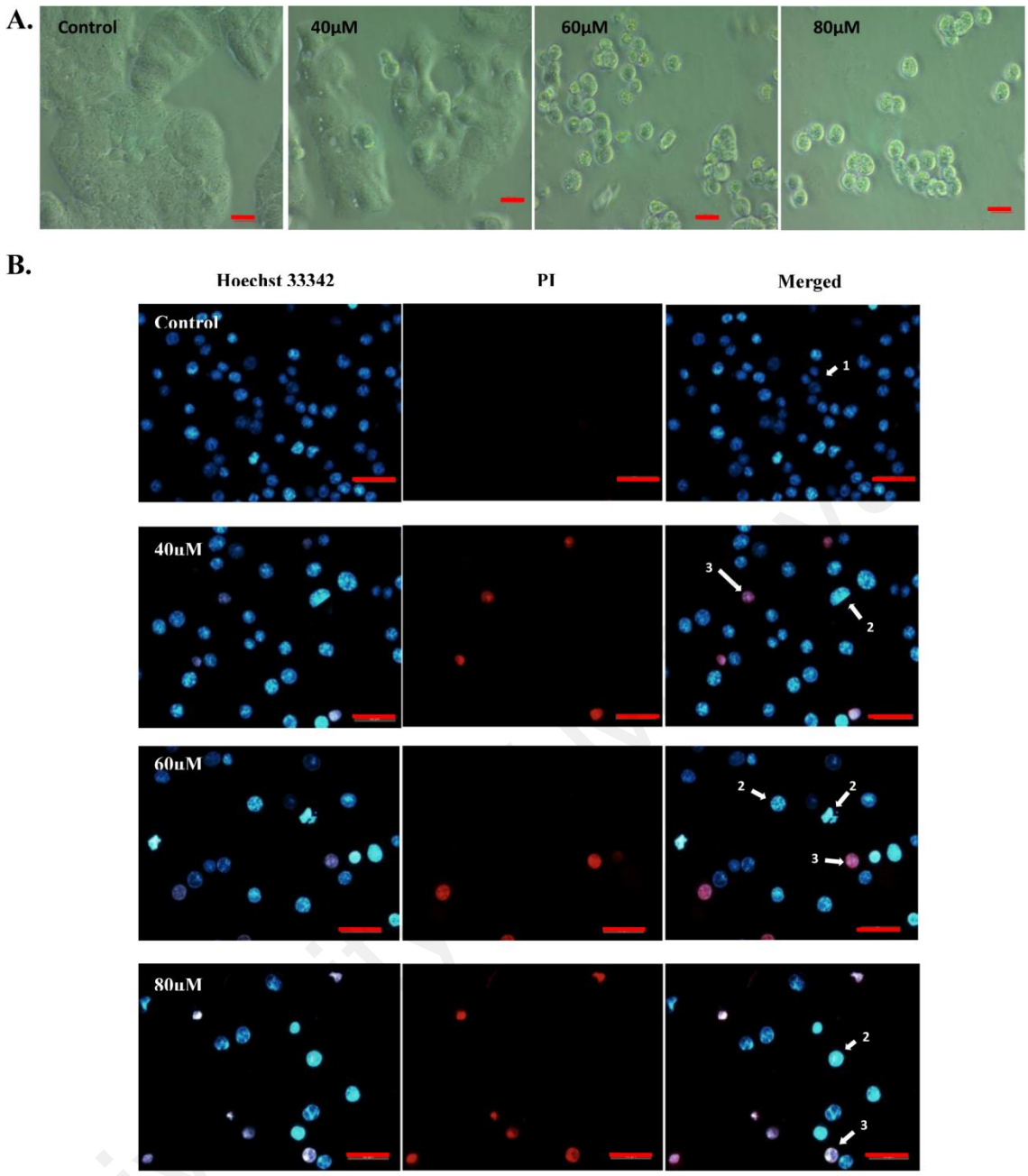

Figure 4.4: Cellular and nuclear morphological changes in HT-29 cells upon FKC treatment. HT-29 cells were treated with FKC at the indicated concentrations for 48 hours, and subsequently observed under an inverted phase contrast microscope at magnification of ×40. (A) Control cells showing normal morphology (well spread and normal nuclei structure) while treated cells showing the typical morphological features of apoptosis include cell shrinkage, condensed or fragmented nuclei, membrane blebbing, increased vacuolation formation and formation of apoptotic bodies. (B) Representative fluorescence microscopy images of HCT 116 and HT-29 cells stained with Hoechst 34222 and PI after treated without or with the indicated concentrations of FKC for 48 hours and visualized using fluorescence microscope at magnification of ×40 (red scale bar=50µm). Arrows labelled with the following number and letter indicates: (1) viable cells with normal nuclei; (2) early apoptotic cells with highly condensed chromatin or fragmented chromatin (b); (3) late apoptotic cells with highly condensed chromatin or fragmented chromatin; (4) dead cells/necrosis. Untreated cells in 0.5% DMSO served as the control.

4.3 Analysis of externalization of phosphatidylserine (PS) in HCT 116 and HT-29 cells upon FKC treatment

To further characterize the apoptotic features of HCT 116 and HT-29 cells after treatment with FKC, Annexin V-PI double staining was performed. It was found that there was a significant increase ($p<0.05$) in early and late apoptotic cells after treatment with increasing concentrations of FKC and incubation times in HCT 116 and HT-29 cells when compared to control (Figures 4.5 and 4.6). After 24 hours incubation of HCT 116 and HT-29 cells with FKC, there was a higher increase in the percentage of early apoptotic cells compared to late apoptotic cells as the concentration of FKC was increased (Figures 4.5 and 4.6). Extending the incubation period to 48 hours resulted in a greater increase in the percentage of late apoptotic cells compared to early apoptotic cells for all concentrations of FKC.

4.4 Analysis of DNA fragmentation in HCT 116 and HT-29 cells upon FKC treatment

As shown in Figure 4.7, there was a concentration-dependent increase in the amount of apoptotic cells with fragmented DNA for both colon cancer cell lines following treatment with FKC for 48 hours. Compared to the control, there was a significant increase in the amount of TUNEL-positive cells with increasing concentrations of FKC as shown in quantitative data (Figure 4.7B). These results were consistent with the results obtained from Hoechst 33342/PI staining. This suggested that FKC caused DNA fragmentation in HCT 116 cells which may be associated with the induction of apoptosis.

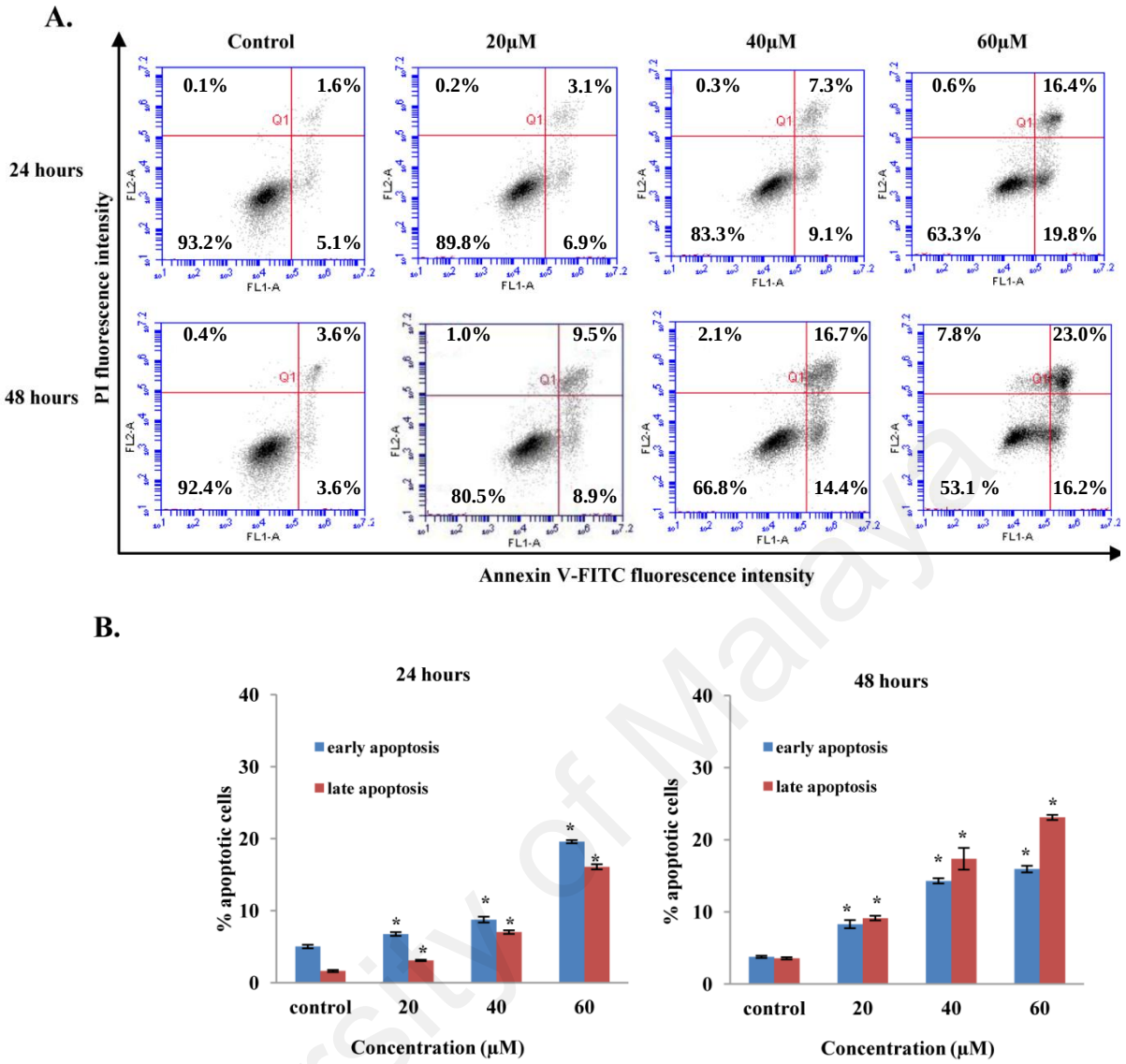

Figure 4.5: **FKC induces phosphotidylserine (PS) externalization in HCT 116 cells.** (A) HCT 116 cells were treated with increasing concentrations of FKC (20, 40 and 60 µM) for 48 hours and stained with AnnexinV-FITC and PI, followed by flow cytometric analysis. Each dot plot is the representative result of three independent experiments. Cell populations are distinguished based on the four quadrants from a dot plot: viable (bottom left), early apoptotic (bottom right), late apoptotic (top right), and dead cells/debris (top left) cells. (B) Quantification of number of early and late apoptotic cells (from total 10,000 cells) of HCT 116 cells measured by flow cytometry for 24 and 48 hours are presented as percentages in bar charts. Values given are expressed as mean±SD of triplicates obtained from three independent experiments. The asterisk (*) shows statistically significant differences in comparison to the control, $p<0.05$.Untreated cells in 0.5% DMSO served as the control.

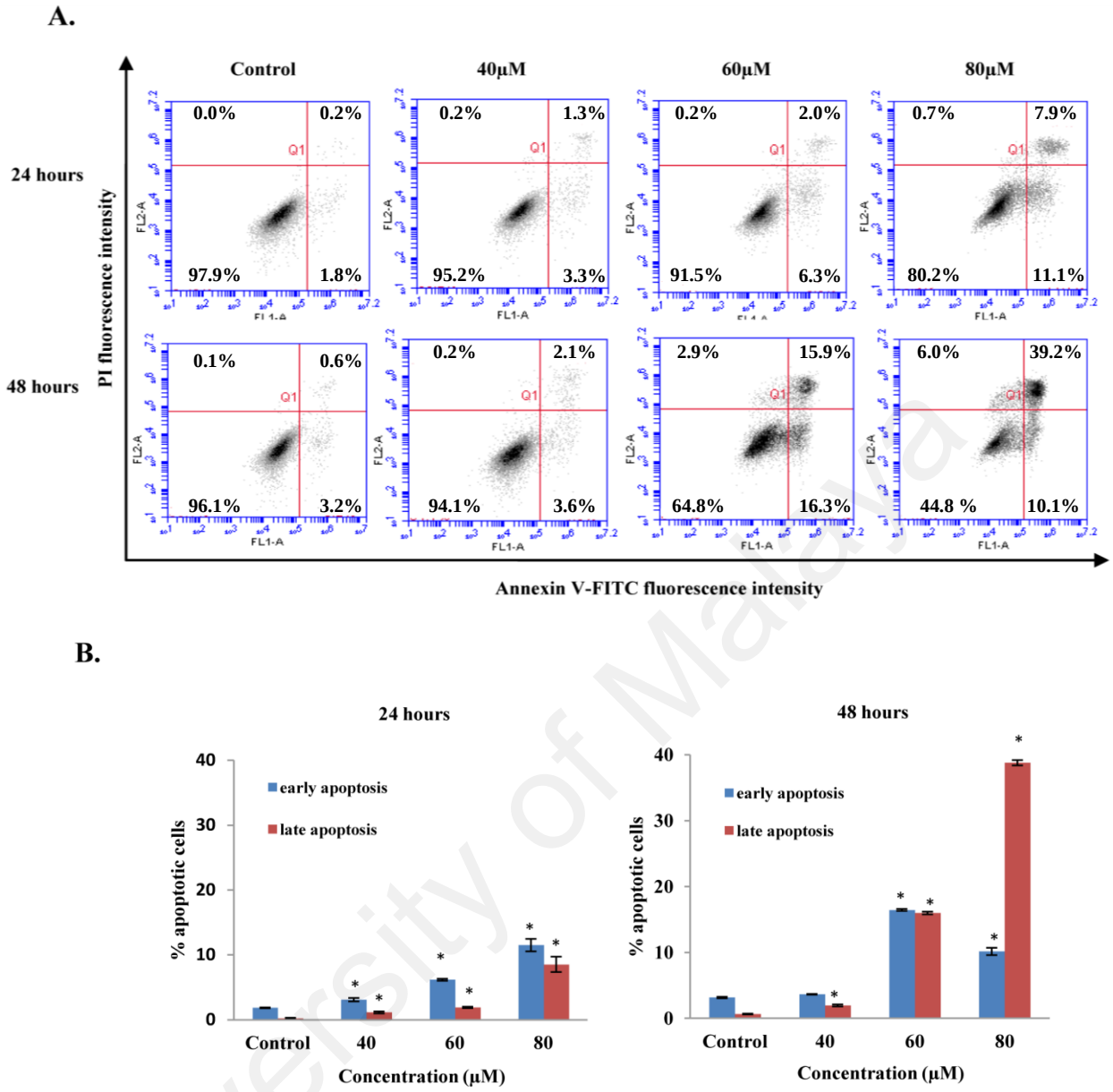

Figure 4.6: **FKC induces phosphotidylserine (PS) externalization in HT-29 cells.** (A) HT-29 cells were treated with increasing concentrations of FKC (40, 60 and 80 µM) for 48 hours and stained with AnnexinV-FITC and PI, followed by flow cytometric analysis. Each dot plot is the representative result of three independent experiments. Cell populations are distinguished based on the four quadrants from a dot plot: viable (bottom left), early apoptotic (bottom right), late apoptotic (top right), and dead cells/debris (top left) cells. (B) Quantification of number of early and late apoptotic cells (from total 10,000 cells) of HT-29 cells measured by flow cytometry for 24 and 48 hours are presented as percentages in bar charts. Values given are expressed as mean±SD of triplicates obtained from three independent experiments. The asterisk (*) shows statistically significant differences in comparison to the control, $p<0.05$.Untreated cells in 0.5% DMSO served as the control.

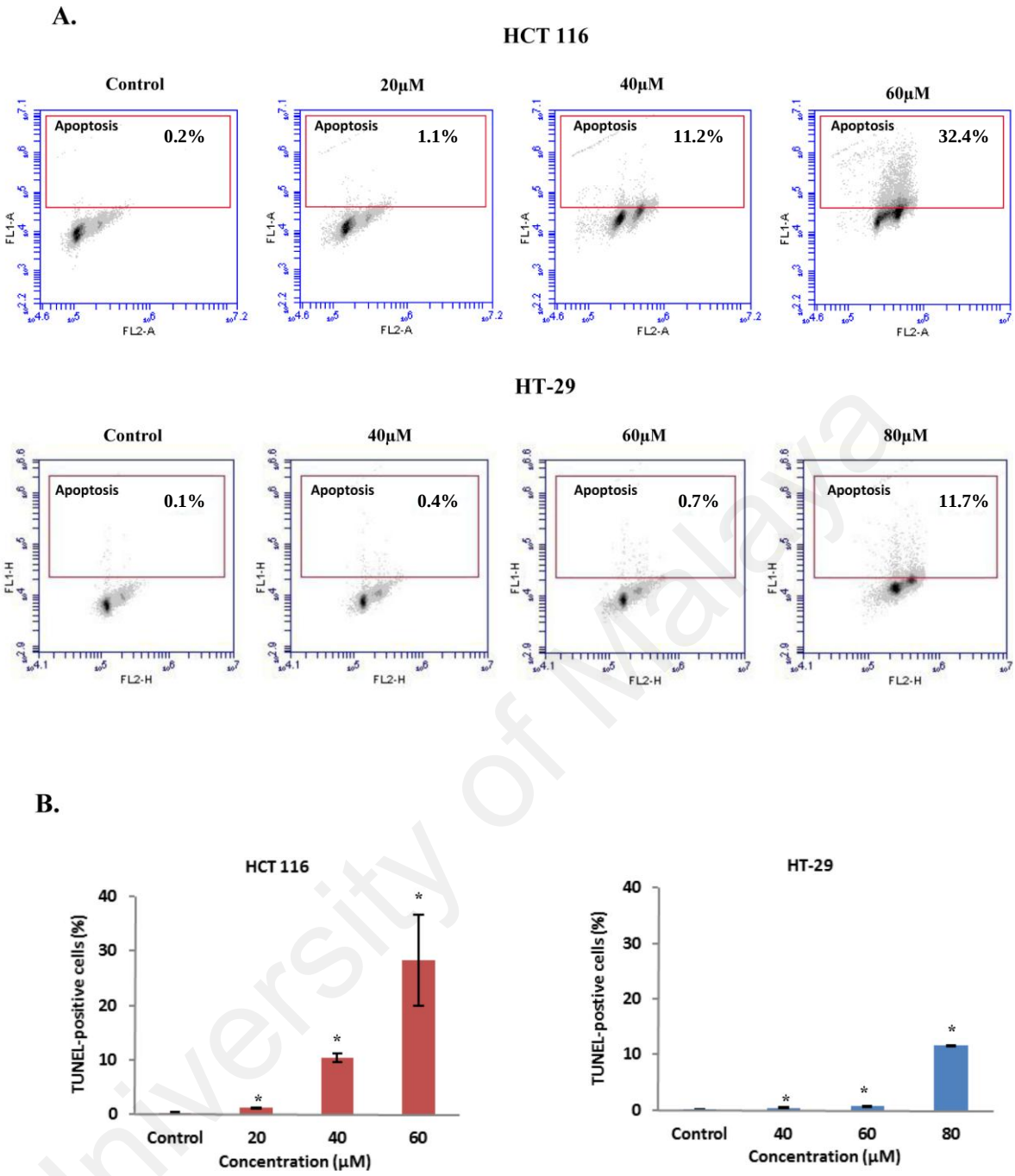

Figure 4.7: Induction of DNA fragmentation by FKC in HCT 116 and HT-29 cells. Cells were treated with absence or presence of FKC at the indicated concentrations for 48 hours, and assessed using TUNEL assay kit. (A) The percentages of cells with fragmented DNA were analyzed using flow cytometry as indicated in the upper quadrant from a dot plot. Each dot plot is the representative result of three independent experiments. (B) Percentages of HCT 116 and HT-29 cells which showed positive DNA fragmentation measured by flow cytometry are presented in bar diagram. Values given are expressed as mean±SD of triplicates obtained from three independent experiments. The asterisk (*) shows statistically significant differences in comparison to the control, $p<0.05$.Untreated cells in 0.5% DMSO served as the control.

4.5 Analysis of changes in mitochondrial membrane potential in HCT 116 and HT-29 cells

One important biochemical event in the intrinsic pathway which is indicative of early apoptosis is the sharp reduction in the mitochondrial membrane potential due to an increase in the permeability of the mitochondrial membrane, leading to the release of apoptotic factors into the cytosol (Tait & Green, 2010). To ascertain the involvement of the mitochondrial pathway in the induction of apoptosis by FKC, the effect of FKC on the mitochondrial membrane potential (MMP) in HCT 116 and HT-29 cells was assessed using a fluorescent dye, JC-1 and analyzed by flow cytometry. A shift of fluorescent emission from red to green indicates a reduction in MMP. As shown in Figure 4.8A and 4.9A, an increase in green fluorescence of JC-1 monomers was observed in HCT 116 and HT-29 cells following 24 and 48 hour of treatment with various concentrations of FKC compared to control. As shown in the quantitative data of the ratio of monomer/dimer of JC-1 (Figure 4.8B and 4.9B), there was a significant increase ($p<0.05$) in ratio in both cell lines treated with increasing concentrations of FKC for 24 and 48 hours compared to control. These findings suggested that exposure to FKC caused a significant change in mitochondrial membrane depolarisation in HCT 116 and HT-29 cells.

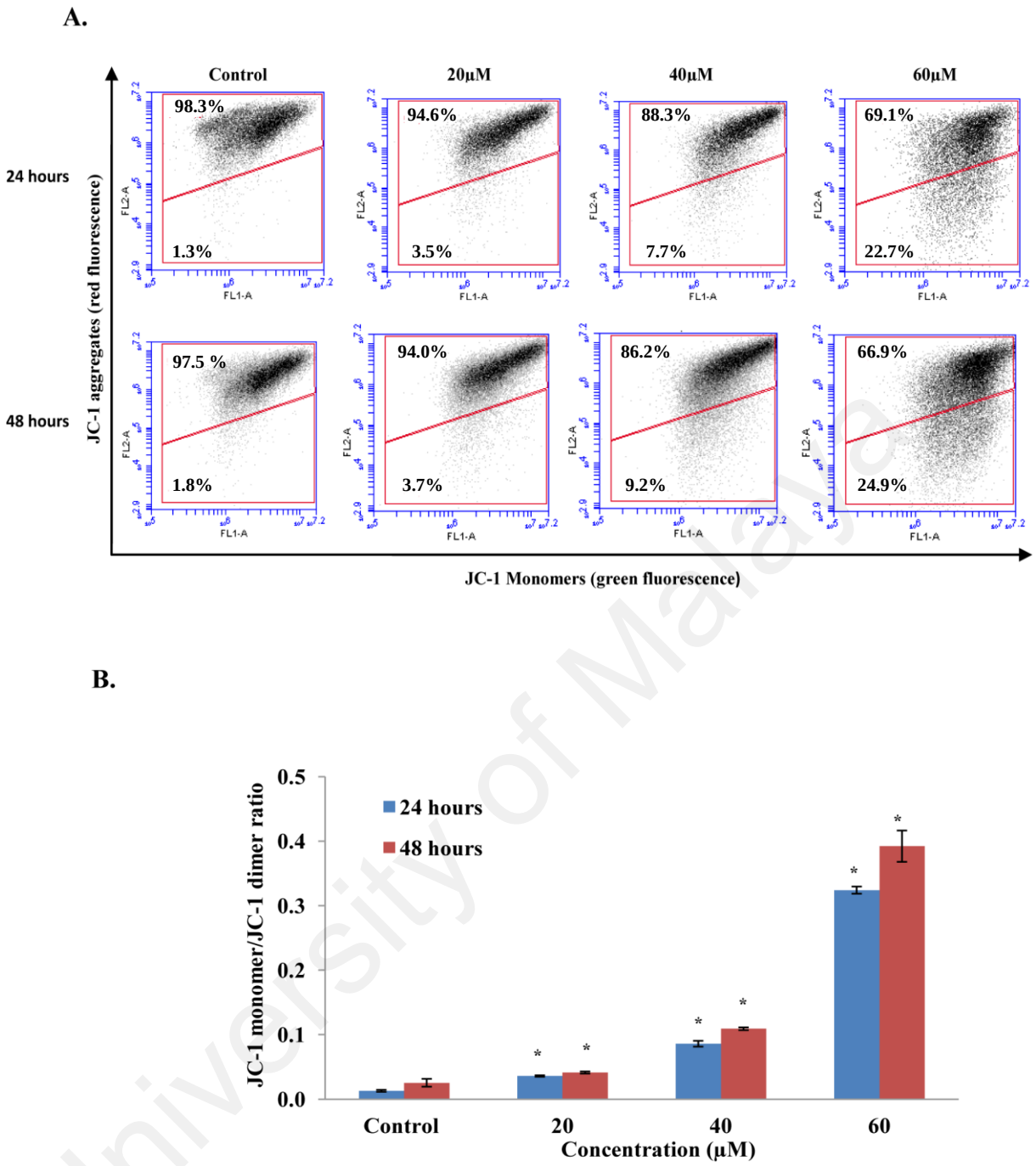

Figure 4.8: Flow cytometric analysis of mitochondrial membrane potential of HCT 116 cells upon FKC treatment using JC-1 staining. (A) Cells were treated with increasing concentrations of FKC (20, 40 and 60 µM) for 24 and 48 hours. Cells were then incubated with JC-1 probe, and then analyzed using flow cytometry. Untreated cells in 0.5% DMSO served as the control. Upper quadrant indicates percentage of cells with polarized mitochondrial membranes which emit red fluorescence whereas bottom quadrant indicates percentages of cells with depolarized mitochondrial membranes which emit green fluorescence. Each dot plot is the representative result of three independent experiments. (B) The bar charts showing the ratio of mean intensity of JC-1 red fluorescence to JC-1 green fluorescence in HCT 116 cells treated with the indicated concentrations for 24 and 48 hours. Values given are expressed as mean±SD of triplicates obtained from three independent experiments. The asterisk (*) indicated $p<0.05$ when compared to the control.

A.

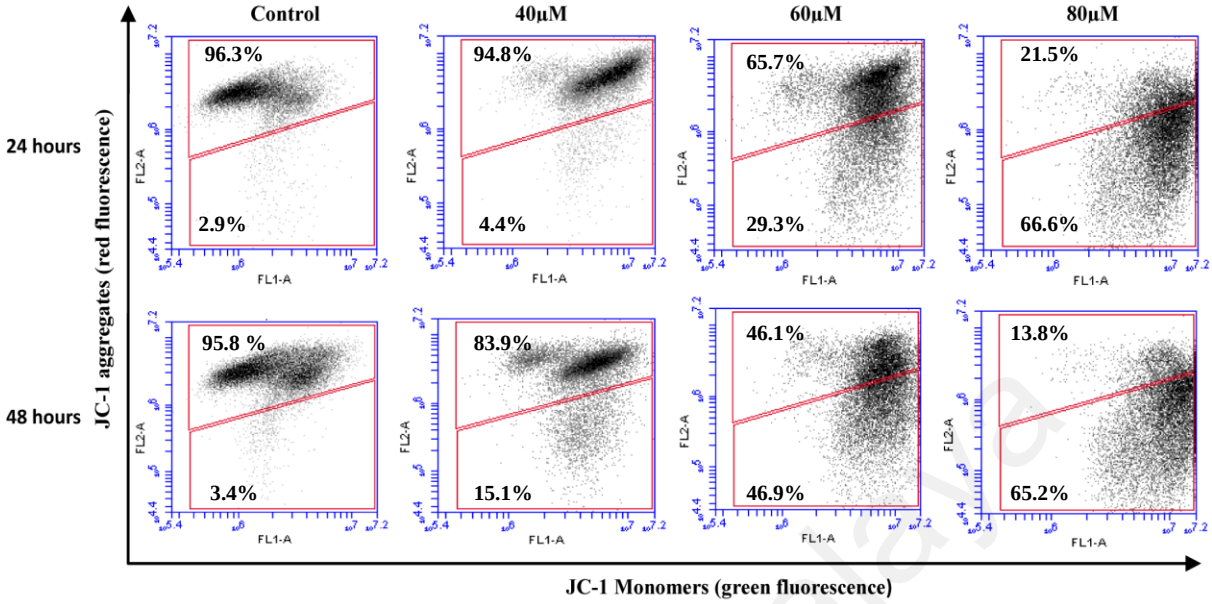

B.

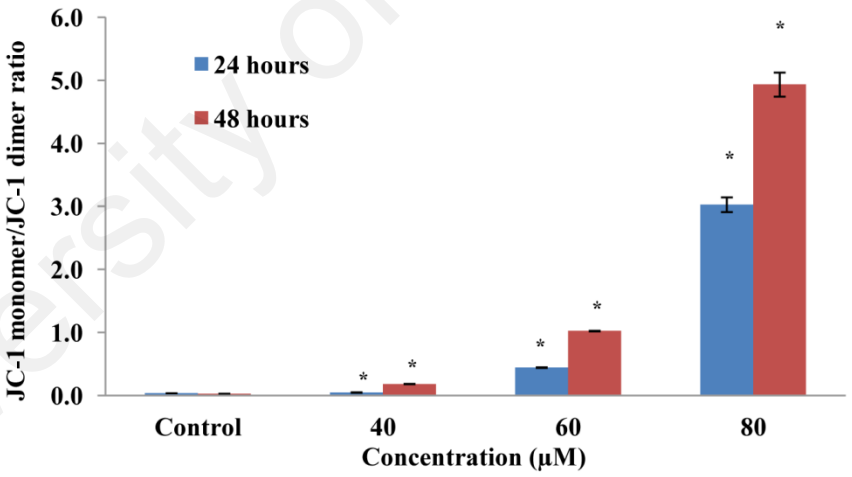

Figure 4.9: Flow cytometric analysis of mitochondrial membrane potential of HT-29 cells upon FKC treatment using JC-1 staining. (A) Cells were treated with increasing concentrations of FKC (40, 60 and 80 µM) for 24 and 48 hours. Cells were then incubated with JC-1 probe, and then analyzed using flow cytometry. Untreated cells in 0.5% DMSO served as the control. Upper quadrant indicates percentage of cells with polarized mitochondrial membranes which emit red fluorescence whereas bottom quadrant indicates percentages of cells with depolarized mitochondrial membranes which emit green fluorescence. Each dot plot is the representative result of three independent experiments. (B) The bar charts showing the ratio of mean intensity of JC-1 red fluorescence to JC-1 green fluorescence in HT-29 cells treated with the indicated concentrations for 24 and 48 hours. Values given are expressed as mean±SD of triplicates obtained from three independent experiments. The asterisk (*) indicated $p<0.05$ when compared to the control.

4.6 Analysis of induction of caspase-3, -8 and -9, and cleavage of PARP-1 in HCT 116 and HT-29 cells upon FKC treatment

To determine whether the apparent induction of apoptosis was associated with the activation of caspase-3, -8 and -9, caspase activities were examined by western blotting and flow cytometry. Through flow cytometric analysis (Figure 4.10), the percentages of activated caspase-3, -8 and -9 were found to have increased significantly in HCT 116 and HT-29 cells after treatment with increasing concentrations of FKC (20, 40 and 60 µM) in comparison to the control. Upon treatment on HCT 116 cells, active caspase-8 was found to be generally more prominent than active caspase-9, and appeared to be the major initiator caspase during the demolition phase of apoptosis. However, it was found that the FKC induced a lesser extent in caspase-3, -8 and -9 levels in HT-29 cells in comparison to HCT 116 cells.

Activation of caspase-3 was further confirmed by western blot analysis of the p25 fragment of poly-ADP-ribose polymerase (PARP) which results from the caspase-3 cleavage of the intact PARP (116 kDa) during apoptosis. Western blot analysis (Figure 4.11) showed that exposure of HCT 116 and HT-29 cells to FKC increased the level of the 25 kDa fragment of PARP as compared to the control. The increased level of cleaved PARP was shown to be correlated with increased activation of caspase-3 in HCT 116 and HT-29 cells in this study. Taken together, these results showed that FKC activated caspase-8, -9 and -3 in a dose- and time-dependent manner.

Figure 4.10

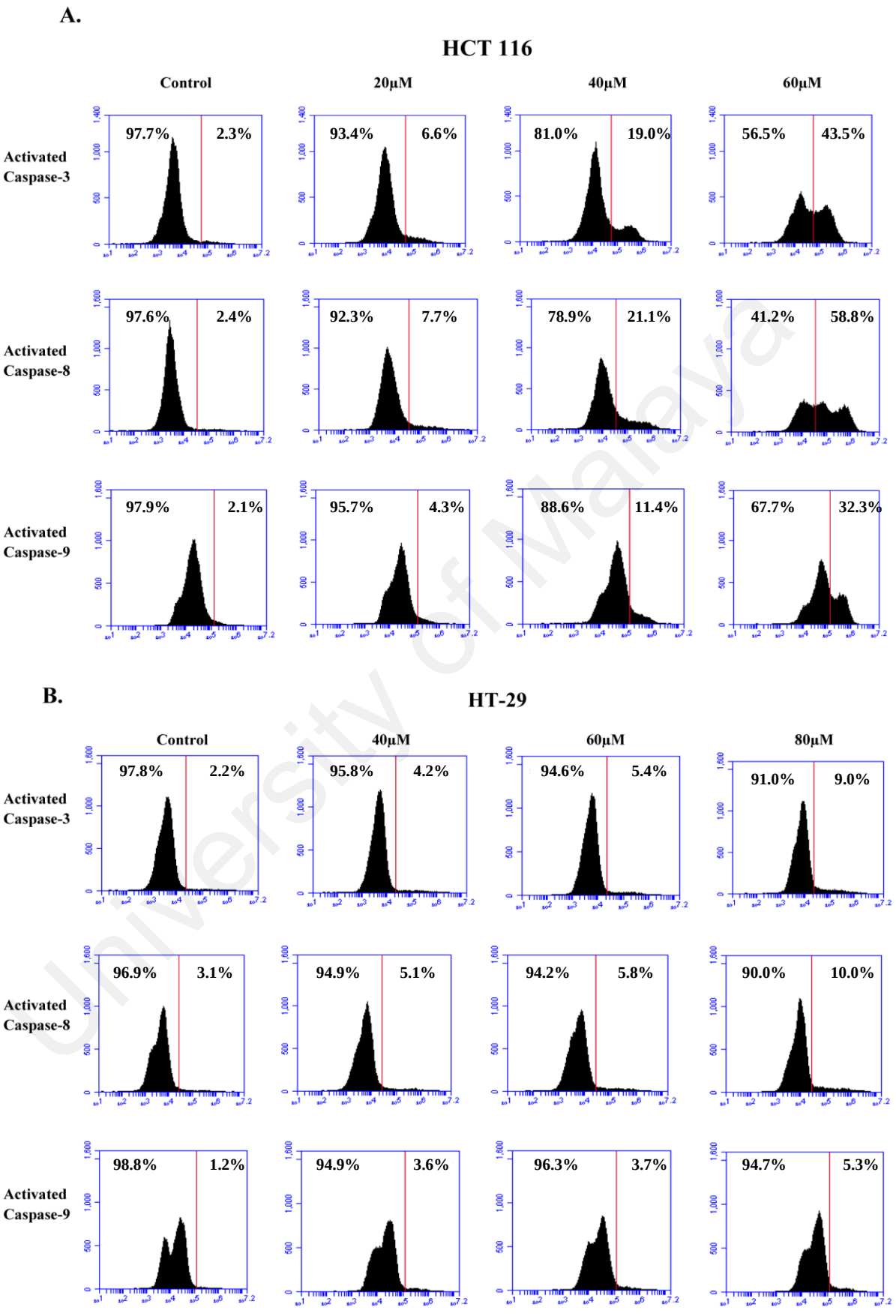

Figure 4.10 continued.

C.

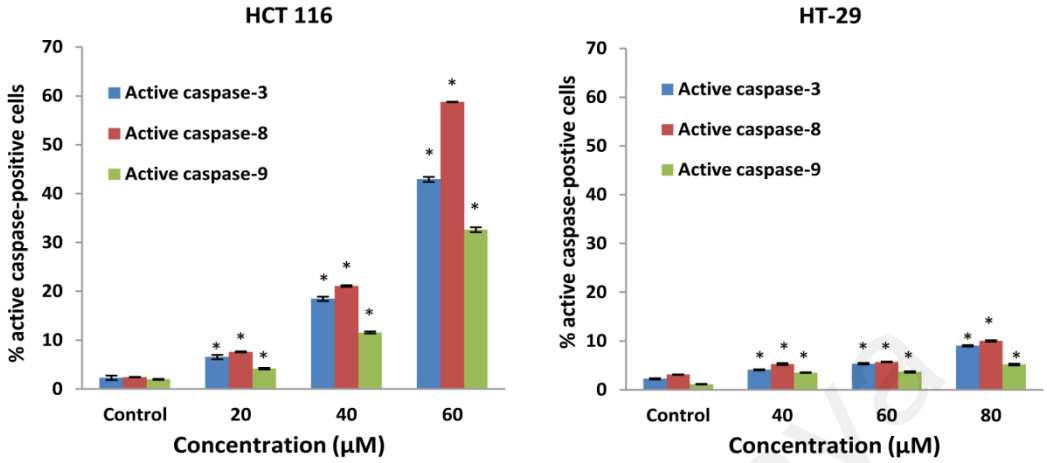

Figure 4.10: Flow cytometric analysis of the effects of FKC on the activation of caspases-3, -8 and -9 in HCT 116 and HT-29 cells. (A) and (B) Cells were treated in the absence or presence of FKC at the indicated concentrations for 48 hours, and assessed using caspILLUME green Active caspase-3, -8 and -9 staining kit. The percentages of (from a total 10,000 cells) of HCT 116 and HT-29 cells showing positive DNA fragmentation were measured by flow cytometric. (C) The percentage of HCT 116 and HT-29 cells that showed positive for active caspase-3, -8 and -9 are presented in the bar chart. Values given are expressed as mean±SD of triplicates obtained from three independent experiments. The asterisk (*) indicated $p<0.05$ when compared to the control. Untreated cells in 0.5% DMSO served as the control

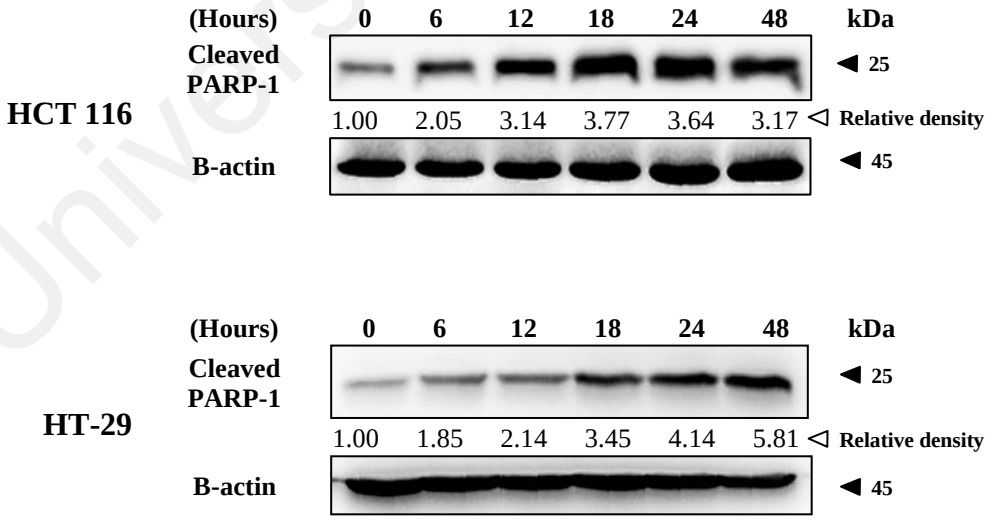

Figure 4.11: Western blot analysis on the levels of cleaved PARP-1 in HCT 116 and HT-29 cells upon FKC treatment. (A) and (B) Cells were treated with FKC (60 µM) at the indicated time points. Cleaved PARP-1 was analyzed by western blot and β-actin served as loading control. The band intensities were quantified using Image J software. The relative density of each band was calculated as fold change relative to the control bands (the protein level at 0 hr) after normalization to β-actin band density.

4.7 Analysis of the activation of death receptor and the level of $cFLIP_L$ by FKC in HCT 116 cells

The involvement of death receptor mediated apoptotic pathway induced by FKC by evaluating the levels of procaspase-8, death receptors, DR5, DR4 and $cFLIP_L$ in HCT 116 cells was investigated via western blot. Western blot analysis showed that the level of the procaspase-8 precursor was decreased in a time-dependent manner after FKC treatment, thereby suggesting cleavage and activation of the enzyme (Figure 4.12A). Western blot analysis revealed that levels of DR5, and to a lesser extent DR4, are increased in a time-dependent manner after FKC treatment (Figure 4.12B). The level of c-$FLIP_L$ was found to be downregulated after 12 hours of FKC treatment (Figure 4.12B). Our results suggested that the death receptors play a role in the extrinsic apoptosis induced by FKC. Thus these data demonstrated that FKC can induce apoptosis in HCT 116 cells through the death receptor apoptotic pathways.

4.8 Effect of FKC on the cytochrome c release, bax, AIF and Smac/DIABLO in the cytosol and mitochondrial fractions of HCT 116 cells

To determine whether the mitochondrial apoptotic pathway causes the translocation of pro-apoptotic proteins from mitochondria to cytosol, the concentrations of cytochrome c, Bax, apoptosis-inducing factor (AIF) and Smac/DIABLO present in the mitochondria and cytosol were examined using western blotting. The content of cytochrome c, AIF and Smac/DIABLO was found to be gradually increased in the cytosol fractions after exposure to FKC, indicating that both proteins were released to the cytosol from the mitochondria (Figure 4.13). Since Bax has been shown to induce permeability of outer mitochondrial membrane, the level of Bax in the mitochondrial fraction was examined by western blot. The content of Bax was increased in the mitochondrial fraction after exposure to FKC (Figure 4.13B). These results suggested that FKC targeted the mitochondria causing a collapse in MMP.

A.

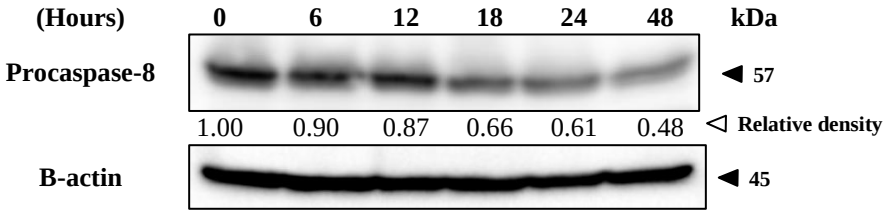

B.

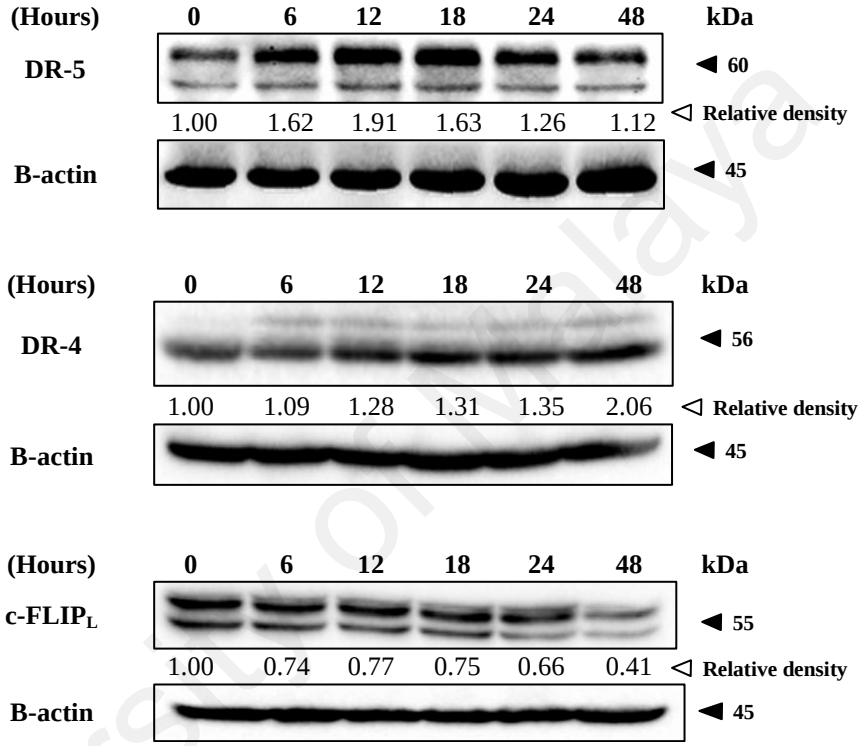

Figure 4.12: Western blot analysis of the effects of FKC on the activation of extrinsic pathway in HCT 116 cells. Cells were treated with FKC (60 µM) at the indicated time points. The levels of caspase-8, and DR-4, DR-5 and c-FLIP$_L$ were analyzed by western blot and β-actin served as loading control. The band intensities were quantified using Image J software. The relative density of each band was calculated as fold change relative to the control bands (the protein level at 0 hr) after normalization to β-actin band density.

A.

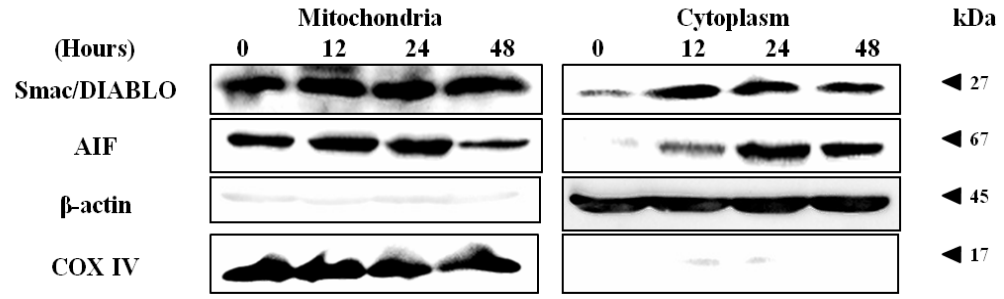

B.

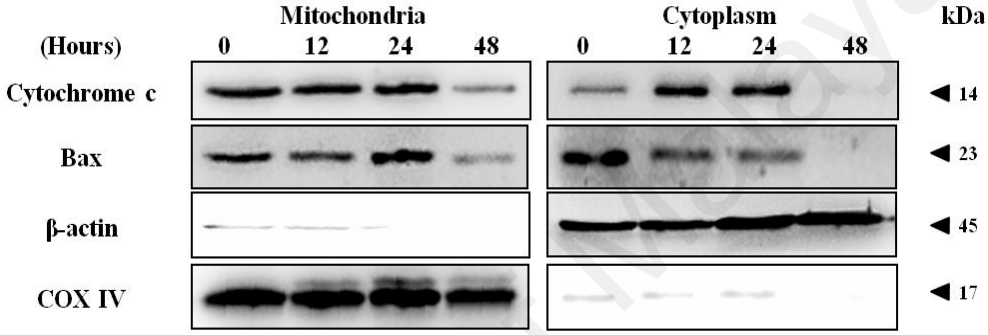

Figure 4.13: FKC induces mitochondrial-mediated apoptosis in HCT 116 cells. After treatment with FKC (60μM) for 12, 24 and 48 hours, whole cell lysates were fractionated into cytosolic and mitochondrial portions. Western blotting was used to examine the levels of cytochrome c, bax, smac/DIABLO and AIF in both fractions. β-actin and COX IV were served as loading control for cytoplasm and mitochondria, respectively.

4.9 Effect of FKC on Bcl-2 family proteins in the regulation of the intrinsic apoptotic pathway in HCT 116 cells

Western blotting was performed to explore the potential role of the Bcl-2 family members in the regulation of the intrinsic and/or mitochondrial apoptotic pathway in HCT 116 cells treated with FKC. It was of particular interest to investigate whether the levels of anti-apoptotic and pro-apoptotic proteins were altered in HCT 116 cells after treatment with FKC. The level of the pro-apoptotic protein Bak was found to increase in HCT 116 cells in a time-dependent manner. However, the level of Bax was found to decrease after 18 hours of incubation with FKC. As shown in Figure 4.14, the levels of the anti-apoptotic protein Bcl-2 were unaffected after the treatment. The level of Bcl-xL remained unaffected only in the first 18 hours and the level was markedly reduced after 18 hours of treatment (Figure 4.14). The level of another pro-apoptotic protein, Bid was also examined, and it was found that there were no significant changes in its total protein level.

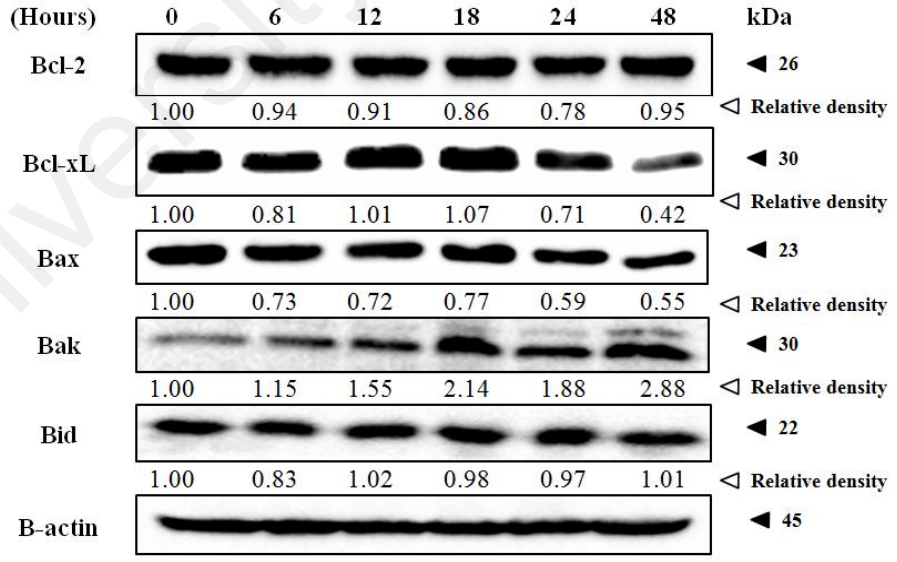

Figure 4.14: Western blot analysis of the effects of FKC on the levels of Bcl-2 family proteins in HCT 116 cells. HCT 116 cells were treated with FKC (60 µM) for indicated time points, and followed by protein extraction and western blot analysis. β-actin was used as the internal control. The band intensities were quantified using Image J software. The relative density of each band was calculated as fold change relative to the control bands (the protein level at 0 hr) after normalization to β-actin band density.

4.10 Effect of FKC on the level of GADD153/CHOP in HCT 116 and HT-29 cells

To further elucidate the possible apoptotic pathway triggered by FKC, we investigated the level of GADD153/CHOP using western blot analysis in HCT 116 and HT-29 cells treated with 60 and 80 µM of FKC, respectively. The protein level of ER stress-associated molecules, GADD153 was investigated by western blotting. GADD153, also known as CHOP, encodes a member of the CCAAT/enhancer-binding protein family and acts as an inhibitor or activator of transcription, leading to apoptosis (Yamaguchi & Wang, 2004).

As shown in Figure 4.15, it was observed that GADD153 was largely upregulated in HCT 116 and HT-29 cells after treatment with FKC throughout the 48 hours incubation, while no expression of the protein was detected in non-treated cells. This implied that ER stress induced by FKC occurred in both intrinsic and extrinsic pathways in HCT 116 and HT-29 cells.

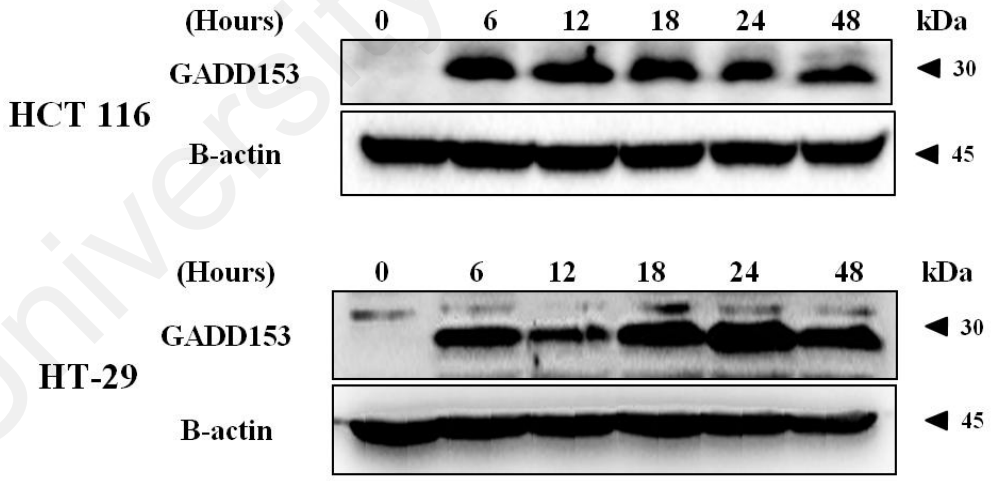

Figure 4.15: Western blot analysis of the effect of FKC on the level of GADD153/CHOP in HCT 116 and HT-29 cells. HCT 116 (A) and HT-29 (B) cells were incubated with FKC (60µM for HCT 116 cells and 80 µM for HT-29 cells) for the indicated time points and followed by protein extraction. The changes in level of GADD153/CHOP were evaluated by western blot. β-actin in the western blot was used as the internal control. The band intensities were quantified using Image J software. The relative density of each band was calculated as fold change relative to the control bands (the protein level at 0 hr) after normalization to β-actin band density.

4.11 Effect of FKC on the inhibitor of apoptosis proteins (IAPs) by FKC in HCT 116 and HT-29 cells

The levels of anti-apoptotic proteins, XIAP, cIAP-1, cIAP-2 and survivin in HCT 116 and HT-29 cells were evaluated by western blot following FKC treatment. Western blot analysis (Figure 4.16A & B) showed that there was a dramatic decrease in the levels of cIAP-1, cIAP-2, XIAP, survivin in HCT 116 and HT-29 cells with increasing incubation time. However, survivin was undetected in HCT 116 cells while cIAP-2 was undetected in HT-29 cells. Taken together, these findings suggested that the levels of pro-apoptotic proteins increased concurrently with a decrease in the levels of anti-apoptotic proteins in HCT 116 cells exposed to FKC.

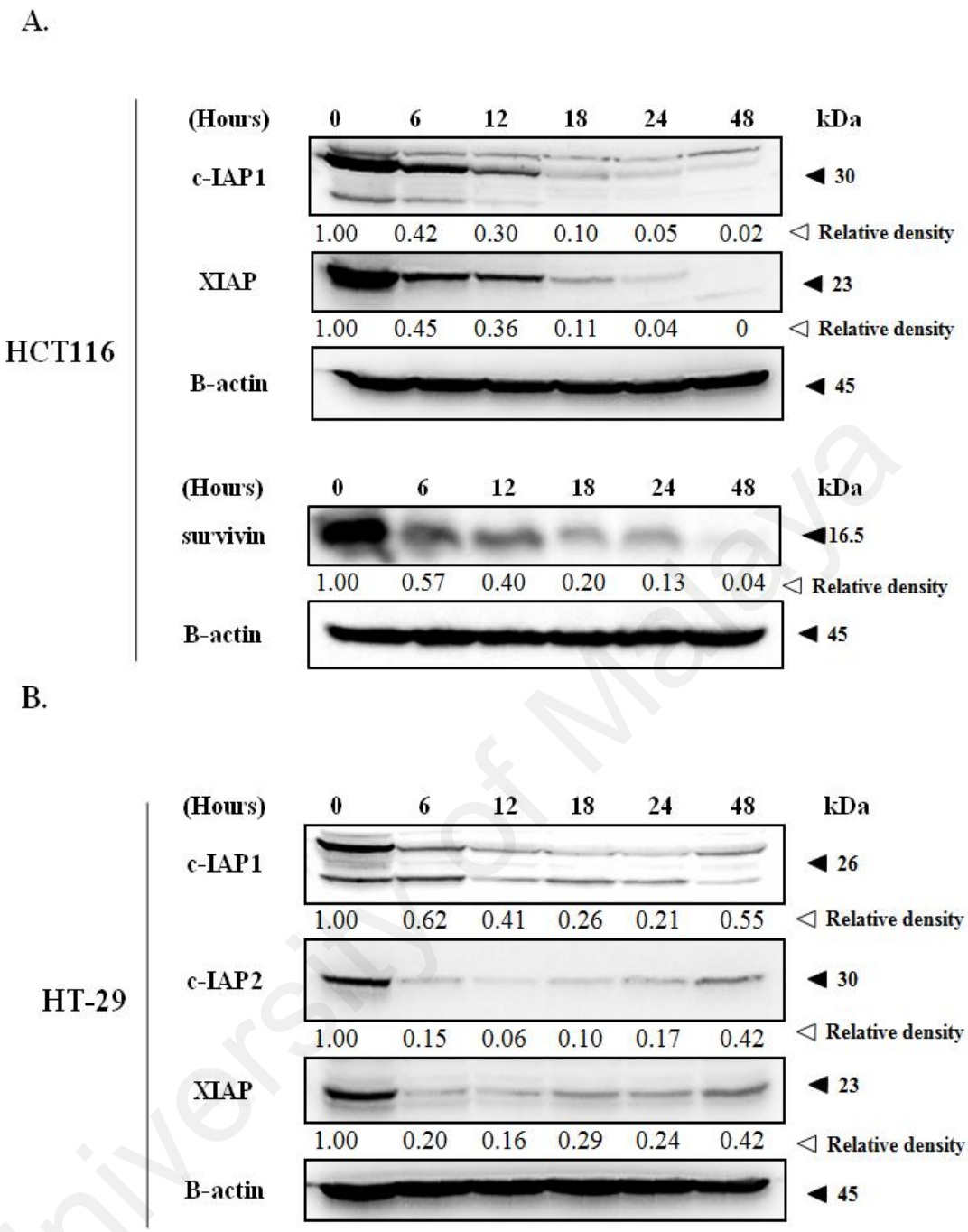

Figure 4.16: Effects of FKC on the levels of inhibitor of apoptosis proteins (IAPs) in HCT 116 and HT-29 cells. HCT 116 (A) and HT-29 (B) cells were treated with FKC for indicated time points, and followed by protein extraction and western blot analysis. FKC decreased the levels of cIAP-1, cIAP-2, XIAP and survivin. β-actin in the western blot was used as the internal control. The band intensities were quantified using Image J software. The relative density of each band was calculated as fold change relative to the control bands (the protein level at 0 hr) after normalization to β-actin band density.

4.12 Effect of FKC on MAPKs and AKT signaling pathways in HCT 116 cells

MAPKs and Akt signaling pathways are known to be involved in cellular proliferation, survival and differentiation (Johnson *et al.*, 2010). Therefore, western blot analysis was performed to investigate whether these signaling pathway were functionally involved in the apoptosis effect of FKC on HCT 116 cells after treatment with 60 µM of FKC at different time intervals. The activation of Akt was detected using a phospho-specific Akt (Ser473) antibody. As shown in Figure 4.17A, there was a slight increase in Akt phosphorylation after 6 hours of treatment, after which the level of phosphorylation gradually decreased while no apparent change was observed in total Akt under the same treatment condition.

We next investigated the effect of FKC on the activation of MAPKs cascade including extracellular regulated protein kinase (ERK), c-Jun N-terminal kinase (JNK) and p38 in HCT 116 cells. Western blot analysis (Figure 4.17B) revealed that FKC decreased the phosphorylation (Thr202/Tyr204) of ERK at the early time points (6, 12 and 18 hours post-FKC), whereas the drug caused dramatic increase in phosphorylation at later time points (24 and 48 hours post-FKC). No significant change in p38 phosphorylation was observed, whereas small reductions in JNK phosphorylation were noted at 24 and 48 hours post-FKC (Figure 4.17B). The levels of total ERK, JNK and p38 protein remain unchanged after treatment with FKC. Together, these results suggested that apoptosis-induced FKC is involved in the inactivation of Akt pathway, and modulation of MAPKs pathway.

A.

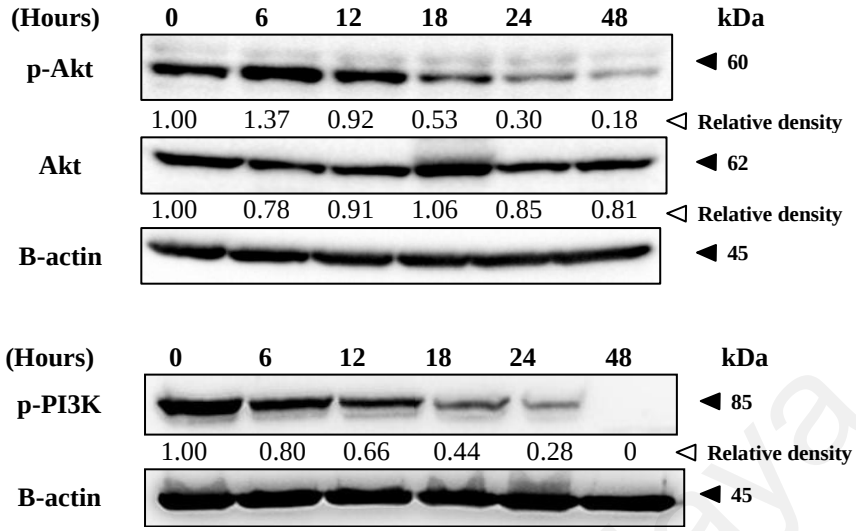

B.

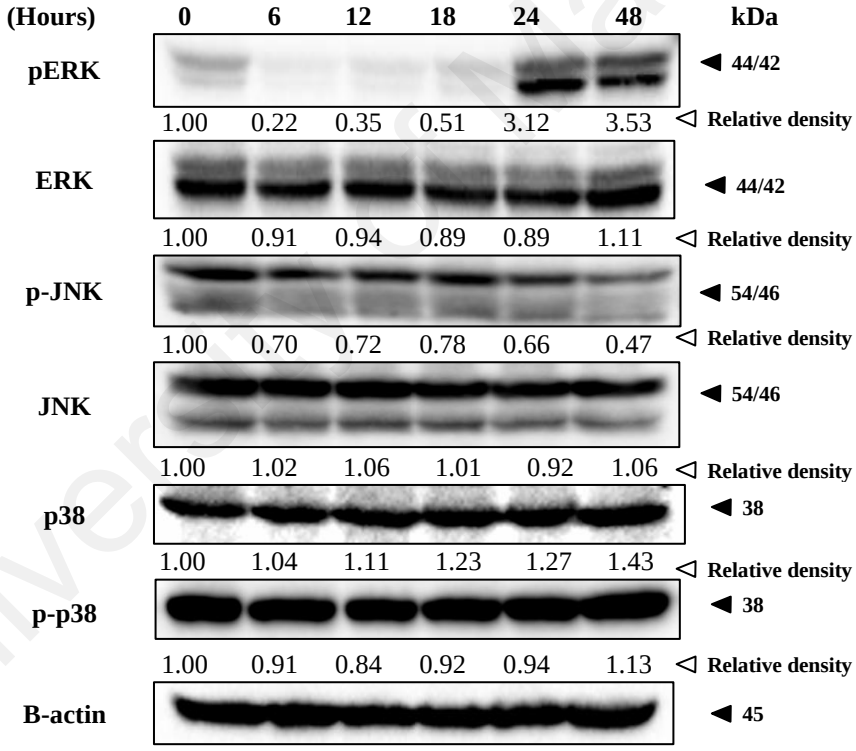

Figure 4.17: Western blot analysis of the effect of FKC on the protein levels involved in MAPK and Akt/PI3K signaling pathways. Cells were incubated with FKC (60µM) for the indicated time points and followed by protein extraction. Cell lysates were subjected to western blot analysis using antibodies indicated to detect the levels of phosphorylated and total proteins of Akt, ERK, JNK and p38, and the level of phosphorylated PI3K. β-actin in the western blot was used as the internal control. The band intensities were quantified using Image J software. The relative density of each band was calculated as fold change relative to the control bands (the protein level at 0 hr) after normalization to β-actin band density.

4.13 Effects of FKC on the cell cycle in HCT 116 and HT-29 cells

Cell proliferation is correlated with the regulation of cell cycle progression. An additional investigation was conducted to examine whether FKC trigger the molecular mechanisms underlying cell cycle arrest in HCT 116 cells. The cell cycles of HCT 116 and HT-29 cells were evaluated using flow cytometry with propidium iodide labelling to determine which phases of the cell cycle were arrested in cells treated with FKC.

As shown in Figure 4.18A & B, there was an accumulation of cells in sub-G_1 phase in HCT 116 cells treated with FKC after 48 hours incubation at 40 and 60 µM (8.65% and 8.69%, respectively) compared to the control. The percentage of cells in the S phase also increased significantly after FKC treatment for 24 and 48 hours accompanied by a decrease in the percentage of cells in the G_1 phase. For instance, treatment of FKC at 40 and 60 µM for 24 hours significantly increased the percentages of cells in S phase (46.51% and 51.65%, respectively) compared to 16.76% in the control. We observed that treatment with FKC at 48 hours resulted in a slight increase in G_2/M phase; however the induced S phase arrest was more apparent compared to G_2/M arrest. These results indicated that there was a concentration- and time-dependent increase in the percentage of cells entering sub-G_1 and S phases of the cell cycle in HCT 116 cells.

In the case of HT-29, a significant increase in the percentage of cells in G_2/M was observed (Figure 4.19A & B) after 24 and 48 hours of FKC treatment compared to the control, indicating that cell cycle arrest occurred at the G_2/M phase. However, there was only a slight increase in percentage of cells in sub-G_1 phase after FKC treatment at 40 and 60 µM for 24 and 48 hours. These results indicated that there was a concentration- and time-dependent increase in the percentage of cells entering G_2/M phases of the cell cycle in HT-29 cells.

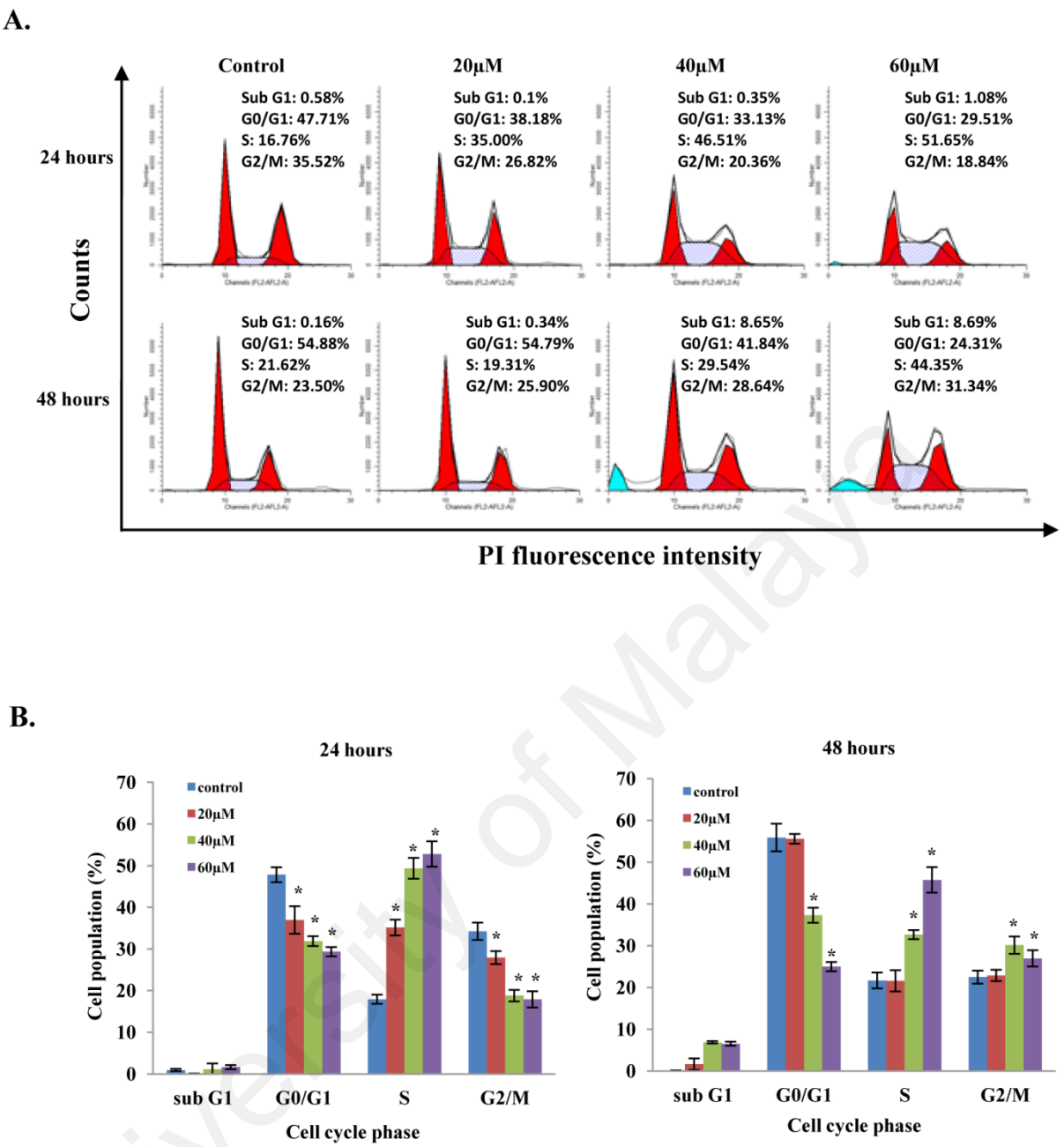

Figure 4.18: Effect of FKC on the cell cycle in HCT 116 cells. (A) Cells were treated with the indicated concentrations (20, 40 and 60 µM) of FKC for 24 and 48 hours, and stained with PI. DNA content of HCT 116 cells were analyzed using flow cytometry and quantification of cell cycle distribution (sub-G_1, G_0/G_1, S and G_2/M phases) was performed using ModFit software. Untreated cells in 0.5% DMSO served as the control. Each histogram is the representative cell cycle profile of three independent experiments. (B) The quantitative data of mean of percentages of cells in each phase for HCT 116 cells for 24 and 48 hours are presented in bar chart. Values given are expressed as mean±SD of triplicates obtained from three independent experiments. The asterisk (*) indicated $p<0.05$ when compared to the control.

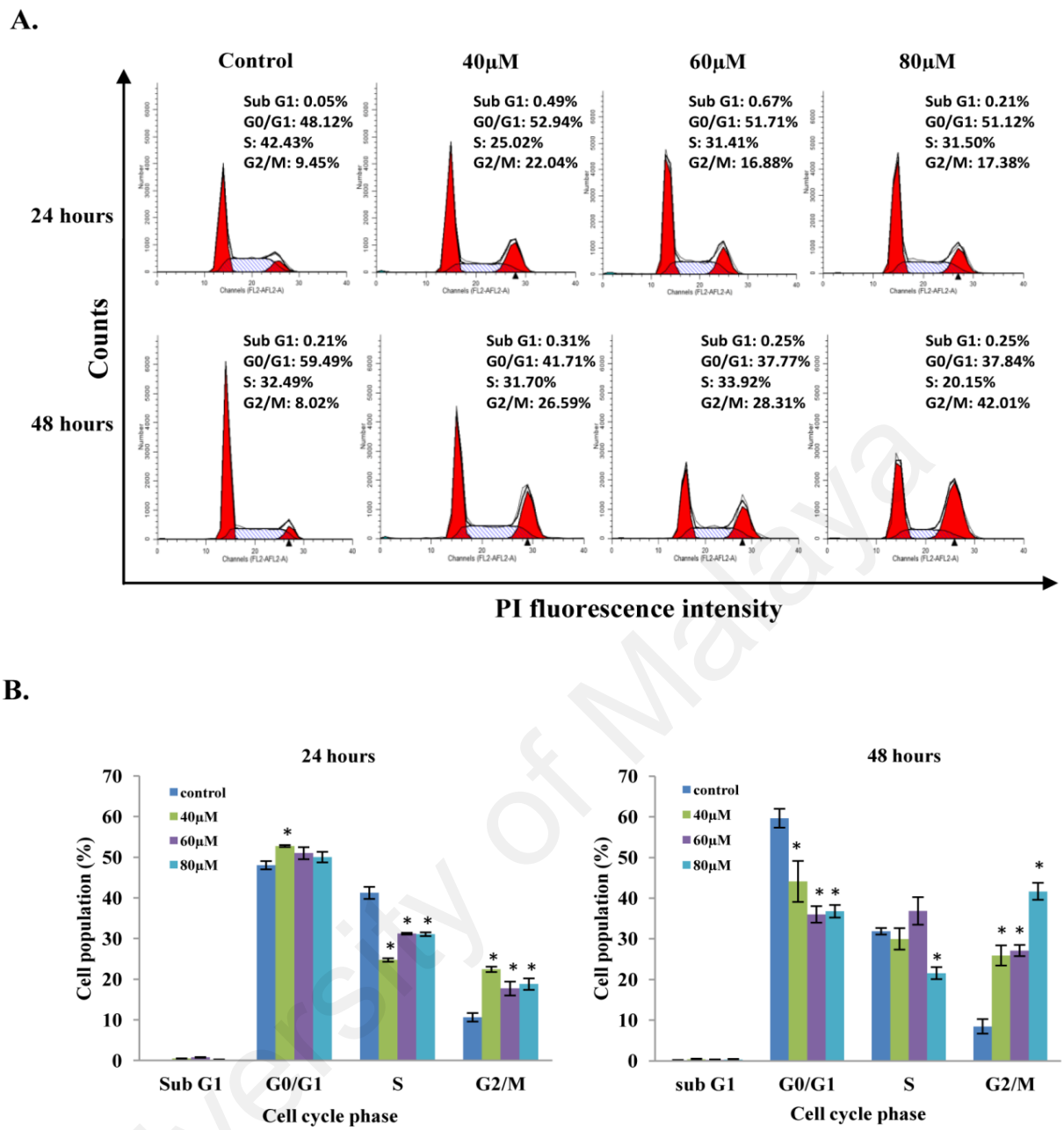

Figure 4.19: Effect of FKC on the cell cycle in HT-29 cells. (A) Cells were treated with the indicated concentrations (40, 60 and 80 µM) of FKC for 24 and 48 hours, and stained with PI. DNA content of HCT 116 and HT-29 cells were analyzed using flow cytometry and quantification of cell cycle distribution (sub-G_1, G_0/G_1, S and G_2/M phases) was performed using ModFit software. Untreated cells in 0.5% DMSO served as the control. Each histogram is the representative cell cycle profile of three independent experiments. (B) The quantitative data of mean of percentages of cells in each phase for HT-29 cells for 24 and 48 hours are presented in bar chart. Values given are expressed as mean±SD of triplicates obtained from three independent experiments. The asterisk (*) indicated $p<0.05$ when compared to the control.

4.14 Effect of FKC on the levels of cyclin, cyclin dependent kinase and pRb phosphorylation (p-pRb) in HCT 116 cells

To examine the mechanism responsible for cell cycle arrest induced by FKC, the effects of FKC on cell cycle regulatory proteins (cyclins), cyclin dependent kinases (Cdks), phosphorylation status of pRb (which are involved in the regulation of the cell cycle progression) were evaluated by western blotting. As shown in Figure 4.20A, FKC treatment induced a dramatic decrease in the protein levels of Cdk2 and Cdk4 in HCT 116 cells. However, no changes in cyclin D1 and cyclin E were observed (Figure 4.20B). FKC markedly inhibited the phosphorylation of pRb (p-pRb) as early as 6 hours, with minimal changes in the level of total pRb protein (Figure 4.20C).

4.15 Effect of FKC on the levels of p53, $p21^{Cip1}$ and $p27^{Kip1}$ in HCT 116 and HT-29 cells

The changes in levels of p53, p21 and p27 were examined by western blot in HCT 116 and HT-29 cells. As shown in Figure 4.21A & B, FKC treatment resulted in a time-dependent increase in the protein expression of p53 in HCT 116 cells, which was particularly evident at first 12 hours of treatment. However, it was decreased after 12 hours of treatment. In the case of HT-29 cells, it was interesting to note that the level of p53 was found to be decreased after FKC treatment

As shown in Figures 4.20A & B the level of p21 was increased at the first 12 hours of FKC treatment in HCT 116 cells. However, the level was decreased afterwards. The level of p27 was gradually increased after FKC treatment in HCT 116 cells. However, the levels were markedly upregulated following FKC treatment after 18 hours. Interestingly, similar results were observed in HT-29 cells after being treated with the same treatment period.

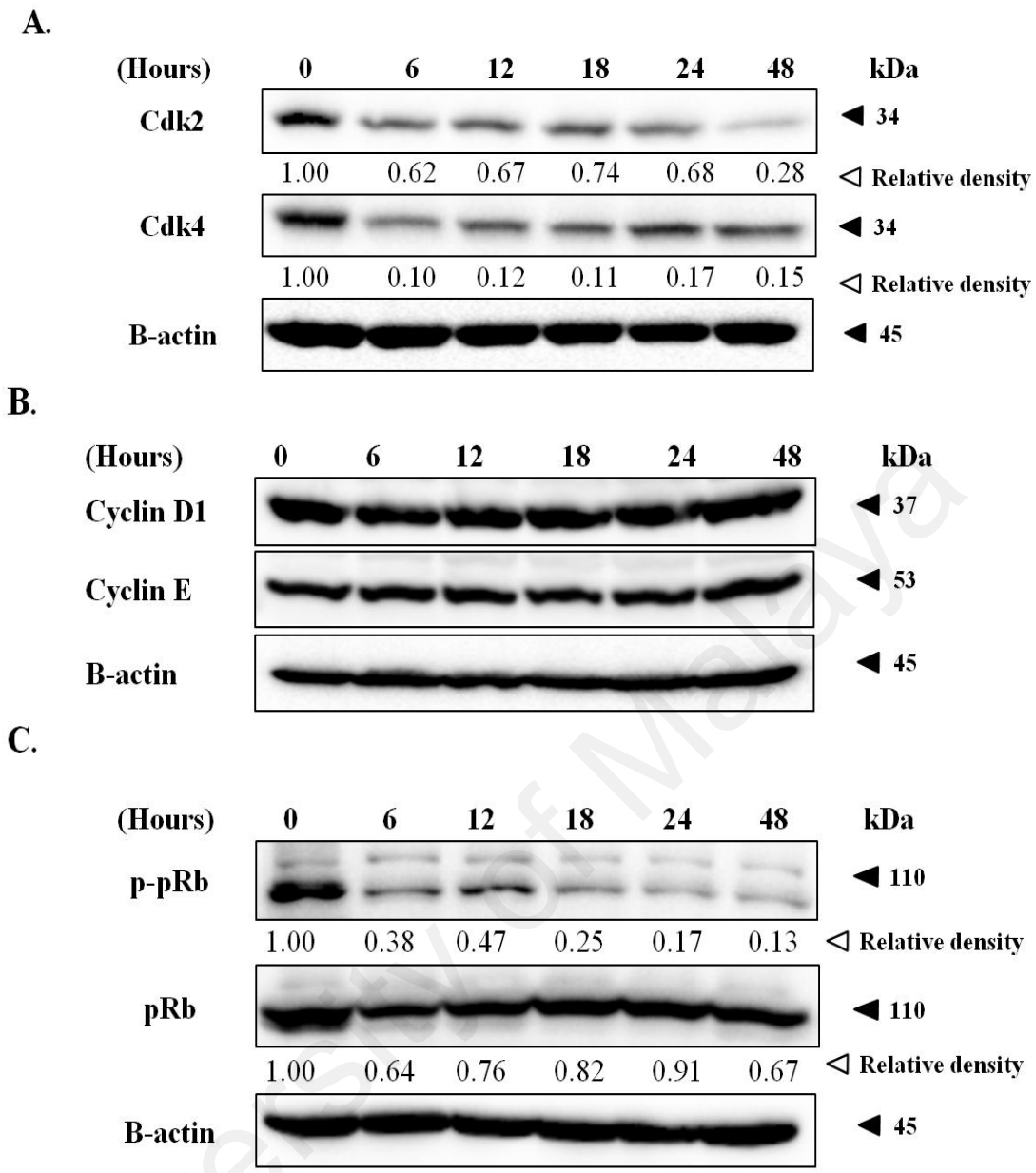

Figure 4.20: Western blot analysis of the effect of FKC on the cell cycle regulatory proteins in HCT 116 cells. Cells were incubated in the absence or presence of FKC (60μM) for the indicated times, and followed by protein extraction. Changes in levels of cell cycle regulatory proteins (cyclin D1 and E), cyclin dependent kinase (Cdk2 and Cdk4) pRb and p-pRb in HCT 116 cells were analyzed by western blot. Untreated cells in 0.5% DMSO served as the control. β-actin was used as the loading control. The band intensities were quantified using Image J software. The relative density of each band was calculated as fold change relative to the control bands (the protein level at 0 hr) after normalization to β-actin band density.

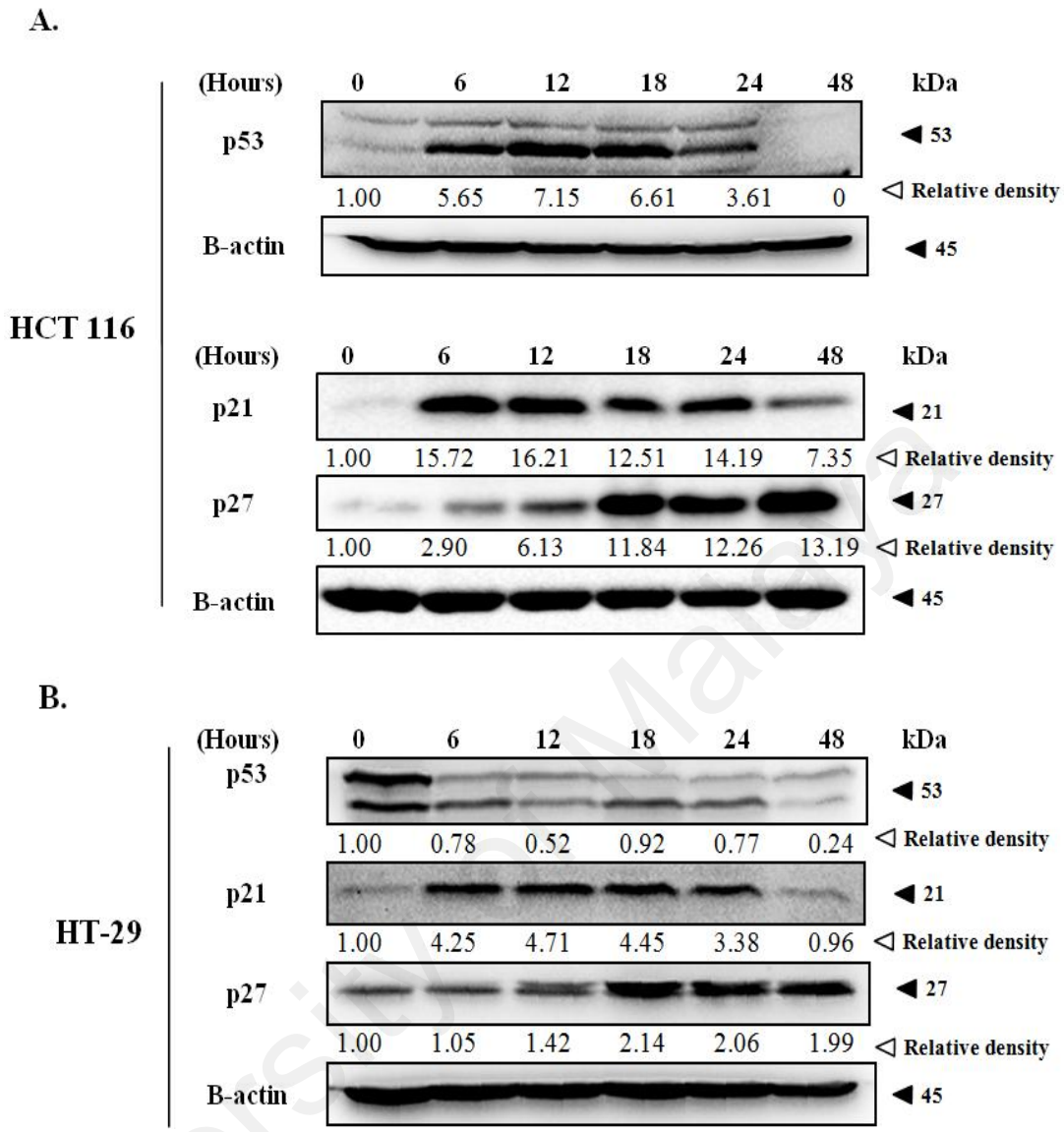

Figure 4.21: Western blot analysis of the effect of FKC on the level of p53, p21 and p27 upon FKC treatment in HCT 116 and HT-29 cells. HCT 116 (A) and HT-29 (B) cells were incubated with FKC (60 µM for HCT 116 and 80 µM for HT-29) for the indicated time points and followed by protein extraction. The changes in level of p53, cdk interacting protein/kinase inhibitory proteins ($p21^{Cip1}$ and $p27^{Kip1}$) were evaluated by western blot. β-actin in the western blot was used as the loading control. The band intensities were quantified using Image J software. The relative density of each band was calculated as fold change relative to the control bands (the protein level at 0 hr) after normalization to β-actin band density.

4.16 Effect of FKC on ROS generation and SOD activity

ROS generation plays an important role in pro-apoptotic activities. To examine whether oxidative stress damage was involved in FKC-induced apoptosis in HT-29 and HCT 116 cells, cells treated with FKC were stained with DCF-DA dye and also examined for SOD activity. As shown in Figure 4.22(A), the intracellular ROS level of HT-29 and HCT 116 cells was significantly increased by FKC treatment in a dose-dependent manner. In addition, the activity of superoxide dismutase (SOD), an enzymatic antioxidant in HT-29 and HCT 116 cells was evaluated. The SOD activity was significantly decreased by FKC in a dose-dependent manner as shown in Figure 4.22(B). The results suggested the involvement of the changes in redox status in FKC-induced apoptosis.

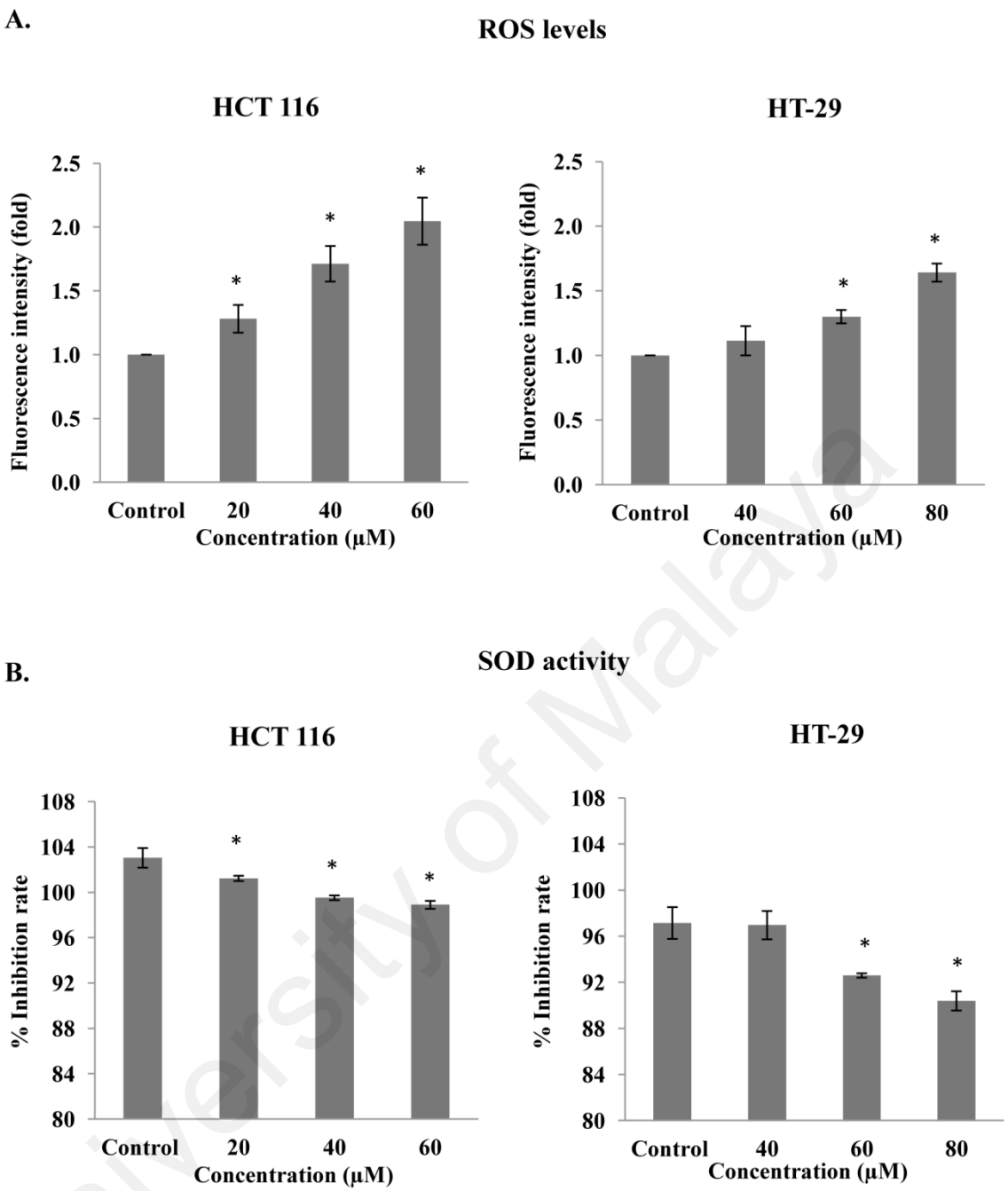

Figure 4.22: Concentration-dependent effect of FKC on ROS generation and SOD activities in HCT 116 and HT-29 cells. Cells were treated with FKC (20, 40 and 60 µM for HCT 116 cells while 40, 60 and 80 µM for HT-29 cells) for 4 hours, and the intracellular level of total ROS (A) and the SOD activity (B) were measured. The ROS levels were significantly increased compared with their levels in the control in both cell lines. The SOD activity was significantly decreased compared with their levels in the control in both cell lines. The data are presented as the mean±SD for three independent experiments. An asterisks (*) indicates a significant difference (p<0.05) in comparison to control. Untreated cells in 0.5% DMSO served as the control.

4.17 2-DE: Identification of proteins that change in abundance with FKC treatment

A representative 2DE map is shown in Figure 4.23. Image analysis of gels revealed that 70 protein spots changed in abundance with FKC treatment. The framed areas in Figure 4.23 are magnified in Figure 4.24, with numbered spots indicating proteins that changed in abundance. A total 35 individual protein spots were unambiguously identified (17 increased and 18 decrease in abundance) using mass spectrometry. The average normalized spot volumes for each identified protein of the control and FKC-treated groups are shown in appendix D. The normalized spot volumes were calculated using Progenesis SameSpot software. The identities of these proteins are shown in Table 4.2. The spot numbers in Figure 4.23 correspond to numbers in Table 4.2. From this point forward, the identified proteins will be referred to by their gene symbols as shown in Table 4.2.

4.17.1 *In silico* analysis of identified proteins

The identified proteins were classified based on their known function, involvement in biological processes, and intracellular localization using information from the Human Protein Reference Database (HPRD) (http://www.hprd.org/queary) and Uniprot Knowledgebase (UniProtKB). Among them, majority were located in cytoplasm (52%) while others found in nucleus (14%), endoplasmic reticulum (7%), mitochondria (5%) and mitochondrial membrane (2%) as shown in Figure 4.27(A). The molecular functions involved with catalytic activity which accounted for 26% of the protein identified and followed by chaperones (17%), cytoskeletal organization (11%), translation (8%), transporter (8%), transcription (6%), RNA binding (6%), DNA binding (6%), ubiquitin proteasome system (3%), protein binding (3%) and unknown (6%) as shown in Figure 4.27(B).

Table 4.2 shows the identified proteins as classified based on their molecular function together, relative abundance, biological functions, and the MS identification. IPA analysis predicted that the identified proteins may be involved in regulating post-translational modifications, protein folding, cell death and survival, protein synthesis and amino acid metabolism (Table 4.3B). The protein ubiquitination pathway and unfolded protein response were predicted to be the top canonical pathways affected by the changes in protein abundance observed (Table 4.3A). The top networks associated with the identified proteins were those associated with cell death and survival, cell cycle, cellular growth, and proliferation as shown in Table 4.3C. The details of the top canonical pathways, molecular and cellular functions and top networks are shown in Table 4.2. Figure 4.26 shows the protein-protein interactions and protein networks relevant to cancer and cell death.

4.17.2 Transcript analysis by qPCR

The transcript expression of 12 proteins: TCEB, SKP1, HMOX1, EEF2, EIF3I, EIF5A, P4HB, ATP5H, RAD23B, RanBP1, SFPQ and HSPA1A, were evaluated (Figure 4.24). Figure 4.25 shows relative mRNA expression levels of the selected targeted proteins after normalization against β-actin. The mRNA expression levels of these proteins showed a similar trend change with protein abundance as observed on 2DE with the exception of SKP1, TCEB, RAD23B and SFPQ. A number of possible factors may be contributing towards this observed inconsistency. They include the existence of proteins in various forms due to post-translational modifications. This will lead to the possible identification of the same proteins in different spots on 2DE gels. This has been observed in many experiments involving 2DE (Thiede *et al.*, 2013).

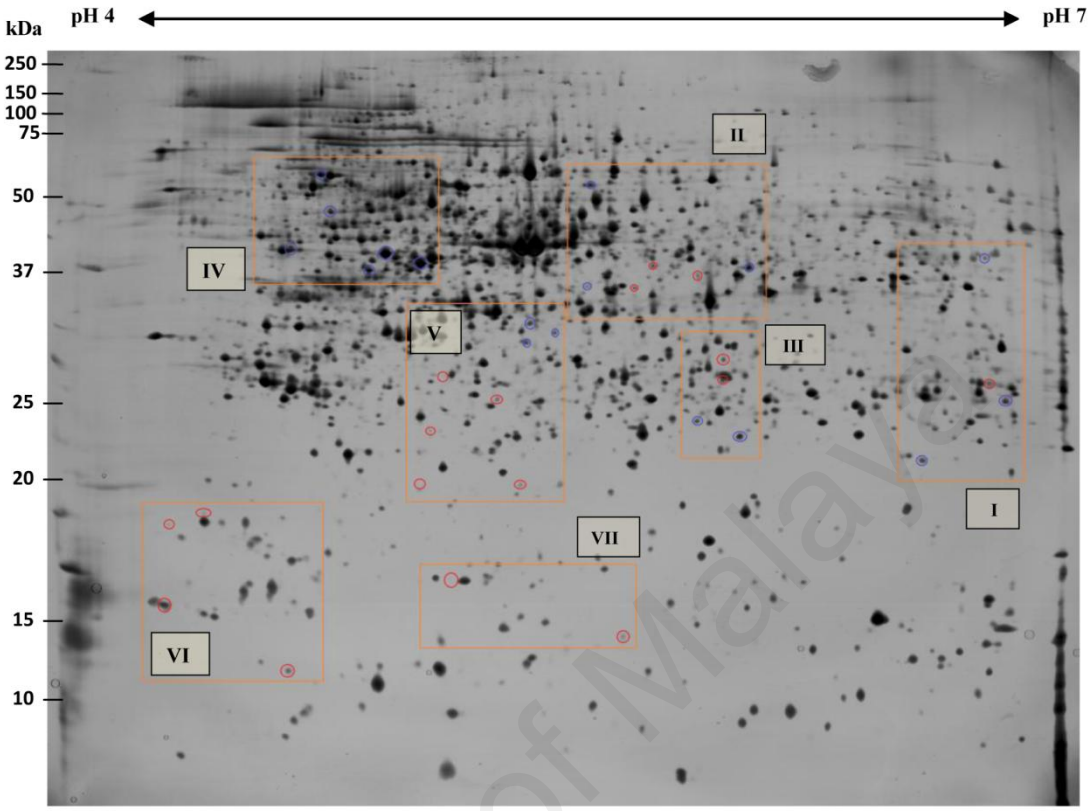

Figure 4.23: Representative proteome map of cell lysate from FKC treated HCT 116 cells. One hundred fifty micrograms of untreated and FKC-treated HCT 116 cells were resolved on 24 cm linear immobiline DryStrip, pH 4–7 in the first dimension, followed by 12.5% SDS-PAGE gel in the second dimension and the proteins were stained with silver. Image analysis was performed using Nonlinear Progenesis SameSpot software. A total of 35 protein spots were identified to be differentially abundant (labelled with circle), 17 were up-regulated (circled in blue) and 18 were down-regulated (circled in red). Framed areas (I, II, III, IV, V, VI and VII) (in orange color) are magnified in Figure 4.24. Protein spots are highlighted according to a 2-fold difference and *p*-value less than 0.05.

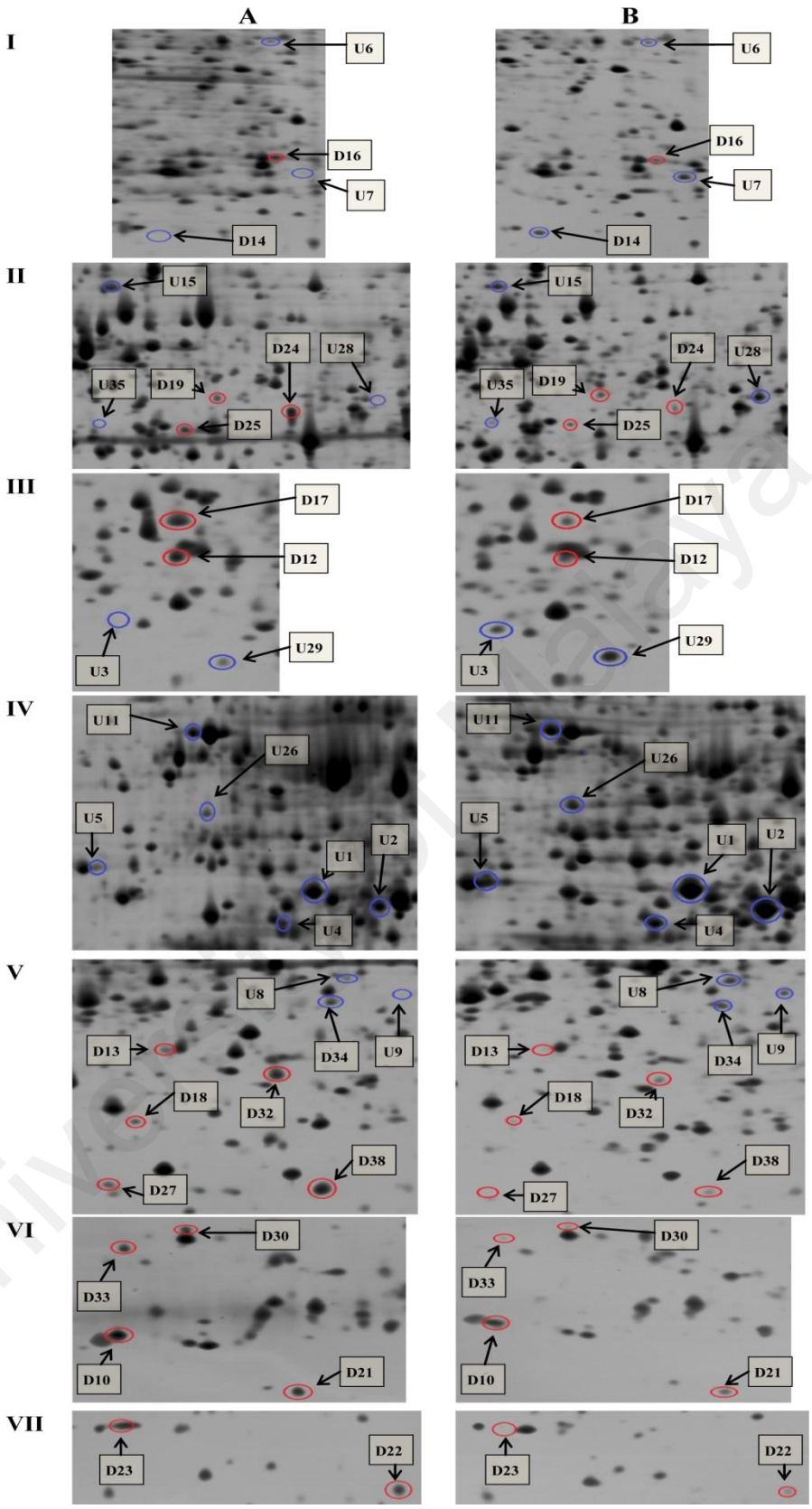

Figure 4.24: Magnified views showing the location of differentially abundant spots on the untreated and FKC-treated HCT 116 cells gels. Expanded view of seven sections (I, II, III, IV, V, VI and VII) showing differentially abundant proteins between A: untreated HCT 116 cells and B: FKC-treated HCT 116 cells. The uppercase 'U'/blue cicle and 'D'/red circle refer to up-regulated and down-regulated spots, respectively. Seven biological replicates per group (n=7) were used in the analysis.

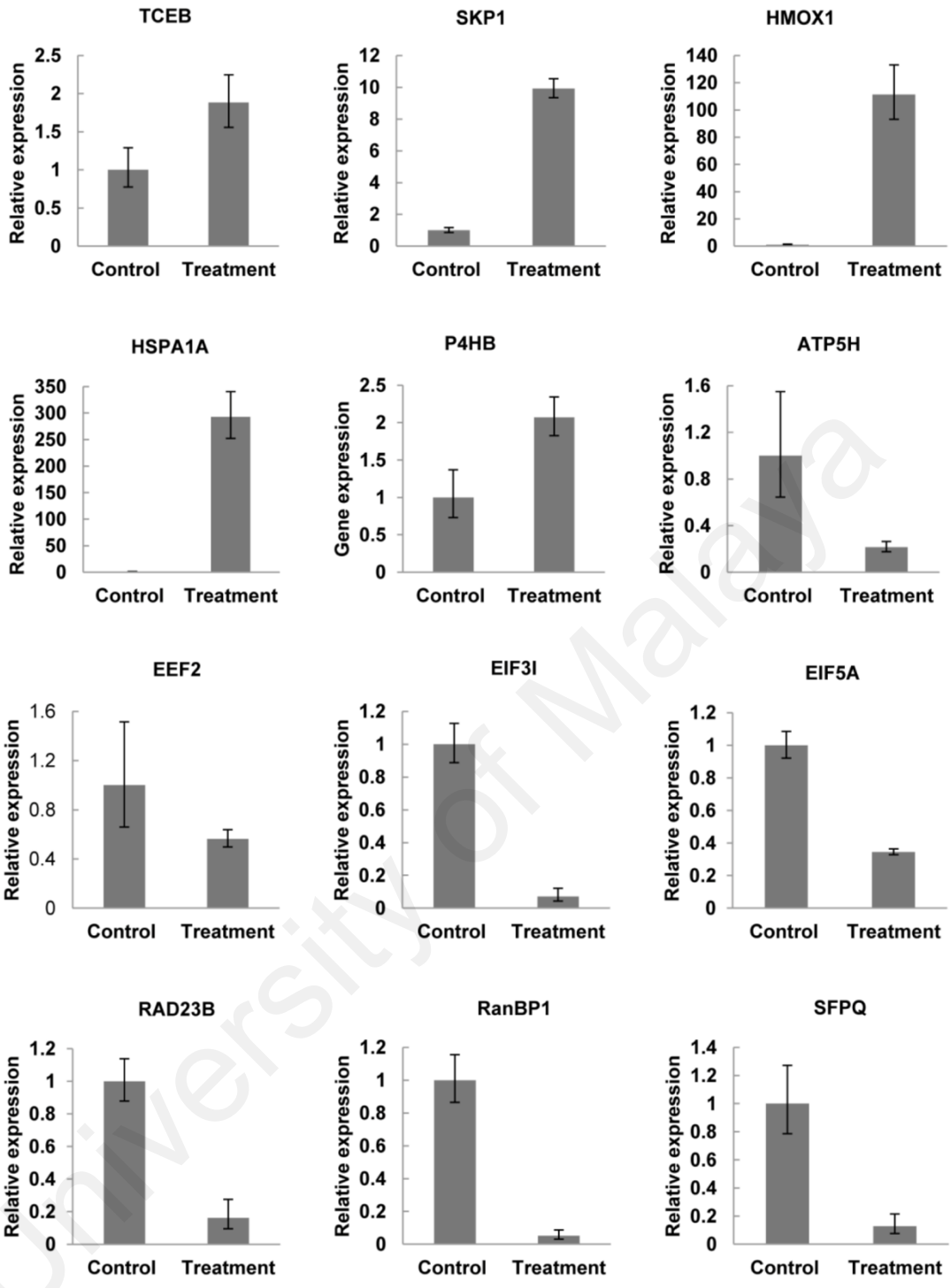

Figure 4.25: RT-qPCR validation of 12 proteins that changed in abundances after FKC treatment in HCT 116 cells. Relative mRNA expression levels of the selected proteins after normalization with reference gene β-actin were analzyed by RT-qPCR. The relative quantification of gene expression was analyzed by the ΔΔCt method. Experiments were repeated three times.

Table 4.2: List of proteins identified by MALDI TOF/TOF-MS that are differentially abundant in FKC treated HCT 116 cells

Spot no.	Protein name	Gene symbol	Accession number	Subcellular Localization	Biological Process	pI/MW (kDa)		MASCOT Score	Peptides matched (% seq coverage)	Fold change	*p*-value
						Exp.	Theo.				
Chaperones											
U1	Heat shock cognate 70kDa protein 8 (Hspa8)	HSPA8	P11142	Cytoplasm	Protein refolding	4.97/ 41117	5.37/ 70854	228	21 (23%)	2	3.54E-05
U2	Heat shock 70 kDa protein 1-like (HSP70-Hom)	HSPA1L	P34931	Cytoplasm	Protein refolding	5.08/ 39925	5.76/ 70331	75	18 (19%)	2.3	1.64E-05
U3	Heat shock protein 27 kDa	HSPB1	P04792	Cytoplasm	Response to unfolded protein	5.88/ 24296	5.98/ 22768	85	12 (37%)	2.2	5.25E-04
U4	Heat shock 70 kDa protein 1A/1B (HSP70-1/HSP70-2)	HSPA1A	P08107	Cytoplasm	Protein stabilization	4.92/ 38625	5.48/ 69995	263	18 (16%)	4.1	4.58E-07
U5	Heat shock protein 90kDa alpha (HSP 86)	HSP90AA1	P07900	Cytoplasm	Protein folding	4.62/ 43283	4.94/ 84529	548	22 (21%)	2.5	3.86E-05
U6	T-complex protein 1 subunit eta (TCP-1 eta)	CCT7	Q99832	Cytoplasm	Protein folding	6.75/ 39817	7.55/ 59329	64	22 (28%)	2.2	2.21E-04
Cytoskeleton											
U7	Keratin, type I cytoskeletal 18 (CK-18)	KRT18	P05783	Cytoplasm	Intermediate filament cytoskeleton organization	6.81/ 26165	5.34/ 48029	140	21 (36%)	8.2	8.83E-07
U8	Tubulin beta-2C chain (Tubulin beta-2 chain)	TUBB4B	P68371	Cytoplasm	Organelle organization; protein folding	5.4/ 33621	4.79/ 49799	155	18 (31%)	2.3	2.60E-04

Table 4.2 continued.

U9	Actin, cytoplasmic 2 (Gamma actin)	ACTG1	P63261	Cytoplasm	Membrane organization; movement of cell or subcellular component	5.47/ 32718	5.31/ 41766	67	21 (37%)	3.8	7.50E-06
D10	Myosin light polypeptide 6 (MLC-3)	MYL6	P60660	Cytoplasm	Muscle contraction	4.48/ 15545	4.56/ 16919	62	8 (43%)	- 2.3	2.86E-03
Catalytic activity											
U11	Protein disulfide-isomerase precursor (PDI) (EC 5.3.4.1)	P4HB	P07237	Endoplasmic reticulum	Cell redox homeostasis	4.77/ 58898	4.76/ 57081	179	23 (29%)	2.6	3.84E-05
D12	Guanidinoacetate N-methyltransferase (EC 2.1.1.2)	GAMT	Q14353	Cytoplasm	Creatine biosynthetic process	5.96/ 27913	5.75/ 26301	194	14 (47%)	- 2.1	2.80E-04
D13	Deoxycytidine kinase (dCK) (EC 2.7.1.74)	DCK	P27707	Cytoplasm	Nucleotide biosynthetic process	5.15/ 28553	5.14/ 30499	57	7 (21%)	- 2.3	1.01E-03
U14	Heme oxygenase-1 (HO-1) (EC 1.14.99.3)	HMOX1	P09601	Endoplasmic reticulum	Heme catabolic process; response to oxidative stress	6.58/ 21432	7.88/ 32798	92	12 (30%)	5.7	2.50E-06
U15	Peptidylprolyl cis-trans isomerise (Rotamase) (EC 5.2.1.8)	FKBP4	Q02790	Cytoplasm	Chaperone-mediated protein folding	5.57/ 57627	5.35/ 51772	150	29 (39%)	2	4.66E-03
D16	Phosphoglycerate mutase 1 (EC 3.1.3.13)	PGAM1	P18669	Cytoplasm	Glycolytic process	6.65/ 27913	6.67/ 28786	177	8 (22%)	- 2.1	5.50E-03
D17	Glutathione S-transferase omega-1 (EC 2.5.1.18)	GSTO1	P78417	Nucleus	Xenobiotic catabolic process	5.96/ 29777	6.23/ 27548	102	6 (27%)	- 2.6	1.99E-03

Table 4.2 continued.

D18	Catechol O-methyltransferase (EC 2.1.16)	COMT	P21964	Cytoplasm	Neurotransmitter catabolic process	5.11/ 23685	5.26/ 30018	71	14 (38%)	- 2.7	3.32E-05
D19	3'(2'),5'-bisphosphate nucleotidase 1 (PIP) (EC 3.1.3.7)	BPNT1	O95861	Cytoplasm	Phosphatidylinositol phosphorylation	5.74/ 39004	5.46/ 33371	98	3 (7%)	- 2.7	6.94E-03
Protein binding											
D20	Protein canopy homolog 2	CNPY2	Q9Y2B0	Endoplasmic reticulum	Negative regulation of gene expression	4.86/ 17369	4.81/ 18542	61	4 (17%)	- 2.1	8.36E-04
Transcriptional regulatory activity											
D21	Transcription elongation factor B polypeptide 1 (Elongin C)	TCEB1	Q15369	Nucleus	Transcription elongation; protein ubiquitination	4.62/ 12475	4.74/ 12473	100	8 (49%)	- 2.5	7.00E-06
D22	Cellular retinoic acid-binding protein 2 (CRABP-II)	CRABP2	P29373	Cytoplasm	Retinoic acid metabolic process	5.67/ 15042	5.42/ 15683	103	7 (33%)	- 2.4	1.84E-05
Translational regulatory activity											
D23	Eukaryotic translation initiation factor 5A-1 (eIF-5A1)	EIF5A	P63241	Cytoplasm	Translational elongation and termination; apoptotic process	5.67/ 15042	5.08/ 16821	144	8 (40%)	- 2.9	3.98E-04
D24	Elongation factor 2 (EF-2)	EEF2	P13639	Cytoplasm	Translational elongation	5.89/ 37108	6.07/ 38276	214	16 (14%)	- 3.3	1.34E-08

Table 4.2 continued.

D25	Eukaryotic translation initiation factor 3 subunit 1 (eIF-3I)	EIF3I	Q13347	Cytoplasm	Translational initiation	5.7/ 35777	5.83/ 36502	290	17 (37%)	- 2.2	7.76E-05
DNA binding											
U26	UV excision repair protein RA23 homolog B (HR23B)	RAD23B	P54727	Nucleus	DNA damage recognition	4.8/ 47833	4.79/ 43145	54	11 (18%)	2.5	3.22E-06
D27	Chromobox protein homolog 3	CBX3	Q13185	Nucleus	Chromatin remodelling	5.07/ 20023	5.23/ 20680	85	6 (22%)	- 3.4	2.11E-04
RNA binding											
U28	Splicing factor proline/glutamine rich protein (PSF)	SFPQ	P23246	Nucleus	Transcription regulation; mRNA splicing	6.06/ 39817	9.45/ 76102	188	14 (11%)	3.7	8.47E-07
U29	Protein deglycase DJ-1	PARK7	Q99497	Cytoplasm	Protein stabilization	6.01/ 22700	6.33/ 19878	71	5 (19%)	2.1	2.67E-04
Ubiquitin-protein transferase activity											
D30	S-phase kinase-associated protein 1A	SKP1	P63208	Nucleus	Protein ubiquitination; Mitotic cell cycle	4.45/ 18585	4.40/ 18527	68	9 (38%)	-2	5.58E-03
Transporter activity											
D31	ATP synthase subunit d, mitochondrial (ATPase subunit d)	ATP5H	O75947	Mitochondrial membrane	Mitochondrial ATP synthesis coupled protein transport	5.39/ 19990	5.21/ 18479	354	14 (62%)	- 2.3	2.40E-03
D32	Ran-specific GTPase-activating protein (RanBP1)	RANBP1	P43487	Cytoplasm	Signal transduction	5.3/ 26748	5.19/ 23296	135	8 (28%)	- 2	6.01E-05

Table 4.2 continued.

D33	Mitochondrial import receptor subunit TOM22 homolog (hTom22)	TOMM22	Q9NS69	Mitochondrial membrane	Translocation	4.36/ 18040	4.27/ 15512	71	8 (45%)	- 2.7	2.75E-05
Unknown											
U34	Glyoxalase domain-containing protein 4	GLOD4	Q9HC38	Mitochondrion	Unknown	5.39/ 32049	5.40/ 33212	112	15 (40%)	5	8.72E-06
U35	Glutaredoxin-3	GLRX3	O76003	Cytoplasm	Cell redox homeostasis	5.57/ 36505	5.31/ 37408	135	14 (26%)	4.5	6.00E-04

The spot numbers listed here correspond to those in Figure 4.23 and 4.24. The proteins were grouped into 11 functional categories: chaperones, structural/cytoskeletal related proteins, enzymes, protein binding, translation, transcription, DNA repair/binding proteins, RNA binding proteins, ubiquitin proteasome system and transport/cargo proteins. Accession numbers were derived from Swiss-Prot/NCBI database. Mascot score, sequence coverage, number of peptides matched, fold change and *p*-value of the differentially abundant proteins of untreated and treated states are displayed. Abbreviation: no., number; MW, molecular mass; pI, isoelectric point; Exp, experimental; Theo, theoretical; seq, sequence. Theoretical Mr (kDa) and pI was obtained from UniProt Knowledgebase (Swiss-Prot or TrEMBL).

Table 4.3: Summary of Ingenuity Pathway Analysis (IPA)-generated functional pathways which associated with differential expressed proteins identified from MALDI-TOF/TOF mass spectrometry

A.

Top canonical pathways	Ratio	*p*-value	Associated proteins
Protein ubiquitination pathway	7/254	3.98E-07	HSP90AA1, HSPA8, HSPA1A/HSPA1B, HSPA1L, HSPB1, SKP1, TCEB1
Unfolded protein response	4/53	2.89E-06	HSPA8, HSPA1A/HSPA1B, HSPA1L, P4HB
Aldosterone signaling in epithelial cells	5/151	8.84E-06	HSP90AA1, HSPA8, HSPA1A/HSPA1B, HSPA1L, HSPB1
eNOS signaling	4/135	1.17E-04	HSP90AA1, HSPA8, HSPA1A/HSPA1B, HSPA1L
Glucocorticoid receptor signaling	5/272	1.47E-04	FKBP4, HSP90AA1, HSPA8, HSPA1A/HSPA1B, HSPA1L
NRF-2-mediated oxidative stress response	4/177	3.31E-04	ACTG1, CCT7, GSTO1, HMOX1
Aryl Hydrocarbon Receptor Signaling	3/135	2.07E-03	GSTO1, HSP90AA1, HSPB1
Epithelial Adherens Junction Signaling	3/143	2.44E-03	ACTG1, MYL6, TUBB4B
L-DOPA Degradation	1/2	3.76E-03	COMT
Glycine degradation (Creatine Biosynthesis)	1/2	3.76E-03	GAMT
ILK Signaling	3/181	4.73E-03	ACTG1, KRT18, MYL6
Diphthamide Biosynthesis	1/3	5.64E-03	EEF2
Ascorbate Recycling (Cytosolic)	1/3	5.64E-03	GSTO1
Hypusine Biosynthesis	1/3	5.64-03	GSTO1
Hypoxia Signaling in the Cardiovascular System	2/63	6.26E-03	HSP90AA1, P4HB
Remodeling of Epithelial Adherens Junctions	2/66	6.85E-03	ACTG1, TUBB4B
Arsenate Detoxification I (Glutaredoxin)	1/4	7.51E-03	GSTO1
Heme Degradation	1/4	7.51E-03	HMOX1
Rapport-Luebering glycolytic shunt	1/4	7.51E-03	PGAM1
Huntington's Disease Signaling	3/226	8.72E-03	HSPA8, HSPAIA/HSPA1B, HSPA1L
Xenobiotic Metabolism Signaling	3/256	1.22E-02	GSTO1, HMOX1, HSP90AA1
Death receptor signaling	2/91	1.27E-02	ACTG1, HSPB1
Fcγ Receptor-mediated Phagocytosis in Macrophages and Monocytes	2/93	1.32E-02	ACTG1, HMOX1
Antioxidant Action of Vitamin C	2/95	1.38E-02	GSTO1, HMOX1
HIFα signaling	2/100	1.52E-02	HSP90AA1, TCEB1
RhoA signaling	2/120	2.14E-02	ACTG1, MYL6
Cellular Effects of Sildenafil (Viagra)	2/124	2.28E-02	ACTG1, MYL6
Choline Biosynthesis III	1/13	2.42E-02	HMOX1
Vitamin-C Transport	1/14	2.61E-02	GSTO1
RAN signaling	1/16	2.97E-02	RANBP1
Parkinson's Signaling	1/16	2.97E-02	PARK7
Gap Junction Signaling	2/151	3.28E-02	ACTG1, TUBB4B

Table 4.3 (A) continued.

D-myo-inositol (1,4,5)-trisphosphate Degradation	1/18	3.34E-02	BPNT1
Germ Cell-Sertoli Cell Junction Signaling	2/156	3.48E-02	ACTG1, TUBB4B
Mitochondrial dysfunction	2/165	3.85E-02	ATP5H, PARK7
Dopamine Degradation	1/21	3.88E-02	COMT
Tight Junction Signaling	2/166	3.89E-02	ACTG1, MYL6
Acute Phase Response Signaling	2/168	3.98E-02	CRABP1, HMOX1
RhoGDI signaling	2/172	4.15E-02	ACTG1, MYL6
Sertoli Cell-Sertoli Cell Junction Signaling	2/173	4.20E-02	ACTG1, TUBB4B
Agranulocyte Adhesion and Diapedesis	2/175	4.28E-02	ACTG1, MYL6
Glutathione-mediated detoxification	1/24	4.43E-02	GSTO1
Superpathway of D-myo-inositol (1,4,5)-trisphosphate Metabolism	1/24	4.43E-02	BPNT1
Glycolysis 1	1/24	4.43E-03	PGAM1
mTOR signaling	2/182	4.6E-02	EIF3I, HMOX1
Gluconeogenesis 1	1/25	1.67E-03	PGAM1
Clathrin-mediated Endocytosis Signaling	2/184	4.69E-02	ACTG1, HSPA8
Antiproliferative Role of TOB in T Cell Signaling	1/26	4.79E-02	SKP1

B.

Molecular and cellular functions	No. of molecules	*p*-value	Associated proteins
Post-Translational modification	8	1.15E-02 – 1.73E-06	HSP90AA1, HSPA1L, HSPA8, FKBP4, P4HB, PARK7, SKP1, TCEB1
Protein folding	4	3.36E-06 – 1.73E-06	HSP90AA1, HSPA1L, HSPA8,FKBP4
Cell death and survival	14	4.35E-02 – 1.97E-05	CNPY2, CRABP2, DCK,HMOX1, HSPA1A/HSPA1B, HSPA8, HSPB1, KRT18, P4HB, PARK7, RAD23B, SFPQ, TCEB1, HOMX1
Protein synthesis	5	4.62E-03 – 2.20E-04	EEF2, EIF3I, HSPA1A/HSPA1B, HSPB1, PARK7
Amino acid metabolism	2	3.76E-03 – 1.88E-03	P4HB, GAMT

Table 4.3 continued.

C.

Top networks	Focus molecules	Score	Associated proteins
Cell death and survival, cell cycle, cellular growth and proliferation	29	55	ACTA2, **ACTG1**, ADRBK2, AGTR1, AIP, ALKBH8, ANGPT2, ATR, BAG2, BAG4, BAG6, C8orf44-SGK3/SGK3, CALD1, CARM1, CASP7, **CBX3**, CCNC, CCND1, CCT5, **CCT7**, CCT6A, CDC25A, CDC37L1, CEBPB,CNPY2, **COMT**, **CRABP2**, CTBP1-AS2, CUL2, CUL5, CUL7, CXCL1, CXCL3, CXCR3, DNAJB11, DSN1, E2F1, **EEF2**, EGLN1, **EIF3I**, **EIF5A**, ENG,EPS8, ESR1, estrogen receptor, nFAF1, FAM76B, FBXO7, FBXO18, FBXW8, FGF1, **FKBP4**, GJB2, GORASP2, **GSTO1**, HGF, **HMOX1**, HNRNPA1, HNRNPD, Hsp90, **HSP90AA1**, **HSPA8**, **HSPA1A/HSPA1B**, **HSPA1L**, **HSPB1**, **HSPB8**, HSPD1, ID1, ID3, ILF3, ITGB3, JUND, KCNH2, KDM5A, KDR, KRT8, KRT14, **KRT18**, KRT19, LDLR, LGALS3, LIMA1, METTL21A, MIF, **MYL6**, NONO, NOTCH1, NPC1, P38 MAPK, **P4HB**, PACRG, **PARK7**, PECAM1, PES1, **PGAM1**, PRKCE, PRKCI, PRMT1, PTGES3, **RAD23B**, **RANBP1**, RCOR1, REV1, RFWD2, RPL5, SERBP1, SERPINB5, SFN, **SFPQ**, **SKP1**, SKP2, SLC6A4, SMARCA4, SMYD3, SNAI1, SNRNP70, SRA1, STIP1, STK17A, STUB1, TAF5, TAGLN, **TCEB1**, TFAP2C, TGFB2, THBS1, thymidine kinase, TIAL1, **TOMM22**, TOP1, TOPBP1, TP53, TRADD, TUBA1C, **TUBB4B**, TYMP, UXT, WISP2, YWHAG, ZEB1
Cellular Function and maintenance, small molecule biochemistry, molecular transport	1	2	ACO1, Ferritin, **GLRX3**, TFRC

Gene names in bold are "focus genes" identified in this experiment and are served to identify other associated molecules in hypothetical networks constructed by IPA. The statistically significant top networks are identified by IPA.

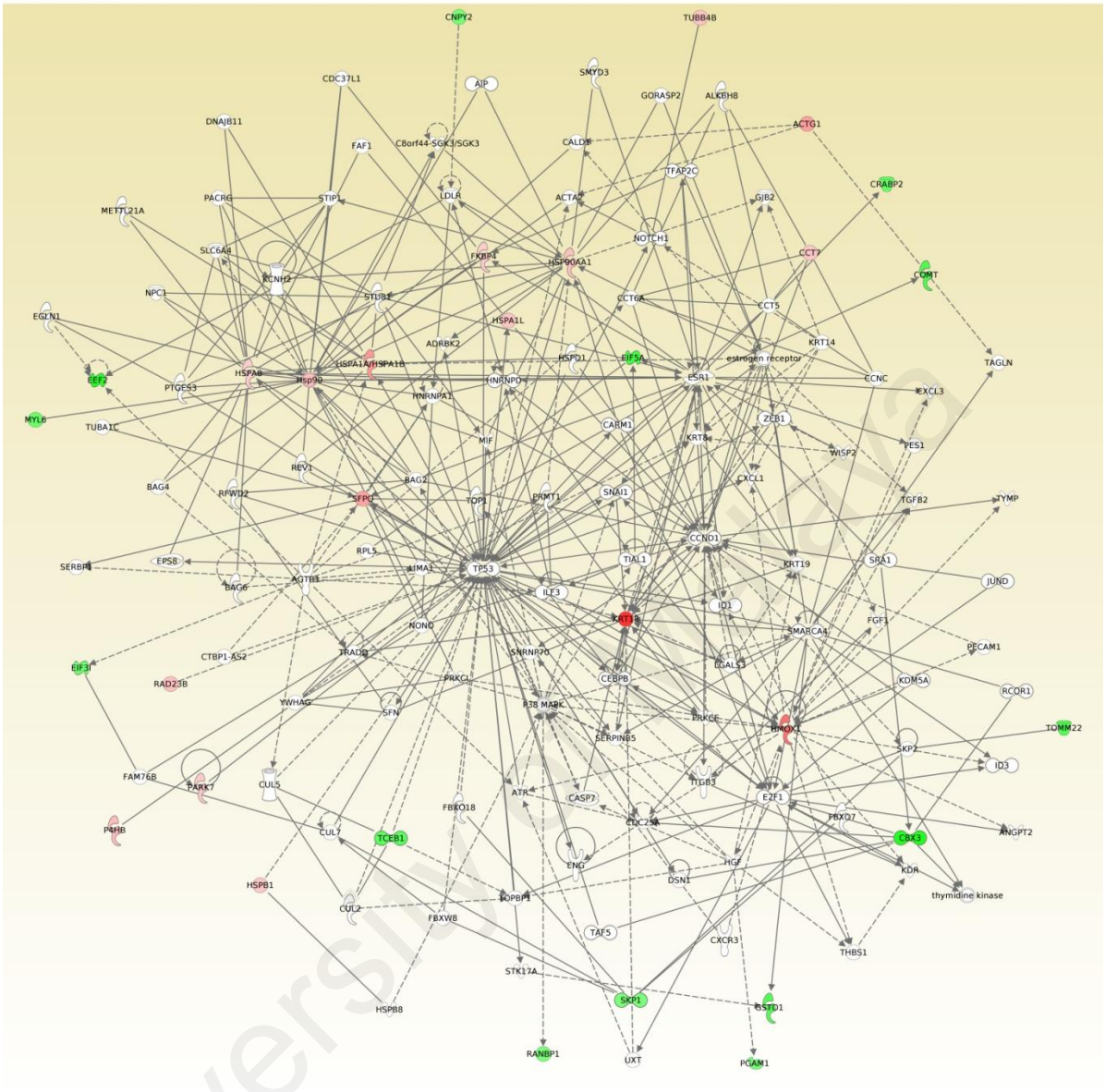

Legends:

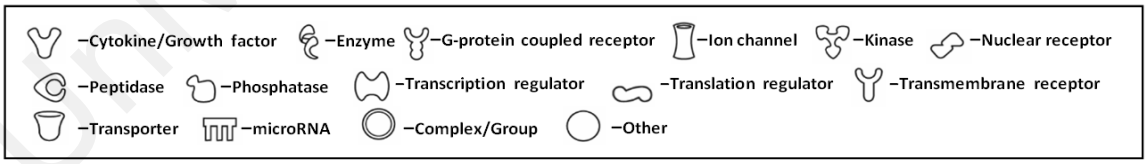

Figure 4.26: Significant signaling pathway networks by IPA analysis. IPA was used to analyze the protein-protein interactions and protein networks relevant to cancer and cell death. The solid lines denote a robust correlation with partner proteins while dashed lines indicate statistically significant but less frequent correlations. The protein-protein interactions are indicated by arrows. The red color represents upregulated proteins whereas the downregulated proteins are shown in green. The un-colored nodes indicate additional proteins of this network that were not spotted by the proteomics analysis. The IPA legend defining the symbols depicted in IPA networks is given in the inset. A curved line means intracellular translocation; a curved arrow means extracellular translocation.

A.

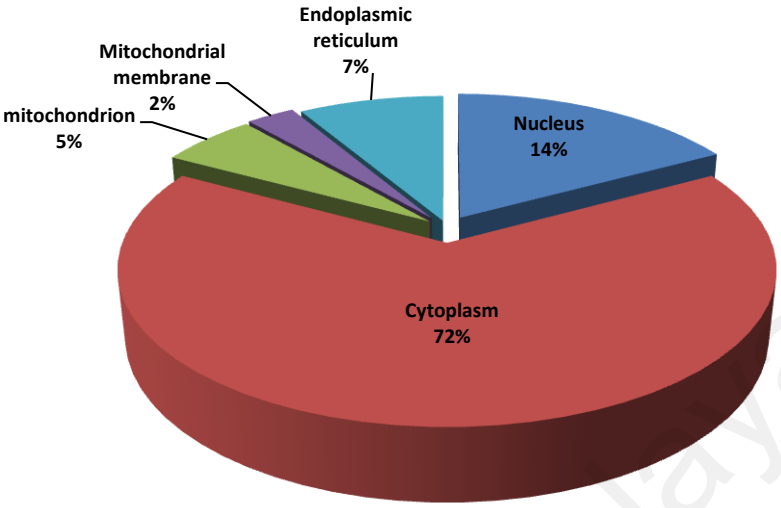

B.

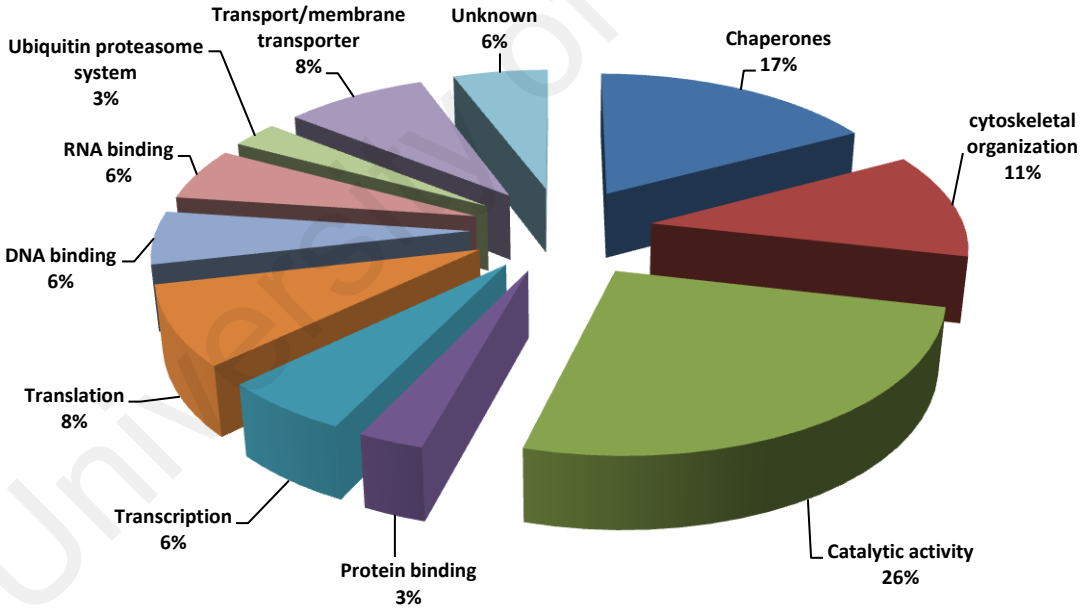

Figure 4.27: Functional classification and subcellular localization of differentially abundant proteins based on bioinformatics. Categorization of the identified differentially abundant proteins in HCT 116 cells following FKC treatment was analyzed based on the UniProt annotations and Human Protein Reference Database (HPRD). Molecular function (A) and subcellular localization (B) of the corresponding identified proteins were classified.

4.18 *In vivo* studies: nude mice model

4.18.1 Effect of FKC on the tumor growth in nude mice bearing HCT 116 colon carcinoma tumor.

To determine the *in vivo* anti-cancer activity of FKC in HCT 116 colon cells, we established HCT 116 cells xenografts nude mice model. The mice were given intraperitoneal administration of FKC at the doses of 1 and 3 mg/kg thrice weekly or vehicle solution for 19 days.

All tumors were harvested at the end of the study and representative tumors are shown in Figure 4.28B. In comparison to the control group, FKC treatment decreased the rate of tumor growth throughout the study (Figure 4.28A). At the end of experiment, the average tumor volume (mean±SD) in the control group had grown greater than 900% of the original size (84.67±17.32 to 859.99±93.04 mm^3), whereas for the low dose (1mg/kg) of FKC-treated group was 600% of their original size (84.48±10.48 to 658.19±115.18 mm^3) and high dose (3mg/kg) of FKC-treated group was 300% of their original size (86.56±18.55 to 411.31±95.82 mm^3).

Drug treatment efficacy was evaluated based on tumor volume inhibition (%T/C) (Figure 4.28C). There was a reduction of 18.73 to 23.99% and 23.43 to 52.17% in tumor volume following the treatment of 1 mg/kg and 3mg/kg, respectively from day 3 to 19 of treatment. It was apparent from these results that FKC could effectively suppress or delay the tumorigenicity of HCT 116 colon carcinoma *in vivo.*

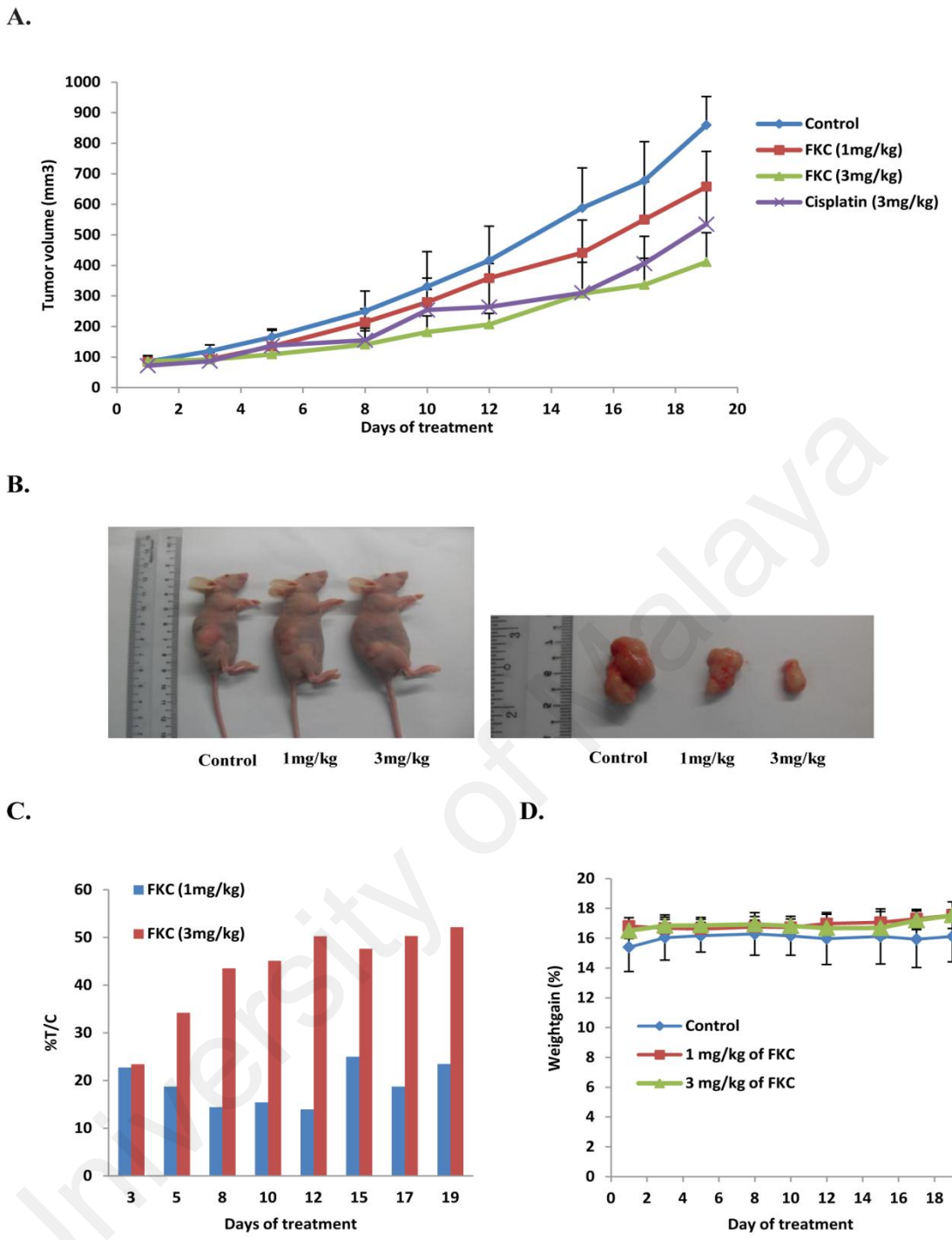

Figure 4.28: Inhibitory effect of FKC on the growth of HCT 116 tumor xenografts in Balb/c nude mice. (A) Balb/c nude mice were first subcutaneously injected with HCT 116 cells to establish tumor xenograft. Once the tumor size reached 75–150 mm^3, the mice were then administrated intraperitoneally with 1 and 3 mg/kg of FKC or vehicle solution for 19 days. The tumor volume of the mice was measured thrice weekly. After 19 days of treatment, the mice were sacrificed and the tumor excised. Values given are expressed as mean±standard deviation (SD) (n=5 per group). (B) Representative photographs of mice from control and treatment groups, and the excised tumors from each group at 19 days of treatment. (C) The bar chart shows the percentage of mean tumor inhibition (%T/C) by FKC at 1 mg/kg and 3 mg/kg in comparison to control group at the indicated day of treatment. D. Body weight of the mice from control and treatment group for 19 days. Values given are expressed as mean±SD.

4.18.2 Toxicity evaluation of FKC in nude mice

To further evaluate whether treatment of FKC in tumor-bearing nude mice for 19 days could affect the vital organs, detailed histological examinations on organs harvested at the end of study was performed. Heart, kidney, liver, lung and spleen in FKC-treated mice did not show any obvious pathological abnormalities when compared to those in the healthy normal and vehicle-treated mice except there are slight fatty changes in the liver tissues treated with 3 mg/kg of FKC (Figure 4.29 & 4.30). In terms of body weight, all mice appeared to be healthy and there was no obvious sign or symptom of drug toxicity throughout the study. There was no serious weight loss in the FKC-treated groups throughout the study (Figure 4.28D).

In addition, analysis of liver function (AST, ALT and ALP) and kidney function (creatinine and urea nitrogen) in serum collected from the three groups (control, 1mg/kg and 3mg/kg) were compared to the normal healthy mice. All values were found within the normal limits in the three groups (Figure 4.31) except a significant increase in the level of urea in control and 1 mg/kg of FKC were observed. The data show that FKC treatment at the dose of 1 and 3 mg/kg did not cause serious damage to the organs and abnormal physiological vital functions in the mice.

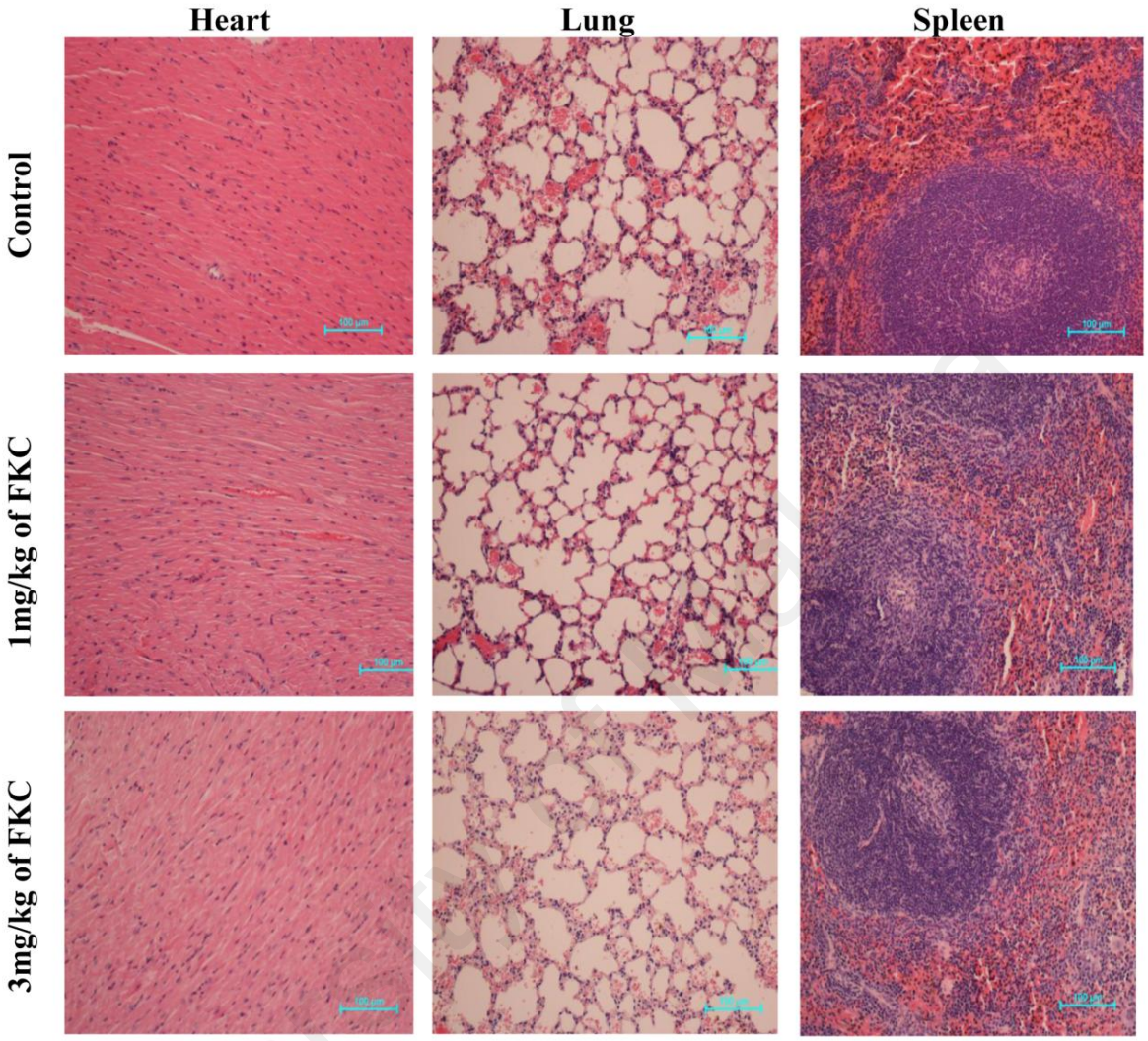

Figure 4.29: Effects of FKC on the histology of heart, lung and spleen in nude mice treated with or without FKC. Heart, lung and spleen were collected from nude mice bearing HCT 116 tumor xenograft treated with vehicle (Control) and FKC (1mg/kg and 3mg/kg). Sections of heart, lung and spleen were stained with hemotoxylin and eosin (H&E) for the analysis of tissue morphology. The pictures were captured at ×20 magnification and the bars represent 100µm. H&E analysis shows that all organs did not show any obvious pathological abnormalities compared to those in the vehicle-treated mice (control).

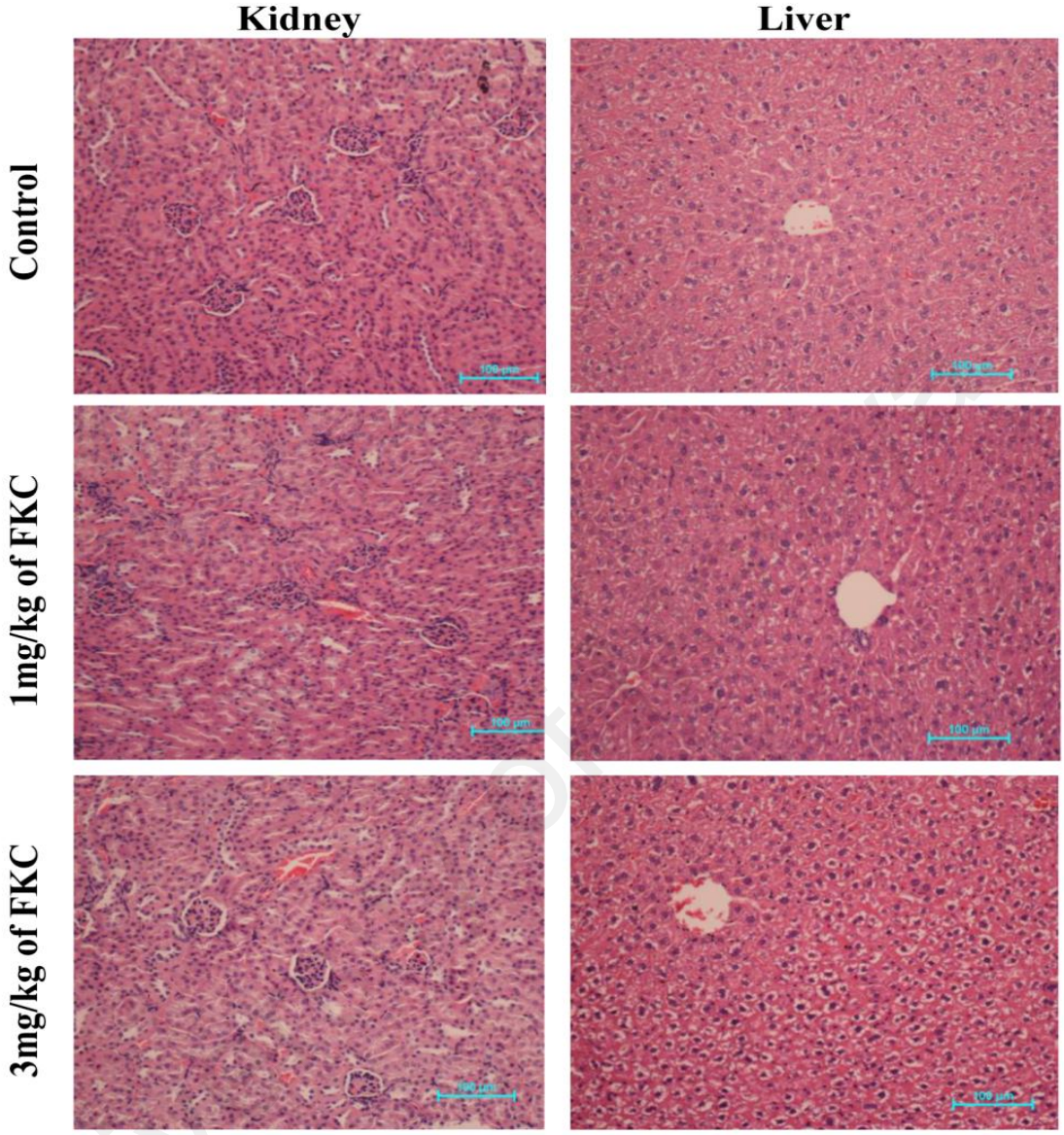

Figure 4.30: Effects of FKC on the histology of kidney and liver in nude mice treated with or without FKC. Kidney and liver were collected from nude mice bearing HCT 116 tumor xenograft treated with vehicle (Control) and FKC (1 mg/kg and 3 mg/kg). Sections of kidney and liver were stained with hemotoxylin and eosin (H&E) for the analysis of tissue morphology. The pictures were captured at ×20 magnification and the bars represent 100 µm. H&E analysis shows that all organs did not show any obvious pathological abnormalities compared to those in the vehicle-treated mice (Control) except there are slight fatty changes in liver tissues treated 3mg/kg of FKC.

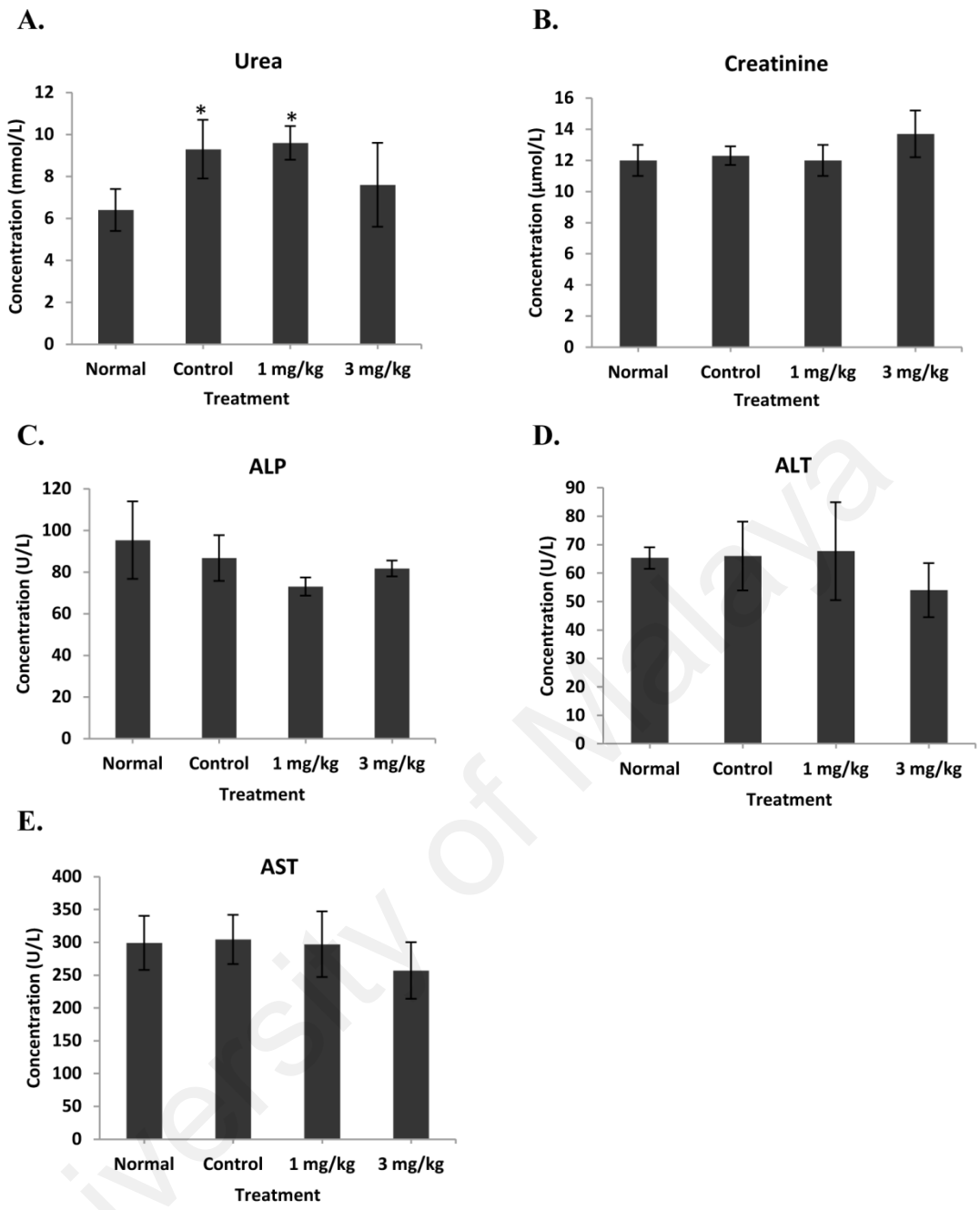

Figure 4.31: Effect of FKC on the serum biochemical parameters in mice bearing HCT 116 tumor treated with and without FKC in comparison to healthy normal nude mice. The concentration of (A) urea, (B) creatinine, (C) alkaline phosphatase (ALP), (D) alanine aminotransferase (ALT) and (E) asparate aminotransferase (AST) was determined in the serum. The analysis showed no significant difference in blood parameters in control and treated groups (1 mg/kg and 3 mg/kg) in comparison to normal group except a significant increase was observed in urea levels in the control and 1mg/kg of FKC. Data given are mean±standard deviation (SD) of three biological replicates. The asterisk (*) indicated $p<0.05$ when compared to the normal group.

4.18.3 Evaluation of induction of apoptosis by FKC in colon tumor tissues

To determine whether FKC-mediated tumor size reduction is associated with induction of apoptosis, we examined the DNA fragmentation in these tumor tissues by H&E staining and TUNEL assay. Figure 4.32 shows the representative tumor sections stained with H&E and TUNEL analysis. H&E staining showed substantially increased necrosis in FKC-treated tumors compared to that of the vehicle-treated tumors. The TUNEL results showed that a greater number of TUNEL-positive cells were observed in the FKC-treated tumors while the vehicle-treated tumors exhibited few and dispersed TUNEL-positive cells. To further clarify that FKC-induced cell death was via apoptosis, we measured the expression of cleaved caspase-3 by immunohistochemistry. The results showed there were a higher number of cleaved caspase-3 positive cells to those of the FKC-treated tumors compared to those found in the vehicle-treated tumors (Figure 4.33).

4.18.4 Evaluation of expression of Ki67 in colon tumor tissues

To determine whether the reduction in tumor growth following FKC treatment was associated with decreased cell proliferation, IHC analysis of Ki67 was performed on the paraffin-embedded tumor tissues from the control and FKC-treated groups. Figure 4.33 shows the representative tumor section of the treated and untreated groups. IHC analysis showed a lower level of expression of Ki67 was observed in the FKC-treated tumor compared to those found in vehicle-treated tumor, indicating that less number of cells were proliferating under FKC treatment. The results indicated FKC has the ability to restrict the colon tumor growth by inhibiting the cell proliferation.

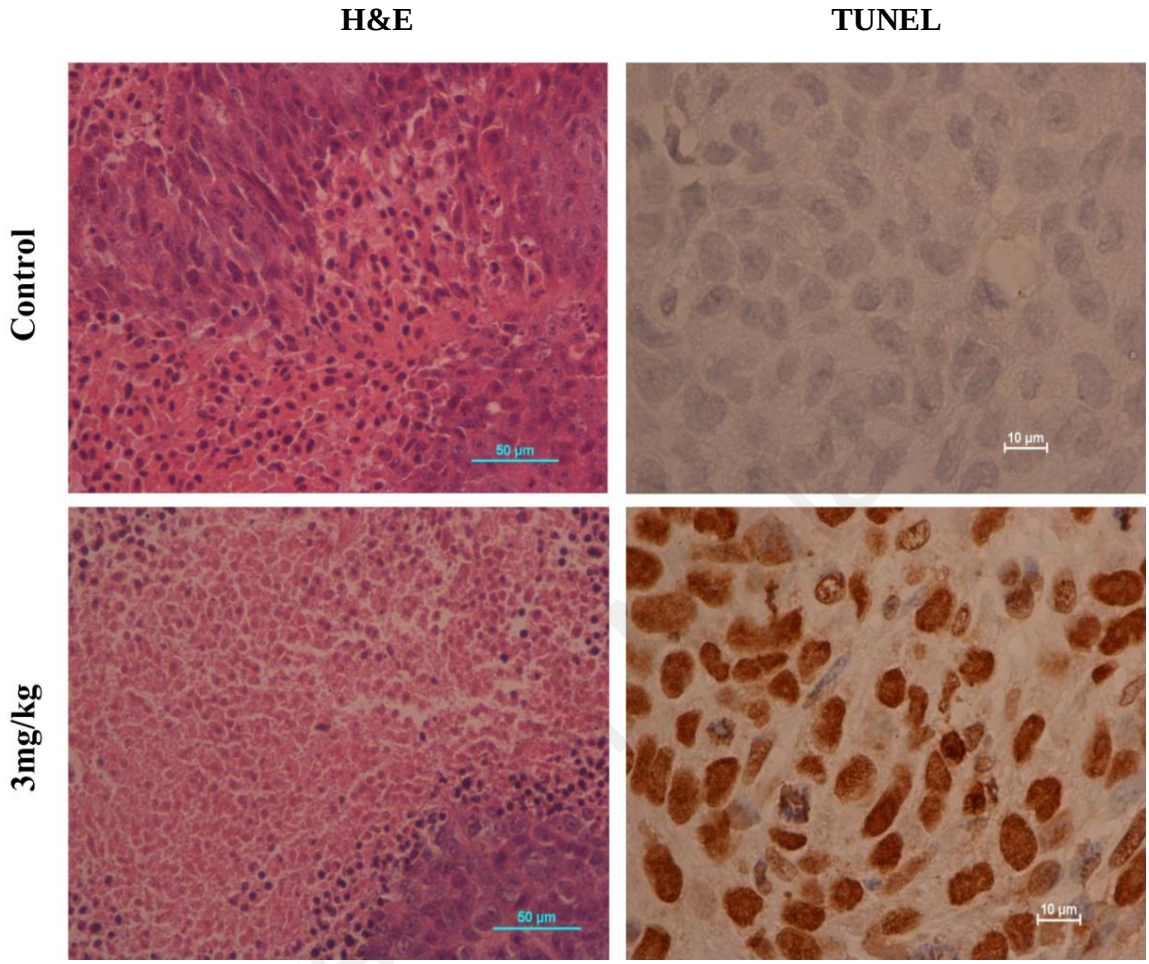

Figure 4.32: Effects of FKC on the tumors and and DNA fragmentation in the tumor tissues. H&E staining and detection of DNA fragmentation in the isolated subcutaneous HCT 116 tumor tissues from control and treated (3 mg/kg) groups are shown. H&E analysis showed an increase in the number of necrosis cells and TUNEL assay showed an increase in TUNEL-positive cells (stained dark brown) in FKC-treated tumor compared to control. Magnification at 40× for H&E and 100× for TUNEL.

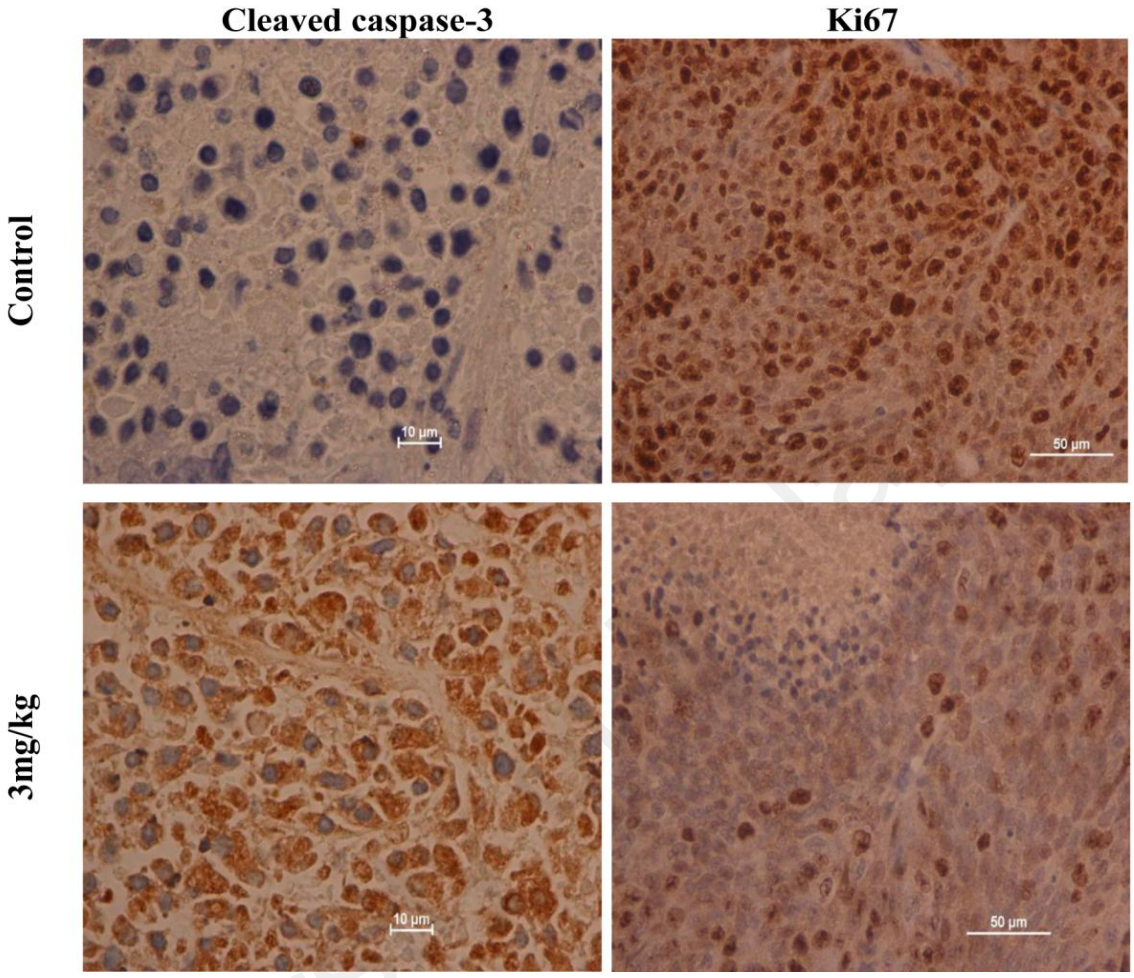

Figure 4.33. **Effects of FKC on the expression of cleaved caspase-3 and Ki67 in the tumor tissues.** IHC analysis of cleaved caspase-3 and Ki-67 expressions in the isolated subcutaneous HCT 116 tumor tissues from control and treated (3 mg/kg) groups are shown. IHC analysis showed an increased in cleaved caspase-3-positive cells while a decrease in Ki67-positive cells in FKC-treated tumor compared to control. Magnification at 100× for cleaved caspase-3 and 40× for Ki67.

4.18.5 2-DE analysis and identification of differentially abundant proteins in sera

To search for serum biomarkers associated with colon carcinoma and response to FKC treatment, serum samples from the healthy nude mice (normal group) and nude mice bearing HCT 116 tumor xenografts following treatment by vehicle solution (control group) and FKC (3 mg/kg) (treated group) were collected and the serum protein profiles were compared by 2-DE.

As shown in Figure 4.34 (A), (B) and (C), the overall protein abundance pattern between these three groups was almost similar. After data processing by progenesis software and MALDI-TOF/TOF-mass spectrometry, five differentially abundant proteins were identified (Table 4.4 and Figure 4.34) which were Ig mu chain C (secreted form) (IgM), hemopexin precursor (hemopexin), kininogen-1 precursor (kininigen-1), 78kDa glucose-regulated protein precursor (GRP78) and apolipoprotein E precursor (ApoE). These proteins showed significantly different expressions between the three groups ($p<0.05$) and the ratio of expression levels was >1.5. Among the five proteins, IgM was up-regulated after FKC treatment whereas the other four proteins were found to be up-regulated in the control groups and down-regulated following the FKC treatment or returned to the levels as in the normal groups.

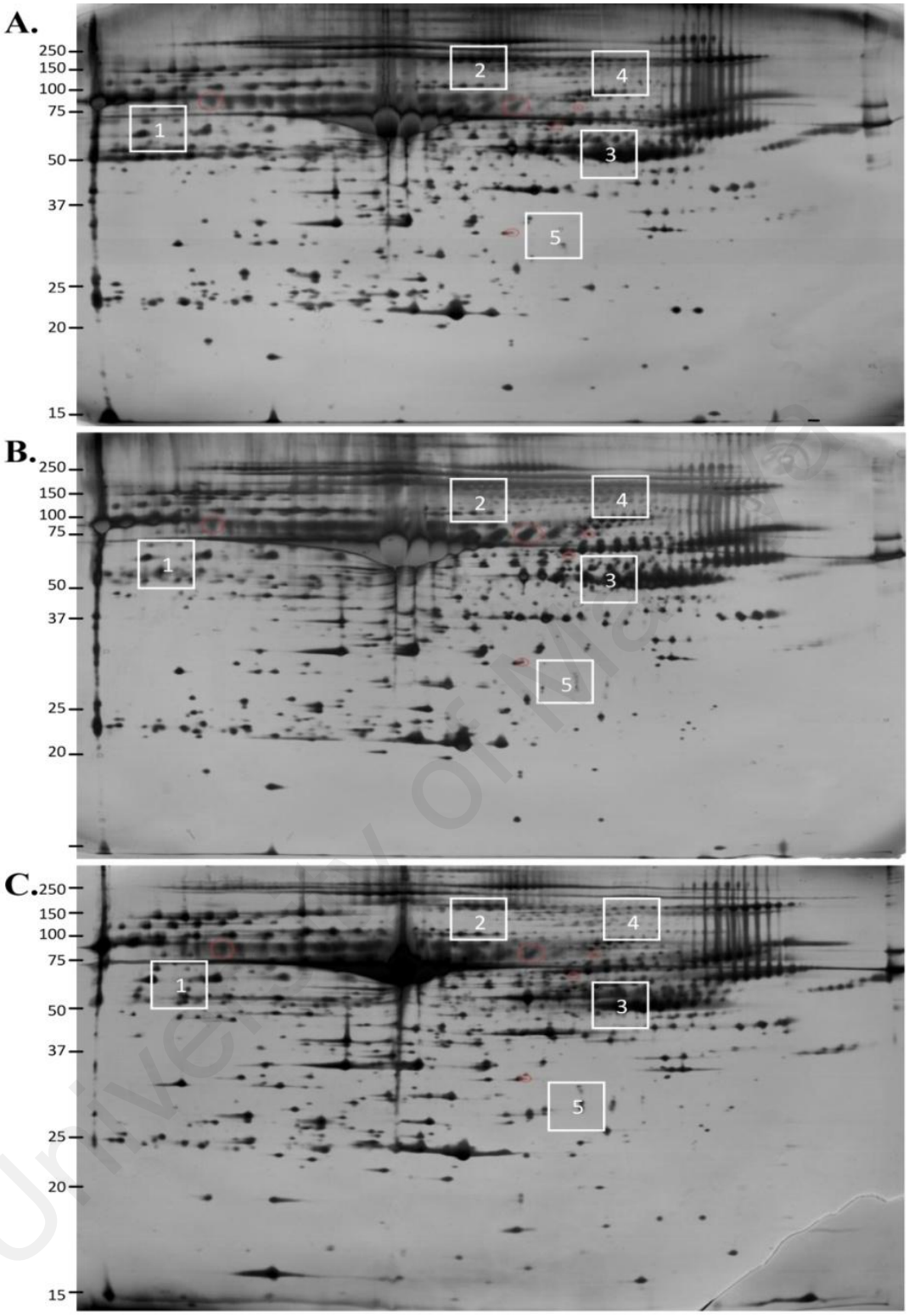

Figure 4.34: Representative of 2DE gel images of serum proteins of the healthy nude mice and nude mice bearing HCT 116 tumor. Serum proteins (125µg) were separated using 24-cm linear IPG strip (pH 4-7) and 11% SDS-PAGE, and were detected by silver staining. (A) Representative 2D gel picture from the normal healthy nude mice; (B) and (C) Representative 2D gel picture from the nude mice bearing HCT 116 tumor xenografts following the treatment with vehicle solution and FKC (3mg/kg), respectively. Five differentially abundant proteins as identified by Progenesis 2D image analysis software are circled in red on the gels and are numbered in white boxes. Four biological replicate per group were used in the analysis. Each spot is numbered corresponds to the Spot number in Table 4.4.

Figure 4.35

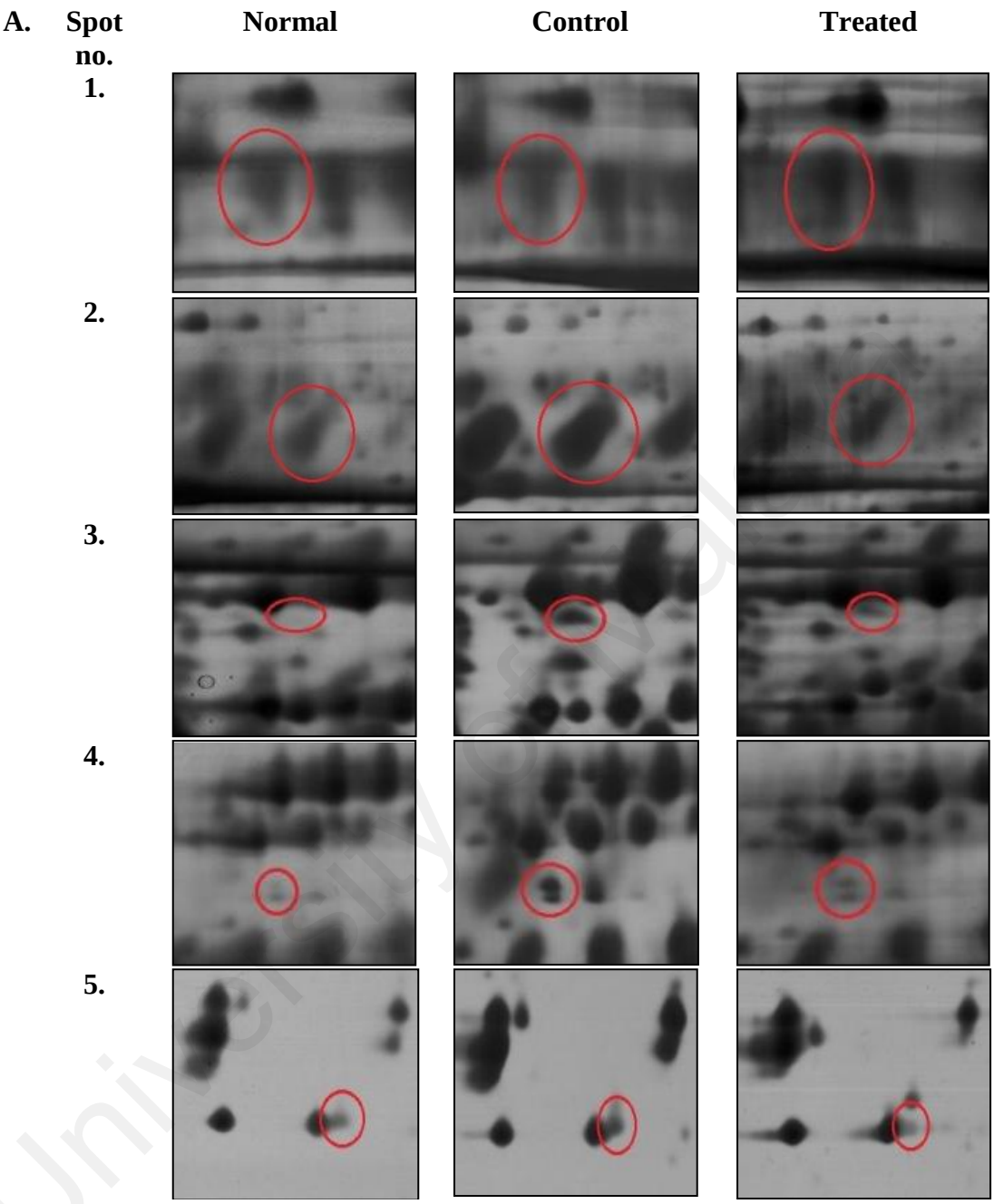

Figure 4.35 continued.

B. Spot no. **Average normalized volumes**

1.

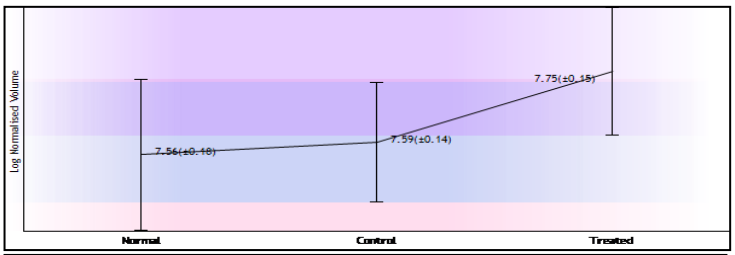

2.

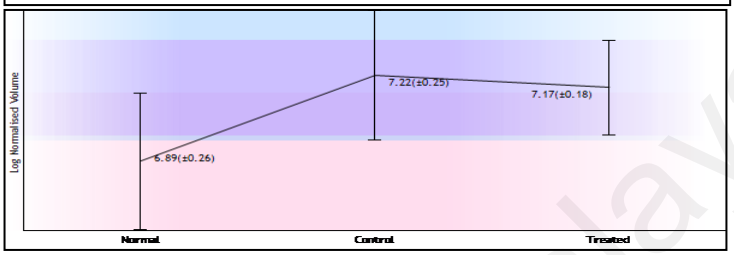

3.

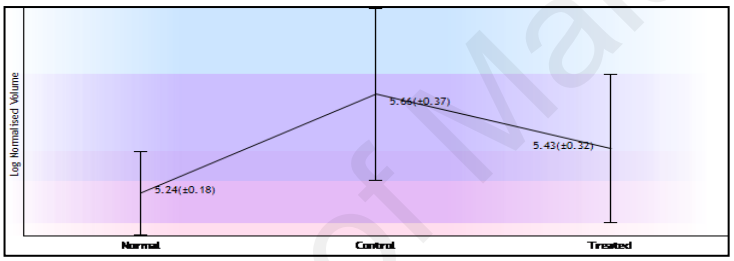

4.

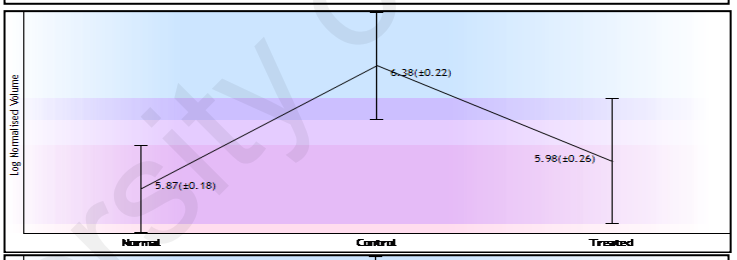

5.

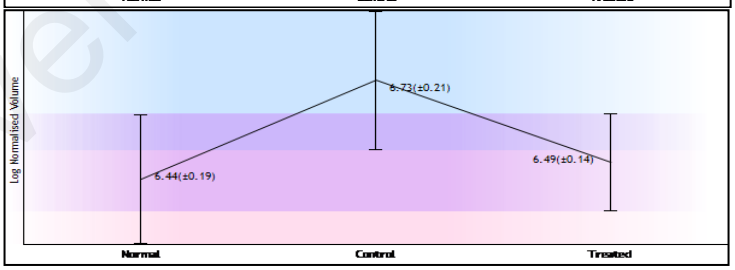

Figure 4.35: Magnification 2DE images of six proteins from the 2D-PAGE presented in Figure 4.34 and comparison between their average normalized volumes. (A) Representative of the magnification 2DE gels picture of the five protein spots corresponding to spot 1, 2, 3, 4 and 5 presented in Figure 1 from the group of normal healthy nude mice (Normal) and nude mice bearing HCT 116 tumor xenografts following the treatment of vehicle solution (Control) and FKC (3 mg/kg) (Treatment). (B) The graphs showing the comparison between the average normalized volume of each spots from the normal, control and treatment groups. The data of the differentially abundant spot proteins were quantified by Progenesis 2D image analysis software. The spot's volumes are expressed as mean of log normalized spot's volume±standard deviation of normalized volume of total spots.

Table 4.4: List of proteins identified by MALDI TOF/TOF-MS/MS that are differentially abundance between normal healthy nude mice (Normal), and nude mice bearing HCT 116 tumor xenograft following the treatment of vehicle solution (Control) and FKC (3mg/kg) (Treated).

Spot No.	Protein name	Gene symbol	Entry number	Accession number	pI/MW		Score	Peptides matched (% Cov)	Fold change (Anova *p*-value)	Log average normalized volumes		
					Theo.	Exp.				Normal	Control	Treated
1	Ig mu chain C region secreted form (IgM)	Ighm	MUC_MOUSE	P01872	6.56/ 50625	4.44/ 79	210	12 (18)	1.5 (0.038)	6.42±0.24	6.43±0.21	6.74±0.38
2	Hemopexin precursor	Hpx	HEMO_MOUSE	Q91X72	7.92/ 52049	5.59/ 71	231	16 (21)	2.1 (0.014)	6.89±0.26	7.22±0.25	7.17±0.18
3	Kininogen-1 precursor	Kng1	KNG1_MOUSE	O08677	6.05/ 74140	5.75/ 62	92	4 (2)	3.3 (0.021)	5.24±018	5.66±0.37	5.43±0.32
4	78 kDa glucose-regulated protein precursor (GRP 78)	HSPA5	GRP78_HUMAN	P11021	5.07/ 72402	5.83/ 71	127	16 (16)	3.3 (1.664E-004)	5.87±0.18	6.38±0.22	5.98±0.26
5	Apolipoprotein E precursor (Apo-E)	Apoe	APOE_MOUSE	P08226	5.56/ 35901	5.59/ 34	71	9 (20)	2.0 (0.006)	6.44±0.19	6.73±0.21	6.49±0.14

The spot numbers listed here correspond to those in Figure 4.34 and 4.35. Gene name, Accession number and Entry number were obtained from UniProtKB/Swiss-Prot; Score: Mascot MOWSE-score; MW and pI: Theoretical molecular mass (Da) and theoretical isoelectric point taken from the Mascot report. The values of log average normalized volume±standard deviation for each protein spots were calculated by Progenesis software. Abbreviation: seq, sequence; % Cov, percentage of coverage.

CHAPTER 5: DISCUSSION

5.1 FKC exerts cytotoxicity against human cancer cell lines and more potent against HCT 116 cell lines

In the present study, the potential growth inhibitory and apoptosis-inducing effect of FKC on human cancer cell lines was explored. Human cancer cell lines have been widely used as a model in the development of new anti-cancer drugs and in investigating the cellular signaling pathways targeted by chemotherapeutic drugs in cancer cells. Cytotoxic screening models provide important preliminary data on the anti-cancer potential of compounds. Based on the SRB assay, FKC selectively inhibits the viability of HCT 116 colon carcinoma cells in comparison with other tested cell lines while showing less cytotoxicity towards normal colon cells (CCD-18Co).

5.2 FKC exerts cell death in colon cancer cells via apoptosis

Apoptosis is defined by typical morphological and biochemical hallmarks (Hengartner, 2000). Exposure of PS on the surface of apoptotic cells is a common marker for apoptosis and serve as a recognition signal for engulfment by phagocytes such as macrophages and dendritic cells and by their neighboring cells (Elliott & Ravichandran, 2010). Internucleosomal DNA fragmentation which is one of the last stages of apoptosis resulted from the cleavage of ICAD (inhibitor of caspase-activated DNase) by caspase-3. The activated CAD (caspase-activated DNase) is released from ICAD and cut the internucleosomal regions into double-stranded fragments of 180 to 200 base pairs (Darzynkiewicz *et al.*, 2008). Another key hallmark which is the activation of caspases, a family of cysteine proteases that act as common death effector molecules in apoptosis that cleaves a number of different substrates such as PARP-1 and results in many morphological features of apoptotic cell death (Fulda & Debatin, 2006).

Two types of colon cancer cells, HCT 116 and HT-29 cell lines were selected for the investigation of apoptosis-inducing activity of FKC. Based on the microscopic and flow cytometric analysis, both cell lines showed typical morphological hallmark of apoptosis such as cell shrinkage, membrane blebbing and chromatin condensation/fragmentation. Associated biochemical hallmark includes a significant phosphatidylserine translocation, DNA fragmentation, activation of caspases and cleavage of PARP-1.

However, the results in the DNA fragmentation and activation of caspases are different for HCT 116 and HT-29 cells upon FKC treatment. In the TUNEL assay, a low amount cells with DNA fragmentation was observed in HT-29 cells compared to HCT 116 cells and a clear increase in DNA fragmentation was only observed at 80µM of FKC treatment. Although both cell lines showed the cleavage of PARP-1 in the western blot analysis, the flow cytometric analysis of activation of caspases showed there was a lower increment in the levels of caspase-3, -8 and -9 in HT-29 cells in comparison to HCT 116 cells upon FKC treatment. The reasons for the differences in both results between two cell lines might be due to their p53 status where HCT 116 cells possess wild type p53 and those in HT-29 cells are of the mutated. Taken together, this might be implicated in the lower cytotoxicty in HT-29 cells in comparison to HCT 116 cells after FKC treatment. It is suggested that the FKC treated HT-29 cells might have undergone cell death via other mechanisms.

5.3 Structure-activity relationship of FKC in comparison FKA and FKB for apoptotic activity in cancer

In order to evaluate whether slight variations in the structure of FKC play an important role in cytotoxic and apoptotic activity, the effect of GMM (substitution at C-2’ and C-4, as shown in Figure 2.2) was investigated. Figure 3.1 show differences in the substitution at position C-2’ and C-4. FKC has a methoxyl group at C-2’ and a hydroxyl

group at C-4 whilst GMM has a hydroxyl and methoxyl substituents at C-2' and C-4 respectively. This change resulted in the absence of cytotoxic effect in both cell lines (IC_{50} > 300 µM) for GMM. Thus, this suggested that reversing the substituents as in FKC resulted in pronounced cytotoxic activity of FKC in the HCT 116 cells. Based on previous studies, replacement of hydroxyl group at C-6' of GMM with a methoxyl substituent as in flavokawain A (FKA) (Figure 2.2) resulted in pronounced cytotoxicity and FKA was able to induce apoptosis in bladder cells (Zi & Simoneau, 2005). The absence of a functional group at aromatic ring B in FKB did not affect its apoptotic activity as FKB has been previously reported to cause cytotoxicity and induced apoptosis in HCT 116 cells (Kuo *et al.*, 2010; Malek *et al.*, 2011). Taken together, these results suggested that the cytotoxic and apoptotic activities of chalcones are clearly dependent on its molecular structure. Further work to understand the structure-activity relationship of this class of compounds is required.

5.4 FKC increases mitochondrial membrane permeability and release of apoptotic factors to the cytosol through modulation of Bcl-2 proteins

In the intrinsic apoptotic pathway, the signals leading to cell death typically originates from within the cell itself. The mitochondria play a major role in the initiation and execution of the intrinsic pathway of apoptosis (Harris & Thompson, 2000; Zeestraten *et al.*, 2013). Bcl-2 family members are key regulators involved in controlling permeability of the mitochondrial outer membrane permeabilization. This causes leakage of apoptogenic proteins such as cytochrome c and other mitochondrial apoptotic factors like Smac/DIABLO, AIF and endoglycosidase G into the cytosol. Released cytochrome c binds to Apaf-1and pro-caspase-9 to form the apoptosome, which in turn activates caspase-9.

In general, Bcl-2 related proteins are categorized into two groups: anti-apoptotic proteins (Bcl-2 and Bcl-xL), pro-apoptotic proteins (Bax, Bak and Bid) (Lindsay *et al.*, 2011). During apoptosis, Bax and Bak are known to be responsible for promoting mitochondrial outer membrane permeabilization by oligomerizing to form pores within the outer mitochondria membrane (Lindsay *et al.*, 2011). On other hand, Bcl-2 and Bcl-xL acts as the inhibitor of apoptosis by binding with pro-apoptotic proteins of the bcl-2 family and thus antagonizing them (Tamm *et al.*, 2001). Therefore, they limit permeabilization of the mitochondrial outer membrane and maintain the mitochondria membrane potential by inhibiting pore formation (Harris & Thompson, 2000; Jain *et al.*, 2013). In addition, Bcl-xL can interact with Apaf-1 and inhibit the activation of capase-9 (Hu *et al.*, 1998).

Western blot analysis showed that FKC caused a downregulation of Bcl-xL and an increase in the amount of Bak (Figure 4.14) in HCT 116 cells which may have caused a disruption in the integrity of the outer mitochondria membrane by increasing its permeability. A previous study reported that Bak deficiency can lead to substantial inhibition of mitochondrial-mediated apoptotic cell death (Indran *et al.*, 2011). The western blot analysis in both mitochondrial and cytosol fractions in HCT 116 cells demonstrated a gradual increase in the level of Bax in the mitochondrial fraction while a gradual increase in the levels of cytochrome c, AIF and Smac/DIABLO in the cytosol fraction upon FKC treatment. The results suggested that FKC causes the release of cytochrome c, AIF and Smac/DIABO from the mitochondria into the cytosol. AIF which is normally present in the mitochondria will translocate into the nucleus following release from the mitochondria where it induces caspase-independent chromatin condensation and DNA fragmentation (Hu & Kavanagh, 2003; Indran *et al.*, 2011).

5.5 FKC induces extrinsic apoptosis by activating caspase-8 and DR-5, and inhibiting cFLIP$_L$

In the extrinsic pathway, apoptosis is initiated through the binding of cognate ligands to the respective death receptors. This will lead to the recruitment of adaptor molecules such as Fas-associated death domain protein (FADD) and TNF receptor-associated death doman protein (TRADD) through their complementary death domains which will then bind to procaspase-8. A death-inducing signaling complex (DISC) is formed, resulting in dimerization and activation of caspase-8. The activated caspase-8 directly cleave and activate caspase-3 (Parrish *et al.*, 2013). However, cellular FLICE-like inhibitory protein (c-FLIP) competes with pro-caspase-8 to bind with the FADD in the formation of DISC (Krueger *et al.*, 2001). Thus c-FLIP inhibits the activation of caspase-8 which in turn inhibits the induction of apoptosis triggered by death receptors.

Based on our findings, we propose that FKC activate the extrinsic pathway by increasing the levels of DR5, and to a lesser extent DR4, and down-regulation of c-FLIP$_L$. These results were consistent with the decrease in the levels of pro-caspase-8. A higher amount of active caspase-8 was detected in comparison to the active caspase-9 in HCT 116 cells upon FKC treatment in dose-dependent manner. A link with the mitochondrial pathway exists via caspase 8-mediated cleavage of Bid in which the truncated Bid migrates to the mitochondria and activates the pro-apoptotic members Bak and Bax. In the western blot analysis, no changes were observed in the level of Bid after FKC treatment, suggesting that Bid was not involved in the FKC-induced apoptosis.

5.6 FKC induces apoptosis through endoplasmic reticulum stress in HCT 116 and HT-29 cells

The ER plays an important role in the proper protein folding, post-translational modification of secreted and membrane proteins, lipid biosynthesis and maintenance of calcium homeostasis (Jin *et al.*, 2014). Accumulation of unfolded proteins and disturbance of calcium homeostasis within ER causes ER stress. Prolonged or severe ER stress can result in apoptosis via intrinsic or extrinsic-mediated pathways to eliminate the damaged cells (Jin *et al.*, 2014; McGuckin *et al.*, 2010).

GADD153/CHOP is a key factor in ER stress-induced apoptosis in which the increased level of CHOP can induce the transcription of various genes that activate the apoptotic pathways, which involves inhibition of Bcl-2 and stimulation of DR5, activation of caspases, increased outer mitochondrial membrane permeabilization and amplification of death signals (Xu *et al.*, 2014). Western blot results showed the increase in the level of CHOP as early as 6 hours after FKC treatment which suggested the occurrence of endoplasmic reticulum stress in HCT 116 and HT-29 cells, leading to apoptotic cell death.

5.7 FKC down-regulates the levels of c-IAPs in HCT 116 and HT-29 cells

The human inhibitor of apoptosis protein (IAP) family members consist of eight proteins which contain either one or three Baculovirus IAP Repeat (BIR) domain (Berthelet & Dubrez, 2013). Among the inhibitor of apoptosis proteins, XIAP, cIAP-1, cIAP-2, ML-IAP and survivin are endogenous caspase inhibitors that inhibit apoptosis and lead to cell survival while others are involved in cell cycle and inflammation (Berthelet & Dubrez, 2013). Based on the western blot results, the levels of inhibitor of apoptosis proteins (XIAP, cIAP-1, cIAP-2 and survivin) were dramatically decreased

after FKC treatment in HCT 116 and HT-29 cells thus paving the way for the activation of caspases.

XIAP are the most potent caspase inhibitor as it directly binds and inhibits the caspases activation. XIAP binds caspase-9 through its BIR3 domain and preventing its dimerization. It also binds to activated caspase-3/7 through its BIR2 domain and the linker region between the BIR1 and BIR2 domains. However, XIAP can be inhibited by Smac/DIABLO which is released into the cytosol from the mitochondria upon loss of outer mitochondrial membrane potential. The released Smac/DIABLO binds to XIAP via its IAP-binding motif, and promote their auto-ubiquitination and consequent degradation (Li *et al.*, 1997). Thus inhibition of XIAP can be caused by binding to Smac/DIABLO which was found to be released into the cytoplasm upon FKC treatment.

In contrast, cIAP-1 indirectly inhibits caspase-3/8 activation through its E3 ligase activity as well as interaction with the TNR receptor-associated factor 1 and 2 (TRAF1 and TRAF2) (Guicciardi *et al.*, 2011). Survivin, the smallest member of the IAP family of proteins, has been found to be highly expressed in tumors and associated with a metastatic phenotype, shorter survival times, and a resistance to chemotherapy in patients. Survivin indirectly inhibits caspase-9 activation by binding to Smac/DIABLO, thus preventing it from binding to XIAP (Johnson & Howerth, 2004).

5.8 FKC induces activation of ERK and inactivation of Akt

Many studies have reported the possible interlink between the Akt/PI3K and MAPKs pathways in the regulation of cell proliferation and apoptosis. Therefore, in this study, we investigated the involvement of ERK1/2, p38 and JNK, and Akt pathways in the mechanism underlying the apoptotic properties of FKC. Interestingly, we found that FKC inhibited activation of Akt and this resulted in a dramatic increase in ERK1/2

phosphorylation (a 3-fold increase after 18 hours over the control) while a decrease in JNK phosphorylation. However, activation of Akt was found to occur in HCT 116 cells following FKC treatment at the beginning of 6 hours. This phenomenon might be due to the transient response of the cells to an apoptotic stimulus as a self-defense mechanism to protect cells against apoptosis. It was noticed that the inhibition of Akt and activation of ERK1/2 occurred at a relatively late event in the response of HCT 116 cells to the FKC treatment (Figure 4.17). These results suggests that there is an opposite regulation between Akt and ERK signaling pathways while a positive correlation between Akt and JNK phosphorylation in FKC-induced apoptosis.

However, the mechanisms that can modulate both the Akt and MAPKs pathways in response to treatment with FKC remain unclear. The activation of the ERK1/2 pathway is normally thought to be associated with cell proliferation and survival. However, many studies have shown that ERK1/2 can exert a dual effect on cell growth. The anti-apoptotic effect of ERK1/2 activation has been shown to stimulate proliferation by increasing expression of cyclin D and inactivating p27 (Kawada *et al.*, 1997; Lenferink *et al.*, 2001). Activation of ERK1/2 has also been shown to be required for the induction of apoptosis by DNA-damaging agents such as doxorubicin and cisplatin which is accompanied by inactivation of Akt (Lee *et al.*, 2006; Wang *et al.*, 2000). Activation of ERK1/2 has been shown to induce apoptosis in T-cells via increasing Fas ligand expression (van den Brink *et al.*, 1999). ERK pathway is also involved in activating mitochondrial-dependent pathway through regulation of Bcl family proteins as well as extrinsic pathway by increasing the expression of ligands and death receptors (Cagnol & Chambard, 2010). Collectively, our results suggested that there is an interplay between the Akt signaling pathway and MAPKs pathway in induction of apoptosis and cell cycle arrest by FKC in HCT 116 cells.

5.9 FKC induces cell cycle arrest in HCT 116 and HT-29 cells

Deregulation of the cell cycle is one of the hallmarks of tumorigenesis and contributes to the uncontrolled proliferation in human cancer. In this study, the growth rate in HCT 116 and HT-29 cells was inhibited after FKC treatment in dose- and time-dependent manner as shown in Figure 4.19. Based on cell cycle analysis, the inhibition of cell proliferation could be due to the cell cycle arrest which was found to be significantly arrested at S phase in HCT 116 cells while G_2/M phase in HT-29 cells upon FKC treatment.

In HCT 116 cells, the blockade of DNA synthesis in S phase may prevent the replication of the damaged or mutated DNA which allows the cells to either repair DNA damage before entering mitosis or undergo apoptosis (Agarwal *et al.*, 1998). In addition, FKC inhibited HT-29 cells from entry into mitosis as a greater number of cells were arrested in the G_2/M phase. Based on the results, it can be proposed that FKC treatment could inhibit the growth in HCT 116 and HT-29 cells by arresting the cell cycle which subsequently led to cell death.

5.10 FKC down-regulates Cdk2 and Cdk4, and inactivates retinoblasma (pRb) in HCT 116 cells

It is well known that eukaryotic cell cycle is tightly coordinated by protein kinase complexes, each consisting of a cyclin and cyclin-dependent kinase (Cdk). As transit from G_1 phase of cell cycle is regulated by the sequential activation of Cdk2 and Cdk4 in early early and mid/late G_1 phase, the level of these two serine-threonine kinases in HCT 116 cells was next assessed after FKC treatment. Western blot analysis in FKC-treated HCT 116 cells showed the down-regulation of Cdk2 and Cdk4. However, no change was observed in the levels of cyclin D1 and E in HCT 116 cells. Moreover, phosphorylation of pRb was found to be inhibited by FKC in HCT 116 cells. De-

phosphorylation of retinoblastoma inhibits the release of the transcription factor E2F to enter the nucleus and activates transcription of cyclin E and cyclin D1 (Figure 2.8).

5.11 FKC up-regulates $p21^{Cip1}$ and $p27^{Kip1}$ in HCT 116 and HT-29 cells via either dependent or independent of p53

The proteins p53, p21 and p27 play a role in preventing the onset of cancer and is involved in the elimination of damaged cells through induction of apoptosis, cell cycle arrest, DNA repair and senescence (Jette *et al.*, 2008). The main difference between the two cell lines is the p53 status in which the p53 in HT-29 cells has a mutated gene with a mutation at codon 273 whilst those in HCT 116 cells are of the wild-type (Kramer *et al.*, 2016). Thus it is interesting to investigate role of p53 status in contributing to the growth arrest in both cell lines upon treatment. In HCT 116 cells, the p53 level was up-regulated after FKC treatment and was barely detected in untreated cells but the level decreased after 12 hours of treatment.

One possible explanation for the reduction maybe due to the complex biphasic nature of p53 alteration in which its activity is regulated by post-translational modifications on multiple sites such as phosphorylation, acetylation, ubiquitination, or methylation (Terzian *et al.*, 2008). These post-translational modifications occur in response to typical cellular stresses such as DNA damage and oncogene activation (such as activation of Ras mutations or increased c-Myc expression) (Terzian *et al.*, 2008). Unlike in HCT 116 cells, high level of p53 was found in untreated HT-29 cells but decreased after treatment with increasing concentrations of FKC. The high level of p53 in HT-29 cells could be due to the mutated p53 gene that give rise to a stable mutant protein in human cancers which results in inhibition of MDM2-mediated p53 ubiquitination (Moll & Petrenko, 2003). There is accumulating evidences supporting the views that p53 mutants are able to actively promote tumor development by several

other means such as increased proliferation, evasion of apoptosis and chemoresistance. Thus the reduction of p53 mutant level in HT-29 cells by FKC may contribute to the growth arrest, however it remained unclear as to how FKC causes reduction in the level of mutant p53 (Figure 4.21).

It is known that the kinase activities of cyclin-Cdk complexes are inhibited by binding with endogenous inhibitor proteins (CKIs), $p21^{WAF1/CIP1}$ and $p27^{Kip1}$, and this prevents cell cycle progression. Western blot analysis (Figure 4.21) showed that p21 and p27 were up-regulated in a similar pattern for HCT 116 and HT-29 cells upon FKC treatment. Based on the western blot analysis on the p53 status in both cell lines, the up-regulation of p21 and p27 may occur in a p53 independent manner.

Unlike p53, the frequency of somatic mutations in the Cip/Kip genes in cancers is very rare, which underlines the importance of these molecules as promising therapeutic targets. Although p21 was initially identified to be transcriptionally up-regulated by p53 in response to DNA damage; however, recent studies have shown that p21 can also be induced by Chk2 kinase and p73 (Aliouat-Denis *et al.*, 2005; Schmelz *et al.*, 2005). p21 mRNA stability can also be posttranscriptionally regulated by HuR, a RNA-binding protein, in response to stress. p27 translation can be regulated by an internal ribosome entry site element in its 5'untranslated region (Roy *et al.*, 2007).

pRb suppresses Cdk kinase activity and G1-S transition through post-transcriptional up-regulation of p27. pRb also stabilize the p27 by the interfering the formation of Skp2-p27 complex, thus preventing p27 ubiquitination. Progression of the cells through G_1 and S phases requires pRb phosphorylation (Giacinti & Giordano, 2006). Thus it can be proposed that the inhibitory effect of FKC on cell cycle arrest is due to the up-regulation of p21 and p27, the reduction in Cdk2 and Cdk4 and hypophosphorylation of pRb. Further studies need to be done to elucidate the molecular events of this pathway.

5.12 FKC increased the ROS generation and reduced the SOD activity

Increased oxidative stress by increasing ROS generation could be a potential therapeutic strategy (Trachootham *et al.*, 2009). ROS act in multiple signaling cascades involving the development of cancer such as proliferation, survival, angiogenesis and metastasis (Wang & Yi, 2008). However, high levels of ROS have been reported to inhibit cell proliferation by inducing cell cycle arrest and apoptosis. The level of ROS is tightly regulated by intracellular antioxidants for maintaining redox homeostasis (Kovacic & Jacintho, 2001). Excessive ROS can induce apoptosis by damaging the mitochondrial membrane integrity which leads to release of pro-apoptotic proteins (Gao *et al.*, 2015). ROS have been shown to induce the activation both caspase-8 and caspase-9 (Zhao *et al.*, 2013).

In this study, apart from enhancing ROS generation in both HT-29 and HCT 116 cells, FKC was also found to inhibit the activity of SOD in both cells. It has been proposed that a relatively high content of Mn-SOD can stimulate the growth of the tumor cells by protecting them against high concentrations of ROS which can be produced by several anti-cancer therapies such as radiotherapy, chemotherapy and photodynamic therapy (Miranda, Janssen *et al.*, 2000). Thus the elevation of ROS and depletion of antioxidant SOD activity may trigger the cancer cells towards apoptosis. This may further explain the results on the disruption of the mitochondria membrane potential by FKC. FKC may have utilized the mitochondria to cause oxidative stress, which led to the activation of apoptotic signaling pathways in HCT 116 and HT-29 cells. In addition, results also showed that the ROS levels were higher in FKC-treated HCT 116 cells at lower doses in comparison to FKC-treated HT-29 cells. This may suggest the higher cytotoxic activity of FKC against HCT 116. Therefore, more studies are needed to explore the underlying mechanisms.

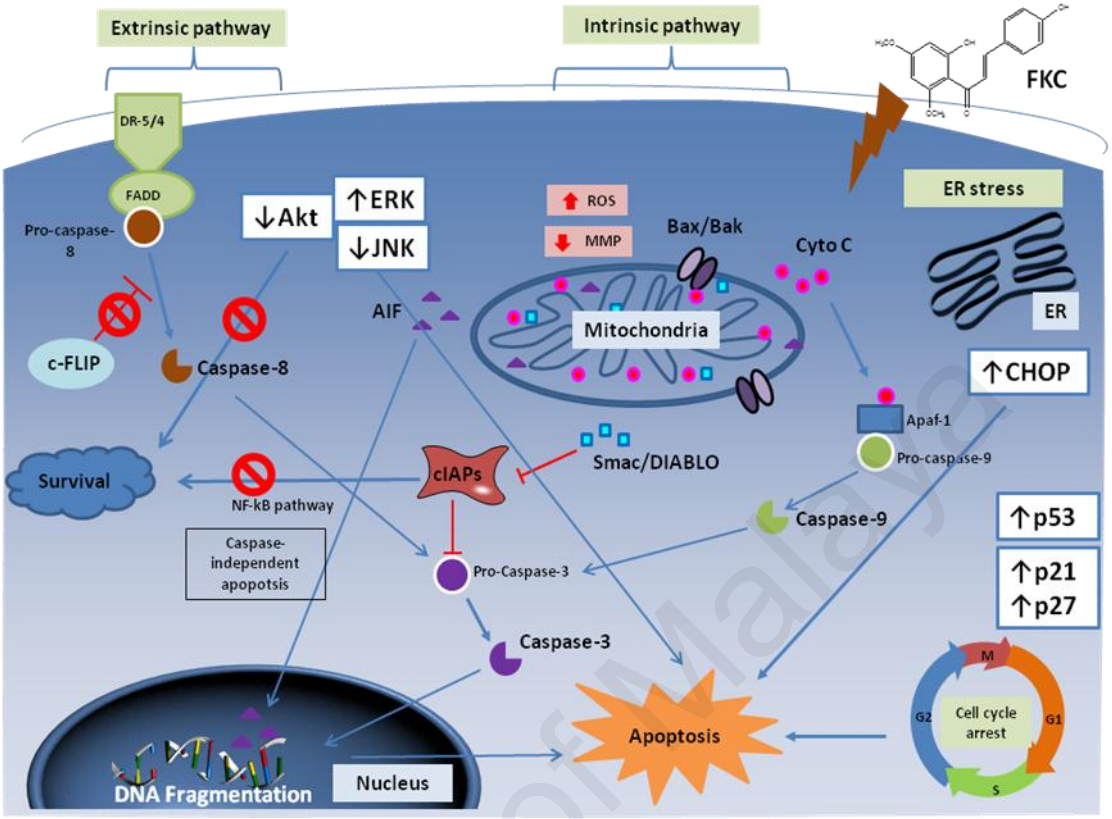

Figure 5.1: Summary of the possible apoptotic signaling pathways and molecular mechanisms underlying FKC in causing cell death in colon cancer cells.

5.13 Identification of the differentially abundant proteins of FKC-treated HCT 116 cells and their involvement in possible signaling pathways

Cell lines established from human colorectal carcinomas have been widely used to identify novel molecular targets which are crucial for carcinogenesis. 2-DE analysis was performed to identify proteins that were affected by FKC treatment of HCT 116 cells. The proteins that changed in abundance suggested that FKC mainly disrupted proteins associated with cell death and survival, cell cycle, cellular growth and proliferation. The identified proteins with their known functions and how they may be associated with the effects of FKC are discussed in the following paragraphs.

5.13.1 Proteins involved in the ubiquitin proteasome pathway (UPP)

UPP is a major intracellular proteolytic pathway in the cell that facilitates intracellular protein degradation, and clearance of misfolded/unfolded and damaged proteins. It is responsible for the constitutive and induced the turnover of proteins that regulate cellular functions involved in cell cycle progression, oncogenesis, cell growth, signal transduction, transcriptional, translation, and antigen processing (Mitsiades *et al.*, 2002). Thus, an alteration of this pathway may affect cell survival.

Seven identified proteins were found to be related to this pathway. Five increased in abundance: heat shock protein 90kDa alpha (HSP90AA1), heat shock cognate 70kDa protein 8 (HSPA8), heat shock protein 70kDa protein 1A/1B (HSPA1A), heat shock 70kDa protein 1-like (HSPA1L) and heat shock protein 27kDa (HSPB1). Two decreased in abundance: transcription elongation factor B polypeptide 1 (TCEB1) and S-phase kinase-associated protein 1A (SKP1).

The induction of HSPs has been shown to occur when cells are stressed and accumulate denatured or malfolded proteins (Mathew & Morimoto, 1998). Up-regulation of HSPs is believed to be a adaptive mechanism for proteasome inhibition

(Kastle & Grune, 2011). Increase of these proteins suggested that FKC treatment caused cellular stress and disruption of ubiquitin-proteasome mediated proteolysis in HCT 116 cells.

SKP1 is an adapter subunit that links the exchangeable F-box protein to Cullin1 scaffold protein to form a multi-protein E3 ubiquitin ligase complex (SCF complex) that targets cell cycle regulatory proteins for ubiquitination-mediated proteolysis (Sheikh *et al.*, 2014). Elongin C is structurally homologous to SKP1 which additionally binds to elongin B and von Hippel-Lindau (VHL) to form a VCB complex and functions as an E3 ubiquitin-ligase (Stebbins *et al.*, 1999). VCB complex promote the ubiquitination and degradation of HIF-1α, resulting in decreased gene expression involved in glycolysis, angiogenesis and proliferation (Imtiyaz & Simon, 2010; Stebbins *et al.*, 1999).

FKC promotes the formation of SKP1/Elongin C containing-complexes. These proteins are capable of binding with other proteins. For instance, SKP1 plays additional role where it binds to cyclin A-Cdk2 complex, inhibiting its activity (Yam *et al.*, 1999). It also found to bind with centrosome to maintain chromosomal stability (Freed *et al.*, 1999). Elongin C and B can form complex with suppressor of cytokine signaling-1 (SOCS-1) protein to inhibit the Jak/STAT signaling (Conaway *et al.*, 1998).

5.13.2 Proteins associated with the unfolded protein response (UPR) and endoplasmic reticulum stress

The UPR plays an important role in the maintenance of ER homeostasis and is activated in response to ER stress when there is an accumulation of unfolded or misfolded proteins. If ER stress is prolonged or too extreme, it will eventually cause cell death by triggering apoptotic pathways (Hetz, 2012). Prolonged ER stress suppresses Akt signaling (Hosoi *et al.*, 2007). ER stress can be caused by disturbances in calcium

homeostasis, glucose/energy depletion, redox changes that impair client protein folding (Brown & Naidoo, 2012). UPR also causes the activation of the heat shock response (Li *et al.*, 2011).

The proteomic results showed that there was increased abundance of an ER stress marker, protein disulfide isomerase (PDI). PDI is a multifunctional protein that catalyzes the formation and rearrangement of disulfide bonds during protein folding in the ER. It acts as a molecular chaperone that helps ameliorate misfolded proteins in response to ER stress (Noiva, 1999).

5.13.3 Antioxidants and detoxification enzymes

The nuclear factor-E2-related factor-2 (NRF2) mediated oxidative stress response pathway was also predicted to be affected (Table 4.3). NRF2 is a transcription factor that regulates the antioxidant response element (ARE)-mediated expression of cellular detoxification enzymes and antioxidant proteins (He *et al.*, 2012). NRF2 signaling pathway can be activated directly by oxidative stress and/or indirectly by UPR through protein kinase RNA-like endoplasmic reticulum kinase (PERK) (Brown & Naidoo, 2012). Four proteins associated with this pathway were identified: T-complex protein 1 subunit eta (CCT7), glutathione S-transferase omega 1 (GSTO1), heme oxygenase 1 (HMOX1), and gamma actin 1 (ACTG1).

HMOX1 which increased in abundance, is a target gene for NRF. It is one of the ARE-regulated phase II detoxifying enzymes that catalyzes the degradation of heme and converts it to biliverdin, iron and carbon monoxide (Itoh *et al.*, 1997; Maines, 1997). It is an essential anti-inflammatory enzyme that is induced in response to oxidative stress (Batovska & Todorova, 2010). Increased abundance of HMOX1 may be the cells' attempt to trigger an adaptive response against FKC-mediated oxidative stress. Furthermore, the expression of HO-1 might be due to the addition of chalcones to

thiol of Keap1 via Michael type reaction (Maydt *et al.*, 2013). Induction of HO-1 was found to be correlated with the production of ROS, as it may serve as a feedback mechanism to balance the intracellular level of ROS (Gottlieb *et al.*, 2000; McNally *et al.*, 2007).

GSTO1 was decreased in abundance upon FKC treatment. GSTO1 belongs to a superfamily of phase II detoxification enzyme that mainly catalyzes the conjugation of glutathione (GSH) to endogenous or exogenous xenobiotic toxins for biotranformation and/or removal as a cellular defence against chemical carcinogens, therapeutic drugs and oxidative stress products. GSTO1 is highly overexpressed in human cancers and is implicated in invasion, metastasis and chemotherapy resistance (Liu *et al.*, 2007; Piaggi *et al.*, 2010). Inhibition of GSTO1 has been shown to increase the sensitivity of cancer cells to apoptosis (Tsuboi *et al.*, 2011).

5.13.4 Translational regulatory proteins

Deregulation of protein synthesis is one of the hallmarks of cancer. Enhanced translation rates in cancer lead to an increase in the translation of mRNAs encoding oncogenic proteins that promote tumor cell survival, transformation, angiogenesis, invasion and metastasis (Silvera *et al.*, 2010). In addition, ER stress can inhibit protein synthesis through phosphorylation of elF2α by activated PERK which prevent translation initiation (Teske *et al.*, 2011).

Most translation control occurs at the rate-limiting step which is regulated by multiple eukaryotic factors (eIFs) before entering the elongation step (Spilka *et al.*, 2013). In this proteomic study, FKC treatment caused a decrease in abundance of proteins involved in mRNA translation or protein synthesis. These proteins were eukaryotic translation initiation factor 5A-1 (eIF5A1), eukaryotic translation initiation factor 3 subunit 1 (eIF3I) and elongation factor-2 (EEF2).

eIF3I is a subunit of the eukaryotic translation initiation factor 3 (eIF3) complex. It has been implicated in the regulation of oncogenic mechansims and tumorigenesis (Hershey, 2015). An increase in eIF3 has been shown to result in malignant transformation of immortal cells (Hershey, 2015; Zhang *et al.*, 2007). An increase in eIF3I has been found in number of cancers including hepatocellular carcinoma, cervical cancer, colon cancer, breast cancer, head and neck cancer (Hershey, 2015; Wang, Lin *et al.*, 2013). eIF3I also been shown to promote oncogenesis in the colon by translationally upregulating COX-2 and activating the β-catenin signaling pathway (Qi *et al.*, 2014). Knockdown of eIF3I has been shown to increase cellular apoptosis by inhibiting the activation of Akt1 signaling pathway (Wang, Lin *et al.*, 2013). It has been found to bind to Akt1 and prevent its dephosphorylation by protein phosphatase, PP2A (Wang, Lin *et al.*, 2013).

eIF5A1 has been found in high abundance in human cancer tissue and is associated with cell proliferation (Mathews & Hershey, 2015). It acts in both the initiation and elongation stages of protein synthesis and has been implicated in transcription, mRNA turnover and nucleocytoplasmic transport (Mathews & Hershey, 2015). eIF5A is upregulated in human PDAC tissues and in premalignant pancreatic intraepithelial neoplasia tissues in mice (Sun *et al.*, 2010; Taylor *et al.*, 2007). Unhypusinated eIF5A1 was found to capable to induce apopotosis in colon cancer (Sun *et al.*, 2010).

Elongation factor 2 (eEF2) is a key component in the elongation step of mRNA translation in the tumorigenesis of gastrointestinal cancers and knockdown of eEF2 was shown to cause a potent growth inhibition in gastric cancer (AZ-521 and MKN-28) and colorectal cancer (SW620) cell lines (Nakamura *et al.*, 2009). Inactivation of eEF2 by silencing eEF-2K had been found to inhibit tumor growth, induce apoptosis and sensitize tumors toward doxorubicin treatment (Tekedereli *et al.*, 2012). Down-

regulation of eEF2 was found to reduce cisplatin resistance in lung adenocarcinoma (Chen *et al.*, 2011).

5.13.5 DNA and RNA binding proteins

RAD23B is linked to nucleotide excision DNA repair (Bergink *et al.*, 2013). In has been shown to exhibit tumor suppression effects in breast cancer (Linge *et al.*, 2014). It has been proposed as a multi-ubiquitin chain receptor that binds to ubiquitylated-HIF1α in the nucleus for proteasomal degradation in colorectal cancer (Nunez de Villavicencio-Diaz *et al.*, 2015).

PTB-associated splicing factor (SFPQ) is an essential nucleic acid-binding protein that has been implicated in a wide range of cellular activities including pre-mRNA splicing, transcription repression, nuclear retention of RNA, DNA repair,3'end processing, apoptosis and viral replication (Yarosh *et al.*, 2015). It has been reported to function as tumor suppressor protein where high abundance of SFPQ represses transcription of multiple oncogenic genes and inhibits cell proliferation (Song *et al.*, 2005).

5.13.6 Structural/cytoskeletal related proteins

FKC treatment caused the changes in abundances of Keratin 18 (KRT18), tubulin beta-2 chain (TUBB4B), gamma actin (ACTG1) and myosin light polypeptide 6 (MYL6). The reorganization of cytoskeletal proteins is associated with the regulation of apoptosis signaling, resulting in partial detachment from the extracellular matrix, cell rounding and contraction and followed by chromatin condensation, membrane blebbing and formation of intact apoptotic bodies (Desouza *et al.*, 2012).

Microfilaments (actin filaments), microtubules and intermediate filaments are the major components of the cytoskeleton. They have important roles in maintaining the

cell shape and internal organization, and provides mechanical support (Ndozangue-Touriguine *et al.,* 2008). With regards to cell death alteration of actin dynamics is required for modulation of apoptotic signals. Formation of membrane blebs and apoptotic bodies is dependent on the contractility of actin-myosin cytoskeletal structures (Coleman *et al.,* 2001). Actin skeleton is involved in clustering of death receptor and ligand in lipid raft to initiate downstream signaling (Mollinedo *et al.*, 2004).

KRT18 is an intermediate filament which supports the cell integrity and are polymerized and cross-linked to other cytoskeletal proteins through plakin family of proteins (Ndozangue-Touriguine *et al.*, 2008). It is cleaved by activated caspases during apoptosis which generates three cleaved form of KRT18 in the 20 - 26 kDa range (Schutte *et al.*, 2004). Collapse of the cytokeratin network is mediated by cleavage of keratin 18 (Liu *et al.*, 2011).

5.13.7 Proteins associated with cellular transport and signaling

RANBP1 is a key regulator of Ran GTPase and is transcriptionally regulated by E2F and retinoblastoma-related factors, which are often deregulated in many tumors (Guarguaglini *et al.*, 2000). It forms a complex with RAN and RANGAP to regulate nucleo-cytoplasmic transport during interphase, mitotic spindle organization and cell cycle progression (Clarke & Zhang, 2001; Guarguaglini *et al.*, 2000; Plafker & Macara, 2000). Downregulation of RANBP1 has been shown to induce apoptosis in taxol-exposed HeLa and MCF7 cells through activation of ERK1/2 and p38 and is independent of p53 (Rensen *et al.*, 2009).

Two mitochondrial transporters were identified to be decreased in abundance which are ATPase subunit d (ATP5H) and mitochondrial import receptor subunit (TOM22), which could be implicated in mitochondria-mediated apoptosis. TOM22 is a central component of the mitochondria outer membrane protein translocation pore and has been

implicated as the receptor for the proapoptotic protein Bax (Bellot *et al.*, 2007). ATP5A is a subunit of mitochondrial ATP synthase F0 complex that catalyzes ATP synthesis using an electrochemical gradient of protons across the inner membrane during oxidative phosphorylation (Cao *et al.*, 2009).

5.13.8 Effect of FKC on energy metabolism

A canonical pathway analysis of IPA also highlighted one major pathway, glycolysis and gluconeogenesis 1. Studies had showed that cancer cells exhibited a high rate of glycolysis (Pelicano *et al.*, 2006). PGAM1 is the key enzyme in glycolysis and found to be upregulated in human cancers (Hitosugi *et al.*, 2012). Inhibition of PGAM1 resulted in significantly decreased glycolysis and reduction in tumor growth (Hitosugi *et al.*, 2012). Therefore, the down-regulation of this protein suggests that FKC may inhibit cell proliferation by reducing ATP synthesis.

5.14 *In vivo* studies using nude mice xenograft model

Taking into consideration the tumor heterogeneity and microenvironment that play an important role in cancer development and progression, the use of animal model may reflect the drug's efficacy for treatment in cancer patients. Unsuccessful outcomes in many forms of chemotherapy in most cancer patients are often caused by its failure to induce apoptosis signaling pathways in cancer (Housman *et al.*, 2014). In this regard, we further investigate the clinical relevance of FKC for its anti-tumor activity using nude mice model in which FKC was used to evaluate the activity associated with induction of apoptosis as found in *in vitro* study.

5.14.1 FKC suppresses tumor growth in nude mice bearing HCT 116 xenografts is associated with induction apoptosis.

The results of the present study showed that FKC was able to suppress tumor growth in nude mice carrying the HCT 116 tumor xenografts when given intraperitonal

injection. Histopathological examination of major organs and biochemical analysis of serum in FKC-treated mice indicated no obvious adverse effects *in vivo*. FKC also displayed apoptotic features in tumor tissues where there was an increase in DNA fragmentation and expression of cleaved caspase-3. These findings were consistent with our earlier *in vitro* finding in which FKC inhibited HCT 116 tumor growth via induction apoptosis.

5.14.2 FKC decreases cell proliferation in colon tumor tissues

Tumor growth depends on both the rate of neoplastic cell proliferation and cell death. Tumor cells consist of proliferating cells (G_1, S, G_2, and M stages of cell cycle), temporarily non-proliferating cells (G_0) and non-proliferating cells. Ki67 is a nuclear antigen that is expressed in proliferating cells in all cell cycle phases except those in G_0 phase, and is degraded after mitosis (Georgescu *et al.*, 2007). An increase in Ki67 expression indicates a high proliferation rate and the mitotic activity. Ki67 has been frequently used as prognostic marker for colorectal cancer (Oshima *et al.*, 2005). Our results in IHC analysis showed there was a decrease in the expression of Ki67 in tumor tissues treated with FKC compared to the control tumor tissues. This showed that FKC is able to inhibit the cell proliferation and prevent colon cancer progression.

5.15 Identification of differentially abundant proteins in serums as cancer biomarker

Discovery of highly sensitive and specific serum biomarker for the diagnosis, early disease detection and monitoring treatment response allows patients to benefit from the treatment with higher survival rate at the time of diagnosis (Ludwig & Weinstein, 2005). The tumor-specific marker also provides a basis for development of future targeted therapies. Cancer xenograft models have been shown to facilitate the identification of potential biomarkers from tumor and host response. Proteomic

technologies have been the relevant technique for identification of new diagnostic or therapeutic serum biomarkers for cancer. In the present proteomic analysis, it was revealed that five proteins were differentially regulated in the serum before and after treatment by FKC. Of the five differentially regulated protein identified in mice serum, the level of IgM was found to be elevated following the treatment while the levels of hemopexin, GRP78, apoE and kininogen-1 were increased in the control group but decreased after the treatment and returned to a similar level as in the normal nude mice.

IgM plays important role in the first line of defense in immune surveillance against invading microbes, but also for removal of cellular waste, modified structures and transformed cells (Brandlein & Vollmers, 2004). It is also involved in recognition and elimination of precancerous and cancerous lesions (Vollmers & Brandlein, 2006). IgM has gained increasingly interest in cancer therapy as studies have shown that IgM antibodies can kill malignant cells by apoptosis (Vollmers & Brandlein, 2006). The up-regulation of IgM in the serum following FKC treatment in this study may contribute to the suppression of the HCT 116 tumor growth.

GRP78 is known as a major endoplasmic reticulum (ER) chaperone which serves as a regulator of the unfolded protein response (UPR) and promote cell survival under ER stress (Lee, 2007). Over-expression of GRP78 has been found in many cancers including colon (Xing *et al.*, 2006), breast (Fernandez *et al.*, 2000), ovarian (Delie *et al.*, 2012), lung (Wang *et al.*, 2005), gastric (Zhang *et al.*, 2006), prostate (Pootrakul *et al.*, 2006) and liver (Luk *et al.*, 2006) cancers. The over-expression has been correlated with tumor growth, apoptosis resistance, metastasis, angiogenesis, cancer recurrence and resistance to chemotherapeutics (Lee, 2007). GRP78 has been found to be the target for tumor-specific apoptosis or lipoptosis by the natural IgM antibodies (Rauschert *et al.*,

2008). The expression of GRP may serve as a biomarker for tumor behavior and treatment response (Lee, 2007).

Kininogen-1 is a multifunctional protein that is involved in many pathophysiological processes including blood coagulation, fibrinolysis, regulation of vascular tone and inflammation response (Yousef & Diamandis, 2001). Recently, kininogen-1 has been identified as a potential serum biomarker for the early detection of advanced colorectal adenoma and colorectal cancer as the level was found to be higher compared to healthy persons (Wang, Wang *et al.*, 2013). However, its role in carcinogenesis still remains unclear.

Hemopexin (Hpx) is a serum glycoprotein that binds heme and transports it to the liver for breakdown and iron recovery, after which the free hemopexin is recycled back in circulation (Tolosano & Altruda, 2002). Increased Hpx concentrations have been found in melanoma and breast cancers (Coombes *et al.*, 1977; Manuel *et al.*, 1971). Increased Hpx concentration is implicated in cancer metastasis and invasion by cooperating with multiple matrix metalloproteinases (MMPs) (Dufour *et al.*, 2011; Piccard *et al.*, 2007). The down-regulation of hemopexin in serum from nude mice bearing tumor xenograft treated with FKC may have caused inhibition of tumor growth.

ApoE is a key regulatory protein in the transport and metabolism of cholesterol and phospholipids by binding to the low-density lipoprotein (LDL) receptor and the low-density lipoprotein receptor-related protein (LRP) (Niemi *et al.*, 2002). It is produced primarily in the liver and also in the brain, adrenal glands, kidney and macrophages (Niemi *et al.*, 2002). It is also involved in other cellular functions including platelet aggregation, immune activities and cellular growth and differentiation (Su *et al.*, 2011). It has been postulated that apoE may modify the tumor microenvironment to maintain the proliferation and survival of tumor (Chen *et al.*, 2005). ApoE may have influenced

CRC development through three potential pathways: cholesterol and bile metabolism, triglyceride and insulin regulation, and prolonged inflammation (Slattery *et al.*, 2005). However, the role of apoE in carcinogenesis is still not fully understood. ApoE has been recently identified as a potential tumor-associated marker in many tumor types including ovarian (Chen *et al.*, 2005), lung (Su *et al.*, 2011), pancreatic (Yu *et al.*, 2005), gastric (Shi *et al.*, 2015), colon (Slattery *et al.*, 2005), prostate (Ifere *et al.*, 2013) and anaplastic thyroid cancers (Ito *et al.*, 2006), and glioblastoma (Nicoll *et al.*, 2003) due to its elevated expression in these tumors.

CHAPTER 6: CONCLUSION

In conclusion, FKC has shown to exert potent cytotoxic effect against colon cancers, particularly HCT 116 cells by inducing apoptosis and cell cycle arrest. FKC treatment induces apoptosis through the mitochondria, death receptors and endoplasmic reticulum mediated pathways. A prolonged FKC treatment was also found to be associated with the inhibition of survival pathways through inactivation of Akt phosphorylation and modulation of MAPKs pathway. FKC also caused the cell cycle arrest in HCT 116 and HT-29 cells. This was correlated with the modulation of the functions of the cell cycle regulatory proteins including p21, p27, p53, the cyclins and pRb. In the proteomic study, it showed that apoptotic mechanisms regulated by FKC in HCT 116 cells involved key player proteins that participate in the ER stress, unfolded protein response, translation, tumor suppression and survival mechanisms. Functional characterization of these proteins will be needed to elucidate the complicated signal cascades related to these altered protein abundances.

In the present study, the *in vitro* findings were also further investigated in nude mice model for its possible application in chemotherapeutic intervention. In the *in vivo* studies, FKC treatment also showed effectiveness in reducing HCT 1116 tumor growth in nude mice model. The reduction of tumor growth following FKC treatment was evidenced by the increase in the number of necrotic cells and decrease in the expression of Ki67. Tumor tissues from FKC-treated mice showed increased DNA fragmentation and expression of cleaved caspase-3, suggesting FKC inhibited the tumor growth via induction of apoptosis.

Furthermore, from the proteomics study, several potential mechanisms or molecular targets of FKC that affect the survival and apoptosis pathways in colon cancer were identified. Knowing how FKC affects cellular proteins may open up a new opportunity

of targeting apoptotic cell death via different signaling pathways in cancers while sparing normal organs and tissues. In addition, potential serum biomarkers from the xenograft model treated with FKC using 2DE approach would be useful in predicting the colorectal cancer patients that are more likely to benefit from the treatment with FKC. Such results would also be useful in avoiding the dose-toxicity associated with the treatment and preventing tumor progression and metastasis upon the time of diagnosis. However, further pharmacological studies are needed to verify the present study.

Although results from the current study are still at the preliminary stage and therefore rquire more work in further elucidating the underlying mechanisms triggered by FKC, it however provides evidences to support FKC's potential to be developed into anti-cancer drug for the treatment of colon carcinoma. FKC may have the potential to be used in combination with standard therapeutic agents such as cisplatin to enchance drug efficacy and possibly eliminate residual resistant tumor. An in-depth understanding of the molecular mechanisms underlying oncogenesis and cell death may provide a new approach for the treatment of cancer that aims at a wide range of high priority targets. Taken together, the results may provide better therapeutic opportunities for treatment of colon cancer patients.

REFERENCES

Abu Hassan, M. R., Ismail, I., Mohd Suan, M. A., Ahmad, F., Wan Khazim, W. K., Othman, Z. (2016). Incidence and mortality rates of colorectal cancer in Malaysia. *Epidemiology and Health, 38*(0), e2016007-2016000

Abu, N., Akhtar, M. N., Yeap, S. K., Lim, K. L., Ho, W. Y., Zulfadli, A. J. (2014). Flavokawain A induces apoptosis in MCF-7 and MDA-MB231 and inhibits the metastatic process *in vitro*. *PLoS One, 9*(10), e105244

Abu, N., Ho, W. Y., Yeap, S. K., Akhtar, M. N., Abdullah, M. P., Omar, A. R. (2013). The flavokawains: uprising medicinal chalcones. *Cancer Cell International, 13*(1), 102

Acevedo, A., Diaz, Y., Perez, C. M., Garau, M., Baron, J., & Cruz-Correa, M. (2012). Diabetes Mellitus and Colorectal Neoplasia. *Journal of Cancer Therapy, 3*(6A), 859-865

Aebersold, R., & Mann, M. (2003). Mass spectrometry-based proteomics. *Nature, 422*(6928), 198-207

Agarwal, M. L., Agarwal, A., Taylor, W. R., Chernova, O., Sharma, Y., & Stark, G. R. (1998). A p53-dependent S-phase checkpoint helps to protect cells from DNA damage in response to starvation for pyrimidine nucleotides. *Proceedings of the National Academy of Sciences of the United States of America, 95*(25), 14775-14780

Aisha, A. F., Abu-Salah, K. M., Ismail, Z., & Majid, A. M. (2012). *In vitro* and *in vivo* anti-colon cancer effects of Garcinia mangostana xanthones extract. *BMC Complementary Alternative Medicine, 12*, 104

Alaiya, A. A., Franzen, B., Auer, G., & Linder, S. (2000). Cancer proteomics: from identification of novel markers to creation of artifical learning models for tumor classification. *Electrophoresis, 21*(6), 1210-1217

Albuquerque, H. M. T., Santos, C. M. M., Cavaleiro, J. A. S., & Silva, A. M. S. (2014). Chalcones as Versatile Synthons for the Synthesis of 5-and 6-membered Nitrogen Heterocycles. *Current Organic Chemistry, 18*(21), 2750-2775

Aliouat-Denis, C. M., Dendouga, N., Van den Wyngaert, I., Goehlmann, H., Steller, U., van de Weyer, I. (2005). p53-independent regulation of p21Waf1/Cip1 expression and senescence by Chk2. *Molecular Cancer Research, 3*(11), 627-634

Alvarez-Chaver, P., Otero-Estevez, O., Paez de la Cadena, M., Rodriguez-Berrocal, F. J., & Martinez-Zorzano, V. S. (2014). Proteomics for discovery of candidate colorectal cancer biomarkers. *World Journal of Gastroenterology, 20*(14), 3804-3824

Amin, A. R. M. R., Kucuk, O., Khuri, F. R., & Shin, D. M. (2009). Perspectives for Cancer Prevention With Natural Compounds. *Journal of Clinical Oncology, 27*(16), 2712-2725

An, J., Gao, Y., Wang, J., Zhu, Q., Ma, Y., Wu, J. (2012). Flavokawain B induces apoptosis of non-small cell lung cancer H460 cells via Bax-initiated mitochondrial and JNK pathway. *Biotechnology Letters, 34*(10), 1781-1788

Arnedos, M., Vielh, P., Soria, J. C., & Andre, F. (2014). The genetic complexity of common cancers and the promise of personalized medicine: is there any hope? *The Journal of Pathology, 232*(2), 274-282

Avila, H. P., Smania Ede, F., Monache, F. D., & Smania, A., Jr. (2008). Structure-activity relationship of antibacterial chalcones. *Bioorganic & Medicinal Chemistry, 16*(22), 9790-9794

Baba, A. I., Câtoi, C. (2007). *Comparative Oncology*. Bucharest, Romania: The Publishing House of the Romanian Academy.

Baba, Y., Nosho, K., Shima, K., Hayashi, M., Meyerhardt, J. A., Chan, A. T. (2011). Phosphorylated AKT Expression is Associated with PIK3CA Mutation, Low Stage and Favorable Outcome in 717 Colorectal Cancers. *Cancer, 117*(7), 1399-1408

Baldwin, M. A. (2004). Protein identification by mass spectrometry: issues to be considered. *Molecular & Cellular Proteomics, 3*(1), 1-9

Barnhart, B. C., Lee, J. C., Alappat, E. C., & Peter, M. E. (2003). The death effector domain protein family. *Oncogene, 22*(53), 8634-8644

Barrett, J., Brophy, P. M., & Hamilton, J. V. (2005). Analysing proteomic data. *International Journal of Parasitology, 35*(5), 543-553

Batovska, D., Parushev, S., Slavova, A., Bankova, V., Tsvetkova, I., Ninova, M. (2007). Study on the substituents' effects of a series of synthetic chalcones against the yeast Candida albicans. *European Journal of Medicinal Chemistry, 42*(1), 87-92

Batovska, D. I., & Todorova, I. T. (2010). Trends in utilization of the pharmacological potential of chalcones. *Current Clinical Pharmacology, 5*(1), 1-29

Bazzaro, M., Anchoori, R. K., Mudiam, M. K. R., Issaenko, O., Kumar, S., Karanam, B. (2011). α,β-unsaturated carbonyl system of chalcone-Based Derivatives is Responsible for Broad Inhibition of proteasomal activity and preferential killing of human papilloma virus (HPV)-positive cervical cancer cells. *Journal of medicinal chemistry, 54*(2), 449-456

Bellot, G., Cartron, P. F., Er, E., Oliver, L., Juin, P., Armstrong, L. C. (2007). TOM22, a core component of the mitochondria outer membrane protein translocation pore, is a mitochondrial receptor for the proapoptotic protein Bax. *Cell Death & Differentiation, 14*(4), 785-794

Bergink, S., Theil, A. F., Toussaint, W., De Cuyper, I. M., Kulu, D. I., Clapes, T. (2013). Erythropoietic defect associated with reduced cell proliferation in mice lacking the 26S proteasome shuttling factor Rad23b. *Molecular and Cellular Biology, 33*(19), 3879-3892

Berth, M., Moser, F. M., Kolbe, M., & Bernhardt, J. (2007). The state of the art in the analysis of two-dimensional gel electrophoresis images. *Applied Microbiology and Biotechnology, 76*(6), 1223-1243

Berthelet, J., & Dubrez, L. (2013). Regulation of Apoptosis by Inhibitors of Apoptosis (IAPs). *Cells, 2*(1), 163-187

Bevers, T. B., Brown, P. H., Maresso, K. C., & Hawk, E. T. (2014). Cancer Prevention, Screening, and Early Detection. In J .E. Tepper, J. E. Niederhuber, J. O. Armitage, J. H. Doroshow, M. B. Kastan (Eds.), *Abeloff's Clinical Oncology* (5th ed.) (pp. 322-359). Philadelphia, PA: Saunders Elsevier.

Bhanot, A., Sharma, R., & Noolvi, M. N. (2011). Natural sources as potential anti-cancer agents: A review. *International Journal of Phytomedicine, 3*(1), 18

Bilia, A. R., Scalise, L., Bergonzi, M. C., & Vincieri, F. F. (2004). Analysis of kavalactones from Piper methysticum (kava-kava). *Journal of Chromatography. B, Analytical Technologies in the Biomedical and Life Sciences, 812*(1-2), 203-214

Blume-Jensen, P., & Hunter, T. (2001). Oncogenic kinase signalling. *Nature, 411*(6835), 355-365

Boumendjel, A., Boccard, J., Carrupt, P. A., Nicolle, E., Blanc, M., Geze, A. (2008). Antimitotic and antiproliferative activities of chalcones: forward structure-activity relationship. *Journal of medicinal chemistry, 51*(7), 2307-2310

Boyle, P., & Leon, M. E. (2002). Epidemiology of colorectal cancer. *British Medical Bulletin, 64*, 1-25

Bradley, A. (2002). Mining the mouse genome. *Nature, 420*(6915), 512-514

Brandlein, S., & Vollmers, H. P. (2004). Natural IgM antibodies, the ignored weapons in tumour immunity. *Journal of Histology & Histopathology, 19*(3), 897-905

Bresalier, R. S., Boland, C. R., & Kim, Y. S. (1984). Characteristics of colorectal carcinoma cells with high metastatic potential. *Gastroenterology, 87*(1), 115-122

Bretthauer, M. (2011). Colorectal cancer screening. *Journal of Internal Medicine, 270*(2), 87-98

Brown, M. K., & Naidoo, N. (2012). The endoplasmic reticulum stress response in aging and age-related diseases. *Frontiers in Physiology, 3*, 263

Burrell, R. A., & Swanton, C. (2014). Tumour heterogeneity and the evolution of polyclonal drug resistance. *Molecular Oncology, 8*(6), 1095-1111

Cagnol, S., & Chambard, J. C. (2010). ERK and cell death: mechanisms of ERK-induced cell death--apoptosis, autophagy and senescence. *The FEBS Journal, 277*(1), 2-21

Calvino, V., Picallo, M., López-Peinado, A. J., Martín-Aranda, R. M., & Durán-Valle, C. J. (2006). Ultrasound accelerated Claisen–Schmidt condensation: A green route to chalcones. *Applied Surface Science, 252*(17), 6071-6074

Calvo, K. R., Liotta, L. A., & Petricoin, E. F. (2005). Clinical Proteomics: From Biomarker Discovery and Cell Signaling Profiles to Individualized Personal Therapy. *Bioscience Reports, 25*(1-2), 107-125

Cao, H., Yu, J., Xu, W., Jia, X., Yang, J., Pan, Q. (2009). Proteomic analysis of regenerating mouse liver following 50% partial hepatectomy. *Proteome Science, 7*, 48

Cardone, M. H., Roy, N., Stennicke, H. R., Salvesen, G. S., Franke, T. F., Stanbridge, E. (1998). Regulation of cell death protease caspase-9 by phosphorylation. *Science, 282*(5392), 1318-1321

Cartwright, T. H. (2012). Treatment decisions after diagnosis of metastatic colorectal cancer. *Clinical Colorectal Cancer, 11*(3), 155-166

Cazarolli, L. H., Kappel, V. D., Zanatta, A. P., Suzuki, D. O. H., Yunes, R. A., Nunes, R. J. (2013). Natural and synthetic chalcones: tools for the study of targets of action—Insulin secretagogue or insulin mimetic? In R. Atta ur (Ed.), *Studies in natural products chemistry* (pp. 47-89). Amsterdam, Netherlands: Elsevier

Chandramouli, K., & Qian, P. Y. (2009). Proteomics: challenges, techniques and possibilities to overcome biological sample complexity. *Human Genomics and Proteomics, 2009*

Chaurand, P., Luetzenkirchen, F., & Spengler, B. (1999). Peptide and protein identification by matrix-assisted laser desorption ionization (MALDI) and MALDI-post-source decay time-of-flight mass spectrometry. *Journal of the American Society for Mass Spectrometry, 10*(2), 91-103

Chen, C. Y., Fang, H. Y., Chiou, S. H., Yi, S. E., Huang, C. Y., Chiang, S. F. (2011). Sumoylation of eukaryotic elongation factor 2 is vital for protein stability and anti-apoptotic activity in lung adenocarcinoma cells. *Cancer Science, 102*(8), 1582-1589

Chen, S. P., Yang, H. L., Her, G. M., Lin, H. Y., Jeng, M. F., Wu, J. L. (2006). Betanodavirus induces phosphatidylserine exposure and loss of mitochondrial membrane potential in secondary necrotic cells, both of which are blocked by bongkrekic acid. *Virology, 347*(2), 379-391

Chen, Y. C., Pohl, G., Wang, T. L., Morin, P. J., Risberg, B., Kristensen, G. B. (2005). Apolipoprotein E is required for cell proliferation and survival in ovarian cancer. *Cancer Research, 65*(1), 331-337

Cheung-Ong, K., Giaever, G., & Nislow, C. (2013). DNA-Damaging Agents in Cancer Chemotherapy: Serendipity and Chemical Biology. *Chemistry & Biology, 20*(5), 648-659

Chevalier, F. (2010). Highlights on the capacities of "Gel-based" proteomics. *Proteome Science, 8*, 23

Chiaradia, L. D., Mascarello, A., Purificacao, M., Vernal, J., Cordeiro, M. N., Zenteno, M. E. (2008). Synthetic chalcones as efficient inhibitors of Mycobacterium tuberculosis protein tyrosine phosphatase PtpA. *Bioorganic & Medicinal Chemistry Letters, 18*(23), 6227-6230

Cho, W. C. (2007). Contribution of oncoproteomics to cancer biomarker discovery. *Molecular Cancer, 6*, 25

Clarke, H. J., Chambers, J. E., Liniker, E., & Marciniak, S. J. (2014). Endoplasmic reticulum stress in malignancy. *Cancer Cell, 25*(5), 563-573

Clarke, P. R., & Zhang, C. (2001). Ran GTPase: a master regulator of nuclear structure and function during the eukaryotic cell division cycle? *Trends in Cell Biology, 11*(9), 366-371

Coleman, M. L., Sahai, E. A., Yeo, M., Bosch, M., Dewar, A., & Olson, M. F. (2001). Membrane blebbing during apoptosis results from caspase-mediated activation of ROCK I. *Nature Cell Biology, 3*(4), 339-345

Conaway, J. W., Kamura, T., & Conaway, R. C. (1998). The Elongin BC complex and the von Hippel-Lindau tumor suppressor protein. *Biochimica et Biophysica Acta, 1377*(2), M49-54

Coombes, R. C., Powles, T. J., & Neville, A. M. (1977). Evaluation of biochemical markers in breast cancer. *Journal of the Royal Society of Medicine, 70*(12), 843-845

Cote, C. S., Kor, C., Cohen, J., & Auclair, K. (2004). Composition and biological activity of traditional and commercial kava extracts. *Biochemical and Biophysical Research Communications, 322*(1), 147-152

Cristea, I. M., Gaskell, S. J., & Whetton, A. D. (2004). Proteomics techniques and their application to hematology. *Blood, 103*(10), 3624-3634

Croxatto, A., Prod'hom, G., & Greub, G. (2012). Applications of MALDI-TOF mass spectrometry in clinical diagnostic microbiology. *FEMS Microbiology Reviews, 36*(2), 380-407

Dangi, S., Chen, F. M., & Shapiro, P. (2006). Activation of extracellular signal-regulated kinase (ERK) in G2 phase delays mitotic entry through p21CIP1. *Cell Proliferation, 39*(4), 261-279

Danielsen, S. A., Eide, P. W., Nesbakken, A., Guren, T., Leithe, E., & Lothe, R. A. (2015). Portrait of the PI3K/AKT pathway in colorectal cancer. *Biochimica et Biophysica Acta, 1855*(1), 104-121

Darzynkiewicz, Z., Galkowski, D., & Zhao, H. (2008). Analysis of apoptosis by cytometry using TUNEL assay. *Methods, 44*(3), 250-254

David, J. N., Gordon, M. C., Susan, H., & Edward, A. S. (2002). Natural products and derivatives as leads to cell cycle pathway targets in cancer chemotherapy. *Current Cancer Drug Targets, 2*(4), 279-308

de Wit, M., Fijneman, R. J., Verheul, H. M., Meijer, G. A., & Jimenez, C. R. (2013). Proteomics in colorectal cancer translational research: biomarker discovery for clinical applications. *Clinical Biochemistry, 46*(6), 466-479

Delie, F., Petignat, P., & Cohen, M. (2012). GRP78 protein expression in ovarian cancer patients and perspectives for a drug-targeting approach. *Journal of Oncology, 2012*, 468615

Denayer, T., Stöhr, T., & Van Roy, M. (2014). Animal models in translational medicine: Validation and prediction. *New Horizons in Translational Medicine, 2*(1), 5-11

Deng, J., Carlson, N., Takeyama, K., Dal Cin, P., Shipp, M., & Letai, A. (2007). BH3 profiling identifies three distinct classes of apoptotic blocks to predict response to ABT-737 and conventional chemotherapeutic agents. *Cancer Cell, 12*(2), 171-185

DePinto, W., Chu, X. J., Yin, X., Smith, M., Packman, K., Goelzer, P. (2006). *In vitro* and *in vivo* activity of R547: a potent and selective cyclin-dependent kinase inhibitor currently in phase I clinical trials. *Molecular Cancer Therapeutics, 5*(11), 2644-2658

DeSantis, M., Bowne, W., Ferretti, J., & Franceschi, A. (2014). Long term evaluation of mouse toxicity using application of spherical nanocarbon injected into known human prostatic carcinoma in nude mouse with microwave assisted therapy. *Journal of Nuclear Medcine, 55*(Supplement 1, Meeting Abstracts), 1515

Desouza, M., Gunning, P. W., & Stehn, J. R. (2012). The actin cytoskeleton as a sensor and mediator of apoptosis. *Bioarchitecture, 2*(3), 75-87

Dharmaratne, H. R., Nanayakkara, N. P., & Khan, I. A. (2002). Kavalactones from *Piper methysticum*, and their 13C NMR spectroscopic analyses. *Phytochemistry, 59*(4), 429-433

Diaz, L. A., Jr., Williams, R. T., Wu, J., Kinde, I., Hecht, J. R., Berlin, J. (2012). The molecular evolution of acquired resistance to targeted EGFR blockade in colorectal cancers. *Nature, 486*(7404), 537-540

Doke, S. K., & Dhawale, S. C. (2015). Alternatives to animal testing: A review. *Saudi Pharmaceutical Journal, 23*(3), 223-229

Dominguez, D. C., Lopes, R., & Torres, M. L. (2007). Proteomics: clinical applications. *Clinical Laboratory Science, 20*(4), 245-248

Dominguez, J. N., Charris, J. E., Lobo, G., Gamboa de Dominguez, N., Moreno, M. M., Riggione, F. (2001). Synthesis of quinolinyl chalcones and evaluation of their antimalarial activity. *European Journal of Medicinal Chemistry, 36*(6), 555-560

Donjerkovic, D., & Scott, D. W. (2000). Regulation of the G1 phase of the mammalian cell cycle. *Cell Research, 10*(1), 1-16

Du, W. (2003). Towards new anticancer drugs: a decade of advances in synthesis of camptothecins and related alkaloids. *Tetrahedron, 59*(44), 8649-8687

Dufour, A., Sampson, N. S., Li, J., Kuscu, C., Rizzo, R. C., Deleon, J. L. (2011). Small-molecule anticancer compounds selectively target the hemopexin domain of matrix metalloproteinase-9. *Cancer Research, 71*(14), 4977-4988

Dunn, B. K., Jegalian, K., & Greenwald, P. (2011). Biomarkers for early detection and as surrogate endpoints in cancer prevention trials: issues and opportunities. *Recent Results in Cancer Research, 188*, 21-47

Duprez, L., Wirawan, E., Vanden Berghe, T., & Vandenabeele, P. (2009). Major cell death pathways at a glance. *Microbes and Infection, 11*(13), 1050-1062

Duronio, V. (2008). The life of a cell: apoptosis regulation by the PI3K/PKB pathway. *Biochemical Journal, 415*(3), 333-344

Elfant, A. B. (2015). Hot topics in primary care: colorectal cancer screening. *The Journal of Family Practice, 64*(12 Suppl), S10-15

Elliott, M. R., & Ravichandran, K. S. (2010). Clearance of apoptotic cells: implications in health and disease. *The Journal of Cell Biology, 189*(7), 1059-1070

Eskander, R. N., Randall, L. M., Sakai, T., Guo, Y., Hoang, B., & Zi, X. (2012). Flavokawain B, a novel, naturally occurring chalcone, exhibits robust apoptotic effects and induces G2/M arrest of a uterine leiomyosarcoma cell line. *Journal of Obstetrics and Gynaecology Research, 38*(8), 1086-1094

Fang, J. Y., & Richardson, B. C. (2005). The MAPK signalling pathways and colorectal cancer. *Lancet Oncology, 6*(5), 322-327

Fearon, E. R., & Vogelstein, B. (1990). A genetic model for colorectal tumorigenesis. *Cell, 61*(5), 759-767

Ferlay, J., Soerjomataram, I., Dikshit, R., Eser, S., Mathers, C., Rebelo, M. (2015). Cancer incidence and mortality worldwide: sources, methods and major patterns in GLOBOCAN 2012. *International Journal of Cancer, 136*(5), E359-386

Fernandez, P. M., Tabbara, S. O., Jacobs, L. K., Manning, F. C., Tsangaris, T. N., Schwartz, A. M. (2000). Overexpression of the glucose-regulated stress gene GRP78 in malignant but not benign human breast lesions. *Breast Cancer Research and Treatment, 59*(1), 15-26

Fink, S. L., & Cookson, B. T. (2005). Apoptosis, pyroptosis, and necrosis: mechanistic description of dead and dying eukaryotic cells. *Infection and Immunity, 73*(4), 1907-1916

Fountoulakis, M., & Takacs, B. (2001). Effect of strong detergents and chaotropes on the detection of proteins in two-dimensional gels. *Electrophoresis, 22*(9), 1593-1602

Freed, E., Lacey, K. R., Huie, P., Lyapina, S. A., Deshaies, R. J., Stearns, T. (1999). Components of an SCF ubiquitin ligase localize to the centrosome and regulate the centrosome duplication cycle. *Genes & Development, 13*(17), 2242-2257

Fulda, S. (2010). Cell death and survival signaling in oncogenesis. *Klinische Pädiatrie, 222*(6), 340-344

Fulda, S., & Debatin, K. M. (2006). Extrinsic versus intrinsic apoptosis pathways in anticancer chemotherapy. *Oncogene, 25*(34), 4798-4811

Fulda, S., Gorman, A. M., Hori, O., & Samali, A. (2010). Cellular stress responses: cell survival and cell death. *International Journal of Cell Biology, 2010,* 214074

Gao, J., Gao, L., Zhang, L., Yao, W., Cao, Y., Bao, B. (2015). 3-O-(2'E,4'Z-decadienoyl)-20-O-acetylingenol induces apoptosis in intestinal epithelial cells of rats via mitochondrial pathway. *Journal of Ethnopharmacology, 174*, 331-338

Garborg, K., Holme, O., Loberg, M., Kalager, M., Adami, H. O., & Bretthauer, M. (2013). Current status of screening for colorectal cancer. *Annals of Oncology, 24*(8), 1963-1972

Georgescu, C. V., Saftoiu, A., Georgescu, C. C., Ciurea, R., & Ciurea, T. (2007). Correlations of proliferation markers, p53 expression and histological findings in colorectal carcinoma. *Journal of Gastrointestinal and Liver Diseases, 16*(2), 133-139

Giacinti, C., & Giordano, A. (2006). RB and cell cycle progression. *Oncogene, 25*(38), 5220-5227

Gottlieb, E., Vander Heiden, M. G., & Thompson, C. B. (2000). Bcl-x(L) prevents the initial decrease in mitochondrial membrane potential and subsequent reactive oxygen species production during tumor necrosis factor alpha-induced apoptosis. *Molecular and Cellular Biology, 20*(15), 5680-5689

Grady, W. M. (2004a). Cancer, Overview A2 - Johnson, Leonard R *Encyclopedia of Gastroenterology* (pp. 256-264). New York: Elsevier.

Grady, W. M. (2004b). Genomic instability and colon cancer. *Cancer and Metastasis Reviews, 23*(1-2), 11-27

Graves, P. R., & Haystead, T. A. J. (2002). Molecular biologist's guide to proteomics. *Microbiology and Molecular Biology Reviews, 66*(1), 39-63

Greene, F. L., & Sobin, L. H. (2008). The staging of cancer: a retrospective and prospective appraisal. *CA: A Cancer Journal for Clinicians, 58*(3), 180-190

Guarguaglini, G., Renzi, L., D'Ottavio, F., Di Fiore, B., Casenghi, M., Cundari, E. (2000). Regulated Ran-binding protein 1 activity is required for organization and function of the mitotic spindle in mammalian cells *in vivo*. *Cell Growth & Differentiation, 11*(8), 455-465

Guicciardi, M. E., & Gores, G. J. (2009). Life and death by death receptors. *The FASEB Journal, 23*(6), 1625-1637

Guicciardi, M. E., Mott, J. L., Bronk, S. F., Kurita, S., Fingas, C. D., & Gores, G. J. (2011). Cellular inhibitor of apoptosis 1 (cIAP-1) degradation by caspase 8 during TNF-related apoptosis-inducing ligand (TRAIL)-induced apoptosis. *Experimental Cell Research, 317*(1), 107-116

Guo, S., Zou, J., & Wang, G. (2013). Advances in the proteomic discovery of novel therapeutic targets in cancer. *Drug Design, Development and Therapy, 7*, 1259-1271

Gygi, S. P., Corthals, G. L., Zhang, Y., Rochon, Y., & Aebersold, R. (2000). Evaluation of two-dimensional gel electrophoresis-based proteome analysis technology. *Proceedings of the National Academy of Sciences of the United States of America, 97*(17), 9390-9395

Haggar, F. A., & Boushey, R. P. (2009a). Colorectal cancer epidemiology: incidence, mortality, survival, and risk factors. *Clin Colon Rectal Surg, 22*(4), 191-197

Haggar, F. A., & Boushey, R. P. (2009b). Colorectal cancer epidemiology: incidence, mortality, survival, and risk factors. *Clinics in Colon and Rectal Surgery, 22*(4), 191-197

Hahn-Windgassen, A., Nogueira, V., Chen, C. C., Skeen, J. E., Sonenberg, N., & Hay, N. (2005). Akt activates the mammalian target of rapamycin by regulating cellular ATP level and AMPK activity. *The Journal of Biological Chemistry, 280*(37), 32081-32089

Han, C. R., Jun do, Y., Woo, H. J., Jeong, S. Y., Woo, M. H., & Kim, Y. H. (2012). Induction of microtubule-damage, mitotic arrest, Bcl-2 phosphorylation, Bak activation, and mitochondria-dependent caspase cascade is involved in human Jurkat T-cell apoptosis by aruncin B from Aruncus dioicus var. kamtschaticus. *Bioorganic & Medicinal Chemistry Letters, 22*(2), 945-953

Han, X., Aslanian, A., & Yates, J. R., 3rd. (2008). Mass spectrometry for proteomics. *Current Opinion in Chemical Biology, 12*(5), 483-490

Hanahan, D., & Weinberg, R. A. (2011). Hallmarks of cancer: the next generation. *Cell, 144*(5), 646-674

Harris, M. H., & Thompson, C. B. (2000). The role of the Bcl-2 family in the regulation of outer mitochondrial membrane permeability. *Cell Death & Differentiation, 7*(12), 1182-1191

He, X., Wang, L., Szklarz, G., Bi, Y., & Ma, Q. (2012). Resveratrol inhibits paraquat-induced oxidative stress and fibrogenic response by activating the nuclear factor erythroid 2-related factor 2 pathway. *Journal of Pharmacology and Experimental Therapeutics, 342*(1), 81-90

Hengartner, M. O. (2000). The biochemistry of apoptosis. *Nature, 407*(6805), 770-776

Henry, N. L., & Hayes, D. F. (2012). Cancer biomarkers. *Molecular Oncology, 6*(2), 140-146

Hershey, J. W. (2015). The role of eIF3 and its individual subunits in cancer. *Biochimica et Biophysica Acta, 1849*(7), 792-800

Hetz, C. (2012). The unfolded protein response: controlling cell fate decisions under ER stress and beyond. *Nature Reviews Molecular Cell Biology, 13*(2), 89-102

Hitosugi, T., Zhou, L., Elf, S., Fan, J., Kang, H. B., Seo, J. H. (2012). Phosphoglycerate mutase 1 coordinates glycolysis and biosynthesis to promote tumor growth. *Cancer Cell, 22*(5), 585-600

Honda, K., Ono, M., Shitashige, M., Masuda, M., Kamita, M., Miura, N. (2013). Proteomic approaches to the discovery of cancer biomarkers for early detection and personalized medicine. *Japanese Journal of Clinical Oncology, 43*(2), 103-109

Hosoi, T., Hyoda, K., Okuma, Y., Nomura, Y., & Ozawa, K. (2007). Akt up- and down-regulation in response to endoplasmic reticulum stress. *Brain Research, 1152*, 27-31

Housman, G., Byler, S., Heerboth, S., Lapinska, K., Longacre, M., Snyder, N. (2014). Drug resistance in cancer: an overview. *Cancers (Basel), 6*(3), 1769-1792

Hu, W., & Kavanagh, J. J. (2003). Anticancer therapy targeting the apoptotic pathway. *Lancet Oncology, 4*(12), 721-729

Hu, Y., Benedict, M. A., Wu, D., Inohara, N., & Nunez, G. (1998). Bcl-XL interacts with Apaf-1 and inhibits Apaf-1-dependent caspase-9 activation. *Proceedings of the National Academy of Sciences of the United States of America, 95*(8), 4386-4391

Hu, Y., Rosen, D. G., Zhou, Y., Feng, L., Yang, G., Liu, J. (2005). Mitochondrial manganese-superoxide dismutase expression in ovarian cancer: role in cell proliferation and response to oxidative stress. *Journal of Biological Chemistry, 280*(47), 39485-39492

Huang, L. Y., Lee, Y. S., Huang, J. J., Chang, C. C., Chang, J. M., Chuang, S. H. (2014a). Characterization of the biological activity of a potent small molecule Hec1 inhibitor TAI-1. *Journal of Experimental & Clinical Cancer Research, 33*, 6

Huang, M., Shen, A., Ding, J., & Geng, M. (2014b). Molecularly targeted cancer therapy: some lessons from the past decade. *Trends in Pharmacological Sciences, 35*(1), 41-50

Huang, X., Zhang, X., Farahvash, B., & Olumi, A. F. (2007). Novel targeted pro-apoptotic agents for the treatment of prostate cancer. *The Journal of Urology, 178*(5), 1846-1854

Hudler, P., Kocevar, N., & Komel, R. (2014). Proteomic approaches in biomarker discovery: new perspectives in cancer diagnostics. *Scientific World Journal, 2014*, 260348

Hughes, J. P., Rees, S., Kalindjian, S. B., & Philpott, K. L. (2011). Principles of early drug discovery. *British Journal of Pharmacology, 162*(6), 1239-1249

Humphries, A., & Wright, N. A. (2008). Colonic crypt organization and tumorigenesis. *Nature Reviews Cancer, 8*(6), 415-424

Ifere, G. O., Desmond, R., Demark-Wahnefried, W., & Nagy, T. R. (2013). Apolipoprotein E gene polymorphism influences aggressive behavior in prostate cancer cells by deregulating cholesterol homeostasis. *International Journal of Oncology, 43*(4), 1002-1010

Imtiyaz, H. Z., & Simon, M. C. (2010). Hypoxia-inducible factors as essential regulators of inflammation. *Current Topics in Microbiology and Immunology, 345*, 105-120

Indran, I. R., Tufo, G., Pervaiz, S., & Brenner, C. (2011). Recent advances in apoptosis, mitochondria and drug resistance in cancer cells. *Biochimica et Biophysica Acta, 1807*(6), 735-745

Issaenko, O. A., & Amerik, A. Y. (2012). Chalcone-based small-molecule inhibitors attenuate malignant phenotype via targeting deubiquitinating enzymes. *Cell Cycle, 11*(9), 1804-1817

Ito, Y., Takano, T., & Miyauchi, A. (2006). Apolipoprotein e expression in anaplastic thyroid carcinoma. *Oncology, 71*(5-6), 388-393

Itoh, K., Chiba, T., Takahashi, S., Ishii, T., Igarashi, K., Katoh, Y. (1997). An Nrf2/small Maf heterodimer mediates the induction of phase II detoxifying enzyme genes through antioxidant response elements. *Biochemical and Biophysical Research Communications, 236*(2), 313-322

Itoh, N., Semba, S., Ito, M., Takeda, H., Kawata, S., & Yamakawa, M. (2002). Phosphorylation of Akt/PKB is required for suppression of cancer cell apoptosis and tumor progression in human colorectal carcinoma. *Cancer, 94*(12), 3127-3134

Jain, M. V., Paczulla, A. M., Klonisch, T., Dimgba, F. N., Rao, S. B., Roberg, K. (2013). Interconnections between apoptotic, autophagic and necrotic pathways: implications for cancer therapy development. *Journal of Cellular and Molecular Medicine, 17*(1), 12-29

Jandial, D. D., Blair, C. A., Zhang, S., Krill, L. S., Zhang, Y. B., & Zi, X. (2014). Molecular targeted approaches to cancer therapy and prevention using chalcones. *Current Cancer Drug Targets, 14*(2), 181-200

Janssen, A. M., Bosman, C. B., Sier, C. F., Griffioen, G., Kubben, F. J., Lamers, C. B. (1998). Superoxide dismutases in relation to the overall survival of colorectal cancer patients. *British Journal of Cancer, 78*(8), 1051-1057

Javadov, S., & Karmazyn, M. (2007). Mitochondrial permeability transition pore opening as an endpoint to initiate cell death and as a putative target for cardioprotection. *Cellular Physiology and Biochemistry, 20*(1-4), 1-22

Jeong, H. J., Lee, C. S., Choi, J., Hong, Y. D., Shin, S. S., Park, J. S. (2015). Flavokawains B and C, melanogenesis inhibitors, isolated from the root of Piper methysticum and synthesis of analogs. *Bioorganic & Medicinal Chemistry Letters, 25*(4), 799-802

Jette, L., Bissoon-Haqqani, S., Le Francois, B., Maroun, J. A., & Birnboim, H. C. (2008). Resistance of colorectal cancer cells to 5-FUdR and 5-FU caused by Mycoplasma infection. *Anticancer Research, 28*(4B), 2175-2180

Ji, T., Lin, C., Krill, L. S., Eskander, R., Guo, Y., Zi, X. (2013). Flavokawain B, a kava chalcone, inhibits growth of human osteosarcoma cells through G2/M cell cycle arrest and apoptosis. *Molecular Cancer, 12*, 55

Jia, Y., & Guo, M. (2013). Epigenetic changes in colorectal cancer. *Chinese Journal of Cancer, 32*(1), 21-30

Jimenez, C. R., & Verheul, H. M. (2014). Mass spectrometry-based proteomics: from cancer biology to protein biomarkers, drug targets, and clinical applications. *American Society of Clinical Oncology Educational Book*, e504-510

Jin, H. R., Liao, Y., Li, X., Zhang, Z., Zhao, J., Wang, C. Z. (2014). Anticancer compound Oplopantriol A kills cancer cells through inducing ER stress and BH3 proteins Bim and Noxa. *Cell Death & Disease, 5*, e1190

Johnson, M. E., & Howerth, E. W. (2004). Survivin: a bifunctional inhibitor of apoptosis protein. *Veterinary Pathology, 41*(6), 599-607

Johnson, T. L., Lai, M. B., Lai, J. C., & Bhushan, A. (2010). Inhibition of cell proliferation and MAP Kinase and Akt pathways in oral squamous cell carcinoma by genistein and biochanin A. *Evidence-Based Complementary and Alternative Medicine, 7*(3), 351-358

Karmakar, S., Banik, N. L., Patel, S. J., & Ray, S. K. (2007). Garlic compounds induced calpain and intrinsic caspase cascade for apoptosis in human malignant neuroblastoma SH-SY5Y cells. *Apoptosis, 12*(4), 671-684

Kasdagly, M., Radhakrishnan, S., Reddivari, L., Veeramachaneni, D. N., & Vanamala, J. (2014). Colon carcinogenesis: influence of Western diet-induced obesity and targeting stem cells using dietary bioactive compounds. *Nutrition, 30*(11-12), 1242-1256

Kastle, M., & Grune, T. (2011). Protein oxidative modification in the aging organism and the role of the ubiquitin proteasomal system. *Current Pharmaceutical Design, 17*(36), 4007-4022

Katkoori, V. R., Suarez-Cuervo, C., Shanmugam, C., Jhala, N. C., Callens, T., Messiaen, L. (2010). Bax expression is a candidate prognostic and predictive marker of colorectal cancer. *Journal of Gastrointestinal Oncology, 1*(2), 76-89

Kawada, M., Yamagoe, S., Murakami, Y., Suzuki, K., Mizuno, S., & Uehara, Y. (1997). Induction of p27Kip1 degradation and anchorage independence by Ras through the MAP kinase signaling pathway. *Oncogene, 15*(6), 629-637

Kelland, L. R. (2004). Of mice and men: values and liabilities of the athymic nude mouse model in anticancer drug development. *European Journal of Cancer, 40*(6), 827-836

Kelloff, G. J., & Sigman, C. C. (2012). Cancer biomarkers: selecting the right drug for the right patient. *Nature Reviews Drug Discovery, 11*(3), 201-214

Kerbel, R. S. (2003). Human tumor xenografts as predictive preclinical models for anticancer drug activity in humans: better than commonly perceived-but they can be improved. *Cancer Biology & Therapy, 2*(4 Suppl 1), S134-139

Kim, Y. H., Kim, J., Park, H., & Kim, H. P. (2007). Anti-inflammatory Activity of the Synthetic Chalcone Derivatives: Inhibition of Inducible Nitric Oxide Synthase-Catalyzed Nitric Oxide Production from Lipopolysaccharide-Treated RAW 264.7 Cells. *Biological and Pharmaceutical Bulletin, 30*(8), 1450-1455

Klamt, F., & Shacter, E. (2005). Taurine chloramine, an oxidant derived from neutrophils, induces apoptosis in human B lymphoma cells through mitochondrial damage. *The Journal of Biological Chemistry, 280*(22), 21346-21352

Kollipara, S., Agarwal, N., Varshney, B., & Paliwal, J. (2011). Technological Advancements in Mass Spectrometry and Its Impact on Proteomics. *Analytical Letters, 44*(8), 1498-1520

Korsmeyer, S. J. (1995). Regulators of cell death. *Trends in Genetics, 11*(3), 101-105

Kovacic, P., & Jacintho, J. D. (2001). Mechanisms of carcinogenesis: focus on oxidative stress and electron transfer. *Current Medicinal Chemistry, 8*(7), 773-796

Kraljevic, S., Stambrook, P. J., & Pavelic, K. (2004). Accelerating drug discovery. *EMBO Reports, 5*(9), 837-842

Kramer, H. B., Lai, C. F., Patel, H., Periyasamy, M., Lin, M. L., Feller, S. M. (2016). LRH-1 drives colon cancer cell growth by repressing the expression of the CDKN1A gene in a p53-dependent manner. *Nucleic Acids Research, 44*(2), 582-594

Kroemer, G. (2003). The mitochondrial permeability transition pore complex as a pharmacological target. An introduction. *Current Medicinal Chemistry, 10*(16), 1469-1472

Krueger, A., Baumann, S., Krammer, P. H., & Kirchhoff, S. (2001). FLICE-inhibitory proteins: regulators of death receptor-mediated apoptosis. *Molecular and Cellular Biology, 21*(24), 8247-8254

Kuick, R., Misek, D. E., Monsma, D. J., Webb, C. P., Wang, H., Peterson, K. J. (2007). Discovery of cancer biomarkers through the use of mouse models. *Cancer Letters, 249*(1), 40-48

Kuninaka, S., Ichinose, Y., Koja, K., & Toh, Y. (2000). Suppression of manganese superoxide dismutase augments sensitivity to radiation, hyperthermia and doxorubicin in colon cancer cell lines by inducing apoptosis. *British Journal of Cancer, 83*(7), 928-934

Kuo, Y. F., Su, Y. Z., Tseng, Y. H., Wang, S. Y., Wang, H. M., & Chueh, P. J. (2010). Flavokawain B, a novel chalcone from *Alpinia pricei Hayata* with potent apoptotic activity: Involvement of ROS and GADD153 upstream of mitochondria-dependent apoptosis in HCT116 cells. *Free Radical Biology & Medicine, 49*(2), 214-226

Laukens, K., Naulaerts, S., & Berghe, W. V. (2015). Bioinformatics approaches for the functional interpretation of protein lists: from ontology term enrichment to network analysis. *Proteomics, 15*(5-6), 981-996

Lee, A. S. (2007). GRP78 induction in cancer: therapeutic and prognostic implications. *Cancer Research, 67*(8), 3496-3499

Lee, E. R., Kim, J. Y., Kang, Y. J., Ahn, J. Y., Kim, J. H., Kim, B. W. (2006). Interplay between PI3K/Akt and MAPK signaling pathways in DNA-damaging drug-induced apoptosis. *Biochimica et Biophysica Acta, 1763*(9), 958-968

Legrain, P., Aebersold, R., Archakov, A., Bairoch, A., Bala, K., Beretta, L. (2011). The human proteome project: Current state and future direction. *Molecular & Cellular Proteomics, 10*(7), M111.009993

Lenferink, A. E., Busse, D., Flanagan, W. M., Yakes, F. M., & Arteaga, C. L. (2001). ErbB2/neu kinase modulates cellular p27(Kip1) and cyclin D1 through multiple signaling pathways. *Cancer Research, 61*(17), 6583-6591

Levitzki, A., & Klein, S. (2010). Signal transduction therapy of cancer. *Molecular Aspects of Medicine, 31*(4), 287-329

Li, B., Blanc, J. M., Sun, Y., Yang, L., Zaorsky, N. G., Giacalone, N. J. (2014). Assessment of M867, a selective caspase-3 inhibitor, in an orthotopic mouse model for non-small cell lung carcinoma. *American Journal of Cancer Research, 4*(2), 161-171

Li, N., Liu, J. H., Zhang, J., & Yu, B. Y. (2008). Comparative evaluation of cytotoxicity and antioxidative activity of 20 flavonoids. *Journal of Agricultural and Food Chemistry, 56*(10), 3876-3883

Li, P., Nijhawan, D., Budihardjo, I., Srinivasula, S. M., Ahmad, M., Alnemri, E. S. (1997). Cytochrome c and dATP-dependent formation of Apaf-1/caspase-9 complex initiates an apoptotic protease cascade. *Cell, 91*(4), 479-489

Li, X., Zhang, K., & Li, Z. (2011). Unfolded protein response in cancer: the physician's perspective. *Journal of Hematology & Oncology, 4*, 8

Lin, E., Lin, W. H., Wang, S. Y., Chen, C. S., Liao, J. W., Chang, H. W. (2012). Flavokawain B inhibits growth of human squamous carcinoma cells: Involvement of apoptosis and cell cycle dysregulation *in vitro* and *in vivo*. *The Journal of Nutritional Biochemistry, 23*(4), 368-378

Lin, F. M., Tsai, C. H., Yang, Y. C., Tu, W. C., Chen, L. R., Liang, Y. S. (2008). A novel diterpene suppresses CWR22Rv1 tumor growth *in vivo* through antiproliferation and proapoptosis. *Cancer Research, 68*(16), 6634-6642

Lindsay, J., Esposti, M. D., & Gilmore, A. P. (2011). Bcl-2 proteins and mitochondria--specificity in membrane targeting for death. *Biochimica et Biophysica Acta, 1813*(4), 532-539

Linge, A., Maurya, P., Friedrich, K., Baretton, G. B., Kelly, S., Henry, M. (2014). Identification and functional validation of RAD23B as a potential protein in human breast cancer progression. *Journal of Proteome Research, 13*(7), 3212-3222

Liu, J., & Wang, Z. (2015). Increased Oxidative Stress as a Selective Anticancer Therapy. *Oxidative Medicine and Cellular Longevity, 2015*, 294303

Liu, L., Zhao, L., Zhang, Y., Zhang, Q., & Ding, Y. (2007). Proteomic analysis of Tiam1-mediated metastasis in colorectal cancer. *Cell Biology International, 31*(8), 805-814

Liu, Y. H., Ho, C. C., Cheng, C. C., Chao, W. T., Pei, R. J., Hsu, Y. H. (2011). Cytokeratin 18-mediated disorganization of intermediate filaments is induced by degradation of plectin in human liver cells. *Biochemical and Biophysical Research Communications, 407*(3), 575-580

Loa, J., Chow, P., & Zhang, K. (2009). Studies of structure-activity relationship on plant polyphenol-induced suppression of human liver cancer cells. *Cancer Chemotherapy and Pharmacology, 63*(6), 1007-1016

Lu, Y., Hou, S. X., & Chen, T. (2003). Advances in the study of vincristine: an anticancer ingredient from *Catharanthus roseus*. *Zhongguo Zhong Yao Za Zhi, 28*(11), 1006-1009

Ludwig, J. A., & Weinstein, J. N. (2005). Biomarkers in cancer staging, prognosis and treatment selection. *Nature Reviews Cancer, 5*(11), 845-856

Luk, J. M., Lam, C. T., Siu, A. F., Lam, B. Y., Ng, I. O., Hu, M. Y. (2006). Proteomic profiling of hepatocellular carcinoma in Chinese cohort reveals heat-shock proteins (Hsp27, Hsp70, GRP78) up-regulation and their associated prognostic values. *Proteomics, 6*(3), 1049-1057

Luo, H. Y., & Xu, R. H. (2014). Predictive and prognostic biomarkers with therapeutic targets in advanced colorectal cancer. *World Journal of Gastroenterology, 20*(14), 3858-3874

Macaluso, M., Paggi, M. G., & Giordano, A. (2003). Genetic and epigenetic alterations as hallmarks of the intricate road to cancer. *Oncogene, 22*(42), 6472-6478

Magdeldin, S., Enany, S., Yoshida, Y., Xu, B., Zhang, Y., Zureena, Z. (2014). Basics and recent advances of two dimensional- polyacrylamide gel electrophoresis. *Clinical proteomics, 11*(1), 16-16

Mahapatra, D. M., Bharti, S. K., & Asati, V. (2015). Anti-cancer chalcones: Structural and molecular target perspectives. *European Journal of Medicinal Chemistry, 98*, 69-114

Maines, M. D. (1997). The heme oxygenase system: a regulator of second messenger gases. *Annual Review of Pharmacology and Toxicology, 37*, 517-554

Majors, B. S., Betenbaugh, M. J., & Chiang, G. G. (2007). Links between metabolism and apoptosis in mammalian cells: applications for anti-apoptosis engineering. *Metabolic Engineering, 9*(4), 317-326

Malek, S. N., Phang, C. W., Ibrahim, H., Norhanom, A. W., & Sim, K. S. (2011). Phytochemical and cytotoxic investigations of *Alpinia mutica* rhizomes. *Molecules, 16*(1), 583-589

Manuel, Y., Defontaine, M. C., Bourgoin, J. J., Dargent, M., & Sonneck, J. M. (1971). Serum haemopexin levels in patients with malignant melanoma. *Clinica Chimica Acta, 31*(2), 485-486

Mara, C., & Marina, C. (2013). Proteomics-based drug discovery and chemoproteomics. In L. Sleno (Ed.), *Applications of high-resolution mass spectrometry in drug discovery and development* (pp. 120-139). London, UK: Future Science Ltd

Marusyk, A., Almendro, V., & Polyak, K. (2012). Intra-tumour heterogeneity: a looking glass for cancer? *Nature Reviews Cancer, 12*(5), 323-334

Marusyk, A., & Polyak, K. (2010). Tumor heterogeneity: causes and consequences. *Biochimica et Biophysica Acta, 1805*(1), 105-117

Mathew, A., & Morimoto, R. I. (1998). Role of the heat-shock response in the life and death of proteins. *Annals of the New York Academy of Sciences, 851*, 99-111

Mathews, M. B., & Hershey, J. W. (2015). The translation factor eIF5A and human cancer. *Biochimica et Biophysica Acta, 1849*(7), 836-844

Maydt, D., De Spirt, S., Muschelknautz, C., Stahl, W., & Muller, T. J. (2013). Chemical reactivity and biological activity of chalcones and other alpha,beta-unsaturated carbonyl compounds. *Xenobiotica, 43*(8), 711-718

McGuckin, M. A., Eri, R. D., Das, I., Lourie, R., & Florin, T. H. (2010). ER stress and the unfolded protein response in intestinal inflammation. *The American Journal of Physiology-Gastrointestinal and Liver Physiology, 298*(6), G820-832

McNally, S. J., Harrison, E. M., Ross, J. A., Garden, O. J., & Wigmore, S. J. (2007). Curcumin induces heme oxygenase 1 through generation of reactive oxygen species, p38 activation and phosphatase inhibition. *International Journal of Molecular Medicine, 19*(1), 165-172

Mekahli, D., Bultynck, G., Parys, J. B., De Smedt, H., & Missiaen, L. (2011). Endoplasmic-reticulum calcium depletion and disease. *Cold Spring Harbor Perspectives in Biology, 3*(6)

Melet, A., Song, K., Bucur, O., Jagani, Z., Grassian, A. R., & Khosravi-Far, R. (2008). Apoptotic pathways in tumor progression and therapy. *Advances in Experimental Medicine and Biology, 615*, 47-79

Merrick, B. A. (2008). The plasma proteome, adductome and idiosyncratic toxicity in toxicoproteomics research. *Briefings in Functional Genomics, 7*(1), 35-49

Mesri, M. (2014). Advances in Proteomic Technologies and Its Contribution to the Field of Cancer. *Advances in Medicine, 2014*, 238045

Michor, F., & Polyak, K. (2010). The origins and implications of intratumor heterogeneity. *Cancer Prevention Research, 3*(11), 1361-1364

Miranda, A., Janssen, L., Bosman, C. B., van Duijn, W., Oostendorp-van de Ruit, M. M., Kubben, F. J. G. M. (2000). Superoxide Dismutases in Gastric and Esophageal Cancer and the Prognostic Impact in Gastric Cancer. *Clinical Cancer Research, 6*(8), 3183-3192

Miranda, C. L., Stevens, J. F., Ivanov, V., McCall, M., Frei, B., Deinzer, M. L. (2000). Antioxidant and prooxidant actions of prenylated and nonprenylated chalcones and flavanones *in vitro*. *Journal of Agricultural and Food Chemistry, 48*(9), 3876-3884

Mitsiades, N., Mitsiades, C. S., Poulaki, V., Chauhan, D., Fanourakis, G., Gu, X. (2002). Molecular sequelae of proteasome inhibition in human multiple myeloma cells. *Proceedings of the National Academy of Sciences of the United States of America, 99*(22), 14374-14379

Moll, U. M., & Petrenko, O. (2003). The MDM2-p53 interaction. *Molecular Cancer Research, 1*(14), 1001-1008

Mollinedo, F., Gajate, C., Martin-Santamaria, S., & Gago, F. (2004). ET-18-OCH3 (edelfosine): a selective antitumour lipid targeting apoptosis through intracellular activation of Fas/CD95 death receptor. *Current Medicinal Chemistry, 11*(24), 3163-3184

Moudi, M., Go, R., Yien, C. Y., & Nazre, M. (2013). Vinca alkaloids. *International Journal of Preventive Medicine, 4*(11), 1231-1235

Nakamura, J., Aoyagi, S., Nanchi, I., Nakatsuka, S., Hirata, E., Shibata, S. (2009). Overexpression of eukaryotic elongation factor eEF2 in gastrointestinal cancers and its involvement in G_2/M progression in the cell cycle. *International Journal of Oncology, 34*(5), 1181-1189

Nakamura, S., Otani, T., Ijiri, Y., Motoda, R., Kurimoto, M., & Orita, K. (2000). IFN-gamma-dependent and -independent mechanisms in adverse effects caused by concomitant administration of IL-18 and IL-12. *The Journal of Immunology, 164*(6), 3330-3336

Ndozangue-Touriguine, O., Hamelin, J., & Breard, J. (2008). Cytoskeleton and apoptosis. *Biochemical Pharmacology, 76*(1), 11-18

Neutzner, A., Li, S., Xu, S., & Karbowski, M. (2012). The ubiquitin/proteasome system-dependent control of mitochondrial steps in apoptosis. *Seminars in Cell and Developmental Biology, 23*(5), 499-508

Ng, S. C., & Wong, S. H. (2013). Colorectal cancer screening in Asia. *British Medical Bulletin, 105*, 29-42

Nibbe, R. K., & Chance, M. R. (2009). Approaches to biomarkers in human colorectal cancer: looking back, to go forward. *Biomarkers in Medicine, 3*(4), 385-396

Nicoll, J. A., Zunarelli, E., Rampling, R., Murray, L. S., Papanastassiou, V., & Stewart, J. (2003). Involvement of apolipoprotein E in glioblastoma: immunohistochemistry and clinical outcome. *Neuroreport, 14*(15), 1923-1926

Niemi, M., Hakkinen, T., Karttunen, T. J., Eskelinen, S., Kervinen, K., Savolainen, M. J. (2002). Apolipoprotein E and colon cancer. Expression in normal and malignant human intestine and effect on cultured human colonic adenocarcinoma cells. *European Journal of Internal Medicine, 13*(1), 37-43

Nishitoh, H. (2012). CHOP is a multifunctional transcription factor in the ER stress response. *The Journal of Biochemistry, 151*(3), 217-219

Noiva, R. (1999). Protein disulfide isomerase: the multifunctional redox chaperone of the endoplasmic reticulum. *Seminars in Cell and Developmental Biology, 10*(5), 481-493

Nunez de Villavicencio-Diaz, T., Ramos Gomez, Y., Oliva Arguelles, B., Fernandez Masso, J. R., Rodriguez-Ulloa, A., Cruz Garcia, Y. (2015). Comparative proteomics analysis of the antitumor effect of CIGB-552 peptide in HT-29 colon adenocarcinoma cells. *Journal of Proteomics, 126*, 163-171

Onyilagha, J. C., Malhotra, B., Elder, M., French, C. J., & Towers, G. H. N. (1997). Comparative studies of inhibitory activities of chalcones on tomato ringspot virus (ToRSV). *Canadian Journal of Plant Pathology, 19*(2), 133-137

Orlikova, B., Tasdemir, D., Golais, F., Dicato, M., & Diederich, M. (2011). Dietary chalcones with chemopreventive and chemotherapeutic potential. *Genes & Nutrition, 6*(2), 125-147

Ortega, J., Vigil, C. E., & Chodkiewicz, C. (2010). Current progress in targeted therapy for colorectal cancer. *Cancer Control, 17*(1), 7-15

Oshima, C. T., Iriya, K., & Forones, N. M. (2005). Ki-67 as a prognostic marker in colorectal cancer but not in gastric cancer. *Neoplasma, 52*(5), 420-424

Ozes, O. N., Mayo, L. D., Gustin, J. A., Pfeffer, S. R., Pfeffer, L. M., & Donner, D. B. (1999). NF-kappaB activation by tumour necrosis factor requires the Akt serine-threonine kinase. *Nature, 401*(6748), 82-85

Palma, S., Zwenger, A. O., Croce, M. V., Abba, M. C., & Lacunza, E. (2015). From Molecular Biology to Clinical Trials: Toward Personalized Colorectal Cancer Therapy. *Clinical Colorectal Cancer, 15*(2), 104-115

Pandey, U. B., & Nichols, C. D. (2011). Human disease models in Drosophila melanogaster and the role of the fly in therapeutic drug discovery. *Pharmacological Reviews, 63*(2), 411-436

Park, E. J., Kwon, H. K., Choi, Y. M., Shin, H. J., & Choi, S. (2012). Doxorubicin induces cytotoxicity through upregulation of pERK-dependent ATF3. *PLoS One, 7*(9), e44990

Parrish, A. B., Freel, C. D., & Kornbluth, S. (2013). Cellular mechanisms controlling caspase activation and function. *Cold Spring Harbor Perspectives in Biology, 5*(6)

Patridge, E., Gareiss, P., Kinch, M. S., & Hoyer, D. (2016). An analysis of FDA-approved drugs: natural products and their derivatives. *Drug Discovery Today, 21*(2), 204-207

Patterson, S. D., & Aebersold, R. H. (2003). Proteomics: the first decade and beyond. *Nature Genetics, 33 Suppl*, 311-323

Paul, G. G., Gordon, M. C., & David, J. N. (2010). Plant Natural Products in Anticancer Drug Discovery. *Current Organic Chemistry, 14*(16), 1781-1791

Pelicano, H., Martin, D. S., Xu, R. H., & Huang, P. (2006). Glycolysis inhibition for anticancer treatment. *Oncogene, 25*(34), 4633-4646

Piaggi, S., Raggi, C., Corti, A., Pitzalis, E., Mascherpa, M. C., Saviozzi, M. (2010). Glutathione transferase omega 1-1 (GSTO1-1) plays an anti-apoptotic role in cell resistance to cisplatin toxicity. *Carcinogenesis, 31*(5), 804-811

Piccard, H., Van den Steen, P. E., & Opdenakker, G. (2007). Hemopexin domains as multifunctional liganding modules in matrix metalloproteinases and other proteins. *Journal of Leukocyte Biology, 81*(4), 870-892

Pietenpol, J. A., & Stewart, Z. A. (2002). Cell cycle checkpoint signaling: cell cycle arrest versus apoptosis. *Toxicology, 181-182*, 475-481

Pietrogrande, M. C., Marchetti, N., Dondi, F., & Righetti, P. G. (2003). Spot overlapping in two-dimensional polyacrylamide gel electrophoresis maps: relevance to proteomics. *Electrophoresis, 24*(1-2), 217-224

Pino, M. S., & Chung, D. C. (2010). The chromosomal instability pathway in colon cancer. *Gastroenterology, 138*(6), 2059-2072

Plafker, K., & Macara, I. G. (2000). Facilitated nucleocytoplasmic shuttling of the Ran binding protein RanBP1. *Molecular and Cellular Biology, 20*(10), 3510-3521

Pohle, T., Brandlein, S., Ruoff, N., Muller-Hermelink, H. K., & Vollmers, H. P. (2004). Lipoptosis: tumor-specific cell death by antibody-induced intracellular lipid accumulation. *Cancer Research, 64*(11), 3900-3906

Pomastowski, P., & Buszewski, B. (2014). Two-dimensional gel electrophoresis in the light of new developments. *TrAC Trends in Analytical Chemistry, 53*, 167-177

Pootrakul, L., Datar, R. H., Shi, S. R., Cai, J., Hawes, D., Groshen, S. G. (2006). Expression of stress response protein Grp78 is associated with the development of castration-resistant prostate cancer. *Clinical Cancer Research, 12*(20 Pt 1), 5987-5993

Qi, J., Dong, Z., Liu, J., & Zhang, J. T. (2014). EIF3i promotes colon oncogenesis by regulating COX-2 protein synthesis and beta-catenin activation. *Oncogene, 33*(32), 4156-4163

Rabilloud, T., & Lelong, C. (2011). Two-dimensional gel electrophoresis in proteomics: a tutorial. *Journal of Proteomics, 74*(10), 1829-1841

Rafiee, E., & Rahimi, F. (2013). A green approach to the synthesis of chalcones via Claisen-Schmidt condensation reaction using cesium salts of 12-tungstophosphoric acid as a reusable nanocatalyst. *Monatshefte für Chemie - Chemical Monthly, 144*(3), 361-367

Ramalho, R. M., Viana, R. J., Low, W. C., Steer, C. J., & Rodrigues, C. M. (2008). Bile acids and apoptosis modulation: an emerging role in experimental Alzheimer's disease. *Trends in Molecular Medicine, 14*(2), 54-62

Rao, C. V., & Yamada, H. Y. (2013). Genomic instability and colon carcinogenesis: from the perspective of genes. *Frontiers in Oncology, 3*, 130

Rao, V. S., Srinivas, K., Sujini, G. N., & Kumar, G. N. S. (2014). Protein-Protein Interaction Detection: Methods and Analysis. *International Journal of Proteomics, 2014*, 12

Rates, S. M. (2001). Plants as source of drugs. *Toxicon, 39*(5), 603-613

Rauschert, N., Brandlein, S., Holzinger, E., Hensel, F., Muller-Hermelink, H. K., & Vollmers, H. P. (2008). A new tumor-specific variant of GRP78 as target for antibody-based therapy. *Laboratory Investigation, 88*(4), 375-386

Rayees Ahmad, M., Girija Sastry, V., Bano, N., & Anwar, S. (2016). Synthesis of novel chalcone derivatives by conventional and microwave irradiation methods and their pharmacological activities. *Arabian Journal of Chemistry, 9*, S931-S935

Rensen, W. M., Roscioli, E., Tedeschi, A., Mangiacasale, R., Ciciarello, M., Di Gioia, S. A. (2009). RanBP1 downregulation sensitizes cancer cells to taxol in a caspase-3-dependent manner. *Oncogene, 28*(15), 1748-1758

Reubold, T. F., Wohlgemuth, S., & Eschenburg, S. (2011). Crystal structure of full-length Apaf-1: how the death signal is relayed in the mitochondrial pathway of apoptosis. *Structure, 19*(8), 1074-1083

Reuter, S., Gupta, S. C., Chaturvedi, M. M., & Aggarwal, B. B. (2010). Oxidative stress, inflammation, and cancer: how are they linked? *Free Radical Biology & Medicine, 49*(11), 1603-1616

Roberts, P. J., & Der, C. J. (2007). Targeting the Raf-MEK-ERK mitogen-activated protein kinase cascade for the treatment of cancer. *Oncogene, 26*(22), 3291-3310

Roy, S., Kaur, M., Agarwal, C., Tecklenburg, M., Sclafani, R. A., & Agarwal, R. (2007). p21 and p27 induction by silibinin is essential for its cell cycle arrest effect in prostate carcinoma cells. *Molecular Cancer Therapeutics, 6*(10), 2696-2707

Safa, A. R. (2012). c-FLIP, a master anti-apoptotic regulator. *Experimental Oncology, 34*(3), 176-184

Sak, K. (2012). Chemotherapy and dietary phytochemical agents. *Chemotherapy Research and Practice, 2012*, 282570

Sakai, T., Eskander, R. N., Guo, Y., Kim, K. J., Mefford, J., Hopkins, J. (2012). Flavokawain B, a kava chalcone, induces apoptosis in synovial sarcoma cell lines. *Journal of Orthopaedic Research, 30*(7), 1045-1050

Salvesen, G. S., & Dixit, V. M. (1999). Caspase activation: the induced-proximity model. *Proceedings of the National Academy of Sciences of the United States of America, 96*(20), 10964-10967

Sano, Y., Byeon, J. S., Li, X. B., Wong, M. C., Chiu, H. M., Rerknimitr, R. (2016). Colorectal cancer screening of the general population in East Asia. *Digestive Endoscopy, 28*(3), 243-249

Savino, R., Paduano, S., Preiano, M., & Terracciano, R. (2012). The proteomics big challenge for biomarkers and new drug-targets discovery. *International Journal of Molecular Sciences, 13*(11), 13926-13948

Schluter, K., Gassmann, P., Enns, A., Korb, T., Hemping-Bovenkerk, A., Holzen, J. (2006). Organ-specific metastatic tumor cell adhesion and extravasation of colon carcinoma cells with different metastatic potential. *American Journal of Pathology, 169*(3), 1064-1073

Schmelz, K., Wagner, M., Dorken, B., & Tamm, I. (2005). 5-Aza-2'-deoxycytidine induces p21WAF expression by demethylation of p73 leading to p53-independent apoptosis in myeloid leukemia. *International Journal of Cancer, 114*(5), 683-695

Schmidt, A., Forne, I., & Imhof, A. (2014). Bioinformatic analysis of proteomics data. *BMC Systems Biology, 8 Suppl 2*, S3

Schreiber, K. (2015). MALDI-TOF MS for the diagnosis of infectious diseases. Retrieved from https://news.mayomedicallaboratories.com/2015/2004/2013/maldi-tof-ms-for-the-diagnosis-of-infectious-diseases-2012/

Schutte, B., Henfling, M., Kolgen, W., Bouman, M., Meex, S., Leers, M. P. (2004). Keratin 8/18 breakdown and reorganization during apoptosis. *Experimental Cell Research, 297*(1), 11-26

Selimovic, D., Ahmad, M., El-Khattouti, A., Hannig, M., Haikel, Y., & Hassan, M. (2011). Apoptosis-related protein-2 triggers melanoma cell death by a mechanism including both endoplasmic reticulum stress and mitochondrial dysregulation. *Carcinogenesis, 32*(8), 1268-1278

Sharkey, F. E., & Fogh, J. (1984). Considerations in the use of nude mice for cancer research. *Cancer Metastasis Reviews, 3*(4), 341-360

Sheikh, M. O., Schafer, C. M., Powell, J. T., Rodgers, K. K., Mooers, B. H., & West, C. M. (2014). Glycosylation of Skp1 affects its conformation and promotes binding to a model f-box protein. *Biochemistry, 53*(10), 1657-1669

Shi, X., Xu, J., Wang, J., Cui, M., Gao, Y., Niu, H. (2015). Expression analysis of apolipoprotein E and its associated genes in gastric cancer. *Oncology Letters, 10*(3), 1309-1314

Siegel, R., DeSantis, C., Virgo, K., Stein, K., Mariotto, A., Smith, T. (2012). Cancer treatment and survivorship statistics, 2012. *CA: A Cancer Journal for Clinicians, 62*(4), 220-241

Silvera, D., Formenti, S. C., & Schneider, R. J. (2010). Translational control in cancer. *Nature Reviews Cancer, 10*(4), 254-266

Singh, P., Anand, A., & Kumar, V. (2014). Recent developments in biological activities of chalcones: a mini review. *European Journal of Medicinal Chemistry, 85*, 758-777

Singh, S., Upadhyay, A. K., Ajay, A. K., & Bhat, M. K. (2007). p53 regulates ERK activation in carboplatin induced apoptosis in cervical carcinoma: a novel target of p53 in apoptosis. *FEBS Letters, 581*(2), 289-295

Slattery, M. L., Sweeney, C., Murtaugh, M., Ma, K. N., Potter, J. D., Levin, T. R. (2005). Associations between apoE genotype and colon and rectal cancer. *Carcinogenesis, 26*(8), 1422-1429

Slichenmyer, W. J., & Von Hoff, D. D. (1991). Taxol: a new and effective anti-cancer drug. *Anticancer Drugs, 2*(6), 519-530

Song, X., Sun, Y., & Garen, A. (2005). Roles of PSF protein and VL30 RNA in reversible gene regulation. *Proceedings of the National Academy of Sciences of the United States of America, 102*(34), 12189-12193

Soreide, K., Janssen, E. A., Soiland, H., Korner, H., & Baak, J. P. (2006). Microsatellite instability in colorectal cancer. *British Journal of Surgery, 93*(4), 395-406

Spilka, R., Ernst, C., Mehta, A. K., & Haybaeck, J. (2013). Eukaryotic translation initiation factors in cancer development and progression. *Cancer Letters, 340*(1), 9-21

Srinivasan, B., Johnson, T. E., Lad, R., & Xing, C. G. (2009). Structure-activity relationship studies of chalcone leading to 3-hydroxy-4,3',4',5'-tetramethoxychalcone and its analogues as potent nuclear factor kappa B inhibitors and their anticancer activities. *Journal of medicinal chemistry, 52*(22), 7228-7235

Srivastava, V., Negi, A. S., Kumar, J. K., Gupta, M. M., & Khanuja, S. P. (2005). Plant-based anticancer molecules: a chemical and biological profile of some important leads. *Bioorganic & Medicinal Chemistry, 13*(21), 5892-5908

Stebbins, C. E., Kaelin, W. G., Jr., & Pavletich, N. P. (1999). Structure of the VHL-ElonginC-ElonginB complex: implications for VHL tumor suppressor function. *Science, 284*(5413), 455-461

Steiner, G. G. (2000). The correlation between cancer incidence and kava consumption. *Hawaii Medical Journal, 59*(11), 420-422

Steller, H. (1995). Mechanisms and genes of cellular suicide. *Science, 267*(5203), 1445-1449

Su, B. B., Shi, H., & Wan, J. (2012). Role of serum carcinoembryonic antigen in the detection of colorectal cancer before and after surgical resection. *World Journal of Gastroenterology, 18*(17), 2121-2126

Su, T. T., Goh, J. Y., Tan, J., Muhaimah, A. R., Pigeneswaren, Y., Khairun, N. S. (2013). Level of colorectal cancer awareness: a cross sectional exploratory study among multi-ethnic rural population in Malaysia. *BMC Cancer, 13*, 376

Su, W. P., Chen, Y. T., Lai, W. W., Lin, C. C., Yan, J. J., & Su, W. C. (2011). Apolipoprotein E expression promotes lung adenocarcinoma proliferation and migration and as a potential survival marker in lung cancer. *Lung Cancer, 71*(1), 28-33

Sugiyama, T., Shimizu, S., Matsuoka, Y., Yoneda, Y., & Tsujimoto, Y. (2002). Activation of mitochondrial voltage-dependent anion channel by apro-apoptotic BH3-only protein Bim. *Oncogene, 21*(32), 4944-4956

Sun, Z., Cheng, Z., Taylor, C. A., McConkey, B. J., & Thompson, J. E. (2010). Apoptosis induction by eIF5A1 involves activation of the intrinsic mitochondrial pathway. *Journal of Cellular Physiology, 223*(3), 798-809

Sung, J. J., Lau, J. Y., Goh, K. L., & Leung, W. K. (2005). Increasing incidence of colorectal cancer in Asia: implications for screening. *Lancet Oncology, 6*(11), 871-876

Tabas, I., & Ron, D. (2011). Integrating the mechanisms of apoptosis induced by endoplasmic reticulum stress. *Nature Cell Biology, 13*(3), 184-190

Tait, S. W., & Green, D. R. (2010). Mitochondria and cell death: outer membrane permeabilization and beyond. *Nature Reviews Molecular Cell Biology, 11*(9), 621-632

Tamm, I., Schriever, F., & Dorken, B. (2001). Apoptosis: implications of basic research for clinical oncology. *Lancet Oncology, 2*(1), 33-42

Tanaka, T. (2009). Colorectal carcinogenesis: Review of human and experimental animal studies. *Journal of Carcinogenesis, 8*, 5

Tang, Y., Simoneau, A. R., Xie, J., Shahandeh, B., & Zi, X. (2008). Effects of the kava chalcone flavokawain A differ in bladder cancer cells with wild-type versus mutant p53. *Cancer Prevention Research, 1*(6), 439-451

Taylor, C. A., Sun, Z., Cliche, D. O., Ming, H., Eshaque, B., Jin, S. (2007). Eukaryotic translation initiation factor 5A induces apoptosis in colon cancer cells and associates with the nucleus in response to tumour necrosis factor alpha signalling. *Experimental Cell Research, 313*(3), 437-449

Tekedereli, I., Alpay, S. N., Tavares, C. D., Cobanoglu, Z. E., Kaoud, T. S., Sahin, I. (2012). Targeted silencing of elongation factor 2 kinase suppresses growth and sensitizes tumors to doxorubicin in an orthotopic model of breast cancer. *PLoS One, 7*(7), e41171

Terzian, T., Suh, Y. A., Iwakuma, T., Post, S. M., Neumann, M., Lang, G. A. (2008). The inherent instability of mutant p53 is alleviated by Mdm2 or p16INK4a loss. *Genes & Development, 22*(10), 1337-1344

Teske, B. F., Wek, S. A., Bunpo, P., Cundiff, J. K., McClintick, J. N., Anthony, T. G. (2011). The eIF2 kinase PERK and the integrated stress response facilitate activation of ATF6 during endoplasmic reticulum stress. *Molecular Biology of the Cell, 22*(22), 4390-4405

Thiede, B., Koehler, C. J., Strozynski, M., Treumann, A., Stein, R., Zimny-Arndt, U. (2013). High resolution quantitative proteomics of HeLa cells protein species using stable isotope labeling with amino acids in cell culture(SILAC), two-dimensional gel electrophoresis(2DE) and nano-liquid chromatograpohy

coupled to an LTQ-OrbitrapMass spectrometer. *Molecular & Cellular Proteomics : MCP, 12*(2), 529-538

Tolosano, E., & Altruda, F. (2002). Hemopexin: structure, function, and regulation. *DNA and Cell Biology, 21*(4), 297-306

Torre, L. A., Bray, F., Siegel, R. L., Ferlay, J., Lortet-Tieulent, J., & Jemal, A. (2015). Global cancer statistics, 2012. *CA: A Cancer Journal for Clinicians, 65*(2), 87-108

Trachootham, D., Alexandre, J., & Huang, P. (2009). Targeting cancer cells by ROS-mediated mechanisms: a radical therapeutic approach? *Nature Reviews Drug Discovery, 8*(7), 579-591

Tsuboi, K., Bachovchin, D. A., Speers, A. E., Spicer, T. P., Fernandez-Vega, V., Hodder, P. (2011). Potent and selective inhibitors of glutathione S-transferase omega 1 that impair cancer drug resistance. *Journal of the American Chemical Society, 133*(41), 16605-16616

Tunon, J., Martin-Ventura, J. L., Blanco-Colio, L. M., Lorenzo, O., Lopez, J. A., & Egido, J. (2010). Proteomic strategies in the search of new biomarkers in atherothrombosis. *Journal of the American College of Cardiology, 55*(19), 2009-2016

Tzifi, F., Economopoulou, C., Gourgiotis, D., Ardavanis, A., Papageorgiou, S., & Scorilas, A. (2012). The role of BCL2 family of apoptosis regulator proteins in acute and chronic leukemias. *Advances in Hematology, 2012*, 524308

Ulivieri, C. (2010). Cell death: insights into the ultrastructure of mitochondria. *Tissue Cell, 42*(6), 339-347

Ungefroren, H., Sebens, S., Seidl, D., Lehnert, H., & Hass, R. (2011). Interaction of tumor cells with the microenvironment. *Cell Communication and Signaling, 9*(1), 18

Vaiopoulos, A. G., Athanasoula, K., & Papavassiliou, A. G. (2014). Epigenetic modifications in colorectal cancer: molecular insights and therapeutic challenges. *Biochimica et Biophysica Acta, 1842*(7), 971-980

van den Brink, M. R., Kapeller, R., Pratt, J. C., Chang, J. H., & Burakoff, S. J. (1999). The extracellular signal-regulated kinase pathway is required for activation-induced cell death of T cells. *The Journal of Biological Chemistry, 274*(16), 11178-11185

Van Schaeybroeck, S., Lawler, M., Johnston, B., Salto-Tellez, M., Lee, J., Loughlin, P. (2014). Colorectal Cancer. In J .E. Tepper, J. E. Niederhuber, J. O. Armitage, J. H. Doroshow, M. B. Kastan (Eds.), *Abeloff's Clinical Oncology* (5th ed.) (pp. 1278-1335). Philadelphia, PA: Saunders Elsevier

Vermeulen, K., Van Bockstaele, D. R., & Berneman, Z. N. (2003). The cell cycle: a review of regulation, deregulation and therapeutic targets in cancer. *Cell Proliferation, 36*(3), 131-149

Vichai, V., & Kirtikara, K. (2006). Sulforhodamine B colorimetric assay for cytotoxicity screening. *Nature Protocols, 1*(3), 1112-1116

Virk, R., Gill, S., Yoshida, E., Radley, S., & Salh, B. (2010). Racial differences in the incidence of colorectal cancer. *Canadian Journal of Gastroenterology, 24*(1), 47-51

Vogel, S., Ohmayer, S., Brunner, G., & Heilmann, J. (2008). Natural and non-natural prenylated chalcones: synthesis, cytotoxicity and anti-oxidative activity. *Bioorganic & Medicinal Chemistry, 16*(8), 4286-4293

Vollmers, H. P., & Brandlein, S. (2006). Natural IgM antibodies: the orphaned molecules in immune surveillance. *Advanced Drug Delivery Reviews, 58*(5-6), 755-765

Wang, J., Wang, X., Lin, S., Chen, C., Wang, C., Ma, Q. (2013). Identification of kininogen-1 as a serum biomarker for the early detection of advanced colorectal adenoma and colorectal cancer. *PLoS One, 8*(7), e70519

Wang, J., & Yi, J. (2008). Cancer cell killing via ROS: to increase or decrease, that is the question. *Cancer Biology & Therapy, 7*(12), 1875-1884

Wang, Q., He, Z., Zhang, J., Wang, Y., Wang, T., Tong, S. (2005). Overexpression of endoplasmic reticulum molecular chaperone GRP94 and GRP78 in human lung cancer tissues and its significance. *Cancer Detection and Prevention, 29*(6), 544-551

Wang, X., Martindale, J. L., & Holbrook, N. J. (2000). Requirement for ERK activation in cisplatin-induced apoptosis. *The Journal of Biological Chemistry, 275*(50), 39435-39443

Wang, Y. W., Lin, K. T., Chen, S. C., Gu, D. L., Chen, C. F., Tu, P. H. (2013). Overexpressed-eIF3I interacted and activated oncogenic Akt1 is a theranostic target in human hepatocellular carcinoma. *Hepatology, 58*(1), 239-250

Wasinger, V. C., Cordwell, S. J., Cerpa-Poljak, A., Yan, J. X., Gooley, A. A., Wilkins, M. R. (1995). Progress with gene-product mapping of the Mollicutes: Mycoplasma genitalium. *Electrophoresis*, *16*(7), 1090-1094

Watson, A. J. (2004). Apoptosis and colorectal cancer. *Gut, 53*(11), 1701-1709

Weiss, J., Sauer, A., Frank, A., & Unger, M. (2005). Extracts and kavalactones of Piper methysticum G. Forst (kava-kava) inhibit P-glycoprotein *in vitro*. *Drug Metabolism and Disposition, 33*(11), 1580-1583

Whitton, P. A., Lau, A., Salisbury, A., Whitehouse, J., & Evans, C. S. (2003). Kava lactones and the kava-kava controversy. *Phytochemistry, 64*(3), 673-679

Witzmann, F. A., & Grant, R. A. (2003). Pharmacoproteomics in drug development. *Pharmacogenomics Journal, 3*(2), 69-76

Workman, P., Aboagye, E. O., Balkwill, F., Balmain, A., Bruder, G., Chaplin, D. J. (2010). Guidelines for the welfare and use of animals in cancer research. *British Journal of Cancer, 102*(11), 1555-1577

Workman, P., & Kaye, S. B. (2002). Translating basic cancer research into new cancer therapeutics. *Trends in Molecular Medicine, 8*(4 Suppl), S1-9

Worthley, D. L., & Leggett, B. A. (2010). Colorectal cancer: molecular features and clinical opportunities. *The Clinical Biochemist Reviews, 31*(2), 31-38

Wu, C. C., Peng, P. H., Chang, Y. T., Huang, Y. S., Chang, K. P., Hao, S. P. (2008). Identification of potential serum markers for nasopharyngeal carcinoma from a xenografted mouse model using Cy-dye labeling combined with three-dimensional fractionation. *Proteomics, 8*(17), 3605-3620

Wu, J. H., Wang, X. H., Yi, Y. H., & Lee, K. H. (2003). Anti-AIDS agents 54. A potent anti-HIV chalcone and flavonoids from genus Desmos. *Bioorganic & Medicinal Chemistry Letters, 13*(10), 1813-1815

Xing, X., Lai, M., Wang, Y., Xu, E., & Huang, Q. (2006). Overexpression of glucose-regulated protein 78 in colon cancer. *Clinica Chimica Acta, 364*(1-2), 308-315

Xu, Y., Wang, C., & Li, Z. (2014). A new strategy of promoting cisplatin chemotherapeutic efficiency by targeting endoplasmic reticulum stress. *Molecular and Clinical Oncology, 2*(1), 3-7

Yam, C. H., Ng, R. W., Siu, W. Y., Lau, A. W., & Poon, R. Y. (1999). Regulation of cyclin A-Cdk2 by SCF component Skp1 and F-box protein Skp2. *Molecular and Cellular Biology, 19*(1), 635-645

Yamaguchi, H., & Wang, H. G. (2004). CHOP is involved in endoplasmic reticulum stress-induced apoptosis by enhancing DR5 expression in human carcinoma cells. *The Journal of Biological Chemistry, 279*(44), 45495-45502

Yan, J. X., Wait, R., Berkelman, T., Harry, R. A., Westbrook, J. A., Wheeler, C. H. (2000). A modified silver staining protocol for visualization of proteins compatible with matrix-assisted laser desorption/ionization and electrospray ionization-mass spectrometry. *Electrophoresis, 21*(17), 3666-3672

Yarosh, C. A., Iacona, J. R., Lutz, C. S., & Lynch, K. W. (2015). PSF: nuclear busy-body or nuclear facilitator? *Wiley Interdisciplinary Reviews: RNA, 6*(4), 351-367

Yin, X. M. (2000). Signal transduction mediated by Bid, a pro-death Bcl-2 family proteins, connects the death receptor and mitochondria apoptosis pathways. *Cell Research, 10*(3), 161-167

Yousef, G. M., & Diamandis, E. P. (2001). The new human tissue kallikrein gene family: structure, function, and association to disease. *Endocrine Reviews, 22*(2), 184-204

Yu, K. H., Rustgi, A. K., & Blair, I. A. (2005). Characterization of proteins in human pancreatic cancer serum using differential gel electrophoresis and tandem mass spectrometry. *Journal of Proteome Research, 4*(5), 1742-1751

Zeestraten, E. C., Benard, A., Reimers, M. S., Schouten, P. C., Liefers, G. J., van de Velde, C. J. (2013). The prognostic value of the apoptosis pathway in colorectal cancer: a review of the literature on biomarkers identified by immunohistochemistry. *Biomarkers in cancer, 5*, 13-29

Zhang, E.-H., Wang, R.-F., Guo, S.-Z., & Liu, B. (2013). An update on antitumor activity of naturally occurring chalcones. *Evidence-based Complementary and Alternative Medicine : eCAM, 2013*, 815621

Zhang, J., Jiang, Y., Jia, Z., Li, Q., Gong, W., Wang, L. (2006). Association of elevated GRP78 expression with increased lymph node metastasis and poor prognosis in patients with gastric cancer. *Clinical and Experimental Metastasis, 23*(7-8), 401-410

Zhang, L., Pan, X., & Hershey, J. W. (2007). Individual overexpression of five subunits of human translation initiation factor eIF3 promotes malignant transformation of immortal fibroblast cells. *The Journal of Biological Chemistry, 282*(8), 5790-5800

Zhang, W., & Liu, H. T. (2002). MAPK signal pathways in the regulation of cell proliferation in mammalian cells. *Cell Research, 12*(1), 9-18

Zhang, X., Tang, N., Hadden, T. J., & Rishi, A. K. (2011). Akt, FoxO and regulation of apoptosis. *Biochimica et Biophysica Acta, 1813*(11), 1978-1986

Zhang, Z., Burnley, P., Coder, B., & Su, D.-M. (2012). Insights on Foxn1 biological significance and usages of the "nude" mouse in studies of T-lymphopoiesis. *International Journal of Biological Sciences, 8*(8), 1156-1167

Zhao, J., Bowman, L., Magaye, R., Leonard, S. S., Castranova, V., & Ding, M. (2013). Apoptosis induced by tungsten carbide-cobalt nanoparticles in JB6 cells involves ROS generation through both extrinsic and intrinsic apoptosis pathways. *International Journal of Oncology, 42*(4), 1349-1359

Zheng, N., Wang, Z., & Wei, W. (2016). Ubiquitination-mediated degradation of cell cycle-related proteins by F-box proteins. *The International Journal of Biochemistry & Cell Biology, 73*, 99-110

Zhou, B., & Xing, C. (2015). Diverse Molecular Targets for Chalcones with Varied Bioactivities. *Medicinal chemistry (Los Angeles), 5*(8), 388-404

Zi, X., & Simoneau, A. R. (2005). Flavokawain A, a novel chalcone from kava extract, induces apoptosis in bladder cancer cells by involvement of Bax protein-dependent and mitochondria-dependent apoptotic pathway and suppresses tumor growth in mice. *Cancer Research, 65*(8), 3479-3486

LIST OF PUBLICATIONS AND PAPERS PRESENTED

Publications arising from this study

1) **Phang, C-W**, Karsani, S.A., Sethi, G., Malek, S.N.A. (2016). Flavokawain C inhibits cell cycle and promotes apoptosis, associated with endoplasmic reticulum stress and regulation of MAPKs and Akt signaling pathways in HCT 116 human colon carcinoma cells. *PLoS ONE*. *11*(2): e0148775

2) **Phang, C-W**, Karsani, S.A., Malek, S.N.A. (2017). Induction of apoptosis and cell cycle arrest by flavokawain C on HT-29 human colon adenocarcinoma via enhancement of reactive oxygen species generation, up-regulation of p21, p27 and GADD153, and inactivation of inhibitor of apoptosis proteins. *Pharmacognosy Magazine*. *13*(50): 321-328. DOI: 10.4103/0973-1296.210180

Poster presentation

Phang, C-W, Karsani, S.A., Malek, S.N.A. (2012, December). Investigation of cytotoxic and apoptotic effects of flavokawain C against selected cancer cell lines. Poster session at the 17th Biological Sciences Graduate Congress (BSGC), 8-10 Dec 2012, Chulalongkorn University, Bangkok.

Oral presentation

Phang, C-W, Karsani, S.A., Malek, S.N.A. (2015, December). An investigation of underlying mechanisms involved in flavokawain C-inducing apoptosis and cell cycle arrest in human colon carcinoma cells. Oral session presented at the 20th Biological Sciences Graduate Congress (BSGC), 9-11 Dec 2015, Chulalongkorn University, Bangkok.

APPENDIX

Appendix A: Percentage of growth inhibition (%) of flavokawain C and cisplatin on selected cancer cell lines and a normal cell line (CCD-18Co)

Table 1: Percentage of growth inhibition (%) of flavokawain C on HCT 116, HT-29, A549, CaSki, MCF7 and CCD-18Co cell lines

Cell lines	Concentration (μM)	Percentage of growth inhibition (%)				
		Test 1	Test 2	Test 3	Average	Standard deviation
HCT 116	333	87.30	87.77	87.73	87.60	0.261
	166	85.48	86.98	86.52	86.33	0.767
	83	84.48	84.81	83.50	84.26	0.681
	42	76.61	78.70	76.26	77.19	1.229
	21	56.85	59.96	63.18	60.00	3.162
	10	47.78	47.14	46.48	47.13	0.652
	5	24.80	22.29	24.95	24.01	1.495
HT-29	333	86.45	86.07	85.64	86.05	0.408
	166	84.90	84.75	84.42	84.69	0.248
	83	82.84	83.29	82.66	82.93	0.326
	42	55.35	53.98	54.74	54.69	0.689
	21	18.32	17.64	15.85	17.27	1.275
	10	3.23	0.13	1.08	1.48	1.584
	5	0.13	0.13	1.22	0.49	0.629
A549	333	85.17	85.31	84.68	85.05	0.329
	166	84.67	82.80	82.27	83.25	1.257
	83	80.83	79.80	79.69	80.11	0.631
	42	53.67	49.25	54.73	52.55	2.908
	21	16.50	16.53	21.86	18.30	3.086
	10	8.50	7.01	6.54	7.35	1.023
	5	6.83	7.01	4.82	6.22	1.218
CaSki	333	78.13	77.57	78.50	78.07	0.467
	166	76.01	76.95	77.48	76.82	0.748
	83	74.95	75.31	75.05	75.10	0.186
	42	51.80	53.50	54.16	53.15	1.214
	21	21.02	15.23	12.58	16.27	4.318
	10	1.70	2.06	0.81	1.52	0.642
	5	0.21	1.23	0.41	0.62	0.543
MCF7	333	72.05	74.14	72.98	73.06	1.048
	166	69.00	73.38	70.97	71.12	2.198
	83	69.43	70.72	68.95	69.70	0.916
	42	41.92	49.81	47.18	46.30	4.016
	21	17.03	27.76	25.81	23.53	5.714
	10	7.42	17.87	10.48	11.93	5.371
	5	9.17	4.18	1.61	4.99	3.843
CCD-18Co	333	55.17	56.25	53.70	55.04	1.281
	166	52.04	50.63	52.09	51.58	0.831
	83	30.41	29.06	26.05	28.51	2.234
	42	9.09	13.75	11.58	11.47	2.331
	21	5.96	1.88	9.00	5.61	3.577
	10	1.88	0.31	3.86	2.02	1.777
	5	5.02	1.56	2.57	3.05	1.775

Table 2: Percentage of growth inhibition (%) of cisplatin on HCT 116, HT-29, A549, CaSki, MCF7 and CCD-18Co cell lines

Cell lines	Concentration (µM)	Percentage of growth inhibition (%)				
		Test 1	Test 2	Test 3	Average	Standard deviation
HCT 116	333	91.25	91.55	89.88	90.89	0.894
	166	90.83	90.41	88.75	90.00	1.099
	83	90.52	88.22	88.24	88.99	1.321
	42	81.77	78.94	73.72	78.14	4.082
	21	56.80	57.04	57.57	57.13	0.394
	10	46.58	49.01	46.52	47.37	1.420
	5	32.67	45.46	39.37	39.17	6.401
HT-29	333	89.64	89.52	88.97	89.38	0.358
	166	80.77	81.45	80.15	80.79	0.653
	83	80.37	80.24	78.89	79.83	0.824
	42	60.26	59.88	60.82	60.32	0.473
	21	28.40	26.41	36.03	30.28	5.077
	10	19.63	10.28	21.01	16.97	5.835
	5	14.50	9.68	18.38	14.19	4.361
A549	333	88.00	86.45	87.64	87.36	0.809
	166	88.00	84.67	86.40	86.36	1.665
	83	81.50	75.94	79.29	78.91	2.802
	42	74.00	73.26	70.63	72.63	1.769
	21	53.83	45.81	51.93	50.53	4.192
	10	46.67	35.12	39.88	40.55	5.805
	5	36.33	25.67	26.28	29.43	5.990
CaSki	333	75.84	77.98	74.87	76.23	1.592
	166	64.22	66.05	66.83	65.70	1.341
	83	33.94	36.34	34.67	34.99	1.228
	42	42.51	49.87	42.96	45.11	4.124
	21	39.45	45.89	36.93	40.76	4.618
	10	35.78	41.91	30.65	36.11	5.636
	5	27.52	20.95	20.35	22.94	3.978
MCF7	333	25.87	28.51	26.20	26.86	1.436
	166	19.40	23.53	16.16	19.70	3.695
	83	14.43	18.55	10.04	14.34	4.255
	42	11.44	14.93	13.54	13.30	1.756
	21	7.46	14.03	17.03	12.84	4.893
	10	3.98	8.14	4.80	5.64	2.206
	5	1.49	5.88	0.44	2.60	2.888
CCD-18Co	333	60.52	63.32	61.92	61.92	1.403
	166	63.10	60.90	58.36	60.79	2.370
	83	44.65	45.67	45.55	45.29	0.560
	42	32.84	31.83	35.59	33.42	1.943
	21	25.09	28.72	21.00	24.94	3.864
	10	22.51	26.64	17.08	22.08	4.795
	5	14.02	23.88	20.64	19.51	5.023

Table 3: Inhibition of cell viability (%) by flavokawain C on HCT 116 cells at 20, 40 and 60 µM for the indicated time points

Time (Hours)	Concentration (µM)	Percentage of growth inhibition (%)				
		Test 1	Test 2	Test 3	Average	Standard deviation
6	Control	116.53	115.70	113.01	115.08	1.841
	20	107.38	107.44	105.74	106.85	0.965
	40	100.00	100.00	100.83	100.28	0.477
	60	98.40	99.18	100.00	99.19	0.800
12	Control	120.66	120.66	120.33	120.55	0.194
	20	109.84	110.74	111.48	110.69	0.821
	40	103.23	105.79	104.96	104.66	1.306
	60	97.60	102.46	100.83	100.30	2.473
24	Control	160.33	157.85	156.91	158.36	1.767
	20	122.95	124.79	124.59	124.11	1.010
	40	106.45	108.26	109.92	108.21	1.733
	60	90.40	94.26	95.04	93.23	2.485
48	Control	257.85	262.81	254.47	258.38	4.194
	20	169.67	168.60	171.31	169.86	1.368
	40	118.55	120.66	119.83	119.68	1.065
	60	75.20	74.59	75.21	75.00	0.354
72	Control	311.57	312.40	302.44	308.81	5.526
	20	168.03	168.60	171.31	169.31	1.753
	40	115.32	122.31	123.97	120.53	4.589
	60	59.20	59.84	57.85	58.96	1.014

Table 4: Inhibition of cell viability (%) by flavokawain C on HT-29 cells at 40, 60 and 80 µM for the indicated time points

Time (Hours)	Concentration (µM)	Percentage of growth inhibition (%)				
		Test 1	Test 2	Test 3	Average	Standard deviation
6	Control	136.36	137.19	138.52	137.36	1.09
	20	124.79	126.45	131.15	127.46	3.30
	40	119.01	122.31	122.13	121.15	1.86
	60	116.53	123.14	122.95	120.87	3.76
12	Control	141.32	143.80	142.62	142.58	1.24
	20	115.70	116.53	121.31	117.85	3.03
	40	117.36	118.18	120.49	118.68	1.63
	60	115.70	118.18	122.95	118.95	3.68
24	Control	212.40	214.88	215.57	214.28	1.67
	20	138.02	138.02	137.70	137.91	0.18
	40	121.49	122.31	121.31	121.70	0.54
	60	116.53	119.01	118.85	118.13	1.39
48	Control	408.26	411.57	403.28	407.70	4.17
	20	161.16	163.64	162.30	162.36	1.24
	40	118.18	119.83	121.31	119.78	1.57
	60	115.70	119.83	118.85	118.13	2.16
72	Control	644.63	645.45	643.44	644.51	1.01
	20	185.12	185.95	184.43	185.17	0.76
	40	111.57	112.40	111.48	111.81	0.51
	60	103.31	105.79	105.74	104.94	1.42

Appendix B: Effect of FKC on ROS generation in HCT 116 and HT-29 cells

Table 1: Fluorescence intensity (nm) and fold change of ROS generation in HCT 116 cells in response to FKC treatment at 20, 40 and 60 µM

Con. (µM)	Fluorescence intensity (nm)			Fold Change			Average	Standard deviation
	1	2	3	1	2	3		
Control	1106	1292	1309	1.0	1.0	1.0	1.0	0.0
20	1556	1567	1604	1.4	1.2	1.2	1.3	0.1
40	2072	2122	2124	1.9	1.6	1.6	1.7	0.1
60	2500	2510	2537	2.3	1.9	1.9	2.0	0.2

Table 2: Fluorescence intensity (nm) and fold change of ROS generation in HT-29 cells in response to FKC treatment at 40, 60 and 80 µM

Con. (µM)	Fluorescence intensity (nm)			Fold Change			Average	Standard deviation
	1	2	3	1	2	3		
Control	3681	3994	4039	1.0	1.0	1.0	1.0	0.0
40	4022	4041	4990	1.1	1.0	1.2	1.1	0.1
60	4960	4970	5282	1.3	1.2	1.3	1.3	0.1
80	6058	6268	6902	1.6	1.6	1.7	1.6	0.1

Appendix C: Effect of FKC on SOD activiy in HCT 116 and HT-29 cells

Table 1: Absorbance values at 450 nm of blank 1, blank 3, blank 2 and samples [flavokawain C (20, 40 and 60 µM)] for HCT 116 cells

Sample	Absorbance at 450 nm			Average	Standard deviation
	1	2	3		
Blank 1	0.783	0.778	0.771	0.777	0.006
Blank 3	0.043	0.042	0.043	0.043	0.001
Blank 2:					
Control	0.231	0.228	0.226	0.228	0.003
20µM of FKC	0.21	0.213	0.212	0.212	0.002
40µM of FKC	0.199	0.201	0.198	0.199	0.002
60µM of FKC	0.194	0.2	0.201	0.198	0.004
Samples:					
Control	0.205	0.202	0.211	0.206	0.005
20µM of FKC	0.2	0.203	0.205	0.203	0.003
40µM of FKC	0.201	0.206	0.202	0.203	0.003
60µM of FKC	0.2	0.211	0.206	0.206	0.006

Table 2: Absorbance values at 450 nm of blank 1, blank 3, blank 2 and samples [flavokawain C (40, 60 and 80 µM)] for HT-29 cells

Sample	Absorbance at 450 nm			Average	Standard deviation
	1	2	3		
Blank 1	0.783	0.778	0.771	0.777	0.006
Blank 3	0.043	0.042	0.043	0.043	0.001
Blank 2:					
Control	0.2	0.193	0.209	0.201	0.008
40µM of FKC	0.195	0.208	0.206	0.203	0.007
60µM of FKC	0.219	0.214	0.221	0.218	0.004
80µM of FKC	0.258	0.264	0.259	0.260	0.003
Samples:					
Control	0.219	0.225	0.221	0.222	0.003
40µM of FKC	0.226	0.221	0.229	0.225	0.004
60µM of FKC	0.275	0.268	0.271	0.271	0.004
80µM of FKC	0.334	0.328	0.335	0.332	0.004

Appendix D: Comparison of the average normalized volumes for each spot of the identified proteins of the control and FKC-treated groups (calculated by progenesis samespot software) (The uppercase 'U' and 'D' refer to up-regulated and down-regulated spots, respectively)

U1 - Heat shock cognate 70 kDa protein 8 (Hspa8)

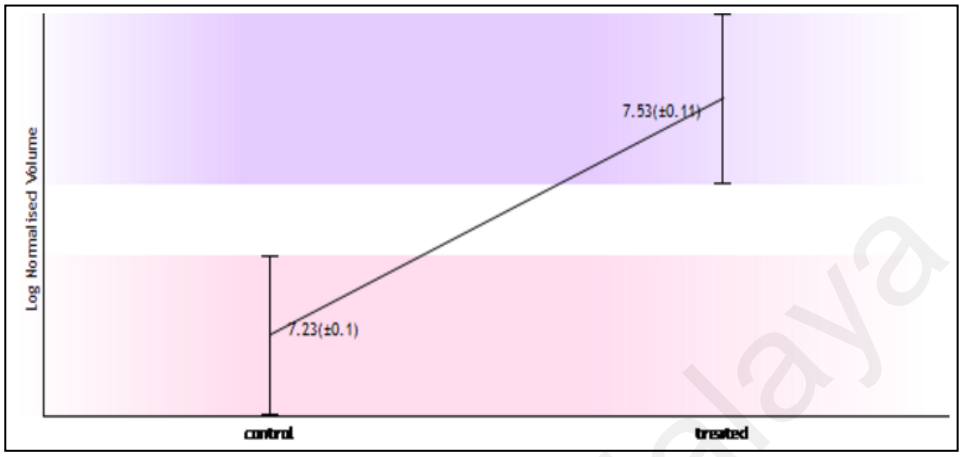

Matched peptides shown in **Bold Red**

```
  1 MSKGPAVGID LGTTYSCVGV FQHGKVEIIA NDQGNRTTPS YVAFTDTERL
 51 IGDAAKNQVA MNPTNTVFDA KRLIGRRFDD AVVQSDMKHW PFMVVNDAGR
101 PKVQVEYKGE TKSFYPEEVS SMVLTKMKEI AEAYLGKTVT NAVVTVPAYF
151 NDSQRQATKD AGTIAGLNVL RIINEPTAAA IAYGLDKKVG AERNVLIFDL
201 GGGTFDVSIL TIEDGIFEVK STAGDTHLGG EDFDNRMVNH FIAEFKRKHK
251 KDISENKRAV RRLRTACERA KRTLSSSTQA SIEIDSLYEG IDFYTSITRA
301 RFEELNADLF RGTLDPVEKA LRDAKLDKSQ IHDIVLVGGS TRIPKIQKLL
351 QDFFNGKELN KSINPDEAVA YGAAVQAAIL SGDKSENVQD LLLLDVTPLS
401 LGIETAGGVM TVLIKRNTTI PTKQTQTFTT YSDNQPGVLI QVYEGERAMT
451 KDNNLLGKFE LTGIPPAPRG VPQIEVTFDI DANGILNVSA VDKSTGKENK
501 ITITNDKGRL SKEDIERMVQ EAEKYKAEDE KQRDKVSSKN SLESYAFNMK
551 ATVEDEKLQG KINDEDKQKI LDKCNEIINW LDKNQTAEKE EFEHQQKELE
601 KVCNPIITKL YQSAGGMPGG MPGGFPGGGA PPSGGASSGP TIEEVD
```

Show predicted peptides also

Sort Peptides By ◉ Residue Number ○ Increasing Mass ○ Decreasing Mass

Start - End	Observed	Mr(expt)	Mr(calc)	ppm	Miss	Sequence
273 - 299	2997.5212	2996.5139	2996.4502	21	0	R.TLSSSTQASIEIDSLYEGIDFYTSITR.A (No match)
273 - 299	2997.5212	2996.5140	2996.4502	21	0	R.TLSSSTQASIEIDSLYEGIDFYTSITR.A (Ions score 43)
300 - 311	1480.7827	1479.7754	1479.7470	19	1	R.ARFEELNADLFR.G (No match)
302 - 311	1253.6398	1252.6325	1252.6088	19	0	R.FEELNADLFR.G (Ions score 30)
302 - 311	1253.6398	1252.6325	1252.6088	19	0	R.FEELNADLFR.G (No match)
329 - 342	1481.8273	1480.8200	1480.7998	14	0	K.SQIHDIVLVGGSTR.I (Ions score 5)
329 - 342	1481.8273	1480.8200	1480.7998	14	0	K.SQIHDIVLVGGSTR.I (No match)
362 - 384	2260.1694	2259.1621	2259.1383	11	0	K.SINPDEAVAYGAAVQAAILSGDK.S (No match)
385 - 415	3238.8774	3237.8701	3237.7782	28	0	K.SENVQDLLLLDVTPLSLGIETAGGVMTVLIK.R (No match)
424 - 447	2774.3892	2773.3819	2773.3195	22	0	K.QTQTFTTYSDNQPGVLIQVYEGER.A (Ions score 117)
424 - 447	2774.3892	2773.3819	2773.3195	23	0	K.QTQTFTTYSDNQPGVLIQVYEGER.A (No match)
459 - 469	1197.6868	1196.6795	1196.6554	20	0	K.FELTGIPPAPR.G (No match)
459 - 469	1197.6868	1196.6795	1196.6554	20	0	K.FELTGIPPAPR.G (No match)
513 - 524	1492.7740	1491.7667	1491.6875	53	1	K.EDIERMVQEAEK.Y Oxidation (M) (No match)

U2 - Heat shock 70 kDa protein 1-like (HSP70-Hom)

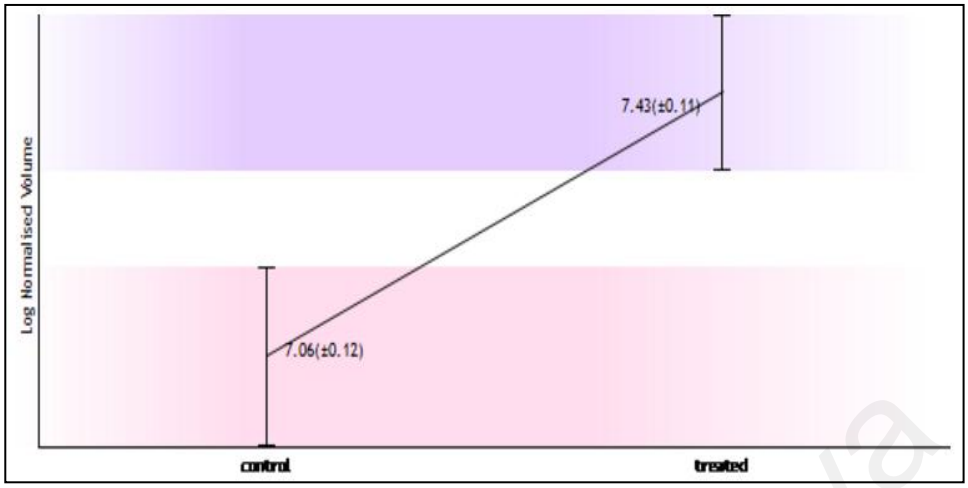

Matched peptides shown in **Bold Red**

```
   1 MATAKGIAIG IDLGTTYSCV GVFQHGKVEI IANDQGNRIT PSYVAFTDTE
  51 RLIGDAAKNQ VAMNPQNTVF DAKRLIGRKF NDPVVQADMK LWPFQVINEG
 101 GKPKVLVSYK GENKAFYPEE ISSMVLTKLK ETAEAFLGHP VTNAVITVPA
 151 YFNDSQRQAT KDAGVIAGLN VLRIINEPTA AAIAYGLDKG GQGERHVLIF
 201 DLGGGTFDVS ILTIDDGIFE VKATAGDTHL GGEDFDNRLV SHFVEEFKRK
 251 HKKDISQNKR AVRRLRTACE RAKRTLSSST QANLEIDSLY EGIDFYTSIT
 301 RARFEELCAD LFRGTLEPVE KALRDAKMDK AKIHDIVLVG GSTRIPKVQR
 351 LLQDYFNGRD LNKSINPDEA VAYGAAVQAA ILMGDKSEKV QDLLLLDVAP
 401 LSLGLETAGG VMTALIKRNS TIPTKQTQIF TTYSDNQPGV LIQVYEGERA
 451 MTKDNNLLGR FDLTGIPPAP RGVPQIEVTF DIDANGILNV TATDKSTGKV
 501 NKITITNDKG RLSKEEIERM VLDAEKYKAE DEVQREKIAA KNALESYAFN
 551 MKSVVSDEGL KGKISESDKN KILDKCNELL SWLEVNQLAE KDEFDHKRKE
 601 LEQMCNPIIT KLYQGGCTGP ACGTGYVPGR PATGPTIEEV D
```

Show predicted peptides also

Sort Peptides By ◉ Residue Number ○ Increasing Mass ○ Decreasing Mass

Start - End	Observed	Mr(expt)	Mr(calc)	ppm	Miss	Sequence	
162 - 173	1197.6459	1196.6386	1196.6877	-41	0	K.DAGVIAGLNVLR.I	(No match)
162 - 173	1197.6459	1196.6386	1196.6877	-41	0	K.DAGVIAGLNVLR.I	(No match)
331 - 344	1465.7853	1464.7780	1464.8413	-43	1	K.AKIHDIVLVGGSTR.I	(Ions score 17)
331 - 344	1465.7853	1464.7780	1464.8413	-43	1	K.AKIHDIVLVGGSTR.I	(No match)
426 - 449	2786.3240	2785.3167	2785.3559	-14	0	K.QTQIFTTYSDNQPGVLIQVYEGER.A	(Ions score 50)
426 - 449	2786.3240	2785.3167	2785.3559	-14	0	K.QTQIFTTYSDNQPGVLIQVYEGER.A	(No match)

U3 - Heat shock protein 27 kDa (HSP 27)

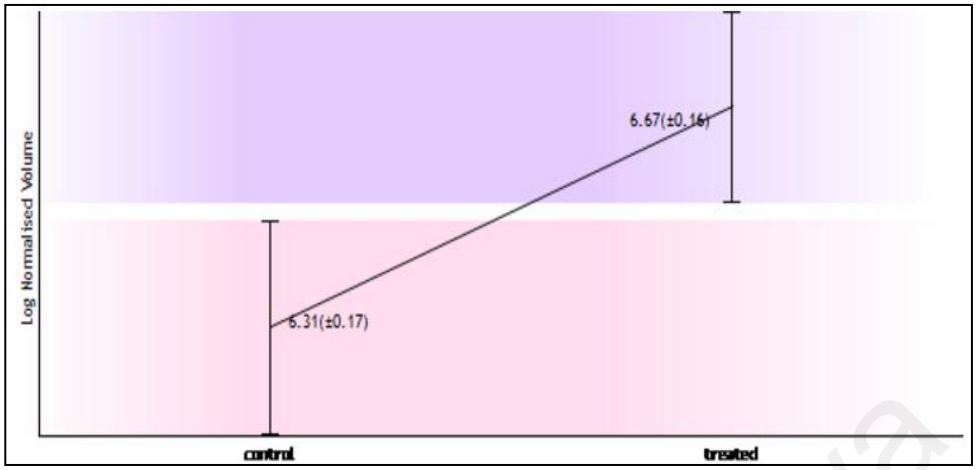

Matched peptides shown in **Bold Red**

```
  1 MTERRVPFSL LRGPSWDPFR DWYPHSRLFD QAFGLPRLPE EWSQWLGGSS
 51 WPGYVRPLPP AAIESPAVAA PAYSRALSRQ LSSGVSEIRH TADRWRVSLD
101 VNHFAPDELT VKTKDGVVEI TGKHEERQDE HGYISRCFTR KYTLPPGVDP
151 TQVSSSLSPE GTLTVEAPMP KLATQSNEIT IPVTFESRAQ LGGPEAAKSD
201 ETAAK
```

Show predicted peptides also

Sort Peptides By ◉ Residue Number ○ Increasing Mass ○ Decreasing Mass

Start - End	Observed	Mr(expt)	Mr(calc)	ppm	Miss	Sequence
13 - 20	961.4633	960.4560	960.4454	11	0	R.GPSWDPFR.D (No match)
21 - 27	960.4493	959.4420	959.4250	18	0	R.DWYPHSR.L (No match)
21 - 27	960.4493	959.4420	959.4250	18	0	R.DWYPHSR.L (No match)
28 - 37	1163.6400	1162.6327	1162.6135	17	0	R.LFDQAFGLPR.L (No match)
28 - 37	1163.6400	1162.6327	1162.6135	17	0	R.LFDQAFGLPR.L (No match)
80 - 89	1075.5863	1074.5790	1074.5669	11	0	R.QLSSGVSEIR.H (No match)
97 - 112	1783.9396	1782.9323	1782.9152	10	0	R.VSLDVNHFAPDELTVK.T (No match)
128 - 136	1104.5254	1103.5181	1103.4996	17	0	R.QDEHGYISR.C (No match)
128 - 136	1104.5254	1103.5181	1103.4996	17	0	R.QDEHGYISR.C (No match)
172 - 188	1906.0120	1905.0047	1904.9843	11	0	K.LATQSNEITIPVTFESR.A (No match)

U4 - Heat shock 70 kDa protein 1A/1B (HSP70-1/HSP70-2)

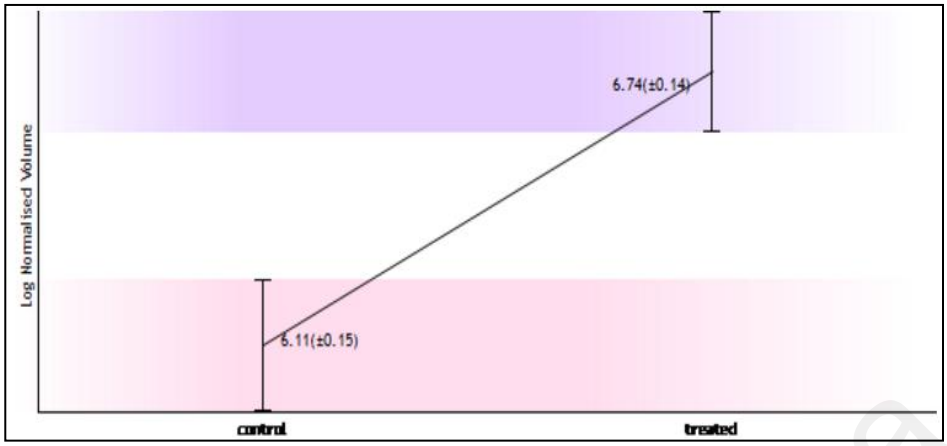

Matched peptides shown in **Bold Red**

```
  1 MAKAAAIGID LGTTYSCVGV FQHGKVEIIA NDQGNRTTPS YVAFTDTERL
 51 IGDAAKNQVA LNPQNTVFDA KRLIGRKFGD PVVQSDMKHW PFQVINDGDK
101 PKVQVSYKGD TKAFYPEEIS SMVLTKMKEI AEAYLGYPVT NAVITVPAYF
151 NDSQRQATKD AGVIAGLNVL RIINEPTAAA IAYGLDRTGK GERNVLIFDL
201 GGGTFDVSIL TIDDGIFEVK ATAGDTHLGG EDFDNRLVNH FVEEFKRKHK
251 KDISQNKRAV RRLRTACERA KRTLSSSTQA SLEIDSLFEG IDFYTSITRA
301 RFEELCSDLF RSTLEPVEKA LRDAKLDKAQ IHDLVLVGGS TRIPKVQKLL
351 QDFFNGRDLN KSINPDEAVA YGAAVQAAIL MGDKSENVQD LLLLDVAPLS
401 LGLETAGGVM TALIKRNSTI PTKQTQIFTT YSDNQPGVLI QVYEGERAMT
451 KDNNLLGRFE LSGIPPAPRG VPQIEVTFDI DANGILNVTA TDKSTGKANK
501 ITITNDKGRL SKEEIERMVQ EAEKYKAEDE VQRERVSAKN ALESYAFNMK
551 SAVEDEGLKG KISEADKKKV LDKCQEVISW LDANTLAEKD EFEHKRKELE
601 QVCNPIISGL YQGAGGPGPG GFGAQGPKGG SGSGPTIEEV D
```

Show predicted peptides also

Sort Peptides By ◉ Residue Number ○ Increasing Mass ○ Decreasing Mass

Start - End	Observed	Mr(expt)	Mr(calc)	ppm	Miss	Sequence
2 - 25	2407.2666	2406.2593	2406.2366	9	1	M.AKAAAIGIDLGTTYSCVGVFQHGK.V (No match)
160 - 171	1197.6459	1196.6386	1196.6877	-41	0	K.DAGVIAGLNVLR.I (No match)
160 - 171	1197.6459	1196.6386	1196.6877	-41	0	K.DAGVIAGLNVLR.I (No match)
273 - 299	2981.4228	2980.4156	2980.4553	-13	0	R.TLSSSTQASLEIDSLFEGIDFYTSITR.A (Ions score 33)
273 - 299	2981.4229	2980.4156	2980.4553	-13	0	R.TLSSSTQASLEIDSLFEGIDFYTSITR.A (No match)
300 - 311	1542.7097	1541.7024	1541.7296	-18	1	R.ARFEELCSDLFR.S Carbamidomethyl (C) (No match)
300 - 311	1542.7097	1541.7024	1541.7296	-18	1	R.ARFEELCSDLFR.S Carbamidomethyl (C) (No match)
302 - 311	1315.5765	1314.5692	1314.5914	-17	0	R.FEELCSDLFR.S Carbamidomethyl (C) (No match)
302 - 311	1315.5765	1314.5693	1314.5914	-17	0	R.FEELCSDLFR.S Carbamidomethyl (C) (Ions score 12)
329 - 342	1465.7853	1464.7780	1464.8049	-18	0	K.AQIHDLVLVGGSTR.I (Ions score 17)
329 - 342	1465.7853	1464.7780	1464.8049	-18	0	K.AQIHDLVLVGGSTR.I (No match)
349 - 357	1109.5566	1108.5493	1108.5665	-16	0	K.LLQDFFNGR.D (No match)
349 - 357	1109.5566	1108.5494	1108.5665	-15	0	K.LLQDFFNGR.D (Ions score 21)
424 - 447	2786.3240	2785.3167	2785.3559	-14	0	K.QTQIFTTYSDNQPGVLIQVYEGER.A (Ions score 50)
424 - 447	2786.3240	2785.3167	2785.3559	-14	0	K.QTQIFTTYSDNQPGVLIQVYEGER.A (No match)

U5 - Heat shock protein 90 kDa alpha (HSP 86)

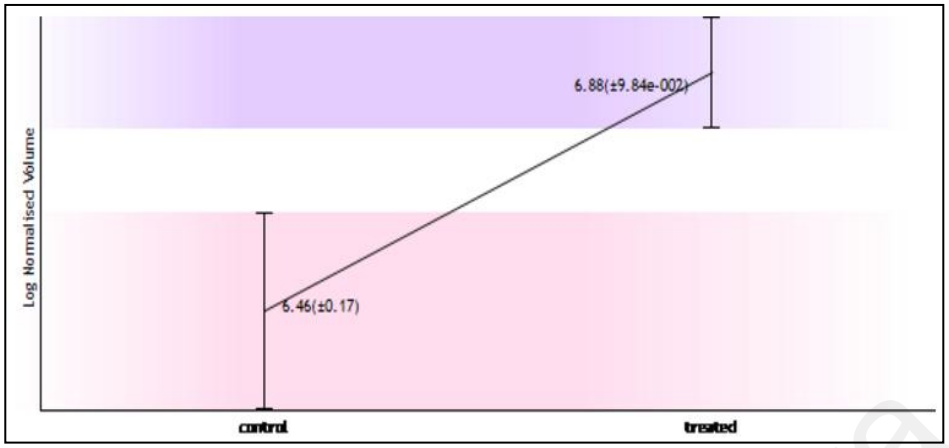

Matched peptides shown in **Bold Red**

```
   1 MPEETQTQDQ PMEEEEVETF AFQAEIAQLM SLIINTFYSN KEIFLRELIS
  51 NSSDALDKIR YESLTDPSKL DSGKELHINL IPNKQDRTLT IVDTGIGMTK
 101 ADLINNLGTI AKSGTKAFME ALQAGADISM IGQFGVGFYS AYLVAEKVTV
 151 ITKHNDDEQY AWESSAGGSF TVRTDTGEPM GRGTKVILHL KEDQTEYLEE
 201 RRIKEIVKKH SQFIGYPITL FVEKERDKEV SDDEAEEKED KEEEKEKEEK
 251 ESEDKPEIED VGSDEEEEKK DGDKKKKKKI KEKYIDQEEL NKTKPIWTRN
 301 PDDITNEEYG EFYKSLTNDW EDHLAVKHFS VEGQLEFRAL LFVPRRAPFD
 351 LFENRKKKNN IKLYVRRVFI MDNCEELIPE YLNFIRGVVD SEDLPLNISR
 401 EMLQQSKILK VIRKNLVKKC LELFTELAED KENYKKFYEQ FSKNIKLGIH
 451 EDSQNRKKLS ELLRYYTSAS GDEMVSLKDY CTRMKENQKH IYYITGETKD
 501 QVANSAFVER LRKHGLEVIY MIEPIDEYCV QQLKEFEGKT LVSVTKEGLE
 551 LPEDEEEKKK QEEKKTKFEN LCKIMKDILE KKVEKVVVSN RLVTSPCCIV
 601 TSTYGWTANM ERIMKAQALR DNSTMGYMAA KKHLEINPDH SIIETLRQKA
 651 EADKNDKSVK DLVILLYETA LLSSGFSLED PQTHANRIYR MIKLGLGIDE
 701 DDPTADDTSA AVTEEMPPLE GDDDTSRMEE VD
```

Show predicted peptides also

Sort Peptides By ◉ Residue Number ○ Increasing Mass ○ Decreasing Mass

Start - End	Observed	Mr(expt)	Mr(calc)	ppm	Miss	Sequence
75 - 87	1589.7900	1588.7827	1588.8685	-54	1	K.ELHINLIPNKQDR.T (No match)
75 - 87	1589.7900	1588.7828	1588.8685	-54	1	K.ELHINLIPNKQDR.T (Ions score 60)
154 - 173	2255.8535	2254.8462	2254.9516	-47	0	K.HNDDEQYAWESSAGGSFTVR.T (No match)
154 - 173	2255.8535	2254.8462	2254.9516	-47	0	K.HNDDEQYAWESSAGGSFTVR.T (Ions score 115)
186 - 201	2014.9364	2013.9291	2014.0371	-54	1	K.VILHLKEDQTEYLEER.R (No match)
192 - 201	1311.4954	1310.4881	1310.5626	-57	0	K.EDQTEYLEER.R (Ions score 39)
192 - 201	1311.4954	1310.4881	1310.5626	-57	0	K.EDQTEYLEER.R (No match)
210 - 224	1778.8544	1777.8471	1777.9403	-52	0	K.HSQFIGYPITLFVEK.E (Ions score 50)
210 - 224	1778.8544	1777.8471	1777.9403	-52	0	K.HSQFIGYPITLFVEK.E (No match)
284 - 292	1151.4863	1150.4790	1150.5506	-62	0	K.YIDQEELNK.T (No match)
293 - 299	901.4667	900.4594	900.5181	-65	0	K.TKPIWTR.N (Ions score 12)
293 - 299	901.4667	900.4594	900.5181	-65	0	K.TKPIWTR.N (No match)
300 - 314	1833.6874	1832.6801	1832.7741	-51	0	R.NPDDITNEEYGEFYK.S (Ions score 130)
300 - 314	1833.6874	1832.6801	1832.7741	-51	0	R.NPDDITNEEYGEFYK.S (No match)
315 - 327	1527.6617	1526.6544	1526.7365	-54	0	K.SLTNDWEDHLAVK.H (No match)
315 - 327	1527.6617	1526.6545	1526.7365	-54	0	K.SLTNDWEDHLAVK.H (Ions score 51)
328 - 338	1348.5880	1347.5807	1347.6572	-57	0	K.HFSVEGQLEFR.A (Ions score 48)
346 - 355	1264.5847	1263.5774	1263.6360	-46	1	R.RAPFDLFENR.K (No match)
347 - 355	1108.4771	1107.4698	1107.5349	-59	0	R.APFDLFENR.K (No match)
347 - 356	1236.5658	1235.5585	1235.6299	-58	1	R.APFDLFENRK.K (No match)
387 - 400	1513.6974	1512.6901	1512.7784	-58	0	R.GVVDSEDLPLNISR.E (No match)
621 - 632	1348.5880	1347.5807	1347.5799	1	1	R.DNSTMGYMAAKK.H 2 Oxidation (M) (No match)

U6 - T-complex protein 1 subunit eta (TCP-1-eta)

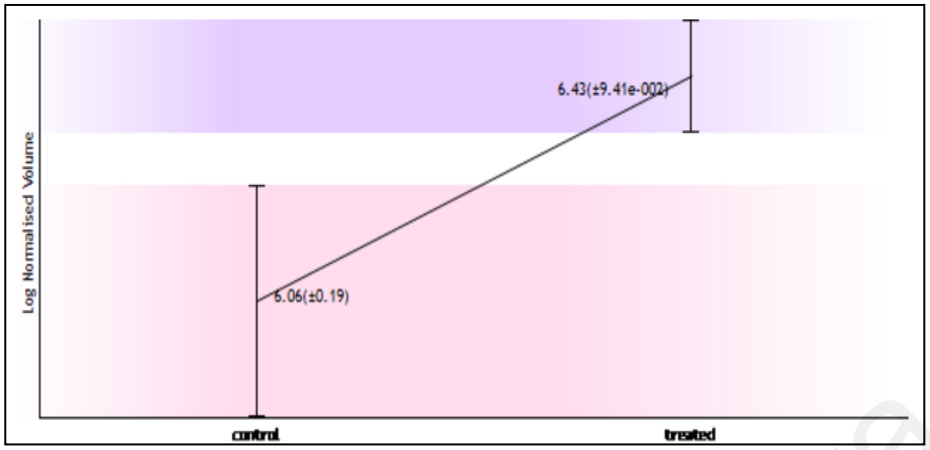

Matched peptides shown in **Bold Red**

```
  1 MMPTPVILLK EGTDSSQGIP QLVSNISACQ VIAEAVRTTL GPRGMDKLIV
 51 DGRGKATISN DGATILKLLD VVHPAAKTLV DIAKSQDAEV GDGTTSVTLL
101 AAEFLKQVKP YVEEGLHPQI IIRAFRTATQ LAVNKIKEIA VTVKKADKVE
151 QRKLLEKCAM TALSSKLISQ QKAFFAKMVV DAVMMLDDLL QLKMIGIKKV
201 QGGALEDSQL VAGVAFKKTF SYAGFEMQPK KYHNPKIALL NVELELKAEK
251 DNAEIRVHTV EDYQAIVDAE WNILYDKLEK IHHSGAKVVL SKLPIGDVAT
301 QYFADRDMFC AGRVPEEDLK RTMMACGGSI QTSVNALSAD VLGRCQVFEE
351 TQIGGERYNF FTGCPKAKTC TFILRGGAEQ FMEETERSLH DAIMIVRRAI
401 KNDSVVAGGG AIEMELSKYL RDYSRTIPGK QQLLIGAYAK ALEIIPRQLC
451 DNAGFDATNI LNKLRARHAQ GGTWYGVDIN NEDIADNFEA FVWEPAMVRI
501 NALTAASEAA CLIVSVDETI KNPRSTVDAP TAAGRGRGRG RPH
```

Show predicted peptides also

Sort Peptides By ◉ Residue Number ○ Increasing Mass ○ Decreasing Mass

Start - End	Observed	Mr(expt)	Mr(calc)	ppm	Miss	Sequence
2 - 10	1011.6710	1010.6637	1010.6198	43	0	M.MPTPVILLK.E (No match)
2 - 10	1011.6710	1010.6637	1010.6198	43	0	M.MPTPVILLK.E (No match)
56 - 77	2247.1543	2246.1470	2246.2634	-52	1	K.ATISNDGATILKLLDVVHPAAK.T (No match)
173 - 193	2414.3074	2413.3001	2413.2459	22	1	K.AFFAKMVVDAVMMLDDLLQLK.M Oxidation (M) (No match)
248 - 256	1045.5887	1044.5815	1044.5199	59	1	K.AEKDNAEIR.V (No match)
293 - 306	1565.8251	1564.8178	1564.7886	19	0	K.LPIGDVATQYFADR.D (No match)
293 - 306	1565.8251	1564.8178	1564.7886	19	0	K.LPIGDVATQYFADR.D (No match)
322 - 344	2298.2278	2297.2205	2297.0814	61	0	R.TMMACGGSIQTSVNALSADVLGR.C Oxidation (M) (No match)
322 - 344	2298.2278	2297.2205	2297.0814	61	0	R.TMMACGGSIQTSVNALSADVLGR.C Oxidation (M) (No match)
358 - 366	1133.5361	1132.5288	1132.5012	24	0	R.YNFFTGCPK.A Carbamidomethyl (C) (No match)
369 - 375	910.5107	909.5034	909.4742	32	0	K.TCTFILR.G Carbamidomethyl (C) (No match)
369 - 387	2234.1309	2233.1236	2233.0143	49	1	K.TCTFILRGGAEQFMEETER.S Oxidation (M) (No match)
376 - 387	1383.6394	1382.6321	1382.5772	40	0	R.GGAEQFMEETER.S (No match)
376 - 387	1383.6394	1382.6321	1382.5772	40	0	R.GGAEQFMEETER.S (No match)
388 - 397	1154.6608	1153.6535	1153.6277	22	0	R.SLHDAIMIVR.R (No match)
388 - 397	1154.6608	1153.6535	1153.6277	22	0	R.SLHDAIMIVR.R (No match)
388 - 397	1170.6547	1169.6474	1169.6227	21	0	R.SLHDAIMIVR.R Oxidation (M) (No match)
441 - 447	811.5270	810.5197	810.4963	29	0	K.ALEIIPR.Q (No match)
525 - 535	1045.5887	1044.5814	1044.5200	59	0	R.STVDAPTAAGR.G (No match)

U7 - Keratin, type I cytoskeletal 18 (CK-18)

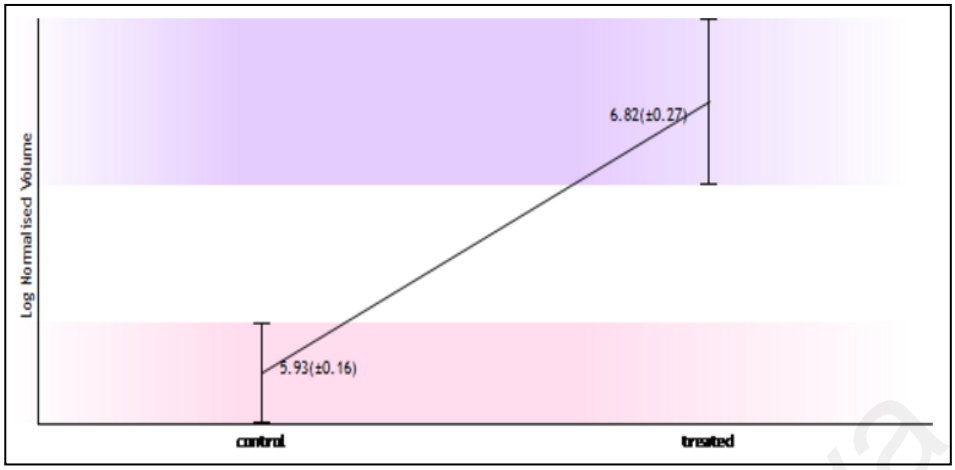

Matched peptides shown in **Bold Red**

```
  1 MSFTTRSTFS TNYRSLGSVQ APSYGARPVS SAASVYAGAG GSGSRISVSR
 51 STSFRGGMGS GGLATGIAGG LAGMGGIQNE KETMQSLNDR LASYLDRVRS
101 LETENRRLES KIREHLEKKG PQVRDWSHYF KIIEDLRAQI FANTVDNARI
151 VLQIDNARLA ADDFRVKYET ELAMRQSVEN DIHGLRKVID DTNITRLQLE
201 TEIEALKEEL LFMKKNHEEE VKGLQAQIAS SGLTVEVDAP KSQDLAKIMA
251 DIRAQYDELA RKNREELDKY WSQQIEESTT VVTTQSAEVG AAETTLTELR
301 RTVQSLEIDL DSMRNLKASL ENSLREVEAR YALQMEQLNG ILLHLESELA
351 QTRAEGQRQA QEYEALLNIK VKLEAEIATY RRLLEDGEDF NLGDALDSSN
401 SMQTIQKTTT RRIVDGKVVS ETNDTKVLRH
```

Show predicted peptides also

Sort Peptides By ◉ Residue Number ○ Increasing Mass ○ Decreasing Mass

Start - End	Observed	Mr(expt)	Mr(calc)	ppm	Miss	Sequence
7 - 14	975.4748	974.4675	974.4458	22	0	R.STFSTNYR.S (No match)
7 - 14	975.4748	974.4675	974.4458	22	0	R.STFSTNYR.S (No match)
56 - 81	2261.1616	2260.1543	2260.0940	27	0	R.GGMGSGGLATGIAGGLAGMGGIQNEK.E (No match)
82 - 90	1093.5197	1092.5124	1092.4870	23	0	K.ETMQSLNDR.L (No match)
82 - 90	1093.5197	1092.5124	1092.4870	23	0	K.ETMQSLNDR.L (No match)
91 - 97	837.4642	836.4569	836.4392	21	0	R.LASYLDR.V (No match)
112 - 118	924.5460	923.5387	923.5188	22	1	K.IREHLEK.K (No match)
125 - 131	982.4609	981.4536	981.4345	20	0	R.DWSHYFK.I (No match)
125 - 131	982.4609	981.4537	981.4345	20	0	R.DWSHYFK.I (No match)
138 - 149	1319.7002	1318.6929	1318.6629	23	0	R.AQIFANTVDNAR.I (Ions score 9)
138 - 149	1319.7002	1318.6929	1318.6629	23	0	R.AQIFANTVDNAR.I (No match)
150 - 158	1041.6255	1040.6182	1040.5978	20	0	R.IVLQIDNAR.L (No match)
150 - 158	1041.6255	1040.6182	1040.5978	20	0	R.IVLQIDNAR.L (No match)
159 - 165	807.4185	806.4112	806.3923	24	0	R.LAADDFR.V (No match)
166 - 175	1239.6665	1238.6592	1238.6329	21	1	R.VKYETELAMR.Q (No match)
166 - 175	1239.6665	1238.6592	1238.6329	21	1	R.VKYETELAMR.Q (No match)
168 - 175	1012.4967	1011.4894	1011.4695	20	0	K.YETELAMR.Q (No match)
176 - 186	1267.6665	1266.6592	1266.6317	22	0	R.QSVENDIHGLR.K (Ions score 32)
176 - 186	1267.6665	1266.6592	1266.6317	22	0	R.QSVENDIHGLR.K (No match)
188 - 196	1046.5731	1045.5658	1045.5404	24	0	K.VIDDTNITR.L (No match)
197 - 214	2177.2256	2176.2183	2176.1700	22	1	R.LQLETEIEALKEELLFMK.K (No match)
197 - 214	2193.1526	2192.1453	2192.1650	-9	1	R.LQLETEIEALKEELLFMK.K Oxidation (M) (No match)
215 - 222	1012.4967	1011.4894	1011.4985	-9	1	K.KNHEEEVK.G (No match)
371 - 381	1292.6904	1291.6831	1291.7136	-24	1	K.VKLEAEIATYR.R (No match)
371 - 381	1292.6904	1291.6832	1291.7136	-24	1	K.VKLEAEIATYR.R (No match)

U8 - Tubulin beta-2C chain (Tubulin beta-2 chain)

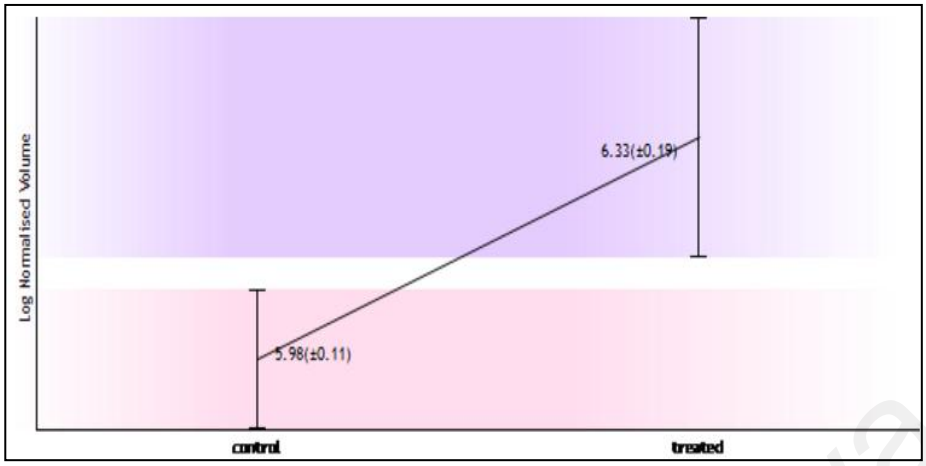

Matched peptides shown in Bold Red

```
  1 MREIVHLQAG QCGNQIGAKF WEVISDEHGI DPTGTYHGDS DLQLERINVY
 51 YNEATGGKYV PRAVLVDLEP GTMDSVRSGP FGQIFRPDNF VFGQSGAGNN
101 WAKGHYTEGA ELVDSVLDVV RKEAESCDCL QGFQLTHSLG GGTGSGMGTL
151 LISKIREEYP DRIMNTFSVV PSPKVSDTVV EPYNATLSVH QLVENTDETY
201 CIDNEALYDI CFRTLKLTTP TYGDLNHLVS ATMSGVTTCL RFPGQLNADL
251 RKLAVNMVPF PRLHFFMPGF APLTSRGSQQ YRALTVPELT QQMFDAKNMM
301 AACDPRHGRY LTVAAVFRGR MSMKEVDEQM LNVQNKNSSY FVEWIPNNVK
351 TAVCDIPPRG LKMSATFIGN STAIQELFKR ISEQFTAMFR RKAFLHWYTG
401 EGMDEMEFTE AESNMNDLVS EYQQYQDATA EEEGEFEEEA EEEVA
```

Show predicted peptides also

Sort Peptides By ◉ Residue Number ○ Increasing Mass ○ Decreasing Mass

Start - End	Observed	Mr(expt)	Mr(calc)	ppm	Miss	Sequence
63 - 77	1601.7505	1600.7432	1600.8131	-44	0	R.AVLVDLEPGTMDSVR.S (Ions score 31)
63 - 77	1601.7505	1600.7432	1600.8131	-44	0	R.AVLVDLEPGTMDSVR.S (No match)
78 - 103	2798.2590	2797.2517	2797.3361	-30	0	R.SGPFGQIFRPDNFVFGQSGAGNNWAK.G (No match)
78 - 103	2798.2590	2797.2518	2797.3361	-30	0	R.SGPFGQIFRPDNFVFGQSGAGNNWAK.G (No match)
104 - 121	1958.9019	1957.8946	1957.9745	-41	0	K.GHYTEGAELVDSVLDVVR.K (Ions score 26)
104 - 121	1958.9019	1957.8946	1957.9745	-41	0	K.GHYTEGAELVDSVLDVVR.K (No match)
155 - 162	1077.4797	1076.4724	1076.5250	-49	1	K.IREEYPDR.I (No match)
217 - 241	2708.2598	2707.2525	2707.3310	-29	0	K.LTTPTYGDLNHLVSATMSGVTTCLR.F Carbamidomethyl (C) (No match)
242 - 251	1130.5441	1129.5368	1129.5880	-45	0	R.FPGQLNADLR.K (Ions score 3)
242 - 251	1130.5441	1129.5368	1129.5880	-45	0	R.FPGQLNADLR.K (No match)
253 - 262	1143.5806	1142.5733	1142.6270	-47	0	K.LAVNMVPFPR.L (Ions score 27)
253 - 262	1143.5806	1142.5733	1142.6270	-47	0	K.LAVNMVPFPR.L (No match)
263 - 276	1620.7688	1619.7615	1619.8283	-41	0	R.LHFFMPGFAPLTSR.G (Ions score 25)
263 - 276	1620.7688	1619.7615	1619.8283	-41	0	R.LHFFMPGFAPLTSR.G (No match)
283 - 297	1707.7213	1706.7140	1706.8549	-83	0	R.ALTVPELTQQMFDAK.N Oxidation (M) (No match)

U9 - Actin, cytoplasmic 2 (Gamma actin)

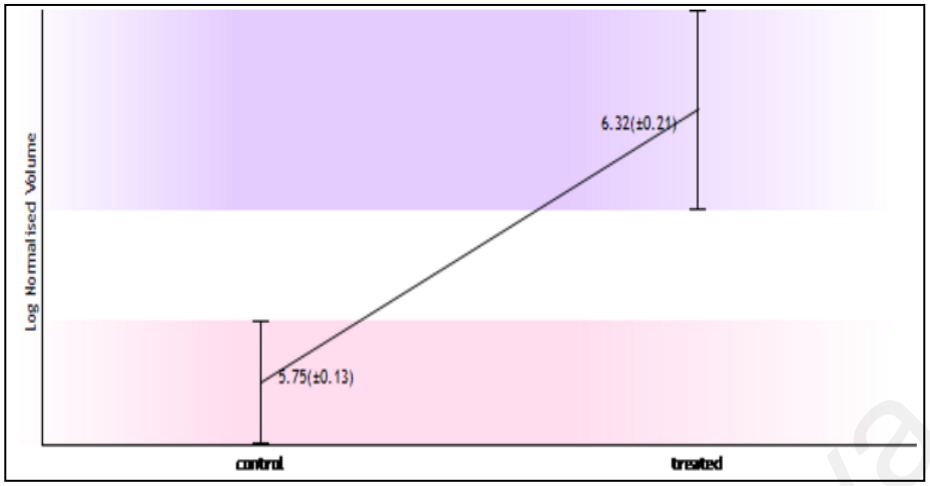

Matched peptides shown in **Bold Red**

```
  1 MEEEIAALVI DNGSGMCKAG FAGDDAPRAV FPSIVGRPRH QGVMVGMGQK
 51 DSYVGDEAQS KRGILTLKYP IEHGIVTNWD DMEKIWHHTF YNELRVAPEE
101 HPVLLTEAPL NPKANREKMT QIMFETFNTP AMYVAIQAVL SLYASGRTTG
151 IVMDSGDGVT HTVPIYEGYA LPHAILRLDL AGRDLTDYLM KILTERGYSF
201 TTTAEREIVR DIKEKLCYVA LDFEQEMATA ASSSSLEKSY ELPDGQVITI
251 GNERFRCPEA LFQPSFLGME SCGIHETTFN SIMKCDVDIR KDLYANTVLS
301 GGTTMYPGIA DRMQKEITAL APSTMKIKII APPERKYSVW IGGSILASLS
351 TFQQMWISKQ EYDESGPSIV HRKCF
```

Show predicted peptides also

Sort Peptides By ◉ Residue Number ○ Increasing Mass ○ Decreasing Mass

Start - End	Observed	Mr(expt)	Mr(calc)	ppm	Miss	Sequence
2 - 18	1794.8590	1793.8517	1793.8175	19	0	M.EEEIAALVIDNGSGMCK.A Oxidation (M) (No match)
29 - 50	2367.3147	2366.3074	2366.2464	26	1	R.AVFPSIVGRPRHQGVMVGMGQK.D Oxidation (M) (No match)
85 - 95	1515.7864	1514.7791	1514.7419	25	0	K.IWHHTFYNELR.V (No match)
85 - 95	1515.7864	1514.7791	1514.7419	25	0	K.IWHHTFYNELR.V (No match)
96 - 113	1954.1036	1953.0963	1953.0571	20	0	R.VAPEEHPVLLTEAPLNPK.A (No match)
96 - 113	1954.1036	1953.0964	1953.0571	20	0	R.VAPEEHPVLLTEAPLNPK.A (No match)
197 - 206	1132.5658	1131.5585	1131.5197	34	0	R.GYSFTTTAER.E (No match)
197 - 206	1132.5658	1131.5585	1131.5197	34	0	R.GYSFTTTAER.E (No match)
239 - 254	1790.9346	1789.9273	1789.8846	24	0	K.SYELPDGQVITIGNER.F (Ions score 24)
239 - 254	1790.9346	1789.9273	1789.8846	24	0	K.SYELPDGQVITIGNER.F (No match)
292 - 312	2215.1438	2214.1365	2214.0627	33	0	K.DLYANTVLSGGTTMYPGIADR.M (No match)
292 - 312	2215.1438	2214.1365	2214.0627	33	0	K.DLYANTVLSGGTTMYPGIADR.M (No match)
292 - 312	2231.2673	2230.2600	2230.0576	91	0	K.DLYANTVLSGGTTMYPGIADR.M Oxidation (M) (No match)
313 - 326	1564.7830	1563.7757	1563.8000	-16	1	R.MQKEITALAPSTMK.I Oxidation (M) (No match)
313 - 326	1564.7830	1563.7757	1563.8000	-16	1	R.MQKEITALAPSTMK.I Oxidation (M) (No match)
360 - 372	1516.7805	1515.7732	1515.6954	51	0	K.QEYDESGPSIVHR.K (No match)

D10 - Myosin light polypeptide 6 (MLC-3)

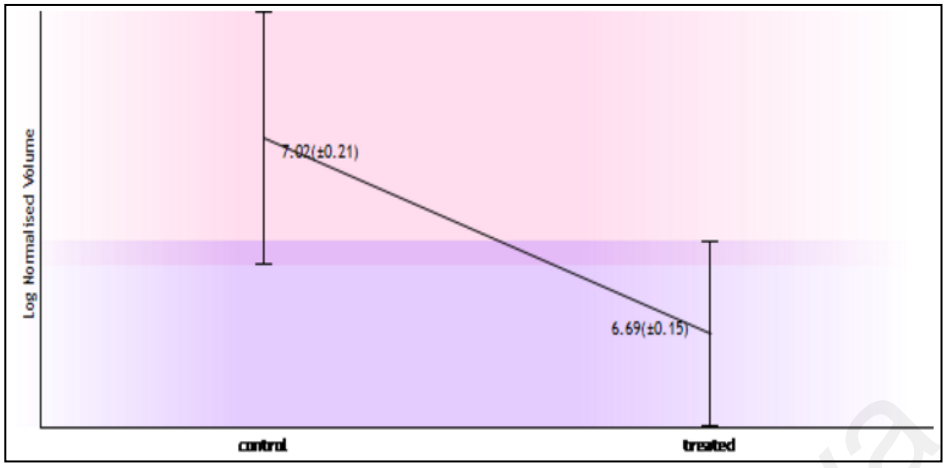

Matched peptides shown in **Bold Red**

```
  1 MCDFTEDQTA EFKEAFQLFD RTGDGKILYS QCGDVMRALG QNPTNAEVLK
 51 VLGNPKSDEM NVKVLDFEHF LPMLQTVAKN KDQGTYEDYV EGLRVFDKEG
101 NGTVMGAEIR HVLVTLGEKM TEEEVEMLVA GHEDSNGCIN YEAFVRHILS
151 G
```

Show predicted peptides also

Sort Peptides By ◉ Residue Number ○ Increasing Mass ○ Decreasing Mass

Start - End	Observed	Mr(expt)	Mr(calc)	ppm	Miss	Sequence
14 - 21	1025.5774	1024.5701	1024.4978	71	0	K.EAFQLFDR.T (No match)
14 - 21	1025.5774	1024.5701	1024.4978	71	0	K.EAFQLFDR.T (No match)
27 - 37	1341.7197	1340.7124	1340.6217	68	0	K.ILYSQCGDVMR.A Carbamidomethyl (C) (No match)
27 - 37	1341.7197	1340.7125	1340.6217	68	0	K.ILYSQCGDVMR.A Carbamidomethyl (C) (Ions score 18)
27 - 37	1357.7262	1356.7189	1356.6166	75	0	K.ILYSQCGDVMR.A Carbamidomethyl (C); Oxidation (M) (No match)
64 - 79	1888.1234	1887.1161	1886.9964	63	0	K.VLDFEHFLPMLQTVAK.N (No match)
64 - 79	1888.1234	1887.1161	1886.9964	63	0	K.VLDFEHFLPMLQTVAK.N (No match)
80 - 94	1786.9353	1785.9280	1785.8169	62	1	K.NKDQGTYEDYVEGLR.V (No match)
82 - 94	1544.7834	1543.7761	1543.6791	63	0	K.DQGTYEDYVEGLR.V (No match)
82 - 94	1544.7834	1543.7762	1543.6791	63	0	K.DQGTYEDYVEGLR.V (No match)
95 - 110	1722.9520	1721.9447	1721.8407	60	1	R.VFDKEGNGTVMGAEIR.H (No match)

U11 - Protein disulfide-isomerase precursor (PDI)

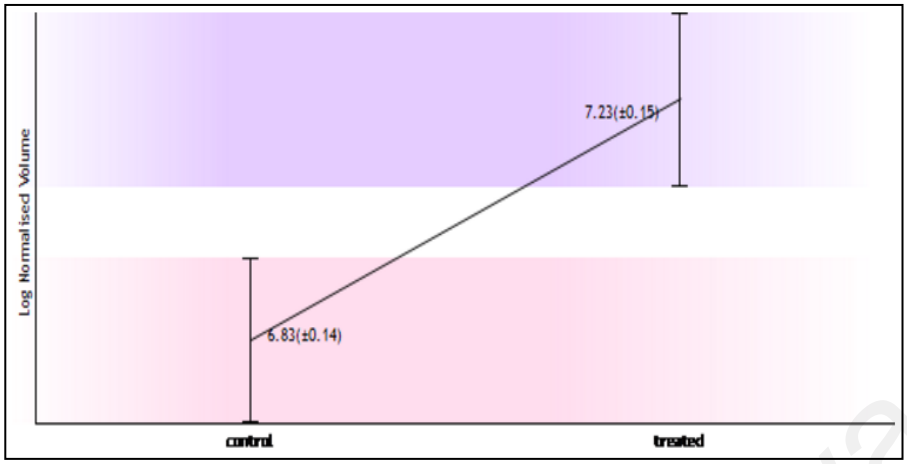

Matched peptides shown in **Bold Red**

```
   1 MLRRALLCLA VAALVRADAP EEEDHVLVLR KSNFAEALAA HKYLLVEFYA
  51 PWCGHCKALA PEYAKAAGKL KAEGSEIRLA KVDATEESDL AQQYGVRGYP
 101 TIKFFRNGDT ASPKEYTAGR EADDIVNWLK KRTGPAATTL PDGAAAESLV
 151 ESSEVAVIGF FKDVESDSAK QFLQAAEAID DIPFGITSNS DVFSKYQLDK
 201 DGVVLFKKFD EGRNNFEGEV TKENLLDFIK HNQLPLVIEF TEQTAPKIFG
 251 GEIKTHILLF LPKSVSDYDG KLSNFKTAAE SFKGKILFIF IDSDHTDNQR
 301 ILEFFGLKKE ECPAVRLITL EEEMTKYKPE SEELTAERIT EFCHRFLEGK
 351 IKPHLMSQEL PEDWDKQPVK VLVGKNFEDV AFDEKKNVFV EFYAPWCGHC
 401 KQLAPIWDKL GETYKDHENI VIAKMDSTAN EVEAVKVHSF PTLKFFPASA
 451 DRTVIDYNGE RTLDGFKKFL ESGGQDGAGD DDDLEDLEEA EEPDMEEDDD
 501 QKAVKDEL
```

Show predicted peptides also

Sort Peptides By ◉ Residue Number ○ Increasing Mass ○ Decreasing Mass

Start - End	Observed	Mr(expt)	Mr(calc)	ppm	Miss	Sequence
82 - 97	1780.8334	1779.8261	1779.8275	-1	0	K.VDATEESDLAQQYGVR.G (Ions score 47)
82 - 97	1780.8334	1779.8261	1779.8275	-1	0	K.VDATEESDLAQQYGVR.G (No match)
133 - 162	2935.4180	2934.4107	2934.4862	-26	0	R.TGPAATTLPDGAAAESLVESSEVAVIGFFK.D (No match)
196 - 207	1424.7783	1423.7710	1423.7711	-0	1	K.YQLDKDGVVLFK.K (No match)
214 - 222	1037.5303	1036.5230	1036.4825	39	0	R.NNFEGEVTK.E (No match)
231 - 247	1965.0284	1964.0211	1964.0367	-8	0	K.HNQLPLVIEFTEQTAPK.I (No match)
231 - 247	1965.0284	1964.0212	1964.0367	-8	0	K.HNQLPLVIEFTEQTAPK.I (Ions score 29)
255 - 263	1081.6752	1080.6679	1080.6695	-2	0	K.THILLFLPK.S (No match)
255 - 263	1081.6752	1080.6679	1080.6695	-1	0	K.THILLFLPK.S (No match)
286 - 300	1833.9047	1832.8974	1832.9057	-5	0	K.ILFIFIDSDHTDNQR.I (Ions score 25)
286 - 300	1833.9047	1832.8974	1832.9057	-5	0	K.ILFIFIDSDHTDNQR.I (No match)
301 - 308	966.5677	965.5604	965.5586	2	0	R.ILEFFGLK.K (No match)
327 - 338	1451.7054	1450.6981	1450.6939	3	0	K.YKPESEELTAER.I (No match)
327 - 338	1451.7054	1450.6982	1450.6939	3	0	K.YKPESEELTAER.I (No match)
339 - 345	962.4598	961.4525	961.4440	9	0	R.ITEFCHR.F Carbamidomethyl (C) (No match)
339 - 345	962.4598	961.4526	961.4440	9	0	R.ITEFCHR.F Carbamidomethyl (C) (Ions score 19)
445 - 452	910.4496	909.4423	909.4345	9	0	K.FFPASADR.T (No match)
445 - 452	910.4496	909.4423	909.4345	9	0	K.FFPASADR.T (No match)
453 - 461	1066.5207	1065.5135	1065.5091	4	0	R.TVIDYNGER.T (No match)
453 - 461	1066.5208	1065.5135	1065.5091	4	0	R.TVIDYNGER.T (No match)

D12 - Guanidinoacetate N-methyltransferase

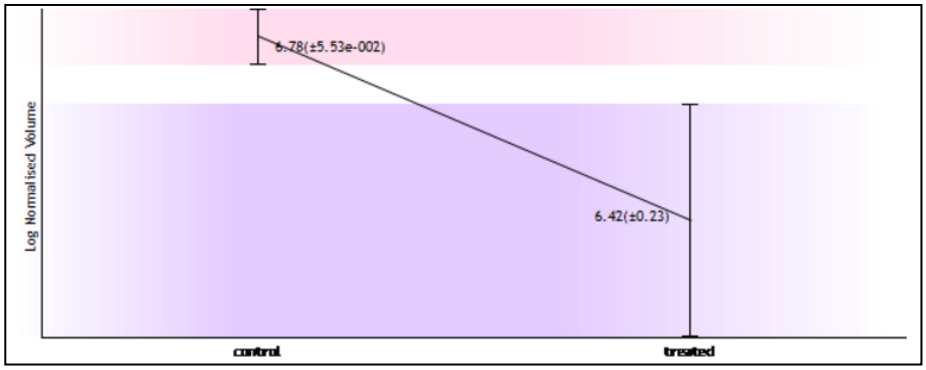

Matched peptides shown in Bold Red

```
  1 MSAPSATPIF APGENCSPAW GAAPAAYDAA DTHLRILGKP VMERWETPYM
 51 HALAAAASSK GGRVLEVGFG MAIAASKVQE APIDEHWIIE CNDGVFQRLR
101 DWAPRQTHKV IPLKGLWEDV APTLPDGHFD GILYDTYPLS EETWHTHQFN
151 FIKNHAFRLL KPGGVLTYCN LTSWGELMKS KYSDITIMFE ETQVPALLEA
201 GFRRENIRTE VMALVPPADC RYYAFPQMIT PLVTKG
```

Show predicted peptides also

Sort Peptides By ◉ Residue Number ○ Increasing Mass ○ Decreasing Mass

Start - End	Observed	Mr(expt)	Mr(calc)	Delta	Miss	Sequence
45 - 60	1733.8956	1732.8883	1732.8242	0.0641	0	R.WETPYMHALAAAASSK.G (No match)
45 - 60	1733.8956	1732.8883	1732.8242	0.0641	0	R.WETPYMHALAAAASSK.G (No match)
78 - 98	2555.2722	2554.2649	2554.1910	0.0739	0	K.VQEAPIDEHWIIECNDGVFQR.L Carbamidomethyl (C) (Ions score 92)
78 - 98	2555.2722	2554.2649	2554.1910	0.0739	0	K.VQEAPIDEHWIIECNDGVFQR.L Carbamidomethyl (C) (No match)
159 - 179	2380.3062	2379.2989	2379.2330	0.0659	0	R.LLKPGGVLTYCNLTSWGELMK.S Carbamidomethyl (C) (Ions score 34)
159 - 179	2380.3062	2379.2989	2379.2330	0.0659	0	R.LLKPGGVLTYCNLTSWGELMK.S Carbamidomethyl (C) (No match)
182 - 203	2530.3213	2529.3140	2529.2460	0.0680	0	K.YSDITIMFEETQVPALLEAGFR.R (Ions score 26)
182 - 203	2530.3213	2529.3140	2529.2460	0.0680	0	K.YSDITIMFEETQVPALLEAGFR.R (No match)
205 - 221	1971.0347	1970.0274	1969.9713	0.0561	1	R.ENIRTEVMALVPPADCR.Y Carbamidomethyl (C) (No match)
205 - 221	1971.0347	1970.0274	1969.9713	0.0561	1	R.ENIRTEVMALVPPADCR.Y Carbamidomethyl (C) (No match)
222 - 236	1728.9584	1727.9511	1727.8956	0.0555	1	R.YYAFPQMITPLVTKG.- (No match)

D13 Deoxycytidine kinase (dCK)

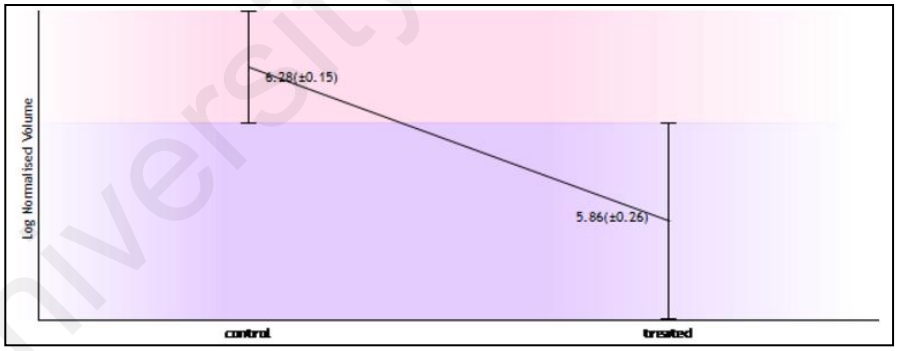

Matched peptides shown in Bold Red

```
  1 MATPPKRSCP SFSASSEGTR IKKISIEGNI AAGKSTFVNI LKQLCEDWEV
 51 VPEPVARWCN VQSTQDEFEE LTMSQKNGGN VLQMMYEKPE RWSFTFQTYA
101 CLSRIRAQLA SLNGKLKDAE KPVLFFERSV YSDRYIFASN LYESECMNET
151 EWTIYQDWHD WMNNQFGQSL ELDGIIYLQA TPETCLHRIY LRGRNEEQGI
201 PLEYLEKLHY KHESWLLHRT LKTNFDYLQE VPILTLDVNE DFKDKYESLV
251 EKVKEFLSTL
```

Show predicted peptides also

Sort Peptides By ◉ Residue Number ○ Increasing Mass ○ Decreasing Mass

Start - End	Observed	Mr(expt)	Mr(calc)	ppm	Miss	Sequence
43 - 57	1826.8684	1825.8611	1825.8669	-3	0	K.QLCEDWEVVPEPVAR.W Carbamidomethyl (C) (No match)
43 - 57	1826.8684	1825.8611	1825.8669	-3	0	K.QLCEDWEVVPEPVAR.W Carbamidomethyl (C) (Ions score 26)
92 - 104	1666.7725	1665.7652	1665.7610	3	0	R.WSFTFQTYACLSR.I Carbamidomethyl (C) (No match)
116 - 128	1591.8995	1590.8922	1590.8770	10	1	K.LKDAEKPVLFFER.S (No match)
118 - 128	1350.7115	1349.7042	1349.6979	5	0	K.DAEKPVLFFER.S (No match)
193 - 207	1774.9187	1773.9114	1773.8897	12	1	R.GRNEEQGIPLEYLEK.L (No match)

U14 Heme oxygenase-1 (HO-1)

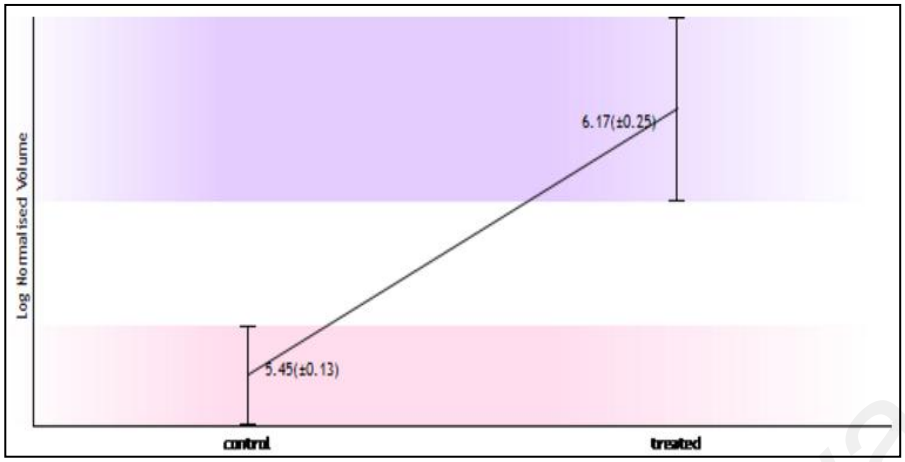

Matched peptides shown in **Bold Red**

```
  1 MERPQPDSMP QDLSEALKEA TKEVHTQAEN AEFMRNFQKG QVTRDGFKLV
 51 MASLYHIYVA LEEEIERNKE SPVFAPVYFP EELHRKAALE QDLAFWYGPR
101 WQEVIPYTPA MQRYVKRLHE VGRTEPELLV AHAYTRYLGD LSGGQVLKKI
151 AQKALDLPSS GEGLAFFTFP NIASATKFKQ LYRSRMNSLE MTPAVRQRVI
201 EEAKTAFLLN IQLFEELQEL LTHDTKDQSP SRAPGLRQRA SNKVQDSAPV
251 ETPRGKPPLN TRSQAPLLRW VLTLSFLVAT VAVGLYAM
```

Show predicted peptides also

Sort Peptides By ◉ Residue Number ○ Increasing Mass ○ Decreasing Mass

Start - End	Observed	Mr(expt)	Mr(calc)	ppm	Miss	Sequence
23 - 35	1561.7354	1560.7281	1560.6991	19	0	K.EVHTQAENAEFMR.N (No match)
49 - 67	2278.2356	2277.2283	2277.1714	25	0	K.LVMASLYHIYVALEEEIER.N (No match)
70 - 85	1916.9965	1915.9892	1915.9468	22	0	K.ESPVFAPVYFPEELHR.K (Ions score 32)
70 - 85	1916.9965	1915.9892	1915.9468	22	0	K.ESPVFAPVYFPEELHR.K (No match)
86 - 100	1764.9457	1763.9384	1763.8995	22	1	R.KAALEQDLAFWYGPR.W (No match)
87 - 100	1636.8502	1635.8429	1635.8045	23	0	K.AALEQDLAFWYGPR.W (No match)
87 - 100	1636.8502	1635.8429	1635.8045	23	0	K.AALEQDLAFWYGPR.W (Ions score 23)
101 - 113	1618.8374	1617.8301	1617.7973	20	0	R.WQEVIPYTPAMQR.Y (No match)
101 - 113	1618.8374	1617.8301	1617.7973	20	0	R.WQEVIPYTPAMQR.Y (No match)
101 - 113	1634.8307	1633.8234	1633.7923	19	0	R.WQEVIPYTPAMQR.Y Oxidation (M) (No match)
124 - 136	1499.8134	1498.8061	1498.7780	19	0	R.TEPELLVAHAYTR.Y (No match)

U15 Peptidylproyl cis-trans isomerise (Rotamase)

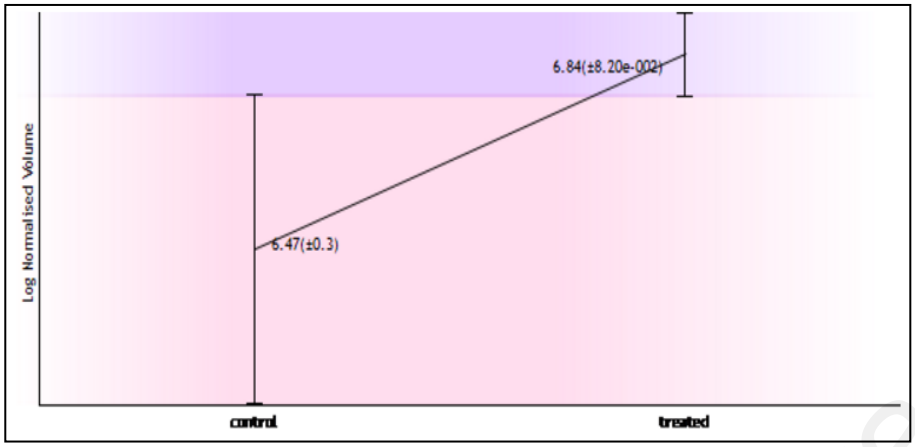

Matched peptides shown in **Bold Red**

```
  1 MTAEEMKATE SGAQSAPLPM EGVDISPKQD EGVLKVIKRE GTGTEMPMIG
 51 DRVFVHYTGW LLDGTKFDSS LDRKDKFSFD LGKGEVIKAW DIAIATMKVG
101 EVCHITCKPE YAYGSAGSPP KIPPNATLVF EVELFEFKGE DLTEEEDGGI
151 IRRIQTRGEG YAKPNEGAIV EVALEGYYKD KLFDQRELRF EIGEGENLDL
201 PYGLERAIQR MEKGEHSIVY LKPSYAFGSV GKEKFQIPPN AELKYELHLK
251 SFEKAKESWE MNSEEKLEQS TIVKERGTVY FKEGKYKQAL LQYKKIVSWL
301 EYESSFSNEE AQKAQALRLA SHLNLAMCHL KLQAFSAAIE SCNKALELDS
351 NNEKGLFRRG EAHLAVNDFE LARADFQKVL QLYPNNKAAK TQLAVCQQRI
401 RRQLAREKKL YANMFERLAE EENKAKAEAS SGDHPTDTEM KEEQKSNTAG
451 SQSQVETEA
```

Show predicted peptides also

Sort Peptides By ◉ Residue Number ○ Increasing Mass ○ Decreasing Mass

Start - End	Observed	Mr(expt)	Mr(calc)	ppm	Miss	Sequence
29 - 38	1128.5690	1127.5617	1127.6550	-83	1	K.QDEGVLKVIK.R (No match)
40 - 52	1393.7196	1392.7123	1392.6013	80	0	R.EGTGTEMPMIGDR.V (No match)
53 - 66	1635.8153	1634.8080	1634.8457	-23	0	R.VFVHYTGWLLDGTK.F (No match)
53 - 66	1635.8153	1634.8080	1634.8457	-23	0	R.VFVHYTGWLLDGTK.F (No match)
99 - 121	2507.1301	2506.1228	2506.1621	-16	0	K.VGEVCHITCKPEYAYGSAGSPPK.I 2 Carbamidomethyl (C) (No match)
158 - 179	2357.1279	2356.1206	2356.1586	-16	0	R.GEGYAKPNEGAIVEVALEGYYK.D (No match)
158 - 179	2357.1279	2356.1207	2356.1586	-16	0	R.GEGYAKPNEGAIVEVALEGYYK.D (No match)
190 - 206	1950.9189	1949.9116	1949.9370	-13	0	R.FEIGEGENLDLPYGLER.A (No match)
190 - 206	1950.9190	1949.9117	1949.9370	-13	0	R.FEIGEGENLDLPYGLER.A (Ions score 69)
214 - 232	2039.0266	2038.0193	2038.0524	-16	0	K.GEHSIVYLKPSYAFGSVGK.E (No match)
296 - 313	2145.9719	2144.9646	2144.9902	-12	0	K.IVSWLEYESSFSNEEAQK.A (No match)
319 - 331	1507.7632	1506.7559	1506.7799	-16	0	R.LASHLNLAMCHLK.L Carbamidomethyl (C) (No match)
359 - 373	1697.8492	1696.8419	1696.8645	-13	1	R.RGEAHLAVNDFELAR.A (No match)
359 - 373	1697.8492	1696.8420	1696.8645	-13	1	R.RGEAHLAVNDFELAR.A (No match)
360 - 373	1541.7552	1540.7479	1540.7634	-10	0	R.GEAHLAVNDFELAR.A (No match)
391 - 399	1046.5188	1045.5115	1045.5339	-21	0	K.TQLAVCQQR.I (No match)
391 - 399	1103.5463	1102.5390	1102.5553	-15	0	K.TQLAVCQQR.I Carbamidomethyl (C) (No match)
391 - 399	1103.5463	1102.5390	1102.5553	-15	0	K.TQLAVCQQR.I Carbamidomethyl (C) (No match)
409 - 417	1171.5792	1170.5719	1170.5855	-12	1	K.KLYANMFER.L (No match)
410 - 417	1043.4896	1042.4823	1042.4906	-8	0	K.LYANMFER.L (No match)

D16 - Phosphoglycerate mutase 1

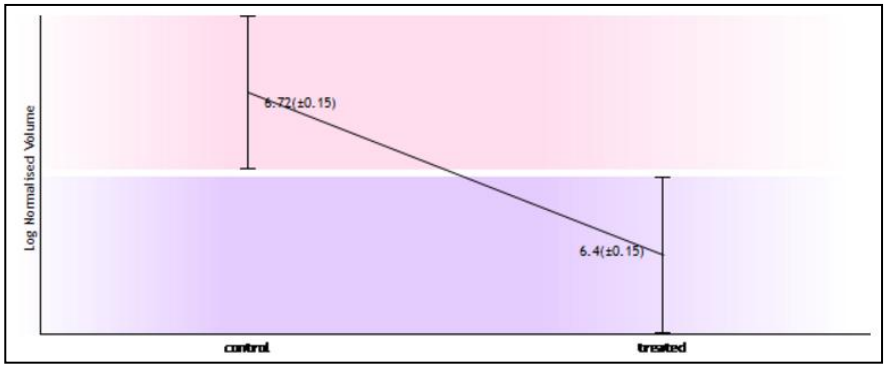

Matched peptides shown in Bold Red

```
  1 MAAYKLVLIR HGESAWNLEN RFSGWYDADL SPAGHEEAKR GGQALRDAGY
 51 EFDICFTSVQ KRAIRTLWTV LDAIDQMWLP VVRTWRLNER HYGGLTGLNK
101 AETAAKHGEA QVKIWRRSYD VPPPPMEPDH PFYSNISKDR RYADLTEDQL
151 PSCESLKDTI ARALPFWNEE IVPQIKEGKR VLIAAHGNSL RGIVKHLEGL
201 SEEAIMELNL PTGIPIVYEL DKNLKPIKPM QFLGDEETVR KAMEAVAAQG
251 KAKK
```

Show predicted peptides also

Sort Peptides By ◉ Residue Number ○ Increasing Mass ○ Decreasing Mass

Start - End	Observed	Mr(expt)	Mr(calc)	Delta	Miss	Sequence
11 - 21	1312.6364	1311.6291	1311.5956	0.0336	0	R.HGESAWNLENR.F (Ions score 29)
11 - 21	1312.6364	1311.6291	1311.5956	0.0336	0	R.HGESAWNLENR.F (No match)
22 - 39	1979.9243	1978.9170	1978.8697	0.0474	0	R.FSGWYDADLSPAGHEEAK.R (No match)
22 - 40	2136.0212	2135.0139	2134.9708	0.0432	1	R.FSGWYDADLSPAGHEEAKR.G (No match)
91 - 100	1059.5769	1058.5696	1058.5508	0.0188	0	R.HYGGLTGLNK.A (No match)
118 - 138	2417.1587	2416.1514	2416.1045	0.0469	0	R.SYDVPPPPMEPDHPFYSNISK.D (No match)
142 - 162	2425.2104	2424.2031	2424.1478	0.0553	1	R.YADLTEDQLPSCESLKDTIAR.A Carbamidomethyl (C) (Ions score 43)
142 - 162	2425.2104	2424.2031	2424.1478	0.0553	1	R.YADLTEDQLPSCESLKDTIAR.A Carbamidomethyl (C) (No match)
163 - 176	1683.9343	1682.9270	1682.9031	0.0239	0	R.ALPFWNEEIVPQIK.E (Ions score 42)
163 - 176	1683.9343	1682.9270	1682.9031	0.0239	0	R.ALPFWNEEIVPQIK.E (No match)
181 - 191	1150.6912	1149.6839	1149.6618	0.0221	0	R.VLIAAHGNSLR.G (Ions score 9)
181 - 191	1150.6912	1149.6839	1149.6618	0.0221	0	R.VLIAAHGNSLR.G (No match)
223 - 240	2115.1660	2114.1587	2114.1193	0.0394	0	K.NLKPIKPMQFLGDEETVR.K (No match)

D17 - Glutathione S-transferase

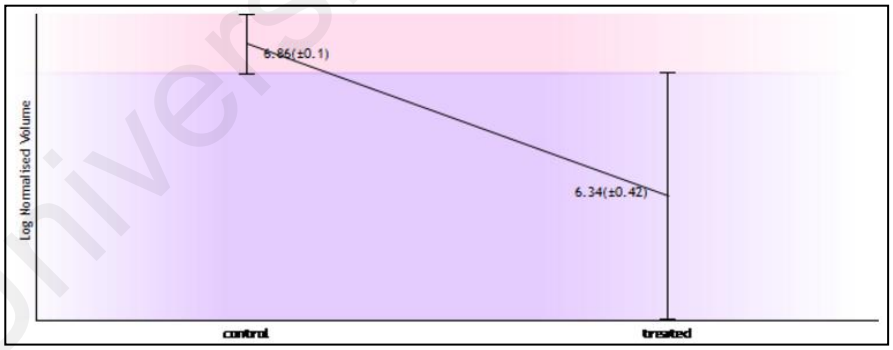

Matched peptides shown in Bold Red

```
  1 MSGESARSLG KGSAPPGPVP EGSIRIYSMR FCPFAERTRL VLKAKGIRHE
 51 VININLKNKP EWFFKKNPFG LVPVLENSQG QLIYESAITC EYLDEAYPGK
101 KLLPDDPYEK ACQKMILELF SKVPSLVGSF IRSQNKEDYA GLKEEFRKEF
151 TKLEEVLTNK KTTFFGGNSI SMIDYLIWPW FERLEAMKLN ECVDHTPKLK
201 LWMAAMKEDP TVSALLTSEK DWQGFLELYL QNSPEACDYG L
```

Show predicted peptides also

Sort Peptides By ◉ Residue Number ○ Increasing Mass ○ Decreasing Mass

Start - End	Observed	Mr(expt)	Mr(calc)	ppm	Miss	Sequence
12 - 25	1320.6099	1319.6026	1319.6834	-61	0	K.GSAPPGPVPEGSIR.I (No match)
31 - 37	926.3599	925.3526	925.4116	-64	0	R.FCPFAER.T Carbamidomethyl (C) (No match)
31 - 37	926.3599	925.3526	925.4116	-64	0	R.FCPFAER.T Carbamidomethyl (C) (Ions score 15)
58 - 65	1095.4977	1094.4904	1094.5549	-59	0	K.NKPEWFFK.K (No match)
123 - 132	1074.5686	1073.5613	1073.6233	-58	0	K.VPSLVGSFIR.S (Ions score 15)
123 - 132	1074.5686	1073.5613	1073.6233	-58	0	K.VPSLVGSFIR.S (No match)

D18 - Catechol O-methyltransferase

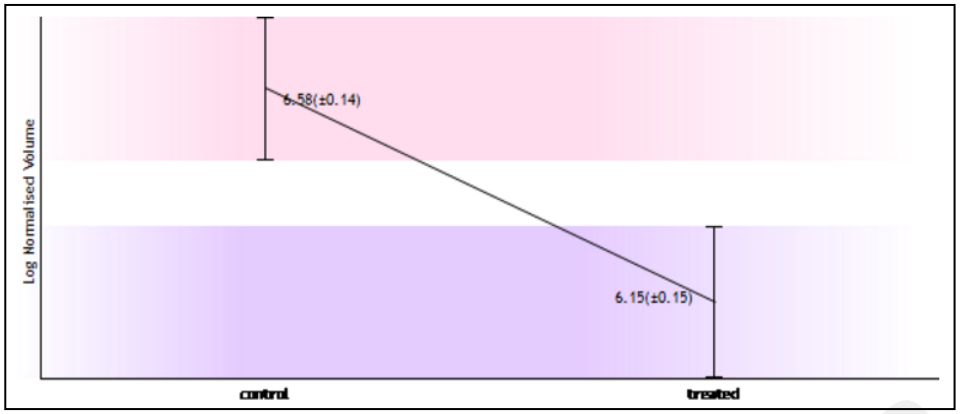

Matched peptides shown in **Bold Red**

```
  1 MPEAPPLLLA AVLLGLVLLV VLLLLLRHWG WGLCLIGWNE FILQPIHNLL
 51 MGDTKEQRIL NHVLQHAEPG NAQSVLEAID TYCEQKEWAM NVGDKKGKIV
101 DAVIQEHQPS VLLELGAYCG YSAVRMARLL SPGARLITIE INPDCAAITQ
151 RMVDFAGVKD KVTLVVGASQ DIIPQLKKKY DVDTLDMVFL DHWKDRYLPD
201 TLLLEECGLL RKGTVLLADN VICPGAPDFL AHVRGSSCFE CTHYQSFLEY
251 REVVDGLEKA IYKGPGSEAG P
```

Show predicted peptides also

Sort Peptides By ◉ Residue Number ○ Increasing Mass ○ Decreasing Mass

Start - End	Observed	Mr(expt)	Mr(calc)	ppm	Miss	Sequence
99 - 125	2987.4106	2986.4033	2986.5222	-40	0	K.IVDAVIQEHQPSVLLELGAYCGYSAVR.M Carbamidomethyl (C) (No match)
136 - 151	1827.8817	1826.8744	1826.9560	-45	0	R.LITIEINPDCAAITQR.M Carbamidomethyl (C) (No match)
136 - 151	1827.8817	1826.8744	1826.9560	-45	0	R.LITIEINPDCAAITQR.M Carbamidomethyl (C) (Ions score 17)
136 - 159	2691.1572	2690.1499	2690.3772	-84	1	R.LITIEINPDCAAITQRMVDFAGVK.D Carbamidomethyl (C); Oxidation (M) (No match)
197 - 211	1804.8831	1803.8758	1803.9440	-38	0	R.YLPDTLLLEECGLLR.K Carbamidomethyl (C) (Ions score 12)
197 - 211	1804.8831	1803.8758	1803.9440	-38	0	R.YLPDTLLLEECGLLR.K Carbamidomethyl (C) (No match)
213 - 234	2335.1316	2334.1243	2334.2155	-39	0	K.GTVLLADNVICPGAPDFLAHVR.G Carbamidomethyl (C) (No match)
213 - 234	2335.1316	2334.1243	2334.2155	-39	0	K.GTVLLADNVICPGAPDFLAHVR.G Carbamidomethyl (C) (No match)
235 - 251	2170.8159	2169.8086	2169.8884	-37	0	R.GSSCFECTHYQSFLEYR.E 2 Carbamidomethyl (C) (No match)
235 - 251	2170.8159	2169.8086	2169.8884	-37	0	R.GSSCFECTHYQSFLEYR.E 2 Carbamidomethyl (C) (No match)

D19 - 3'(2'),5'-bisphosphate nucleotidase 1 (PIP)

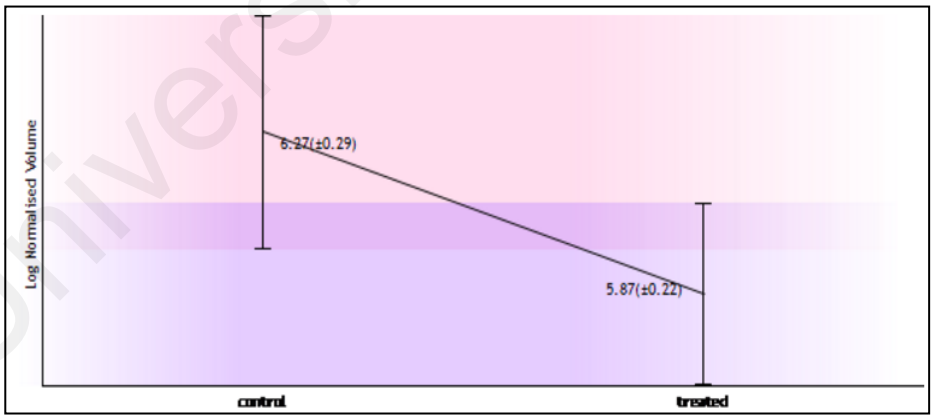

Matched peptides shown in **Bold Red**

```
  1 MASSNTVLMR LVASAYSIAQ KAGMIVRRVI AEGDLGIVEK TCATDLQTKA
 51 DRLAQMSICS SLARKFPKLT IIGEEDLPSE EVDQELIEDS QWEEILKQPC
101 PSQYSAIKEE DLVVWVDPLD GTKEYTEGLL DNVTVLIGIA YEGKAIAGVI
151 NQPYYNYEAG PDAVLGRTIW GVLGLGAFGF QLKEVPAGKH IITTTRSHSN
201 KLVTDCVAAM NPDAVLRVGG AGNKIIQLIE GKASAYVFAS PGCKKWDTCA
251 PEVILHAVGG KLTDIHGNVL QYHKDVKHMN SAGVLATLRN YDYYASRVPE
301 SIKNALVP
```

Show predicted peptides also

Sort Peptides By ◉ Residue Number ○ Increasing Mass ○ Decreasing Mass

Start - End	Observed	Mr(expt)	Mr(calc)	Delta	Miss	Sequence
145 - 167	2451.2847	2450.2774	2450.2229	0.0545	0	K.AIAGVINQPYYNYEAGPDAVLGR.T (Ions score 92)
145 - 167	2451.2847	2450.2774	2450.2229	0.0545	0	K.AIAGVINQPYYNYEAGPDAVLGR.T (No match)

D20 - Protein canopy homolog 2

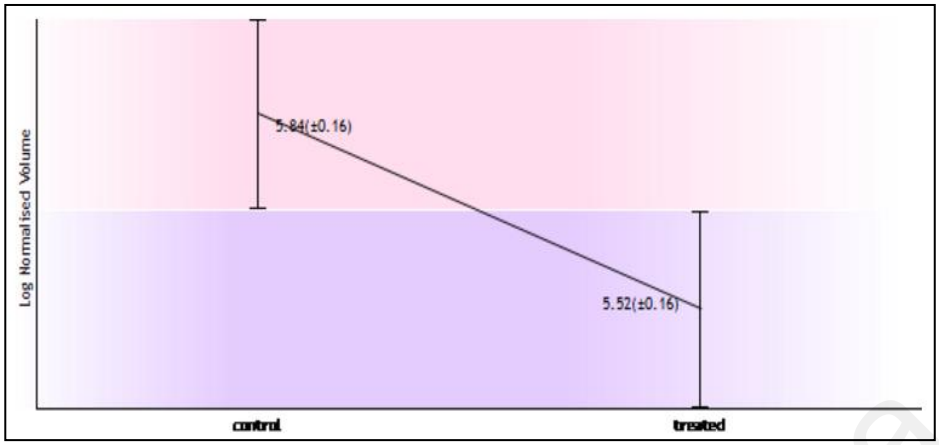

Matched peptides shown in Bold Red

```
  1 MGKKTKRTAD SSSSEDEEEY VVEKVLDRRV VKGQVEYLLK WKGFSEEHNT
 51 WEPEKNLDCP ELISEFMKKY KKMKEGENNK PREKSESNKR KSNFSNSADD
101 IKSKKKREQS NDIARGFERG LEPEKIIGAT DSCGDLMFLM KWKDTDEADL
151 VLAKEANVKC PQIVIAFYEE RLTWHAYPED AENKEKETAK S
```

Show predicted peptides also

Sort Peptides By ◉ Residue Number ○ Increasing Mass ○ Decreasing Mass

Start - End	Observed	Mr(expt)	Mr(calc)	Delta	Miss	Sequence
120 - 141	2383.9998	2382.9925	2383.1473	-0.1547	1	R.GLEPEKIIGATDSCGDLMFLMK.W Oxidation (M) (No match)
120 - 141	2383.9998	2382.9925	2383.1473	-0.1547	1	R.GLEPEKIIGATDSCGDLMFLMK.W Oxidation (M) (No match)
160 - 171	1524.7996	1523.7923	1523.7442	0.0481	0	K.CPQIVIAFYEER.L Carbamidomethyl (C) (Ions score 66)
160 - 171	1524.7996	1523.7923	1523.7442	0.0481	0	K.CPQIVIAFYEER.L Carbamidomethyl (C) (No match)

D21 - Transcription elongation factor B polypeptide 1 (Elong C)

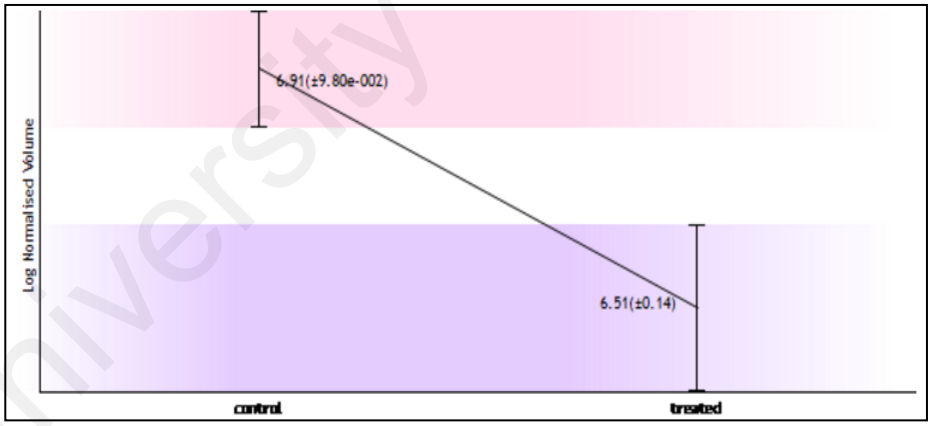

Matched peptides shown in Bold Red

```
  1 MDGEEKTYGG CEGPDAMYVK LISSDGHEFI VKREHALTSG TIKAMLSGPG
 51 QFAENETNEV NFREIPSHVL SKVCMYFTYK VRYTNSSTEI PEFPIAPEIA
101 LELLMAANFL DC
```

Show predicted peptides also

Sort Peptides By ◉ Residue Number ○ Increasing Mass ○ Decreasing Mass

Start - End	Observed	Mr(expt)	Mr(calc)	ppm	Miss	Sequence
7 - 20	1547.6366	1546.6293	1546.6432	-9	0	K.TYGGCEGPDAMYVK.L Carbamidomethyl (C) (No match)
21 - 32	1344.7039	1343.6966	1343.7085	-9	0	K.LISSDGHEFIVK.R (No match)
21 - 32	1344.7039	1343.6966	1343.7085	-9	0	K.LISSDGHEFIVK.R (No match)
21 - 33	1500.8036	1499.7963	1499.8096	-9	1	K.LISSDGHEFIVKR.E (No match)
44 - 63	2211.0093	2210.0020	2210.0062	-2	0	K.AMLSGPGQFAENETNEVNFR.E (No match)
44 - 63	2227.0430	2226.0357	2226.0011	16	0	K.AMLSGPGQFAENETNEVNFR.E Oxidation (M) (Ions score 62)
44 - 63	2227.0430	2226.0357	2226.0011	16	0	K.AMLSGPGQFAENETNEVNFR.E Oxidation (M) (No match)
73 - 80	1111.4891	1110.4818	1110.4878	-5	0	K.VCMYFTYK.V Carbamidomethyl (C) (No match)
73 - 80	1111.4891	1110.4819	1110.4878	-5	0	K.VCMYFTYK.V Carbamidomethyl (C) (No match)

D22 - Cellular retinoic acid-binding protein 2 (CRABP-II)

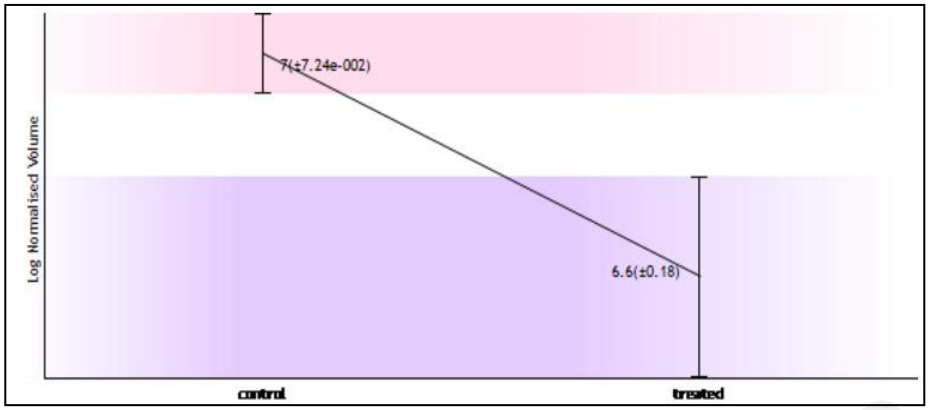

Matched peptides shown in **Bold Red**

```
  1 MPNFSGNWKI IRSENFEELL KVLGVNVMLR KIAVAAASKP AVEIKQEGDT
 51 FYIKTSTTVR TTEINFKVGE EFEEQTVDGR PCKSLVKWES ENKMVCEQKL
101 LKGEGPKTSW TRELTNDGEL ILTMTADDVV CTRVYVRE
```

Show predicted peptides also

Sort Peptides By ◉ Residue Number ○ Increasing Mass ○ Decreasing Mass

Start - End	Observed	Mr(expt)	Mr(calc)	ppm	Miss	Sequence
22 - 30	1000.5953	999.5880	999.5899	-2	0	K.VLGVNVMLR.K (No match)
22 - 30	1000.5953	999.5881	999.5899	-2	0	K.VLGVNVMLR.K (No match)
68 - 83	1879.8403	1878.8330	1878.8418	-5	0	K.VGEEFEEQTVDGRPCK.S Carbamidomethyl (C) (No match)
68 - 83	1879.8403	1878.8331	1878.8418	-5	0	K.VGEEFEEQTVDGRPCK.S Carbamidomethyl (C) (Ions score 23)
113 - 133	2366.1062	2365.0989	2365.1141	-6	0	R.ELTNDGELILTMTADDVVCTR.V Carbamidomethyl (C) (Ions score 61)
113 - 133	2366.1062	2365.0989	2365.1141	-6	0	R.ELTNDGELILTMTADDVVCTR.V Carbamidomethyl (C) (No match)

D23 - Eukaryotic translation initiation factor 5A-1 (eIF-5A1)

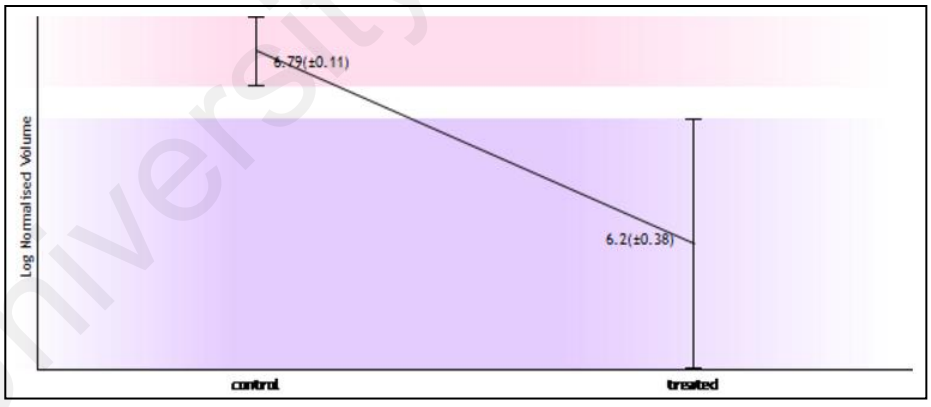

Matched peptides shown in **Bold Red**

```
  1 MADDLDFETG DAGASATFPM QCSALRKNGF VVLKGRPCKI VEMSTSKTGK
 51 HGHAKVHLVG IDIFTGKKYE DICPSTHNMD VPNIKRNDFQ LIGIQDGYLS
101 LLQDSGEVRE DLRLPEGDLG KEIEQKYDCG EEILITVLSA MTEEAAVAIK
151 AMAK
```

Show predicted peptides also

Sort Peptides By ◉ Residue Number ○ Increasing Mass ○ Decreasing Mass

Start - End	Observed	Mr(expt)	Mr(calc)	ppm	Miss	Sequence
1 - 26	2720.3875	2719.3802	2719.1564	82	0	-.MADDLDFETGDAGASATFPMQCSALR.K (No match)
1 - 26	2720.3875	2719.3802	2719.1564	82	0	-.MADDLDFETGDAGASATFPMQCSALR.K (No match)
56 - 67	1298.7753	1297.7680	1297.7394	22	0	K.VHLVGIDIFTGK.K (Ions score 14)
56 - 67	1298.7753	1297.7680	1297.7394	22	0	K.VHLVGIDIFTGK.K (No match)
86 - 109	2736.4595	2735.4522	2735.3878	24	1	K.RNDFQLIGIQDGYLSLLQDSGEVR.E (Ions score 34)
86 - 109	2736.4595	2735.4522	2735.3878	24	1	K.RNDFQLIGIQDGYLSLLQDSGEVR.E (No match)
87 - 109	2580.3599	2579.3526	2579.2867	26	0	R.NDFQLIGIQDGYLSLLQDSGEVR.E (Ions score 73)
87 - 109	2580.3599	2579.3526	2579.2867	26	0	R.NDFQLIGIQDGYLSLLQDSGEVR.E (No match)

D24 - Elongation factor 2 (EF-2)

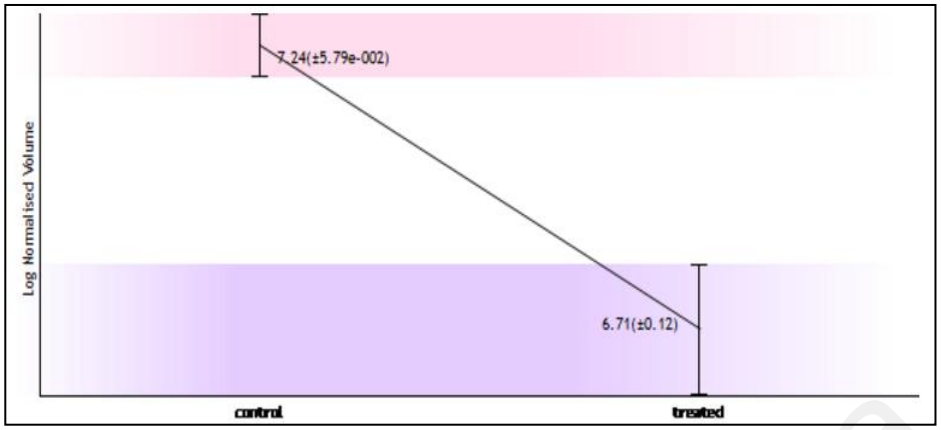

Matched peptides shown in **Bold Red**

```
   1 MVNFTVDQIR AIMDKKANIR NMSVIAHVDH GKSTLTDSLV CKAGIIASAR
  51 AGETRFTDTR KDEQERCITI KSTAISLFYE LSENDLNFIK QSKDGAGFLI
 101 NLIDSPGHVD FSSEVTAALR VTDGALVVVD CVSGVCVQTE TVLRQAIAER
 151 IKPVLMMNKM DRALLELQLE PEELYQTFQR IVENVNVIIS TYGEGESGPM
 201 GNIMIDPVLG TVGFGSGLHG WAFTLKQFAE MYVAKFAAKG EGQLGPAERA
 251 KKVEDMMKKL WGDRYFDPAN GKFSKSAISP EGKKLPRTFC QLILDPIFKV
 301 FDAIMNFKKE ETAKLIEKLD IKLDSEDKDK EGKPLLKAVM RRWLPAGDAL
 351 LQMITIHLPS PVTAQKYRCE LLYEGPPDDE AAMGIKSCDP KGPLMMYISK
 401 MVPTSDKGRF YAFGRVFSGL VSTGLKVRIM GPNYTPGKKE DLYLKPIQRT
 451 ILMMGRYVEP IEDVPCGNIV GLVGVDQFLV KTGTITTFEH AHNMRVMKFS
 501 VSPVVRVAVE AKNPADLPKL VEGLKRLAKS DPMVQCIIEE SGEHIIAGAG
 551 ELHLEICLKD LEEDHACIPI KKSDPVVSYR ETVSEESNVL CLSKSPNKHN
 601 RLYMKARPFP DGLAEDIDKG EVSARQELKQ RARYLAEKYE WDVAEARKIW
 651 CFGPDGTGPN ILTDITKGVQ YLNEIKDSVV AGFQWATKEG ALCEENMRGV
 701 RFDVHDVTLH ADAIHRGGGQ IIPTARRCLY ASVLTAQPRL MEPIYLVEIQ
 751 CPEQVVGGIY GVLNRKRGHV FEESQVAGTP MFVVKAYLPV NESFGFTADL
 801 RSNTGGQAFP QCVFDHWQIL PGDPFDNSSR PSQVVAETRK RKGLKEGIPA
 851 LDNFLDKL
```

Show predicted peptides also

Sort Peptides By ◉ Residue Number ○ Increasing Mass ○ Decreasing Mass

Start - End	Observed	Mr(expt)	Mr(calc)	ppm	Miss	Sequence
2 - 10	1091.5543	1090.5470	1090.5771	-28	0	M.VNFTVDQIR.A (No match)
2 - 10	1091.5543	1090.5470	1090.5771	-28	0	M.VNFTVDQIR.A (Ions score 12)
72 - 90	2204.0688	2203.0615	2203.1048	-20	0	K.STAISLFYELSENDLNFIK.Q (No match)
94 - 120	2801.3440	2800.3367	2800.4032	-24	0	K.DGAGFLINLIDSPGHVDFSSEVTAALR.V (Ions score 28)
94 - 120	2801.3440	2800.3367	2800.4032	-24	0	K.DGAGFLINLIDSPGHVDFSSEVTAALR.V (No match)
121 - 144	2576.2517	2575.2444	2575.2986	-21	0	R.VTDGALVVVDCVSGVCVQTETVLR.Q 2 Carbamidomethyl (C) (No match)
121 - 144	2576.2517	2575.2444	2575.2986	-21	0	R.VTDGALVVVDCVSGVCVQTETVLR.Q 2 Carbamidomethyl (C) (Ions score 73)
163 - 180	2220.1082	2219.1009	2219.1474	-21	0	R.ALLELQLEPEELYQTFQR.I (Ions score 81)
163 - 180	2220.1082	2219.1009	2219.1474	-21	0	R.ALLELQLEPEELYQTFQR.I (No match)
240 - 249	1013.4875	1012.4802	1012.4938	-13	0	K.GEGQLGPAER.A (No match)
288 - 299	1494.7551	1493.7478	1493.7952	-32	0	R.TFCQLILDPIFK.V Carbamidomethyl (C) (No match)
288 - 299	1494.7551	1493.7479	1493.7952	-32	0	R.TFCQLILDPIFK.V Carbamidomethyl (C) (No match)
300 - 308	1084.5308	1083.5235	1083.5423	-17	0	K.VFDAIMNFK.K (No match)

D25 Eukaryotic translation initiation factor 3 subunit 1 (eIF-3I)

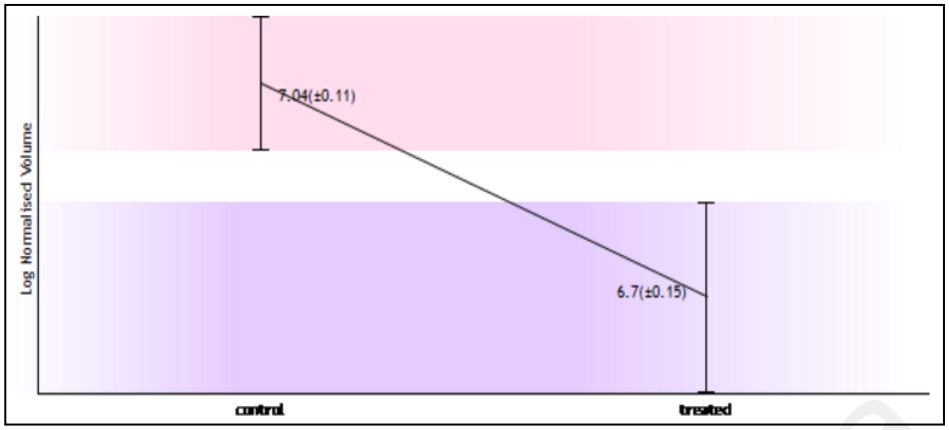

Matched peptides shown in **Bold Red**

```
  1 MKPILLQGHE RSITQIKYNR EGDLLFTVAK DPIVNVWYSV NGERLGTYMG
 51 HTGAVWCVDA DWDTKHVLTG SADNSCRLWD CETGKQLALL KTNSAVRTCG
101 FDFGGNIIMF STDKQMGYQC FVSFFDLRDP SQIDNNEPYM KIPCNDSKIT
151 SAVWGPLGEC IIAGHESGEL NQYSAKSGEV LVNVKEHSRQ INDIQLSRDM
201 TMFVTASKDN TAKLFDSTTL EHQKTFRTER PVNSAALSPN YDHVVLGGGQ
251 EAMDVTITST RIGKFEARFF HLAFEEEFGR VKGHFGPINS VAFHPDGKSY
301 SSGGEDGYVR IHYFDPQYFE FEFEA
```

Show predicted peptides also

Sort Peptides By ◉ Residue Number ○ Increasing Mass ○ Decreasing Mass

Start - End	Observed	Mr(expt)	Mr(calc)	ppm	Miss	Sequence
1 - 11	1321.7317	1320.7244	1320.7336	-7	0	-.MKPILLQGHER.S (No match)
1 - 11	1321.7317	1320.7244	1320.7336	-7	0	-.MKPILLQGHER.S (No match)
31 - 44	1647.7990	1646.7917	1646.8053	-8	0	K.DPIVNVWYSVNGER.L (No match)
115 - 128	1797.7767	1796.7694	1796.8015	-18	0	K.QMGYQCFVSFFDLR.D Carbamidomethyl (C) (No match)
115 - 128	1797.7767	1796.7695	1796.8015	-18	0	K.QMGYQCFVSFFDLR.D Carbamidomethyl (C) (Ions score 6)
149 - 176	2987.3945	2986.3872	2986.4494	-21	0	K.ITSAVWGPLGECIIAGHESGELNQYSAK.S Carbamidomethyl (C) (No match)
149 - 176	2987.3945	2986.3873	2986.4494	-21	0	K.ITSAVWGPLGECIIAGHESGELNQYSAK.S Carbamidomethyl (C) (Ions score 13)
269 - 280	1528.6951	1527.6878	1527.7147	-18	0	R.FFHLAFEEEFGR.V (Ions score 74)
269 - 280	1528.6951	1527.6878	1527.7147	-18	0	R.FFHLAFEEEFGR.V (No match)
283 - 298	1679.8000	1678.7927	1678.8216	-17	0	K.GHFGPINSVAFHPDGK.S (No match)
283 - 298	1679.8001	1678.7928	1678.8216	-17	0	K.GHFGPINSVAFHPDGK.S (No match)
299 - 310	1276.5265	1275.5192	1275.5368	-14	0	K.SYSSGGEDGYVR.I (Ions score 14)
299 - 310	1276.5265	1275.5192	1275.5368	-14	0	K.SYSSGGEDGYVR.I (No match)
311 - 325	1981.7946	1980.7873	1980.8570	-35	0	R.IHYFDPQYFEFEFEA.- (Ions score 101)
311 - 325	1981.7946	1980.7873	1980.8570	-35	0	R.IHYFDPQYFEFEFEA.- (No match)

U26 UV excision repair protein RA23 homolog B (HR23B)

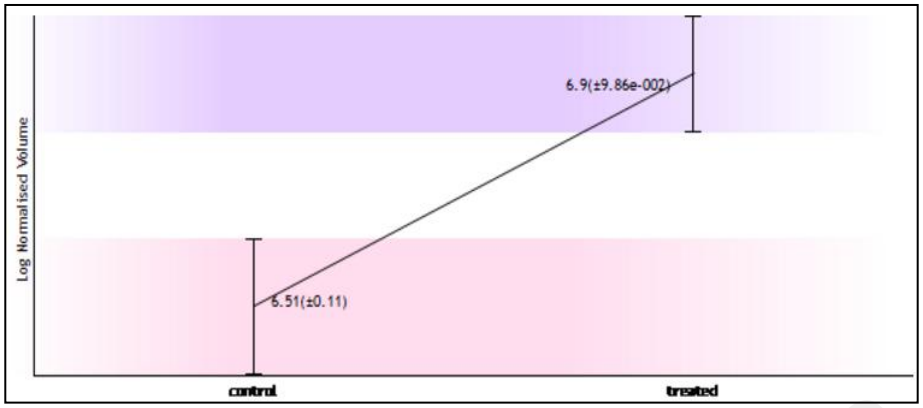

Matched peptides shown in **Bold Red**

```
   1 MQVTLKTLQQ QTFKIDIDPE ETVKALKEKI ESEKGKDAFP VAGQKLIYAG
  51 KILNDDTALK EYKIDEKNFV VVMVTKPKAV STPAPATTQQ SAPASTTAVT
 101 SSTTTTVAQA PTPVPALAPT STPASITPAS ATASSEPAPA SAAKQEKPAE
 151 KPAETPVATS PTATDSTSGD SSRSNLFEDA TSALVTGQSY ENMVTEIMSM
 201 GYERERQVIAA LRASFNNPDR AVEYLLMGIP GDRESQAVVD PPQAASTGAP
 251 QSSAVAAAAA TTTATTTTTS SGGHPLEFLR NQPQFQQMRQ IIQQNPSLLP
 301 ALLQQIGREN PQLLQQISQH QEHFIQMLNE PVQEAGGQGG GGGGGSGGIA
 351 EAGSGHMNYI QVTPQEKEAI ERLKALGFPE GLVIQAYFAC EKNENLAANF
 401 LLQQNFDED
```

Show predicted peptides also

Sort Peptides By ◉ Residue Number ○ Increasing Mass ○ Decreasing Mass

Start - End	Observed	Mr(expt)	Mr(calc)	ppm	Miss	Sequence
7 - 14	993.4894	992.4821	992.5291	-47	0	K.TLQQQTFK.I (No match)
68 - 78	1277.7019	1276.6946	1276.7213	-21	0	K.NFVVVMVTKPK.A Oxidation (M) (No match)
205 - 212	899.5128	898.5055	898.5236	-20	0	R.EQVIAALR.A (No match)
213 - 220	920.4120	919.4047	919.4148	-11	0	R.ASFNNPDR.A (No match)
213 - 220	920.4120	919.4047	919.4148	-11	0	R.ASFNNPDR.A (No match)
221 - 233	1433.7258	1432.7185	1432.7384	-14	0	R.AVEYLLMGIPGDR.E (No match)
221 - 233	1433.7258	1432.7186	1432.7384	-14	0	R.AVEYLLMGIPGDR.E (No match)
281 - 289	1176.5465	1175.5392	1175.5506	-10	0	R.NQPQFQQMR.Q (No match)
281 - 289	1176.5465	1175.5392	1175.5506	-10	0	R.NQPQFQQMR.Q (No match)
290 - 308	2130.1929	2129.1856	2129.2320	-22	0	R.QIIQQNPSLLPALLQQIGR.E (Ions score 18)
290 - 308	2130.1929	2129.1856	2129.2320	-22	0	R.QIIQQNPSLLPALLQQIGR.E (No match)

D27 - Chromobox protein homolog 3

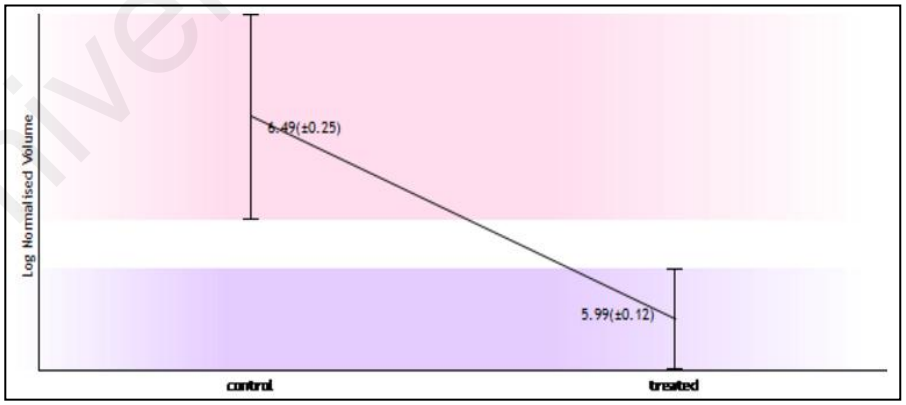

Matched peptides shown in **Bold Red**

```
   1 MGKKTKRTAD SSSSEDEEEY VVEKVLDRRV VKGQVEYLLK WKGFSEEHNT
  51 WEPEKNLDCP ELISEFMKKY KKMKEGENNK PREKSESNKR KSNFSNSADD
 101 IKSKKKREQS NDIARGFERG LEPEKIIGAT DSCGDLMFLM KWKDTDEADL
 151 VLAKEANVKC PQIVIAFYEE RLTWHAYPED AENKEKETAK S
```

Show predicted peptides also

Sort Peptides By ◉ Residue Number ○ Increasing Mass ○ Decreasing Mass

Start - End	Observed	Mr(expt)	Mr(calc)	Delta	Miss	Sequence
120 - 141	2383.9998	2382.9925	2383.1473	-0.1547	1	R.GLEPEKIIGATDSCGDLMFLMK.W Oxidation (M) (No match)
120 - 141	2383.9998	2382.9925	2383.1473	-0.1547	1	R.GLEPEKIIGATDSCGDLMFLMK.W Oxidation (M) (No match)
160 - 171	1524.7996	1523.7923	1523.7442	0.0481	0	K.CPQIVIAFYEER.L Carbamidomethyl (C) (Ions score 66)
160 - 171	1524.7996	1523.7923	1523.7442	0.0481	0	K.CPQIVIAFYEER.L Carbamidomethyl (C) (No match)

U28 - Splicing factor proline/glutamine rich protein (PSF)

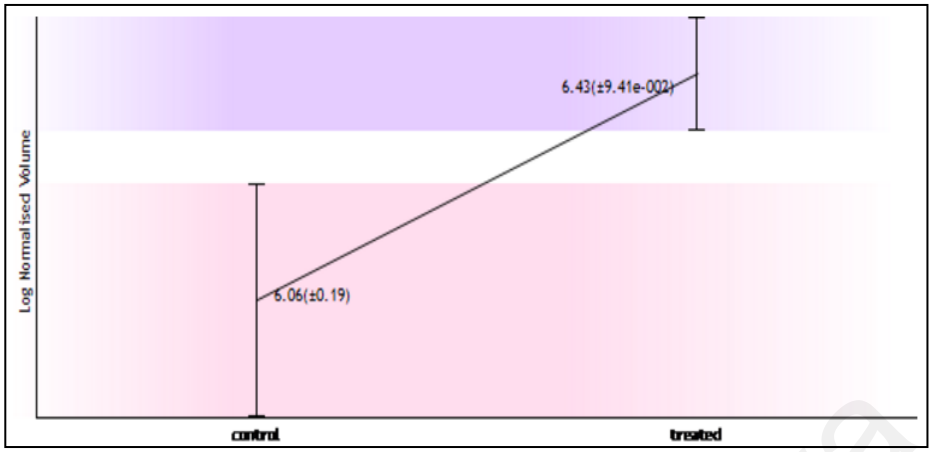

Matched peptides shown in **Bold Red**

```
   1 MSRDRFRSRG GGGGGFHRRG GGGGRGGLHD FRSPPPGMGL NQNRGPMGPG
  51 PGQSGPKPPI PPPPPHQQQQ QPPPQQPPPQ QPPPHQPPPH PQPHQQQQPP
 101 PPPQDSSKPV VAQGPGPAPG VGSAPPASSS APPATPPTSG APPGSGPGPT
 151 PTPPPAVTSA PPGAPPPTPP SSGVPTTPPQ AGGPPPPPAA VPGPGPGPKQ
 201 GPGPGGPKGG KMPGGPKPGG GPGLSTPGGH PKPPHRGGGE PRGGRQHHPP
 251 YHQQHHQGPP PGGPGGRSEE KISDSEGFKA NLSLLRRPGE KTYTQRCRLF
 301 VGNLPADITE DEFKRLFAKY GEPGEVFINK GKGFGFIKLE SRALAEIAKA
 351 ELDDTPMRGR QLRVRFATHA AALSVRNLSP YVSNELLEEA FSQFGPIERA
 401 VVIVDDRGRS TGKGIVEFAS KPAARKAFER CSEGVFLLTT TPRPVIVEPL
 451 EQLDDEDGLP EKLAQKNPMY QKERETPPRF AQHGTFEYEY SQRWKSLDEM
 501 EKQQREQVEK NMKDAKDKLE SEMEDAYHEH QANLLRQDLM RRQEELRRME
 551 ELHNQEMQKR KEMQLRQEEE RRRREEEMMI RQREMEEQMR RQREESYSRM
 601 GYMDPRERDM RMGGGGAMNM GDPYGSGGQK FPPLGGGGGI GYEANPGVPP
 651 ATMSGSMMGS DMRTERFGQG GAGPVGGQGP RGMGPGTPAG YGRGREEYEG
 701 PNKKPRF
```

Show predicted peptides also

Sort Peptides By ◉ Residue Number ○ Increasing Mass ○ Decreasing Mass

Start - End	Observed	Mr(expt)	Mr(calc)	ppm	Miss	Sequence
377 - 399	2639.3708	2638.3635	2638.2915	27	0	R.NLSPYVSNELLEEAFSQFGPIER.A (No match)
377 - 399	2639.3708	2638.3636	2638.2915	27	0	R.NLSPYVSNELLEEAFSQFGPIER.A (Ions score 81)
480 - 493	1762.8167	1761.8094	1761.7747	20	0	R.FAQHGTFEYEYSQR.W (Ions score 66)
480 - 493	1762.8167	1761.8094	1761.7747	20	0	R.FAQHGTFEYEYSQR.W (No match)
517 - 536	2428.1638	2427.1565	2427.1124	18	1	K.DKLESEMEDAYHEHQANLLR.Q (No match)
517 - 536	2428.1638	2427.1565	2427.1124	18	1	K.DKLESEMEDAYHEHQANLLR.Q (Ions score 13)
562 - 571	1347.6858	1346.6785	1346.6248	40	1	K.EMQLRQEEER.R (No match)
667 - 681	1341.6929	1340.6856	1340.6586	20	0	R.FGQGGAGPVGGQGPR.G (Ions score 17)
667 - 681	1341.6929	1340.6856	1340.6586	20	0	R.FGQGGAGPVGGQGPR.G (No match)

U29 - Protein deglycase DJ-1

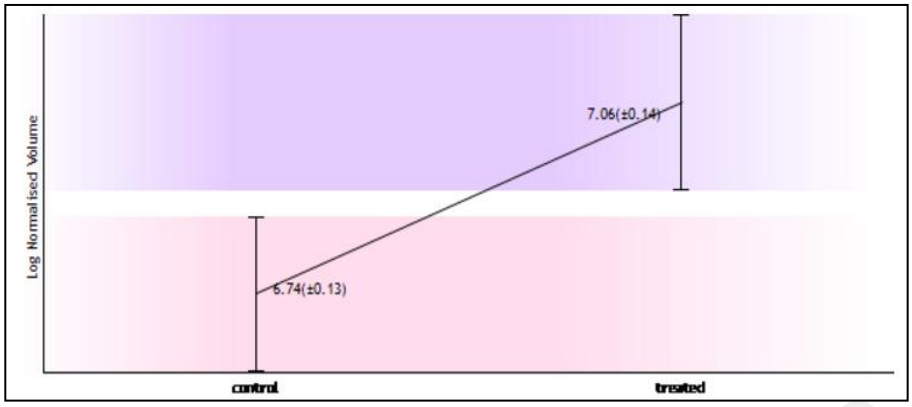

Matched peptides shown in **Bold Red**

```
  1 MASKRALVIL AKGAEEMETV IPVDVMRRAG IKVTVAGLAG KDPVQCSRDV
 51 VICPDASLED AKKEGPYDVV VLPGGNLGAQ NLSESAAVKE ILKEQENRKG
101 LIAAICAGPT ALLAHEIGFG SKVTTHPLAK DKMMNGGHYT YSENRVEKDG
151 LILTSRGPGT SFEFALAIVE ALNGKEVAAQ VKAPLVLKD
```

Show predicted peptides also

Sort Peptides By ◉ Residue Number ○ Increasing Mass ○ Decreasing Mass

Start - End	Observed	Mr(expt)	Mr(calc)	ppm	Miss	Sequence
13 - 27	1675.7585	1674.7512	1674.7957	-27	0	K.GAEEMETVIPVDVMR.R (No match)
13 - 27	1675.7585	1674.7513	1674.7957	-27	0	K.GAEEMETVIPVDVMR.R (Ions score 59)
13 - 27	1707.7262	1706.7189	1706.7855	-39	0	K.GAEEMETVIPVDVMR.R 2 Oxidation (M) (No match)
13 - 27	1707.7262	1706.7189	1706.7855	-39	0	K.GAEEMETVIPVDVMR.R 2 Oxidation (M) (No match)
133 - 145	1559.5905	1558.5832	1558.6293	-30	0	K.MMNGGHYTYSENR.V (No match)
149 - 156	874.4775	873.4702	873.4920	-25	0	K.DGLILTSR.G (No match)

D30 - S-phase kinase-associated protein 1A

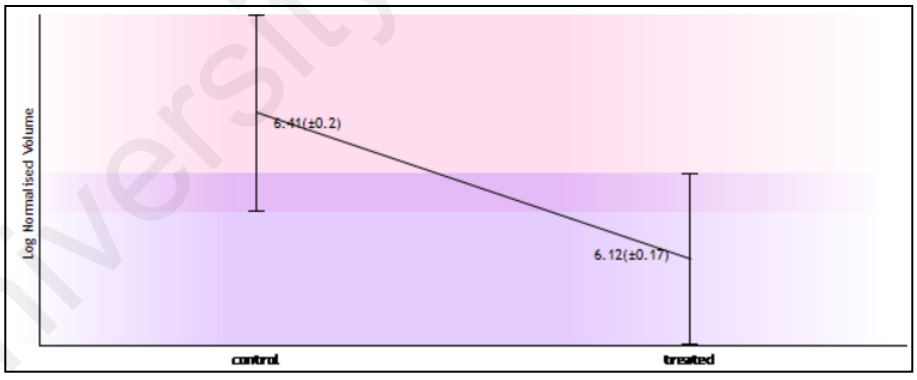

Matched peptides shown in **Bold Red**

```
  1 MPSIKLQSSD GEIFEVDVEI AKQSVTIKTM LEDLGMDDEG DDDPVPLPNV
 51 NAAILKKVIQ WCTHHKDDPP PPEDDENKEK RTDDIPVWDQ EFLKVDQGTL
101 FELILAANYL DIKGLLDVTC KTVANMIKGK TPEEIRKTFN IKNDFTEEEE
151 AQVRKENQWC EEK
```

Show predicted peptides also

Sort Peptides By ◉ Residue Number ○ Increasing Mass ○ Decreasing Mass

Start - End	Observed	Mr(expt)	Mr(calc)	ppm	Miss	Sequence
6 - 22	1878.9972	1877.9899	1877.9258	34	0	K.LQSSDGEIFEVDVEIAK.Q (No match)
81 - 94	1761.9271	1760.9198	1760.8734	26	1	K.RTDDIPVWDQEFLK.V (No match)
81 - 94	1761.9271	1760.9198	1760.8734	26	1	K.RTDDIPVWDQEFLK.V (Ions score 32)
82 - 94	1605.8136	1604.8063	1604.7722	21	0	R.TDDIPVWDQEFLK.V (No match)
95 - 113	2136.1973	2135.1900	2135.1514	18	0	K.VDQGTLFELILAANYLDIK.G (No match)
143 - 154	1466.6819	1465.6746	1465.6321	29	0	K.NDFTEEEEAQVR.K (No match)

D31 - ATP synthase subunit d, mitochondrial (ATPase subunit d)

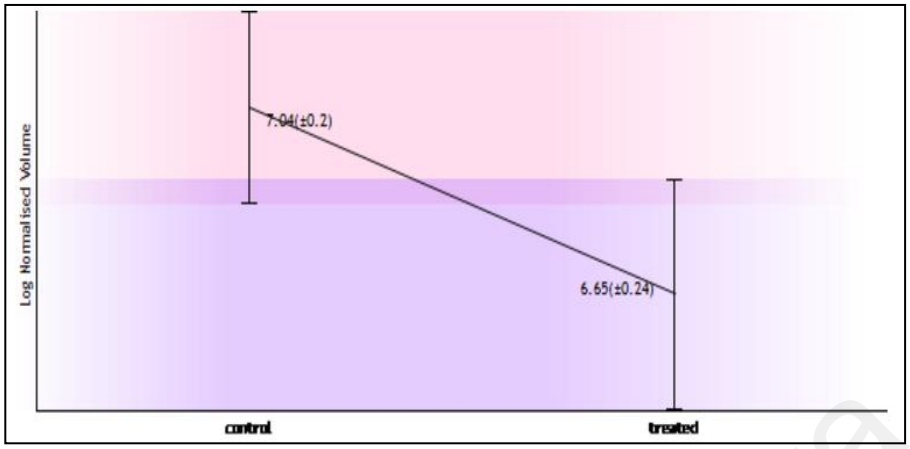

Matched peptides shown in **Bold Red**

```
  1 MAGRKLALKT IDWVAFAEII PQNQKAIASS LKSWNETLTS RLAALPENPP
 51 AIDWAYYKAN VAKAGLVDDF EKKFNALKVP VPEDKYTAQV DAEEKEDVKS
101 CAEWVSLSKA RIVEYEKEME KMKNLIPFDQ MTIEDLNEAF PETKLDKKKY
151 PYWPHQPIEN L
```

Show predicted peptides also

Sort Peptides By ◉ Residue Number ○ Increasing Mass ○ Decreasing Mass

Start - End	Observed	Mr(expt)	Mr(calc)	Delta	Miss	Sequence
10 - 25	1873.0133	1872.0060	1871.9781	0.0279	0	K.TIDWVAFAEIIPQNQK.A (Ions score 52)
33 - 41	1093.5533	1092.5460	1092.5200	0.0261	0	K.SWNETLTSR.L (Ions score 40)
42 - 58	1932.0217	1931.0144	1930.9828	0.0316	0	R.LAALPENPPAIDWAYYK.A (Ions score 62)
124 - 144	2465.2112	2464.2039	2464.1831	0.0208	0	K.NLIPFDQMTIEDLNEAFPETK.L (Ions score 46)
149 - 161	1684.8799	1683.8726	1683.8409	0.0317	1	K.KYPYWPHQPIENL.- (Ions score 53)
150 - 161	1556.7834	1555.7761	1555.7459	0.0302	0	K.YPYWPHQPIENL.- (Ions score 46)

D32 - Ran specific GTPase-activating protein (RanBP1)

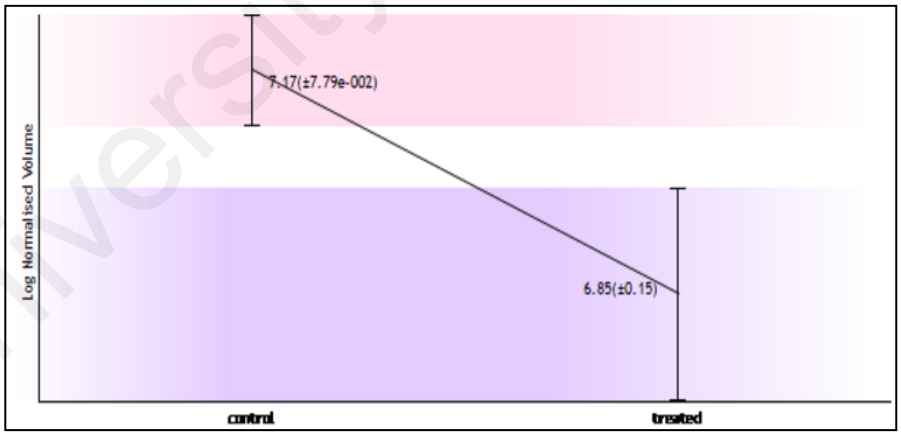

Matched peptides shown in **Bold Red**

```
  1 MAAAKDTHED HDTSTENTDE SNHDPQFEPI VSLPEQEIKT LEEDEEELFK
 51 MRAKLFRFAS ENDLPEWKER GTGDVKLLKH KEKGAIRLLM RRDKTLKICA
101 NHYITPMMEL KPNAGSDRAW VWNTHADFAD ECPKPELLAI RFLNAENAQK
151 FKTKFEECRK EIEEREKKAG SGKNDHAEKV AEKLEALSVK EETKEDAEEK
201 Q
```

Show predicted peptides also

Sort Peptides By ◉ Residue Number ○ Increasing Mass ○ Decreasing Mass

Start - End	Observed	Mr(expt)	Mr(calc)	Delta	Miss	Sequence
58 - 70	1620.8239	1619.8166	1619.7579	0.0587	1	R.FASENDLPEWKER.G (Ions score 9)
58 - 70	1620.8239	1619.8166	1619.7579	0.0587	1	R.FASENDLPEWKER.G (No match)
98 - 118	2418.2146	2417.2073	2417.1290	0.0784	0	K.ICANHYITPMMELKPNAGSDR.A Carbamidomethyl (C) (Ions score 26)
98 - 118	2418.2146	2417.2073	2417.1290	0.0784	0	K.ICANHYITPMMELKPNAGSDR.A Carbamidomethyl (C) (No match)
119 - 141	2739.4038	2738.3965	2738.3275	0.0691	0	R.AWVWNTHADFADECPKPELLAIR.F Carbamidomethyl (C) (Ions score 83)
119 - 141	2739.4038	2738.3965	2738.3275	0.0691	0	R.AWVWNTHADFADECPKPELLAIR.F Carbamidomethyl (C) (No match)

D33 - Mitochondrial import receptor subunit TOM22 homolog (hTom22)

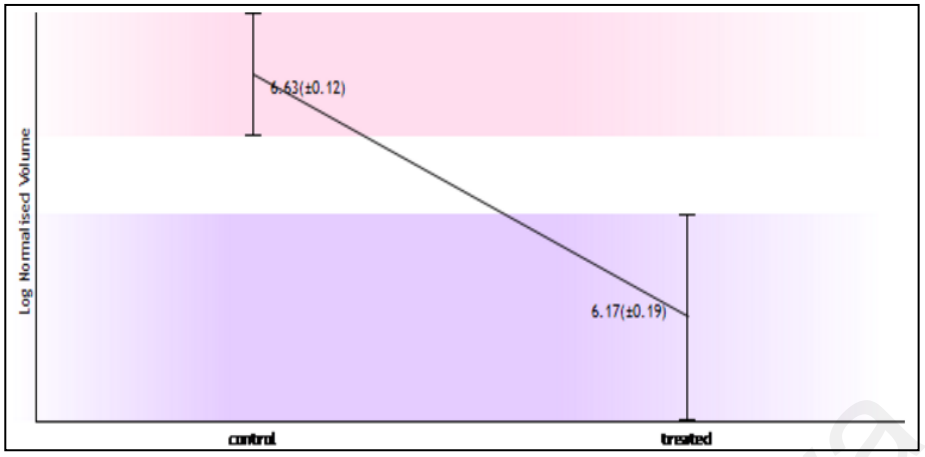

Matched peptides shown in **Bold Red**

```
  1 MAAAVAAAGA GEPQSPDELL PKGDAEKPEE ELEEDDDEEL DETLSERLWG
 51 LTEMFPERVR SAAGATFDLS LFVAQKMYRF SRAALWIGTT SFMILVLPVV
101 FETEKLQMEQ QQQLQQRQIL LGPNTGLSGG MPGALPSLPG KI
```

Show predicted peptides also

Sort Peptides By ◉ Residue Number ○ Increasing Mass ○ Decreasing Mass

Start - End	Observed	Mr(expt)	Mr(calc)	ppm	Miss	Sequence	
48 - 58	1378.6980	1377.6907	1377.6751	11	0	R.LWGLTEMFPER.V	(Ions score 37)
48 - 58	1378.6980	1377.6907	1377.6751	11	0	R.LWGLTEMFPER.V	(No match)
48 - 58	1394.6936	1393.6863	1393.6700	12	0	R.LWGLTEMFPER.V	Oxidation (M) (Ions score 11)
48 - 58	1394.6936	1393.6863	1393.6700	12	0	R.LWGLTEMFPER.V	Oxidation (M) (No match)
106 - 117	1557.8035	1556.7962	1556.7729	15	0	K.LQMEQQQQLQQR.Q	(Ions score 16)
106 - 117	1557.8035	1556.7962	1556.7729	15	0	K.LQMEQQQQLQQR.Q	(No match)
106 - 117	1573.7997	1572.7924	1572.7678	16	0	K.LQMEQQQQLQQR.Q	Oxidation (M) (No match)
106 - 117	1573.7997	1572.7924	1572.7678	16	0	K.LQMEQQQQLQQR.Q	Oxidation (M) (No match)

D34 - Glyoxalase domain-containing protein 4

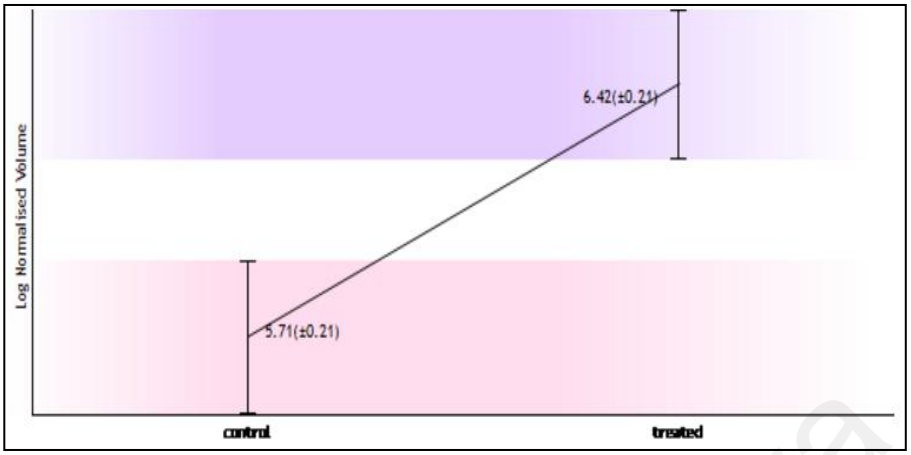

Matched peptides shown in **Bold Red**

```
  1 MAARRALHFV FKVGNRFQTA RFYRDVLGMK VLRHEEFEEG CKAACNGPYD
 51 GKWSKTMVGF GPEDDHFVAE LTYNYGVGDY KLGNDFMGIT LASSQAVSNA
101 RKLEWPLTEV AEGVFETEAP GGYKFYLQNR SLPQSDPVLK VTLAVSDLQK
151 SLNYWCNLLG MKIYEKDEEK QRALLGYADN QCKLELQGVK GGVDHAAAFG
201 RIAFSCPQKE LPDLEDLMKR ENQKILTPLV SLDTPGKATV QVVILADPDG
251 HEICFVGDEA FRELSKMDPE GSKLLDDAMA ADKSDEWFAK HNKPKASG
```

Show predicted peptides also

Sort Peptides By ◉ Residue Number ○ Increasing Mass ○ Decreasing Mass

Start - End	Observed	Mr(expt)	Mr(calc)	ppm	Miss	Sequence
82 - 101	2051.9985	2050.9912	2051.0106	-9	0	K.LGNDFMGITLASSQAVSNAR.K (No match)
82 - 101	2051.9985	2050.9913	2051.0106	-9	0	K.LGNDFMGITLASSQAVSNAR.K (Ions score 18)
102 - 124	2550.2554	2549.2481	2549.2690	-8	1	R.KLEWPLTEVAEGVFETEAPGGYK.F (No match)
125 - 130	840.4340	839.4267	839.4290	-3	0	K.FYLQNR.S (No match)
151 - 162	1498.6984	1497.6911	1497.7108	-13	0	K.SLNYWCNLLGMK.I Carbamidomethyl (C) (No match)
151 - 166	2031.9608	2030.9535	2030.9957	-21	1	K.SLNYWCNLLGMKIYEK.D Carbamidomethyl (C) (No match)
151 - 166	2031.9608	2030.9535	2030.9957	-21	1	K.SLNYWCNLLGMKIYEK.D Carbamidomethyl (C) (No match)
163 - 170	1053.5624	1052.5551	1052.5026	50	1	K.IYEKDEEK.Q (No match)
163 - 170	1053.5624	1052.5551	1052.5026	50	1	K.IYEKDEEK.Q (No match)
191 - 201	1057.5210	1056.5137	1056.5101	3	0	K.GGVDHAAAFGR.I (No match)
238 - 262	2758.3296	2757.3223	2757.3432	-8	0	K.ATVQVVILADPDGHEICFVGDEAFR.E Carbamidomethyl (C) (Ions score 25)
238 - 262	2758.3296	2757.3223	2757.3432	-8	0	K.ATVQVVILADPDGHEICFVGDEAFR.E Carbamidomethyl (C) (No match)
267 - 283	1806.7898	1805.7825	1805.8175	-19	1	K.MDPEGSKLLDDAMAADK.S (No match)
267 - 283	1806.7898	1805.7825	1805.8175	-19	1	K.MDPEGSKLLDDAMAADK.S (No match)

U35 - Glutaredoxin-3

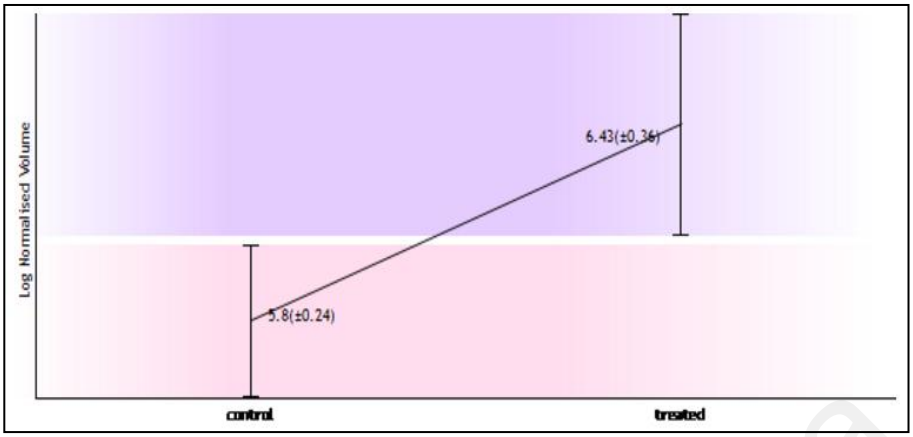

Matched peptides shown in **Bold Red**

```
  1 MAAGAAEAAV AAVEEVGSAG QFEELLRLKA KSLLVVHFWA PWAPQCAQMN
 51 EVMAELAKEL PQVSFVKLEA EGVPEVSEKY EISSVPTFLF FKNSQKIDRL
101 DGAHAPELTK KVQRHASSGS FLPSANEHLK EDLNLRLKKL THAAPCMLFM
151 KGTPQEPRCG FSKQMVEILH KHNIQFSSFD IFSDEEVRQG LKAYSSWPTY
201 PQLYVSGELI GGLDIIKELE ASEELDTICP KAPKLEERLK VLTNKASVML
251 FMKGNKQEAK CGFSKQILEI LNSTGVEYET FDILEDEEVR QGLKAYSNWP
301 TYPQLYVKGE LVGGLDIVKE LKENGELLPI LRGEN
```

Show predicted peptides also

Sort Peptides By ◉ Residue Number ○ Increasing Mass ○ Decreasing Mass

Start - End	Observed	Mr(expt)	Mr(calc)	ppm	Miss	Sequence	
80 - 92	1577.7672	1576.7599	1576.8177	-37	0	K.YEISSVPTFLFFK.N	(No match)
80 - 92	1577.7672	1576.7599	1576.8177	-37	0	K.YEISSVPTFLFFK.N	(No match)
172 - 188	2069.8804	2068.8731	2068.9490	-37	0	K.HNIQFSSFDIFSDEEVR.Q	(Ions score 48)
172 - 188	2069.8804	2068.8731	2068.9490	-37	0	K.HNIQFSSFDIFSDEEVR.Q	(No match)
232 - 238	842.4734	841.4661	841.4657	0	1	K.APKLEER.L	(No match)
266 - 290	2954.3628	2953.3555	2953.4444	-30	0	K.QILEILNSTGVEYETFDILEDEEVR.Q	(Ions score 63)
266 - 290	2954.3628	2953.3555	2953.4444	-30	0	K.QILEILNSTGVEYETFDILEDEEVR.Q	(No match)
295 - 308	1729.7990	1728.7917	1728.8511	-34	0	K.AYSNWPTYPQLYVK.G	(No match)
320 - 332	1523.7964	1522.7891	1522.8718	-54	1	K.ELKENGELLPILR.G	(No match)